Investigations of Holographic Duality in Two Dimensions

Akash Goel

A Dissertation
Presented to the Faculty
of Princeton University
in Candidacy for the Degree
of Doctor of Philosophy

Recommended for Acceptance
by the Department of
Physics
Adviser: Herman Verlinde

September 2022

Abstract

This dissertation explores various structural, geometric, statistical and information-theoretic aspects of models of lower-dimensional holography. Chapter 2 is based on work with Ho Tat Lam, Gustavo J. Turiaci and Herman Verlinde [1]. It explores a class of partially entangled thermal states in the Sachdev-Ye-Kitaev model that interpolates between the thermo-field double state and a pure (product) state. We argue that the holographic dual of this class of states consists of two black holes with their interior regions connected via a domain wall, described by the worldline of a massive particle. We compute the size of the interior region and the entanglement entropy as a function of the temperature of each black hole. We argue that the one-sided bulk reconstruction can access the interior region of the black hole. Chapter 3 is based on work with Luca Iliesiu, Jorrit Kruthoff and Zhenbin Yang [2]. It explores a systematic classification of the possible boundary conditions in Jackiw-Teitelboim gravity and discusses their exact quantization. Each boundary condition that we study will reveal new features in JT gravity related to its matrix integral interpretation, its factorization properties, ensemble averaging interpretation, the definition of the theory at finite cutoff, its relation to the physics of near-extremal black holes and its role as a two-dimensional model of cosmology. Chapter 4 is based partly on [3] and on discussions with Ping Gao, Vladimir Narovlansky and Herman Verlinde. We survey several strategies to explore the UV physics of SYK. We provide a Lorentzian Liouville quantum gravity perspective on the double-scaled model. We then describe the construction of a matrix version of SYK within the framework of minimal string theory.

Acknowledgements

Over the course of my journey, I have had the privilege of interacting and learning from several brilliant mentors, speakers and colleagues that I am thankful for. First, I am grateful to my advisor, Herman Verlinde for his patient guidance and for countless discussions over the years. Herman has been very generous in sharing his ideas and his unique approach to solving problems that have helped sharpen my intuition and shaped my way of thinking. Thanks to Igor Klebanov for his kindness, his wealth of wisdom and advice. To Juan Maldacena, for sharing his insights at various stages. I am also grateful to Atish Dabholkar and Rajesh Gopakumar for valuable advice as an undergrad.

Thank you to my wonderful collaborators - Luca Iliesiu, Jorrit Kruthoff, Ho Tat Lam, Joaquin Turiaci and Zhenbin Yang. I have throughly enjoyed our stimulating discussions and learned so much. I have also benefitted enormously from discussions with Ahmed Almheiri, Yiming Chen, Yale Fan, Ping Gao, Ziming Ji, Himanshu Khanchandani, David Kolchmeyer, Thomas Mertens, Alexei Milekhin, Sanjay Moudgalya, Vladimir Narovlansky, Fedor Popov, Pratik Rath, Mengyang Zhang, Wenli Zhao and many others.

Many thanks to all the wonderful people that I have had the pleasure of befriending, for the fun, laughter and cherished memories. Finally, I thank my parents for their unending patience, affection and support over the years.

Contents

Chapter 1

Introduction and Background

One of the triumphs of modern high energy theoretical physics is a concrete realization of the principle of holography [4, 5]. Indeed, it is now widely believed that the physics of conformally invariant quantum field theories with a large number of degrees of freedom is equivalently described by quantum gravity in one higher dimension on asymptotically Anti de-Sitter space. This Anti de Sitter/Conformal Field Theory correspondence (AdS/CFT) [6–9] has withstood numerous stringent checks and has been a useful tool in understanding various strongly coupled phenomena.

On general grounds, one expects that studying this correspondence in lower dimensions will lead to simplifications. This is indeed what happens in the case of AdS_3/CFT_2 where we find enhanced symmetries on both sides that allow greater analytic control. If we try to go even lower to two dimensions, naively we do not obtain any non-trivial physics since 2D gravity is topological and involves only captures degenerate ground states.

In the past few years however, a systematic framework has been developed to study a deformed version of AdS_2 holography, the *nearly* AdS_2/CFT_1 correspondence [10–15]. In this framework, the boundary dynamics is captured by the Sachdev-Ye-Kitaev model [16, 10] which

is a model of N Majorana fermions interacting via random couplings J

$$H = i^{\frac{p}{2}} \sum_{1 \leq i_1 < i_2 \ldots < i_p}^{N} J_{i_1 \ldots i_p} \ \psi_{i_1} \psi_{i_2} \ldots \psi_{i_p}. \tag{1.1}$$

These couplings are drawn from a Gaussian distribution $\left\langle J^2_{i_1 \ldots i_p} \right\rangle = \binom{N}{p}^{-1} \mathcal{J}^2$. The scaling with N ensures that the model admits analytic solutions for correlation functions of the fermions at strong coupling, $1 \ll \beta J \ll N$ in terms of 'melon' diagrams [10].

This ensemble averaged theory of quantum mechanics has received great attention in recent times since it exhibits various properties characteristic of chaotic black hole dynamics such as a maximal Lyapunov exponent [10] and a ramp in the spectral form factor [17]. In the infrared, the theory has an emergent conformal symmetry described by diffeomorphisms of the time circle. This time reparametrisation symmetry is both spontaneously broken and explicitly broken to $SL(2, R)$ and the IR dynamics is governed by a Schwarzian mode.

The corresponding bulk is described by Jackiw-Teitelboim (JT) dilaton-gravity [18,19] instead of the Einstein Hilbert action given by the action

$$S = -\frac{\phi_0}{16\pi G} \left[\int \sqrt{g} R + \int_\partial K \right] - \frac{1}{16\pi G} \left[\int d^2x \sqrt{g} \ \phi(R+2) + 2 \int_\partial \phi_b K \right]. \tag{1.2}$$

The resulting geometry can be viewed in terms of sections of 2d hyperbolic space. The bulk is rigid and the entire dynamics is governed by fluctuations of the boundary. The boundary is interpreted as the location where the dilaton ϕ achieves a large value[1]. The entire physics is then described by the action of this mode of boundary reparametrizations living on a rigid AdS_2 background which explicitly breaks the asymptotic conformal symmetry group.

One finds that the theory that describes both the dominant infrared mode of SYK as well as

[1] As we will see in chapter 3, other boundary conditions are also possible.

the reparametrization mode of JT gravity is described by the Schwarzian action.

$$S = -C \int_0^\beta d\tau \left(\{f(\tau), \tau\} + \frac{2\pi^2}{\beta^2} f'^2 \right) \tag{1.3}$$

where $C \sim \frac{N}{J}$ is the Schwarzian coupling and the curly brackets denote the Schwarzian derivative,

$$\{f(\tau), \tau\} = \frac{f'''}{f'} - \frac{3}{2} \left(\frac{f''}{f'} \right)^2 . \tag{1.4}$$

This is also the mode responsible for the maximal chaotic behaviour of the model. The action of the $SL(2, R)$ gauge symmetry on the reparametrisation mode is given by

$$f(\tau) \to \frac{af(\tau) + b}{cf(\tau) + d}, \qquad\qquad ad - bc = 1. \tag{1.5}$$

which leaves the Schwazian action invariant.

The quantization of the Schwarzian theory has received much attention and has been carried out using various techniques - using localization [20], interpreting the Schwarzian as a particle moving in a magnetic field [21,22] and through an embedding in Liouville theory by dimensional reduction in a specific scaling limit [23–25].

One can also study correlations functions obtained by insertions of SL(2,R) invariant bilocal operators in the Schwarzian with specific scaling dimensions

$$\mathcal{O}_\ell(\tau_1, \tau_2) = \left(\frac{\sqrt{f'(\tau_1) f'(\tau_2)}}{\frac{\beta}{\pi} \sin\left(\frac{\pi}{\beta} \left[f(\tau_1) - f(\tau_2) \right] \right)} \right)^{2\ell} \tag{1.6}$$

They correspond to insertion of a bulk Liouville vertex operator in the 2d Liouville interpretation. The exact results for the correlation functions of these operators were derived in [24] and their geometric interpretation will be reviewed in chapter 2.

Given the simplicity of these exact results, it is natural to apply this formalism to improve our understanding of information theoretic aspects of holography, in particular how bulk spacetime

emerges and is encoded in the boundary theory. One of the elements of the AdS/CFT dictionary is that thermal states in quantum field theory are described by black hole geometries in the bulk. It is reasonable to expect that we could probe aspects of quantum gravity in the strong coupling regime using this correspondence. This regime is suspected to be relevant to strongly coupled gravitational physics of black hole interiors and the black hole information problem [26–29]. One of the goals of this thesis is to understand better the emergence of the bulk for boundary physics in the context of the simple, solvable quantum mechanical model.

Another important element of the AdS/CFT dictionary that has evolved in recent years is the role of quantum entanglement in giving rise to the structure of spacetime. The celebrated Ryu Takayangi formula [30] states that the entanglement entropy of a region on a given spatial slice in the boundary CFT is given by the bulk extremal surface of minimal area homologous to the boundary region. In the present context, as we will demonstrate explicitly in chapter 2, the role of the extremal surface is played by the value of the dilaton along the bulk Cauchy slice. This can be seen more explicitly by viewing Jackiw Teitelboim gravity as the effective theory upon dimensional reduction on S^2 of the near-horizon region of a four dimensional near-extremal black hole [31]. In this case, the horizon value of the dilaton in the AdS_2 black hole is directly related to the area of the outer horizon of the 4d black hole.

An important state that exemplifies the role played by entanglement in the bulk geometry is the thermofield double state. This is the maximally entangled state in the Hilbert space comprising of two copies of the CFT associated to the temperature β^{-1}

$$|\mathrm{TFD}\rangle = \sum_n e^{-\beta E_n/2} |n\rangle_L |n^*\rangle_R \tag{1.7}$$

The one-sided density matrix looks thermal in this state

$$\mathrm{tr}_L \left(|\mathrm{TFD}\rangle\langle\mathrm{TFD}|\right) = e^{-\beta H} \tag{1.8}$$

This state has a natural interpretation in the bulk. The two CFTs live on the timelike asymp-

totically AdS boundaries of the maximally extended AdS Schwarzschild black hole [32]. The left and right boundaries are causally disconnected and the causal wedges corresponding to the left and the right regions are connected by a wormhole/Einstein-Rosen bridge. The area of the horizon at the bifurcate point measures the minimal cross section of the wormhole and hence the entanglement entropy between the left and right CFTs. This is in contrast to pure state black holes which have a single asymptotic region and the area of the horizon is the thermal entropy. We find an analogous black hole solution in JT gravity.

Having established the correspondence between JT gravity at the level of the disk topology with the Schwarzian theory, one can also extend the analysis to more general surfaces. The corresponding theory is equivalent to a double-scaled matrix model with the expansion in the double-scaling parameter playing the role of the genus expansion [33].

Given these developments, it is natural to consider the following intriguing possibility - if the IR dynamics of SYK is captured by JT gravity, does the full SYK model describe a UV completion? In particular, can one find an embedding of the model within string theory? Initial steps in this direction were taken in [3]. The double-scaling limit of the SYK model introduced in [17] is a particularly useful tool to study this regime since exact results are known in this limit at arbitrary energy scales. In particular, the Schwarzian theory is replaced by a theory described by representations of a quantum group generalisation of $SL(2, R)$.

This thesis is organised as follows - in the rest of this section, we will provide an overview of the background literature relevant to this thesis. We first describe correlation functions in the Schwarzian theory with emphasis on the representation theoretic interpretation. Then, we will describe JT gravity, its genus expansion and corresponding matrix model description. Finally, we will present various elements of non-critical string theory with an emphasis on the study of minimal model CFTs coupled to gravity. Our presentation will be concise and we refer the reader to the primary literature for further details.

In chapter 2, we will study a particular class of partially entangled thermal states in the SYK model. These states are prepared by a Euclidean path integral describing the evolution

over two euclidean time segments separated by a local scaling operator $\mathcal{O}$. We will describe the holographic dual of this class of states geometrically. We will also compute the entanglement entropy in these states as a function of the scale dimension of $\mathcal{O}$ and study bulk reconstruction in the interior region of the black hole.

In chapter 3, we will study a four-fold classification of possible boundary conditions in JT gravity. We will discuss an exact quantization of the theory. In particular, we will show that boundary conditions where the extrinsic curvature K is fixed exhibit unique factorisation properties for $K > 1$. We will also provide an interpretation of each boundary condition from the matrix model point of view and describe an integral kernel that translates to the fixed K boundary conditions from the standard ones.

In chapter 4, we probe aspects of SYK beyond the Schwarzian limit. We expect this regime to include quantum gravity effects and establish connections with non-critical string theory. We introduce the double scaling limit of the SYK model and comment on the dual string interpretation as a sine-dilaton gravity theory. We then discuss a proposed paradigm for realizing a matrix SYK model within string theory. Using the large N matrix description of $c < 1$ string theory, we show that the effective theory on a large number Q of FZZT D-branes in $(p, 1)$ minimal string theory can be mapped to a model that takes the form of disorder averaged SYK with $J\psi^p$ interaction. The SYK fermions represent open strings between the FZZT branes and the ZZ branes that underly the matrix model. We will observe several qualitative and quantitative links between the SYK model and (p, q) minimal string theory and propose that the two describe different phases of a single system. We also derive the chord diagrammatic expansion of double-scaled SYK using a Lorentzian Liouville effective action for SYK. We end with an analysis of the semiclassical limit of double-scaled SYK.

1.1 Schwarzian Quantum Mechanics

In this section, we will briefly describe the evaluation of Schwarzian correlators from Liouville theory and present a Feynman diagram-like prescription to calculate these.

In [24], it was argued that one could view the quantum partition function of the Schwarzian action as a path integral over diffeomorphisms on the circle modulo $SL(2,R)$ transformations. This may be viewed as a double scaling classical limit of the chiral identity character of the Virasoro algebra in which the modular parameter degenerates to that of an infinitesimally thin circular tube. By expanding the identity character in the dual open string channel, one can express this quantity as a transition amplitude between ZZ brane boundary states. One can express insertions of bilocal operators in the Schwarzian $\mathcal{O}_l$ as in (1.6) as insertions of Liouville vertex operators $e^{\ell\phi}$ in the 2D perspective.

Using known results from the literature in Liouville theory, in particular the three point function of primary vertex operators, the correlators were calculated in [24]. The result for the two point function is given by

$$\begin{aligned}\langle \mathcal{O}_\ell(\tau_1,\tau_2)\rangle &= \int \prod_{i=1}^{2} d\mu(k_i)\ \tau_2 \\ &= \int d\mu(k_1)\, d\mu(k_2)\, e^{-(\tau_2-\tau_1)k_1^2-(\beta-\tau_1-\tau_2)k_2^2}\frac{\Gamma(\ell\pm ik_1\pm ik_2)}{\Gamma(2l)} \end{aligned} \tag{1.9}$$

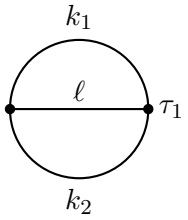

where a product over all possible signs of the gamma functions is implied and the measure $d\mu(k) = k\sinh 2\pi k\ dk$. The diagram above is suggestive of a two dimensional AdS interpretation with the Schwarzian insertions at the boundary Euclidean times as shown and intermediate integrals over continuous $SL(2,R)$ representation labels k_i with the appropriate Plancherel measure in the Schwarzian limit [24].

More generally correlators can be expressed via the following 'Feynman rules'

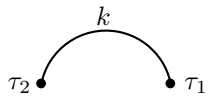

$$= \quad e^{-\,k^2\,(\tau_2-\tau_1)}\ , \qquad \gamma_\ell(k_1,k_2) = \sqrt{\frac{\Gamma(\ell\pm ik_1\pm ik_2)}{\Gamma(2l)}}. \tag{1.10}$$

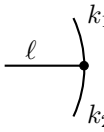

The operator insertions on the thermal circle are supplemented by continuous momentum labels for each region that the diagram is divided into with an appropriate factor for the propagator running on the boundary thermal circle. The bilocal insertions carry discrete $SL(2,R)$ representation labels. A vertex factor is also added as shown which corresponds to the $3j$ symbol for two continuous ans one discrete representation.

The time ordered four point function is thus given by

$$\left\langle \mathcal{O}_{\ell_1}(\tau_1,\tau_2)\,\mathcal{O}_{\ell_2}(\tau_3,\tau_4)\right\rangle \;=\; \int \prod_{i=1,2,s} d\mu(k_i) \tag{1.11}$$

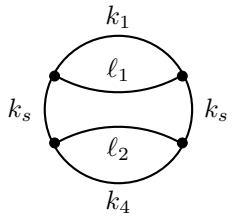

There is a common intermediate momentum k_s because the bilocal operator is $SL(2,R)$ invariant and hence commutes the Schwarzian Hamiltonian which is given by the quadratic Casimir.

Note that for the out of time ordered correlator, one also needs to add an R-matrix factor in the diagram corresponding to crossing of two operators. This matrix is unitary and is related to the 6j symbol of $SL(2,R)$. In [34], it was also verified that this factor is the near horizon scattering matrix of wavepackets in the bulk in the semiclassical limit.

Yet another approach to studying the Schwarzian theory is by using an $SL(2,R)$ BF theory formulation [35,36]. In this case, the constant negative curvature constraint maps to the flatness condition for the gauge field. Boundary-anchored probe geodesics on the hyperbolic surface map to Wilson lines.

1.2 JT Gravity

Let us review briefly the standard analysis of JT gravity which amounts to putting Dirichlet boundary conditions on both the metric and dilaton at asymptotic infinity [13]. We will later generalise this discussion to include alternative boundary conditions. In Euclidean signature, it is convenient to think of fixing the metric as fixing the proper boundary length.

Euclidean JT gravity on a manifold $\mathcal{M}$ and boundary $\partial\mathcal{M}$ is described by the action consisting of three parts - a topological term, a bulk term and a boundary term,

$$S = S_{\text{top}} + S_{\text{bulk}} + S_{\partial}. \tag{1.12}$$

The first of these three terms is given by

$$S_{\text{top}} = -\frac{\phi_0}{4\pi}\left(\int_{\mathcal{M}} \sqrt{g}R + 2\int_{\partial\mathcal{M}} \sqrt{h}K\right) = -\phi_0\chi(\mathcal{M}) \tag{1.13}$$

with ϕ_0 a constant and $\chi(\mathcal{M}) = 2 - 2g - n$ the Euler character of $\mathcal{M}$ for a manifold with genus g and n boundaries. The other two pieces are given by

$$S_{\text{bulk}} = -\frac{1}{16\pi G_N}\int_{\mathcal{M}} d^2x\sqrt{g}\,\phi(R+2), \quad S_{\partial} = -\frac{1}{8\pi G_N}\int_{\partial\mathcal{M}} du\sqrt{h}\,\phi(K-1), \tag{1.14}$$

where in the remainder of this section, we work in units where $16\pi G = 1$. Here, g is the bulk $2d$ metric, ϕ the dilaton and h and K are the induced metric and extrinsic curvature on the boundary $\partial\mathcal{M}$. The boundary term here is chosen so that the variational principle is well-defined (K dependent term) and make the on-shell action finite (second term).

The equations of motion for the metric and dilaton are given by

$$R + 2 = 0, \quad \left(\nabla_\mu\nabla_\nu - g_{\mu\nu}\nabla^2 + g_{\mu\nu}\right)\phi = 0. \tag{1.15}$$

The metric is thus that of Euclidean AdS_2 ($\mathbb{H}^2$). The on-shell solution of the dilaton is pa-

rameterized by a three dimensional vector Z in embedding space corresponding to the different $SL(2,R)$ charges of the dilaton field. Denoting the $\mathbb{H}^2$ embedding coordinates by Y we have $-Y_0^2 + Y_1^2 + Y_2^2 = -1$ and $\phi = Z.Y$. In particular, with Poincaré coordinates the metric and dilaton profile are given by

$$ds^2 = \frac{d\tau^2 + dz^2}{z^2}, \quad \phi = \frac{a_1 + a_2\tau + a_3(\tau^2 + z^2)}{z}. \tag{1.16}$$

The boundary is located at $z \to 0$, but we can consider cutting the geometry along some curve $(\tau(u), z(u))$, with u the intrinsic boundary coordinate. The boundary conditions we then impose [13] on the curve $(\tau(u), z(u))$ are

$$ds^2|_{\partial\mathcal{M}} = g_{uu}du^2 = \frac{du^2}{\epsilon^2}, \quad \phi|_{\partial\mathcal{M}} = \frac{\phi_r(u)}{\epsilon} \tag{1.17}$$

with $\epsilon > 0$ small. We can solve these boundary conditions in an expansion in ϵ and to leading order in ϵ we find, $z(u) = \epsilon\tau'(u)$ and a corresponding solution for the dilaton. The boundary is thus at asymptotic infinity, close to $z = 0$ as $\epsilon \to 0$. The extrinsic curvature in such a case is given by,

$$K = 1 + \epsilon^2 \mathrm{Sch}(\tau, u)\,, \qquad \mathrm{Sch}(\tau, u) = \frac{\tau'''}{\tau'} - \frac{3}{2}\left(\frac{\tau''}{\tau'}\right)^2 \tag{1.18}$$

where $\tau' = \partial_u\tau$ and $\mathrm{Sch}(\tau, u)$ is the Schwarzian derivative. More details related to the bulk dynamics are discussed in section 2.7.

Since the bulk term in (1.12) vanishes after integrating out the dilaton ϕ, the only remaining degree of freedom is given by the reparametrization mode $\tau(u)$, whose action is given by the Schwarzian derivative defined above. Consequently, the quantization of the theory on disk topologies reduces to the quantization of the Schwarzian theory.

1.3 JT Matrix Integral

One can also use the quantization of the Schwarizan theory together with results for the volumes of the moduli space of constant curvatures Rimenann surfaces to compute the contribution of surfaces with any topology to the JT partition function. The quantization of this theory was studied in great detail in [24, 21, 22, 25, 33, 35] and the contribution of higher genus surfaces was computed in [33]. The central tool needed to establish these results is the correspondence with a double-scaled matrix model.

The matrix model we will study in this section takes the form of an integral over arbitrary $N \times N$ Hermitian matrix H weighted by a potential $\mathrm{Tr}\, V(H)$. A natural class of observables in the matrix model are those involving the correlation functions of the loop operator $Z(L) = \mathrm{Tr}\left(e^{-LH}\right)$,

$$\langle Z(L_1)...Z(L_n)\rangle = \frac{1}{\mathcal{Z}}\int dH\, e^{-N\mathrm{Tr}\, V(H)} Z(L_1)...Z(L_n).$$

Here, $\mathcal{Z}$ is an overall normalisation. These observables are related to the correlation functions of the resolvent $R(E) = \mathrm{Tr}\,(E-H)^{-1}$ by a simple integral transform. They will have the interpretation of creating boundaries of renormalised length L in the gravity description.

For a generic potential, one can study the distribution of eigenvalues of the matrix H in this ensemble which can be described by the discontinuity across a branch cut in the resolvent[2]. For the JT matrix model and matrix models corresponding to $(2, p)$ minimal gravity, the resolvent lives on a two-sheet Riemann surface described by the spectral curve. The double scaling limit arises as a result of tuning the potential to a critical point while simultaneously taking the size of the matrix to be large. This corresponds to zooming near the edge of the spectrum of eigenvalues.

The potential that gives rise to the genus expansion of JT gravity corresponds to considering

[2]We will only need to consider here potentials that lead to a single cut.

the following disk spectral density

$$\rho_0(E) = \frac{e^{S_0}}{(2\pi)^2}\sinh(2\pi\sqrt{E}), \qquad E > 0, \tag{1.19}$$

which one may recognise as the Schwarzian spectral density. The double scaled correlation functions are organised in terms of an expansion in the parameter e^{S_0}. In the gravitational language, $S_0 = \phi_0$ is the ground state entropy.

In a general matrix model, one can derive recursion relations between correlation functions of the resolvent called loop equations. What is unique about the JT matrix model is that the loop equations for the resolvents $R_{n,g}$ can be systematically mapped to recursion relations satisfied by the volume of moduli space of constant negative curvature surfaces $V_{g,n}$ derived by Mirzakhani [37]. This happens precisely when the spectral curve of the matrix model is given by

$$y = \frac{\sin(2\pi z)}{4\pi}, \qquad x = z^2, \tag{1.20}$$

in terms of a uniformising coordinate z. Using the BF theory approach, one can also see that the symplectic form in $SL(2,R)$ BF theory precisely maps to the Weil-Peterson form on this moduli space.

This allows us to express the double-scaling expansion as a genus expansion,

$$\begin{aligned} \langle Z(L)\rangle &= e^{\phi_0} Z_{\rm Sch}^{\rm disk}(L) + \sum_{g=1}^{\infty} e^{(1-2g)\phi_0} \int_0^\infty b\, db\; V_{g,1}(b) Z_{\rm Sch}^{\rm trumpet}(L,b). \\ &= \end{aligned} \tag{1.21}$$

where we introduced the amplitudes corresponding to the disk and the trumpet geomtery,

$$Z^{(\rm Disk)}(L) = \frac{1}{\sqrt{2\pi}}\frac{e^{\frac{2\pi^2}{L}}}{L^{3/2}}, \qquad Z^{(\rm Trumpet)}(b;\, L) = \frac{1}{\sqrt{2\pi}}\frac{e^{-\frac{b^2}{2L}}}{L^{1/2}}. \tag{1.22}$$

These can be derived by computing the integral with the symplectic measure weighted by the

Schwarzian action with appropriate boundary conditions.

The recipe for constructing geometries of arbitrary topology describing the contributions to correlation functions with arbitrary number of insertions is now straightforward - to fill in the geometry with a disk, one simply includes the contributions due to boundary wiggles - the Schwarzian disk amplitude. For higher genus and connected geometries, one must integrate the contributions due to boundary wiggles for each trumpet ending at a geodesic with length b_i against the appropriate Mirzakhani volumes $V_{g,n}(b_1, \ldots, b_n)$. The correct measure for this integral that follows from the Weil-Peterson measure is simply b_i and comes from integrating over the twist. We will study the double trumpet geometry from a purely BF perspective in chapter 3.

1.4 Liouville Quantum Gravity

In order to find an embedding of SYK in a UV complete theory, it is natural to look at 2d gravity. The study of the path integral of 2d gravity initiated in [38] leads naturally to non-critical string theory. In conformal gauge, the diffeomorphism invariant sum over two-dimensional worldsheets can be described by conformal matter coupled to Liouville theory. Implementing Weyl symmetry at a quantum level imposes non-trivial constraints on the theory, namely the total central charge must vanish.

The full theory can be organised into the three sectors

$$\left[\begin{array}{c}\text{Conformal}\\ \text{Matter}\end{array}\right] \oplus \left[\begin{array}{c}\text{Liouville}\\ \text{Field } \phi\end{array}\right] \oplus \left[\begin{array}{c}\text{Ghosts}\\ (b,c)\end{array}\right] \tag{1.23}$$

where the action is given by

$$S = S_M + S_L + S_g, \quad S_L = \frac{1}{4\pi}\int d^2z \left((\nabla\phi)^2 + QR\phi + 4\pi\mu e^{2b\phi}\right) \tag{1.24}$$

where $Q = b + b^{-1}$ is the background charge that couples to the curvature and $c_L = 1 + 6Q^2$.

Hence the central charges are constrained via

$$c_M + c_L + c_g = 0, \qquad \text{or} \quad c_M + c_L = 26. \tag{1.25}$$

The physical vertex operators have ghost number 1 and take the form

$$\mathcal{O}_m = c\,\overline{c}\,O_m\,V_\alpha. \tag{1.26}$$

where $V_L(\alpha)$ is the Liouville dressing characterised by a complex parameter α. It is fixed by Weyl symmetry in terms of the conformal dimensions of the matter primary,

$$\Delta(O_m) + \Delta(V_\alpha) = 1 \tag{1.27}$$

With the above application in mind, it is very useful to study the properties of Liouville theory as a CFT on the Euclidean plane. The spectrum consists of scalar primaries which are exponentials of the Liouville field, $V_L(\alpha) = e^{2\alpha\phi}$. It is useful to introduce the real parameter P via $\alpha = \frac{Q}{2} + iP$ which labels the Liouville momentum. The operators are then identified under the reflections $\alpha \leftrightarrow Q - \alpha$ or $P \leftrightarrow (-P)$ [39]. One can impose this contraint by restricting to $P > 0$.

One can express the conformal dimensions of the primaries via

$$\Delta\left(e^{2\alpha\phi}\right) = \alpha(Q - \alpha) = \frac{Q^2}{4} + P^2. \tag{1.28}$$

The theory additionally contains a discrete set of operators with real $\alpha < Q/2$. These operators obey Ward identities that impose constraints on correlation functions coming from degenerate Virasoro representations and render the theory solvable.

The remaining CFT data is completely specified by the Liouville three-point function

$$\langle V_{\alpha_1}(z_1)V_{\alpha_2}(z_2)V_{\alpha_3}(z_3)\rangle = \frac{\mathcal{C}(\alpha_1,\alpha_2,\alpha_3)}{|z_{12}|^{\Delta_1+\Delta_2-\Delta_3}|z_{23}|^{\Delta_2+\Delta_3-\Delta_1}|z_{31}|^{\Delta_3+\Delta_1-\Delta_2}} \tag{1.29}$$

where $z_{ij} = z_i - z_j$. The three point coefficient is given by the DOZZ formula [40, 41]

$$\mathcal{C}(\alpha_1,\alpha_2,\alpha_3) = \frac{\left[\pi\mu\gamma(b^2)b^{2-2b^2}\right]^{\left(Q-\sum_i\alpha_i\right)/b}\Upsilon_b'(0)\Upsilon_b(2\alpha_1)\Upsilon_b(2\alpha_2)\Upsilon_b(2\alpha_3)}{\Upsilon_b(\sum_i\alpha_i - Q)\Upsilon_b(\alpha_1+\alpha_2-\alpha_3)\Upsilon_b(\alpha_1-\alpha_3-\alpha_2)\Upsilon_b(\alpha_2+\alpha_3-\alpha_1)}, \tag{1.30}$$

We refer the reader to [42] for the definition and properties of the special functions used here. The μ-dependent pre-factor here is fixed by the KPZ scaling law [43]. The formula is invariant under Liouville reflections upto a reflection phase. Note also that the formula is analytic in the momenta of the operators.

Notice that the central charge of the theory and the correlation functions are invariant under the transformation $b \to b^{-1}$ if we simultaneously map the cosmological constant to the "dual cosmological constant" via the relation $\left(\tilde{\mu}\gamma(b^{-2})\right)^b = \left(\mu\gamma(b^2)\right)^{1/b}$. This is the weak-strong self-duality of Liouville theory.

It is natural to extend this discussion to include worldsheets with boundary. We will be primarily concerned with Neumann boundary conditions for the Liouville field first studied by Fateev, Zamalodchikov, Zamolodchikov and Teschner (FZZT) [44, 45]. This boundary condition allows us to include an interaction term on the boundary labelled by the boundary cosmological constant μ_B,

$$S_L^{\partial} = \frac{1}{2\pi}\oint du\left(QK\phi + 2\pi\mu_B e^{b\phi}\right). \tag{1.31}$$

where K is the extrinsic curvature at the boundary. It is often useful to introduce the parameter s related to the boundary cosmological constant via $\mu_B = \sqrt{\frac{\mu}{\sin(\pi b^2)}}\cosh(\pi b s)$. If one views the Liouville boundary state as analogous to the Cardy boundary state corresponding to the Lioville primary with momentum P, the corresponding momentum is $s/2$.

One can derive explicit formulas for the bulk one-point function, boundary two- and three-

point functions as well as the bulk to boundary propagator in the CFT on the disk with FZZT boundary conditions. In particular, the boundary two-point function is given by [44],

$$\left\langle B^{\mu_1\mu_2}_{\beta_1} B^{\mu_2\mu_1}_{\beta_2} \right\rangle = \frac{1}{|x|^{2\Delta_{\beta_1}}} \left[\delta(\beta_1 - \beta_2)\, \mathcal{R}(\beta_1|\mu_1,\mu_2) + \delta(Q - \beta_1 - \beta_2)\right] \tag{1.32}$$

where the reflection coefficient $\mathcal{R}$ is

$$\mathcal{R}(\beta|\mu_1,\mu_2) = \left[\pi\mu\gamma(b^2)b^{2-2b^2}\right]^{(Q-2\beta)/b} \left(\frac{\Gamma_b(2\beta - Q)}{\Gamma_b(Q-2\beta)}\right) \frac{1}{S_b\left(\beta \pm \frac{is_1}{2} \pm \frac{is_2}{2}\right)}. \tag{1.33}$$

In specifying the correlation functions, we have used conventional normalisations for the Liouville bulk and boundary vertex operators.

1.5 Minimal Strings

Of particular interest is the case when the conformal matter is described by the (p, q) minimal models for which $c_M < 1$. The case $|p - q| = 1$ specifies the unitary series. The spectrum of primaries is finite and there are $(p-1)(q-1)/2$ primary operators $O_{r,s}$ with $r = 1, 2, \ldots, p-1$ and $s = 1, 2, \ldots, q-1$ along with the identification $O_{(r,s)} \equiv O_{(p-r,q-s)}$. This can be implemented by restricting to $rq - sp \geq 0$. The conformal dimensions are given by

$$\Delta(O_{(r,s)}) = \overline{\Delta}(O_{(r,s)}) = \frac{(rq - sp)^2 - (p-q)^2}{4pq}. \tag{1.34}$$

The corresponding dressed tachyon operators are $\mathcal{O}_{r,s}$. The constraint on the total central charge imposes $b^2 = p/q$ on the Liouville coupling.

Let us review the derivation due of the disk partition function with FZZT boundary conditions for the minimal string due to Seiberg and Shih [46].

The starting point is the observation that

$$\partial_\mu Z|_{\mu_B} = \langle c\bar{c}e^{2b\phi}\rangle\big|_{\mu_B} = \langle \mathcal{O}_{2,1}\rangle|_{\mu_B} \tag{1.35}$$

where the boundary state is a product of the Liouville FZZT and matter Cardy states given by

$$|\mu_B; k, l\rangle_{FZZT} = \sum_{k'} \int_0^\infty dP\, \psi_s^*(P)\, \frac{S_{kl}{}^{k'l'}}{\sqrt{S_{11}{}^{k'l'}}}\, |P\rangle\rangle_L\, |k', l'\rangle\rangle_M. \tag{1.36}$$

The notation $|P\rangle\rangle$ denotes the Ishibashi boundary state in the both the Liouville and minimal matter CFTs. The Lioville FZZT states correspond to the non-degenerate primaries with label $\alpha = \frac{Q}{2} + i\frac{s}{2}$. Recall that s is related to the boundary cosmological constant via $\mu_B = \kappa \cosh(\pi b s)$, $\kappa = \sqrt{\frac{\mu}{\sin(\pi b^2)}}$. The FZZT wavefunction is given by

$$\psi_s(P) = \mu^{-\frac{iP}{b}}\, \cos(2\pi P s)\, \frac{\Gamma\left(1 + \frac{2iP}{b}\right)\Gamma(1 + 2iPb)}{iP} \tag{1.37}$$

and the modular S-matrix elements by

$$S_{kl}{}^{k'l'} = (-1)^{kl'+k'l} \sin\left(\pi b^2 l l'\right) \sin\left(\frac{\pi k k'}{b^2}\right). \tag{1.38}$$

The bulk one-point function on the disk with FZZT boundary for a tachyon operator $\mathcal{O}_{k,l}$ is computed via the overlap $\langle \mathcal{O}_{k',l'}\rangle|_{\mu_B} = \langle \mathcal{O}_{k',l'}|s; k, l\rangle_{FZZT}$ corresponding to the term with P satisfying $\alpha_{k'l'} = \frac{Q}{2} + iP$. In this case,

$$\partial_\mu Z|_{\mu_B} = \frac{1}{2(b^2-1)} (\sqrt{\mu})^{-1+\frac{1}{b^2}} \cosh\left(b - \frac{1}{b}\right)\pi s \tag{1.39}$$

After integrating μ and differentiating with respect to μ_B (keeping μ fixed) we get the 'marked' partition function,

$$\partial_{\mu_B} Z|_\mu = (\sqrt{\mu})^{\frac{1}{b^2}} \cosh\frac{\pi s}{b}. \tag{1.40}$$

This is evaluated by the partition function with a marked point insertion $e^{b\phi}$ at the boundary which fixes the residual gauge symmetry of disk rotations.

As we will see, minimal gravity theories can be equivalently viewed in terms of double-scaled matrix models with up to two matrix fields. From the point of view of the matrix model, this is the quantity that the expectation value of the resolvent computes [47],

$$Z_M(\mu_B) \equiv \partial_{\mu_B} Z|_\mu = \left\langle \mathrm{Tr}\left(\frac{1}{\mu_B - H}\right)\right\rangle = \frac{1}{\mu_B}\sum_{\ell=0}^{\infty} m_\ell\, {\mu_B}^{-\ell} \tag{1.41}$$

where H is the matrix and consequently, the fixed-length partition function is given by [33]

$$Z(\beta) = i\int_{i\mathbb{R}} d\mu_B\, e^{-\mu_B\beta}\, Z_M(\mu_B) = \left\langle \mathrm{Tr}\left(e^{-\beta H}\right)\right\rangle \propto \frac{(\sqrt{\mu})^{\frac{1}{b^2}}}{L} K_{\frac{1}{b^2}}(\kappa L). \tag{1.42}$$

Here, the integral is carried out by deforming the contour around the branch cut at $\mu_B = -\kappa$ and computing the corresponding discontinuity [48, 47].

Defining $x = \mu_B$ and $y = Z_M(\mu_B)$, it follows from Eq (1.40) that the variables x and y live on the Riemann surface described using Chebyshev polynomials,

$$F(x, y) = T_p(y) - T_q(x) = 0 \tag{1.43}$$

which corresponds to the large N spectral curve of the corresponding matrix model [46]. Correlation functions of the dressed vertex operators in minimal gravity were computed in [49, 50].

In fact, JT gravity itself can be understood in terms of the $p \to \infty$ limit of the $(2, p)$ series of matrix models [33] which are one-matrix models. A quick way to see this is by considering the discontinuity across the branch cut in the spectral curve in this case,

$$\rho_0(E) \propto \sinh\left[\frac{p}{2}\mathrm{arccosh}\left(\frac{E}{\kappa}\right)\right] \to \sinh\left(2\pi\sqrt{E_{JT}}\right) \tag{1.44}$$

in terms of the rescaled energies $\frac{E}{\kappa} = 1 + \frac{8\pi}{p^2}E_{JT}$ in the limit $p \to \infty$. This corresponds to the

classical $b \to 0$ limit of the string theory. Further evidence for this correspondence was provided in [47]. In constrast with double-scaled SYK, this theory may be described by representation theory of the non-compact quantum group $\mathcal{U}_q(sl(2,R))$.

Chapter 2

Partially Entangled Thermal States in the SYK model

It is generally believed that black holes must admit a self-consistent quantum description. In AdS/CFT, this microscopic theory takes the form of a finite temperature CFT on the asymptotic AdS boundary. While the rules of quantum mechanics are manifestly obeyed in this holographic setting, it has proven to be a non-trivial task to extract local bulk physics inside the black hole horizon from the dual quantum theory. The logical tension between QM and the semi-classical bulk description is most directly underlined by the firewall argument [26, 27].

As reviewed in the introduction, an often studied finite temperature state in AdS/CFT is the (unnormalized) thermo-field double state (1.7) living in the tensor product Hilbert space of a left- and right CFT. It defines the purification of the thermal density matrix, and can be thought of as obtained by performing a CFT path integral describing the euclidean time evolution over half a thermal circle with period β. The TFD state of a holographic CFT is believed to be dual to a maximally extended black hole space-time with two asymptotic regions separated by a bifurcate horizon [32].

Another type of thermal states are typical pure states of some given total energy. Assuming that the ETH applies, these states will look thermal relative to the set of local bulk observables.

Alternatively, one can consider pure states of the form

$$|\Psi\rangle_R \;=\; e^{-\frac{\beta}{2}H}|B\rangle_R \;=\; {}_L\langle B|\mathrm{TFD}\rangle \tag{2.1}$$

with $|B\rangle$ some typical CFT boundary state. Assuming $|B\rangle$ is uncorrelated with the local bulk observables, this state also looks thermal from the outside. We will call them "thermal pure states". They are believed to describe a one-sided black hole geometry.

Our interest is to learn more about the holographic reconstruction of the black hole interior. For thermal pure states, one can use the mirror operator construction of [28], or more generally, the quantum error correction procedure of [29], to reconstruct the interior operators from a single CFT. This situation must be contrasted with the thermo-field double case. For the TFD state, the one-sided quantum state is a thermal density matrix and the firewall argument of [26, 27] implies that the one-sided bulk reconstruction is limited to the region outside the horizon.

2.1 Partially entangled thermal states

An attractive dual perspective on the thermal pure states was recently suggested in [51], within the context of the SYK model [10]. The SYK model is a quantum theory of N Majorana variables $\{\psi_i, \psi_j\} = \delta_{ij}$ dynamically coupled via the Hamiltonian (1.1).

The SYK Hilbert space contains a natural basis of $2^{N/2}$ boundary states labeled as $|\mathbf{s}\rangle \equiv |s_1, s_2, ..., s_{N/2}\rangle$, with s_i taking values in $\{-1, 1\}$, defined by arranging the Majorana variables into pairs (we assume N is even) and requiring that

$$\left(\psi^{2k-1} - is_k\psi^{2k}\right)|\mathbf{s}\rangle = 0\,. \tag{2.2}$$

The thermal pure state defined via

$$|\Psi\rangle \;=\; |\mathbf{s},\beta\rangle \;\equiv\; e^{-\frac{\beta}{2}H}|\mathbf{s}\rangle \;=\; {}_L\langle\mathbf{s}|\mathrm{TFD}\rangle \tag{2.3}$$

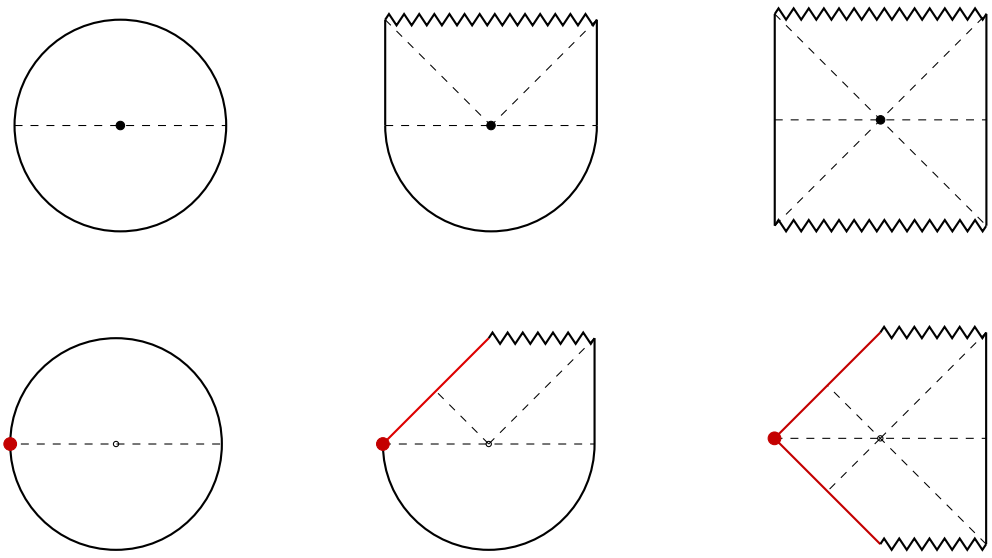

Figure 2.1: The euclidean (left), lorentzian (right) space-time associated with the thermo-field double state (top) and thermal pure state (bottom). The middle column shows the total geometry describing the state preparation and real time evolution, obtained by gluing the euclidean and lorentzian geometry together along the equator of the disc

looks like a thermal state relative to the class of flip invariant operators, that do not depend on the sign of the individual Majorana variables [51]: all n-point correlation functions $\mathrm{tr}(\rho_s\, \mathcal{O}_1 ... \mathcal{O}_n) = \langle \Psi | \mathcal{O}_1 ... \mathcal{O}_n | \Psi \rangle$ of collections of operators that are invariant under the 'flip group' are equal to the thermal expectation values with inverse temperature β (as long as $n \ll N$).

As suggested in [51] [52], the projection ${}_L\langle \mathbf{s} | \mathrm{TFD} \rangle$ of the thermo-field double state onto a particular boundary state can be holographically represented as an 'end-of-the-world particle' that removes the left asymptotic region of the two-sided black hole geometry, but keeps part of the left region in place. The left region thus becomes identified with the black hole interior as seen from the right.

A qualitative description of the proposed dual geometry corresponding to the thermo-field double and the thermal pure states is indicated in figure 2.1, c.f. [51]. The top row indicates the thermal circle (left), which in the holographic setting, constitutes the boundary of a Poincaré disc, the euclidean AdS_2 bulk space-time. The corresponding two-sided black hole geometry is shown on the top right. The middle column shows the total geometry that includes the

state preparation and the real time evolution is obtained by gluing the euclidean and lorentzian geometry together along the equator of the disc. The bifurcate horizon is situated at the center of the disk. The bottom row indicates the geometry of the thermal pure state. The trajectory of the end of the world-particle starts at the intersection point between the left boundary and the equator, where the lorentzian geometry is glued onto the euclidean half-circle. This geometric argument that pure black hole state has a smooth interior geometry provides support for the aforementioned (state-dependent) QEC procedure for constructing interior operators [28, 29].

Thermal pure states and the thermo-field double are both mathematical idealizations. Generic states are somewhere in between: macroscopic systems are never in a pure state nor in a perfect thermally mixed state, since typically we know somewhere between everything or nothing about a system.[1] In current terminology, a class of states compatible with a classical background is called a code subspace [29] [53]. It thus becomes natural to look for a practical generalization of the thermo-field double or thermal pure states, in the form of an interpolating family of partially mixed thermal states.

In the context of the SYK model, there are two natural ways to define such an interpolating family of states. The first method is a straightforward modification of the above construction of the thermal pure states. We will describe this method first. Then we introduce a second class of partially mixed thermal states with a better understood holographic description. This second type of states will be the main focus of this chapter.

Consider the 2^N dimensional Hilbert space $\mathcal{H}$ spanned by $2N$ Majorana variables ψ^i. We assume N is even. Introduce the basis of 2^N states $|\mathbf{s}\rangle$ defined in eqn (2.2). Next we partition the $2N$ Majorana fermions into two groups of N Majorana fermions $\{\psi_{L,R}\}$, each spanning sub-Hilbert spaces $\mathcal{H}_{L,R}$ of dimension $2^{N/2}$. Let H_L and H_R denote two identical SYK Hamiltonians acting on each subsystem. Note that the choice of the Hamiltonian depends on the choice of

[1] By the same token, observables that measure properties of a macroscopic quantum system are usually defined with reference to some classical environment or restriction. So they are typically neither purely state-dependent nor completely state-independent.

partition.[2] Now consider the following class of 2^N entangled states

$$|\Psi\rangle \;=\; |\mathbf{s};\beta_{_L},\beta_{_R}\rangle = e^{-\frac{1}{2}\beta_{_L}H_{_L}-\frac{1}{2}\beta_{_R}H_{_R}}|\mathbf{s}\rangle\,. \tag{2.4}$$

By choosing different partitions, we obtain a large class of states with different degrees of entanglement between the left-sector $\mathcal{H}_{_L}$ and right-sector $\mathcal{H}_{_R}$. The thermo-field double is a state for which the partition into $\{\psi_{_L},\psi_{_R}\}$ precisely coincides with the division into $\{\psi_{\text{even}},\psi_{\text{odd}}\}$, and for which all $s_k = 1$. On the other end of the spectrum, the thermal pure states correspond to the case for which the $\{\psi_{_L}\}$ consists of $N/2$ Majorana pairs (ψ_{2k},ψ_{2k+1}), so that the boundary state (2.2) factorizes into left and right boundary state $|\mathbf{s}\rangle = |\mathbf{s}\rangle_{_L}\otimes|\mathbf{s}\rangle_{_R}$. The state (2.4) then factorizes into a product of two thermal pure states. For the generic choice of partition, the states (2.4) are partially entangled thermal states with an entanglement entropy somewhere in between zero (for the pure product states) and the thermal entropy (for the TFD state). We discuss some further properties of the class of state (2.4) in Appendix 2.6.

In the rest of this chapter, we will study the properties and holographic dual geometry of another class of partially entangled states of the form

$$|\Psi\rangle \;=\; \sum_{m,n} e^{-\frac{1}{2}\beta_{_L}E_m-\frac{1}{2}\beta_{_R}E_n}\,\mathcal{O}_{n,m}\,|m\rangle_{_L}|n\rangle_{_R} \tag{2.5}$$

where $\mathcal{O}_{m,n} = \langle m|\mathcal{O}|n\rangle$ are the matrix elements of some arbitrarily chosen local scaling operator $\mathcal{O}$. This state satisfies the property

$${}_{_L}\langle\psi_1|_{_R}\langle\psi_2|\Psi\rangle \;=\; \langle\psi_1|e^{-\frac{1}{2}\beta_{_L}H}\,\mathcal{O}\,e^{-\frac{1}{2}\beta_{_R}H}|\psi_2^\star\rangle, \tag{2.6}$$

with ψ_1 and ψ_2 labeling generic states in the left and right Hilbert spaces. From (2.6) we recover the expression (2.5) by inserting a complete basis of $\mathcal{H}_{_L}\otimes\mathcal{H}_{_R}$. As seen from the second

[2] Alternatively, we could have picked a fixed partition into left- and right variables $\{\psi_{_{L,R}}\}$, but allowed ourselves the freedom to chose an arbitrary partition into even and odd variables ψ_{even} and ψ_{odd}. In this case, the Hamiltonians $H_{_L}$ and $H_{_R}$ would be held fixed, and the state $|\mathbf{s}\rangle$ would depend on the choice of partition.

representation, the state $|\Psi\rangle$ can be thought of as produced by evolution of a single QM system over a euclidean time interval $\beta_{_R}$, acting with a local operator $\mathcal{O}$, and then evolving over a second euclidean time interval $\beta_{_L}$. It is tempting to identify $\beta_{_{L,R}}$ with the effective temperature of the left- and right QM system, but as we will see, this identification is in general not correct.

The class of states (2.5) includes the TFD and thermal pure states as special limits. If we chose $\mathcal{O} = \mathbb{1}$ with $\langle n|\mathbb{1}|m\rangle = \delta_{nm}$, the state (2.5) reduces to the thermo-field double with inverse temperature $\beta = \beta_{_L} + \beta_{_R}$. On the other end, if we send $\beta_{_L} \to \infty$, we project the left CFT onto the vacuum state. For a sufficiently random choice of the operator $\mathcal{O}$, the state (2.5) then takes the form of a thermal pure state (2.3). We will call the above general class of states 'partially entangled thermal states' (PETS)[3].

The reduced density matrix for $\mathrm{QM}_{_R}$ after tracing over the left Hilbert space $\rho_{_R} = \mathrm{Tr}_{_L}\,|\Psi\rangle\langle\Psi|$ is given by

$$\rho \;=\; \sum_{m,n,n'} e^{-\frac{1}{2}\beta_R E_n}\,\mathcal{O}_{n,m}\,e^{-\beta_L E_m}\,\mathcal{O}_{m,n'}\,e^{-\frac{1}{2}\beta_R E_{n'}}|\,n\,\rangle\,\langle\,n'\,| \tag{2.7}$$

or more succinctly

$$\rho \;=\; e^{-\beta_R H/2}\,\mathcal{O}\,e^{-\beta_L H}\,\mathcal{O}\,e^{-\beta_R H/2} \tag{2.8}$$

In the following, we will usually choose $\mathcal{O}$ to be a scaling operator $\mathcal{O}_\ell$, with scaling dimension ℓ. We will be mostly interested in large scaling dimensions of order $N/\beta J$. More generally, we will also consider the generalization of PETS in which we replace the single operator $\mathcal{O}$ by an incoherent sum of operators $\mathcal{O}_i$ with all approximately the same conformal dimension. The PETS then becomes a partially entangled mixed state.

[3]When $\mathcal{O}_{n,m}$ is constant, the state factorizes into two thermal pure states of inverse temperature β_L and β_R. This can happen if $\ell \to \infty$ for our setup.

2.1.1 A useful graphical notation

We are interested in determining the entanglement and thermal properties of the partially entangled thermal state and of their holographic dual. For this purpose, we briefly pause to introduce a helpful graphical notation for the three types of states.

The thermofield double state represents the purification of the (unnormalized) thermal density matrix

$$\rho \;=\; e^{-\beta H} \;=\;$$ 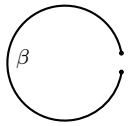

(2.9)

The TFD state can be thought of as being prepared by a euclidean path-integral of a single QM system, evolved over half of the thermal circle

$$|\mathrm{TFD}\rangle \;\cong\; e^{-\frac{\beta}{2}H} \;=\;$$ 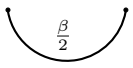

(2.10)

Here for later convenience we adopted the congruence $\sum e^{-\frac{\beta}{2}E_n}|n\rangle_{\mathrm{L}}|n\rangle_{\mathrm{R}} \;\cong\; \sum e^{-\frac{\beta}{2}E_n}|n\rangle\langle n|$ between entangled states of two identical systems and linear operators.

Thermal pure states are states of the form [51]

$$|\,\mathbf{s},\beta\rangle \;=\; e^{-\frac{\beta}{2}H}|\,\mathbf{s}\rangle \;=\;$$ 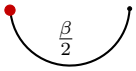

(2.11)

The half circle indicates the euclidean time evolution over $\beta/2$ and the red dot indicates the projection onto the state $|\mathbf{s}\rangle$ defined in eqn (2.2). The corresponding density matrix is denoted by

$$\rho_s \;\equiv\; |\mathbf{s},\beta\rangle\langle\mathbf{s},\beta| \;=\; e^{-\frac{\beta}{2}H}\,\mathrm{P}_{\mathbf{s}}\,e^{-\frac{\beta}{2}H} \;=\;$$ 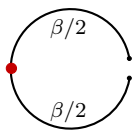

(2.12)

with $\mathrm{P}_{\mathbf{s}} = |\mathbf{s}\rangle\langle\mathbf{s}|$ the projection on the state $|\mathbf{s}\rangle$.

Partially entangled thermal states are represented in this notation as

$$|\,\Psi\,\rangle \;\cong\; e^{-\frac{1}{2}\beta_L H}\,\mathcal{O}_\ell\, e^{-\frac{1}{2}\beta_R H} \;=\; \tag{2.13}$$

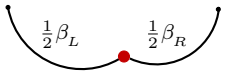

As indicated by the figure, this class of PETS is prepared by performing a path integral over two segments of a thermal circle separated by the insertion of a local scaling operator $\mathcal{O}_\ell$. This insertion has a number of non-trivial effects.

If the dimension ℓ of the operator is small, the operator insertion produces a small perturbation of the TFD state. The dual space-time will just look like the two-sided black hole with a single particle excitation propagating in the bulk. In this chapter, we will instead be interested in the case in which the scale dimension of $\mathcal{O}_\ell$ is of order $\ell \sim N/\beta J$. As we will see, in this regime the insertion of the operator $\mathcal{O}_\ell$ leads to a non-trivial modification of the dual geometry. This backreaction is indicated graphically in eqn (2.13) via the kink connecting the two arcs. Due to the presence of the kink, the two arcs each span an angle bigger than $\pi/2$, reflecting the physical difference between the quantities $\beta_{L,R}$, that specify the left- and right-euclidean time lapse, and the effective temperature as seen by the corresponding one-sided observer. The ratio between the two is parameterized by an angle $\theta_{L,R}$ via

$$\beta_L^{\text{eff}} = \frac{2\pi\beta_L}{2\pi-\theta_L} \qquad\qquad \beta_R^{\text{eff}} = \frac{2\pi\beta_R}{2\pi-\theta_R} \qquad\qquad \theta_{L,R}\in[0,\pi] \tag{2.14}$$

One of our tasks is to compute how these angles $\theta_{L,R}$ depend on the scale dimension ℓ of the local operator and on β_L and β_R.

The density matrix in graphical notation reads

$$\rho \;=\; e^{-\frac{1}{2}\beta_R H}\,\mathcal{O}\,e^{-\beta_L H}\mathcal{O}\,e^{-\frac{1}{2}\beta_R H} \;=\; \tag{2.15}$$

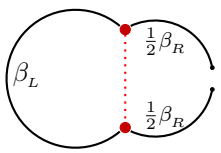

Its partition sum $Z_\ell = \text{tr}\rho$ reduces to the thermal SYK two-point function, with inverse temper-

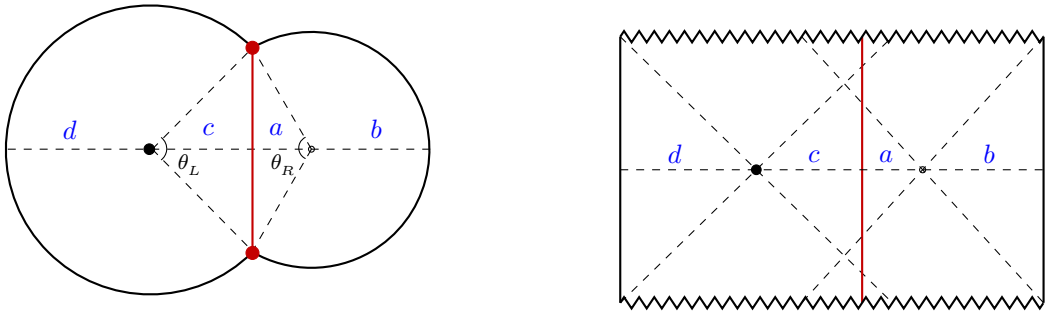

Figure 2.2: The euclidean and lorentzian space-time dual to the partially entangled states (2.5). The worldline of the massive bulk particle created by the operator insertion $\mathcal{O}_\ell$ is indicated by the red line. It divides the space-time into two AdS_2 regions. For a sufficiently massive particle, the worldline is hidden behind two horizons. In this figure, the left-horizon is the true 'extremal surface' with minimal value $\phi_{_L}$ of the dilaton.

ature $\beta = \beta_{_L} + \beta_{_R}$ of two local scaling operators $\mathcal{O}_\ell$

$$Z_\ell(\beta,\tau) \equiv \mathrm{tr}(\rho) = \big\langle \mathcal{O}_\ell(0)\,\mathcal{O}_\ell(\tau)\big\rangle_\beta \quad = \quad \beta-\tau \qquad \tau \tag{2.16}$$

with $\tau \equiv \beta_{_R}$. This thermal two-point function has been analyzed and can be explicitly computed in the Schwarzian limit of the SYK model. This is the appropriate limit for our purpose of extracting the holographic dual interpretation of this class of partially entangled states.

2.1.2 Overview

In this chapter we will determine the 2D space-time dual to the partially entangled states (2.5) in the SYK model (1.1), for $\ell \sim N/\beta J$, and compute the entanglement entropy between the two sides. We will work in the low energy approximation of the SYK model, described by Schwarzian quantum mechanics. This is the appropriate regime for comparison with AdS_2 gravity.

There exists an elegant and for our purpose very useful reformulation of the Schwarzian theory in terms of the motion of a charged particle on AdS_2 in a large constant magnetic (euclidean) or electric (lorentzian) field [54] [11]. The classical action of the 1D effective theory is proportional

to the area of AdS_2 enclosed by the worldline of this charged particle. For the euclidean finite temperature partition function, this worldline follows a circular path, which we identify with the thermal circle. In this description, the two-point function (2.16) is obtained by adding an extra term to the 1D effective action equal to ℓ times the length of a bulk geodesic connects the two points $t = 0$ and $t = \tau$ along the worldline of the charged boundary particle. The semi-classical path of the charged particle then looks like the squeezed thermal circle shown on the left in figure 2.2. The two thermal circle segments represent the piece-wise-circular trajectory of the charged particle, and the red line represents the geodesic worldline of a massive bulk particle with mass ℓ.[4] The holographic dual geometry consists of two AdS_2 regions glued together along the path of the massive particle. As shown in figure 2.2, each AdS_2 region contains a center point, that after analytic continuation to lorentzian signature, corresponds to a bifurcate horizon of a two-sided black hole.

For sufficiently large ℓ above some critical value, determined by $\beta_{L,R}$, the worldline of the bulk particle is hidden in the region behind two horizons. In this regime, the state will look thermal relative to the observables that probe the left and right exterior region. The effective left and right temperature and the opening angles $\theta_{L,R}$ are determined via the effective Schwarzian dynamics. We will compute these effective temperatures in section 2.2.

In figure 2.2, the left-horizon is the true 'extremal surface' with minimal value ϕ_L of the dilaton. In section 2.3, we will show that its value governs the entanglement entropy between the two sides via $S_{\text{ent}} = S_0 + \phi_L/4G_N$ with S_0 the microscopic ground state entropy of the SYK model. In section 2.4 we will argue that this extremal surface separates the regions accessible through one-sided bulk reconstruction from each side. In particular, the right-sided entanglement wedge includes the regions a and c behind the horizon shown in figure 2.2. Finally, in section 2.5 we discuss some generalizations of PETS with more than one operator insertion. In the Appendix we collect some useful formulas for determining and reconstructing the classical bulk geometry.

[4] A very similar geometric set up has been considered previously in [51] and [55].

2.2 Space Time Geometry of PETS

In this section our interest is to determine the holographic dual geometry described by the partially entangled thermal states, in the semiclassical regime. One approach would be to start from the Jackiw-Teitelboim model [18, 19, 12, 13, 15]. As mentioned above, this JT model can be recast as the mechanics of a charge boundary particle in a magnetic field [54] (see also [11] and [55]). Here we will follow a somewhat different route: we will start from the exact correlators of the low energy effective theory of the SYK model, given by Schwarzian quantum mechanics, computed in [24]. We then take their semiclassical limit [34] and derive the semi-classical space-time geometry from the resulting expression. As we will see, this procedure is remarkably efficient.

We denote the JT dilaton by ϕ. Recall that the coupling constant that appears in the Schwarzian action is $C = \frac{\phi_r}{8\pi G_N}$, with $\phi_r = \epsilon\phi_b$ the renormalized boundary dilaton value. In SYK, the coupling C corresponds to the heat capacity $C = \alpha_S N/J$, with α_S an order one constant [10, 56]. For the Schwarzian action we follow the notation in [24]. We summarize the coordinates and our conventions in Appendix 2.7. Following the discussion in section 1.1, we will parametrize the energy E and thermal entropy S of a finite energy state by means of a dimensionless 'momentum' variable k via

$$E(k) = \frac{k^2}{2C}, \qquad\qquad S = S_0 + 2\pi k, \tag{2.17}$$

where S_0 denotes the microscopic SYK ground state entropy.

The partition function associated with a PETS is given by the two-point function of two operators of dimension ℓ. In order to make the connection to the bulk more explicit, we would like to re-express the two point function (1.9) in terms of variables that have a more transparent geometric interpretation. This can be achieved by using the following formula for the product

of gamma functions

$$\frac{\Gamma(\Delta - ik)\Gamma(\Delta + ik)}{\Gamma(2\Delta)} = \int_{-\infty}^{\infty} dx \ \frac{e^{ikx}}{(2\cosh(\frac{x}{2}))^{2\Delta}} \tag{2.18}$$

We can apply this identity to the two point function and introduce 'angle' variables $-\theta_1 = 4\pi + 2ix_1 + 2ix_2$ and $-\theta_2 = 4\pi + 2ix_1 - 2ix_2$ such that

$$\langle \mathcal{O}(\tau)\mathcal{O}(0)\rangle_\beta = \int \prod_{i=1,2} dk_i d\theta_i \ e^{-S(k_i,\theta_i,\tau,\ell)}, \tag{2.19}$$

Hence, the exact two-point function obtained in [24] can be written as [5]

$$\begin{aligned} \langle \mathcal{O}(\tau)\mathcal{O}(0)\rangle_\beta &= \int \prod_{i=1,2} dk_i \rho(k_i) \ e^{-\frac{k_1^2}{2C}\tau - \frac{k_2^2}{2C}(\beta-\tau)} \frac{\Gamma(\ell \pm ik_1 \pm ik_2)}{\Gamma(2\ell)}, & (2.20) \\ &= \int \prod_{i=1,2} dk_i d\theta_i \ e^{-I(k_i,\theta_i,\tau,\ell)}, & (2.21) \end{aligned}$$

where the 'action' appearing in the exponent is given by

$$I(k_i,\theta_i,\tau,\ell) = \sum_{i=1,2}\left(\frac{k_i^2}{2C}\tau_i + \theta_i k_i - \log\rho(k_i)\right) + \ell \log\left(\cos\frac{\theta_1}{2} + \cos\frac{\theta_2}{2}\right)^2 + I_0(\ell), \tag{2.22}$$

and we defined $\tau_1 = \tau$, $\tau_2 = \beta - \tau$ and the density of states $\rho(k) = 2k\sinh 2\pi k$. This second way of expressing the two-point function will be very useful below. We will refer to $I(k_i,\theta_i)$ as the action associated to the two-point function with values k_i and θ_i. At this point this gives an exact expression computing the two-point function, up to an unimportant normalization factor I_0 which appears as a constant term in the action.

We now take a semiclassical limit, C and ℓ both large with ℓ/C fixed. Since ℓ is a dimensionless number it should be compared with a dimensionless ratio such as $2\pi C/\beta$. Since we will take β to be of order one we will simply compare ℓ directly with C. In this case the integrals over k_i and θ_i become dominated by their saddle point. The saddle point scaling is such that

[5] The notation $\pm$ inside the Gamma function means one should take a product over all signs combinations. See [24] for more details.

$k_i \sim C$ and $\theta_i \sim 1$. This approximation is reliable since the action scales as $I \sim C$. We define the (order one) semiclassical action $I_{\text{s.c.}}$ as

$$I(k_i, \theta_i) = C I_{\text{s.c.}}(k_i, \theta_i). \tag{2.23}$$

In this limit the action simplifies to

$$C I_{\text{s.c.}}(k_i, \theta_i, \tau, \ell) = \sum_{i=1,2} \left(\frac{k_i^2}{2C} \tau_i + (\theta_i - 2\pi) k_i \right) + \ell \log \left(\cos \frac{\theta_1}{2} + \cos \frac{\theta_2}{2} \right)^2 + I_0. \tag{2.24}$$

We see that when $\ell \sim \mathcal{O}(C)$, the saddle point will depend on the value of ℓ. We can interpret this as the result of backreaction of the space-time geometry. The saddle-point equations $\partial_{k_i} I_{\text{s.c.}} = \partial_{\theta_i} I_{\text{s.c.}} = 0$ simplify to

$$\frac{k_i}{C} \tau_i = 2\pi - \theta_i, \tag{2.25}$$

$$\frac{k_i}{\sin \frac{\theta_i}{2}} = \frac{\ell}{\cos \frac{\theta_1}{2} + \cos \frac{\theta_2}{2}}, \tag{2.26}$$

for $i = 1, 2$. Using the first equations one can eliminate the angles θ_i. This gives the equivalent system of equations

$$\frac{k_1 \tau_1}{C} + 2 \arctan \frac{k_1 + k_2}{\ell} + 2 \arctan \frac{k_1 - k_2}{\ell} = 2\pi, \tag{2.27}$$

$$\frac{k_2 \tau_2}{C} + 2 \arctan \frac{k_1 + k_2}{\ell} - 2 \arctan \frac{k_1 - k_2}{\ell} = 2\pi. \tag{2.28}$$

The geometric meaning of the above equations will be explained below. [6]

[6] In the small ℓ limit, $\ell/C \ll 1$, the backreaction is turned off. The solution then becomes $k_i \approx 2\pi C/\beta$ and $\theta_i \approx 2\pi \tau_i/\beta$ Keeping track of the subleading $\mathcal{O}(\ell/C)$ terms, one finds the expected form of a thermal two-point function in a 1D CFT

$$\langle \mathcal{O}(\tau) \mathcal{O}(0) \rangle \sim \left(\frac{\pi}{\beta \sin \frac{\pi}{\beta} \tau} \right)^{2\ell}. \tag{2.29}$$

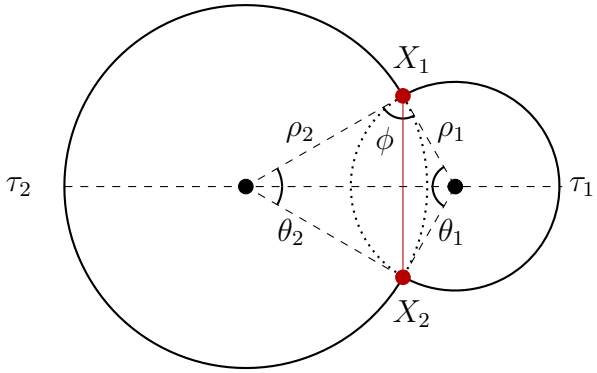

Figure 2.3: The curve that maximizes the action with two operator insertion (red dots) at $\tau_1 = \tau$ and $\tau_2 = \beta - \tau$. The horizons of each side are located at the black dots.

2.2.1 Backreaction

In this subsection we will extract the geometric interpretation of our saddle-point equations (2.25) and compare our results with the action described in [55]. In [55], the authors exploit the fact ([54] and [11]) that the Schwarzian action associated to the reparametrization mode $f(u)$, $u \in (0, \beta)$ is proportional to the area enclosed by the curve $(\rho(u), \theta(u) = \frac{2\pi}{\beta} f(u))$ in a hyperbolic space with metric

$$ds^2 = d\rho^2 + \sinh^2 \rho \, d\theta^2 = \frac{(dr^2 + r^2 d\theta^2)}{(1 - r^2)^2}, \qquad r = \tanh \frac{\rho}{2}, \tag{2.30}$$

where $r(u)$ is determined from the constraint that the induced metric is $g_{uu} = 1/\epsilon^2$, with ϵ a small cut-off scale. This describes a cut-off version of the Poincare disk in Euclidean signature. We summarise the coordinate systems used in Appendix 2.7.

The fixed (large) length of the boundary L is $\beta J = \beta/\epsilon$. This contribution appears in the JT action from a holographic renormalization counterterm. In Poincaré coordinates, it is easy to calculate the area under the boundary curve. Using the induced metric on the boundary,

$$g_{uu} = \frac{1}{\epsilon^2} = \frac{4(r'^2 + r^2 \theta'^2)}{(1 - r^2)^2}. \tag{2.31}$$

This can be solved for the boundary trajectory in an expansion in ϵ

$$r(\theta) = 1 - \epsilon\theta' + \frac{(\epsilon\theta')^2}{2} + \dots \tag{2.32}$$

Plugging this into the expression for the area, one finds that

$$\begin{aligned} A &= \int dr\, d\theta\, \frac{4r}{(1-r^2)^2} \\ &= L - 2\pi + \epsilon \int d\tau \left[\frac{\theta'}{2} - \frac{1}{2}\left(\frac{\theta''}{\theta'}\right)^2\right] + \dots \end{aligned} \tag{2.33}$$

which is precisely the Schwarzian action in the time reparametrisation variable θ.

Also note that the distance between the insertion points on the boundary can be evaluated using

$$\cosh D(X_1, X_2) = -X_1 \cdot X_2 \sim \frac{2J^2}{\theta_1'\theta_2'}\left(\sin\frac{\theta_1 - \theta_2}{2}\right) \tag{2.34}$$

where we used the fact that the radial coordinate at the boundary is large ($r \sim 1$) so that $\frac{2}{1-r} \sim \frac{2}{\epsilon\theta'}$. Comparing the equations (2.33) and (2.34), we find that we can re-express the action of the Schwarzian with a bilocal insertion by identifying $\theta(\tau) = f(\tau)$ as the reparametrization variable

$$-S = -C\int du\ \mathrm{Sch}\left(\tan\frac{\pi}{\beta}f(u), u\right) + \ell \log \frac{f'(u_1)f'(u_2)}{\left(\sin\frac{\pi(f(u_1)-f(u_2))}{\beta}\right)^2} \tag{2.35}$$

$$\simeq -\frac{C}{\epsilon}\left[(A - L + 2\pi) + \frac{\epsilon\ell}{C}\log\left(2\epsilon^2\cosh D(X_1, X_2)\right)\right] \tag{2.36}$$

where $D(X_1, X_2)$ is the geodesic distance between the location of the insertions X_1, X_2. The approximation is valid when the cut-off $\epsilon \ll 1$ so that $\rho(u)$ is large. A denotes the area enclosed by the trajectory of the boundary particle, and $L \sim \beta$ its length.

For a fixed length L, we would like to minimize this action. In the absence of the bilocal operator, this would be achieved by the geometry of a circle which gives the usual Euclidean

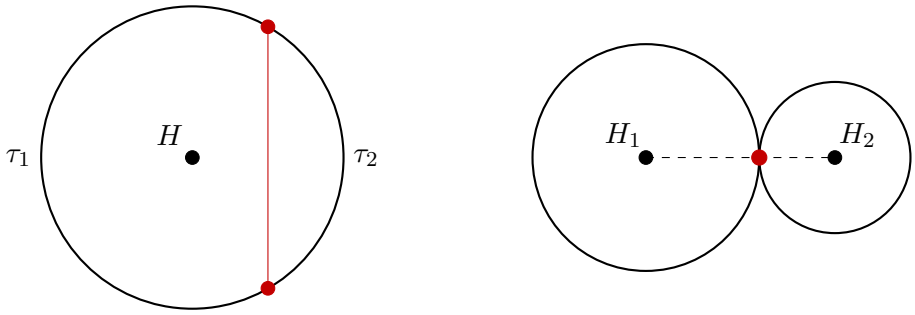

(I) $\ell \to 0$ (II) $\ell \to \infty$

Figure 2.4: Backreaction generated by an operator insertion (red dots) of dimension ℓ when $\ell \to 0$ and $\ell \to \infty$. We indicate the backreaction by depicting the deformations of the boundary curve in the Euclidean Poincare disk. We indicate the (local) horizons by a black dot.

black hole. In the presence of the interaction, for a given geodesic distance D_{12}, the action is minimized by minimizing the area on the left and right. This is achieved by circular arcs on the left and the right terminating on the points of insertion. This gives the geometry of figure 2.3.

For $\ell \ll C$ we can neglect the term in the action depending on the geodesic distance between X_1 and X_2. Then the curve that minimizes the area with a fixed length is given by a circle inside the Poincare disk. In Lorenzian signature this maps to a black hole with the horizon located at the center of the disk. The location of this circle as a function of the length (temperature) is

$$k = \frac{2\pi C}{\beta}, \quad \sinh \rho = \frac{C}{k\epsilon}. \tag{2.37}$$

In this case it is easy to see that the action in (2.35) matches the first terms of our action (2.24) using the explicit expression for the area $A = 2\pi \cosh \rho$ and length $L = 2\pi \sinh \rho$ in for the Poincare disk.

When a heavy operator is inserted we also need to minimize the distance between the insertion points X_1 and X_2. First one can approximate each side of the boundary by circles as shown in figure 2.3. Each has a radius given by

$$\sinh \rho_i = \frac{C}{k_i \epsilon}. \tag{2.38}$$

If we define the opening angle of each circle by θ_i as in figure 2.3 then the length on each side is related to the time insertions as

$$\sinh \rho_i (2\pi - \theta_i) = \frac{\tau_i}{\epsilon}. \tag{2.39}$$

By using this equation and (2.38) one gets precisely the first relation of our saddle-point equations (2.25). With these identifications, the geodesic distance between X_1 and X_2 is given by as

$$\begin{aligned} \cosh D_{12} &= 1 + 2\sinh^2 \rho_1 \sin^2 \frac{\theta_1}{2} = 1 + 2\sinh^2 \rho_2 \sin^2 \frac{\theta_2}{2}, \\ &\approx \frac{C^2}{\epsilon^2} \left(\frac{\sin \frac{\theta_1}{2}}{k_1} \right)^2 = \frac{C^2}{\epsilon^2} \left(\frac{\sin \frac{\theta_2}{2}}{k_2} \right)^2 . \end{aligned} \tag{2.40}$$

The first line of this equation is a purely geometric result. In the second line we have used our proposal to identify our variables with geometry. A first observation is that the two equivalent geometric expressions become consistent when one takes into account the second set of saddle point equations (2.25) since it implies $k_1^{-1} \sin \frac{\theta_1}{2} = k_2^{-1} \sin \frac{\theta_2}{2}$. From the geometry of figure 2.3 this is simply the hyperbolic version of the sine rule. A second observation is that the second equation in (2.25) allows us to write

$$\cosh D_{12} = \frac{C^2}{\epsilon^2 \ell^2} \left(\cos \frac{\theta_1}{2} + \cos \frac{\theta_2}{2} \right)^2 . \tag{2.41}$$

Inserting this relation in the action proposed by [55] we find a match with our on-shell action (2.24). The same is true for the ℓ independent terms in (2.24). This connection allows us to extract the backreaction due to operator insertions in terms of our variables θ and k.

One important parameter of the geometry is the angle ϕ defined in figure 2.3 which can be shown to be equal to $\phi = \ell\epsilon/C$. If we take the cut-off to be $\epsilon \sim 1/\beta J$ in terms of SYK variables, then $\phi \sim \ell/N$. Another interesting parameter of the geometry is the distance between the horizons (specified by the center of each circle segment). This distance D_H can be expressed

as

$$\cosh D_H \;=\; \frac{1+\cos\frac{\theta_1}{2}\cos\frac{\theta_2}{2}}{\sin\frac{\theta_1}{2}\sin\frac{\theta_2}{2}} = \frac{k_1^2+k_2^2+\ell^2}{2k_1k_2}. \tag{2.42}$$

We can separate this into a minimal geodesic distance D_1 (D_2) between the left (right) horizon and the world line of the bulk particle as

$$\sinh D_1 \;=\; \frac{\ell^2+k_2^2-k_1^2}{2\ell k_1}, \qquad \sinh D_2 = \frac{\ell^2+k_1^2-k_2^2}{2\ell k_2}. \tag{2.43}$$

One can verify they add up to the distance between horizons $D_1 + D_2 = D_H$.

Assume $\tau_1 \neq \tau_2$. Then call $k_{\max} = \max(k_1, k_2)$ and $k_{\min} = \min(k_1, k_2)$. For any ℓ, the horizon associated to $k_{\min}$ is always visible from the outside, and it is always part of the geometry. This is not true for the other horizon associated with $k_{\max}$. When ℓ takes values between $\ell = 0$ and a critical ℓ_*, the right horizon is not part of the geometry, it is removed by the gluing procedure across the worldline of the bulk particle. The second horizon becomes visible for $\ell > \ell_*$. From the formulas above (in particular the one for D_1 and D_2) one can write a condition that determines the critical scaling dimension ℓ_* as

$$\ell_*^2 \;=\; k_{\max}^2(\ell_*) - k_{\min}^2(\ell_*), \tag{2.44}$$

where the momenta in the right-hand side are functions of ℓ_*, β and τ, determined by solving the saddle point equations (2.27). From the geometry of figure 2.3 one can see that this is equivalent to the condition $\theta = \pi$ (for which the bulk particle worldline crosses the horizon associated to $k_{\max}$).

Another way of writing the condition of both horizons being part of the geometry is

$$|\Delta E| \;=\; |E_2 - E_1| \;<\; \frac{\ell^2}{2C}. \tag{2.45}$$

In this regime, the trajectory of the bulk particle lies between the two horizons. The corresponding state of the SYK system will look thermal from the perspective of simple observables that can only measure the state outside each horizon. We will elaborate more on bulk reconstruction for these geometries in section 2.4.

Using this knowledge about the backreaction we can analyze the cases $\ell \to 0$ and $\ell \to \infty$. We show both cases in figure 2.4 and we explain below how these simple figures allow us to find approximate solutions to the saddle-point equations.

When $\ell \to 0$ backreaction is negligible, $k_1 \approx k_2 \approx 2\pi C/\beta$. Then the geometry is a circle in the Poincare disk with length $\propto \beta$ and the evaluation of the geodesic distance reproduces equation (2.29). We will study the leading correction to this limit in section 2.3.3.

On the other hand when $\ell \to \infty$ points X_1 and X_2 want to be as close as possible. The two arcs become full circles touching at a point. The renormalized length of each circle is fixed to be $\tau_1 = \tau$ and $\tau_2 = \beta - \tau$. We can anticipate then $k_1 \approx 2\pi C/\tau_1$ and $k_2 \approx 2\pi C/\tau_2$ with $\theta_i \approx 0$. From equation (2.42) we can deduce the distance between horizons as a function of the dimension in this limit as $D_H \approx 2 \log \frac{\beta \ell}{C}$.

2.2.2 Dilaton Profile

The Schwarzian dynamics fixes the backreaction and therefore fixes the boundary curve as explained above. From the boundary curve, one can easily find the dilaton profile inside the bulk. The detailed formulas are left for Appendix 2.7. Here we point out the relevant qualitative features of the euclidean configuration and its continuation to Lorenzian signature.

The dilaton blows up near the asymptotic boundary of AdS. The boundary curve is defined such that $\phi_{\rm b} = \phi_r/\epsilon$ for a cut-off ϵ and a finite renormalized dilaton ϕ_r. The Schwarzian captures the limiting dynamics as ϵ goes to zero. In euclidean space, the dilaton ϕ is smaller than $\phi_{\rm b}$ everywhere inside the cut-off curve and has a local minimum at each horizon. For the TFD in euclidean space (circle in the Poincare disk) one has concentric circles of constant dilaton. In the continuation to Lorentzian signature across the $t = 0$ time slice, the boundary curve splits

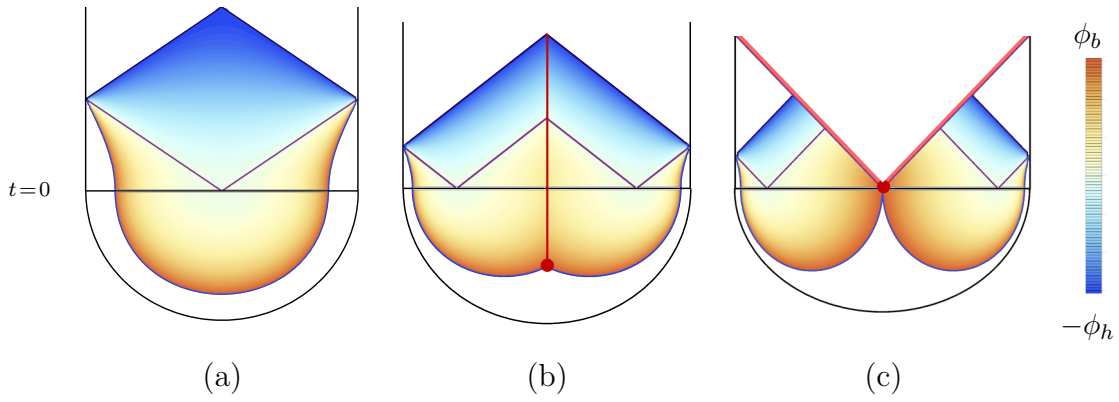

Figure 2.5: Dilaton profile. The values of the dilaton in arbitrary units go from large positive values of ϕ at the boundary (red end of color spectrum) to large negative values ending at the inner horizon (blue end of color spectrum): We show $\ell \sim 0$ (left), $\ell \sim N/\beta J$ (middle) and $\ell \sim N$ (right).

into two hyperbolas (corresponding to the left and right QM) that hit the boundary of AdS after finite global time. Inside of the lorenzian bulk, the 4d singularity is located where $\phi + \phi_0 = 0$ so one could imagine taking as a cut-off $\phi = -\phi_0$ or to be safe $-\phi_{\rm b}$. From the 4d perspective the inner horizon is located $-\phi_h$ and it is well known to be unstable. Therefore we will cut-off the geometry at $-\phi_h$. We show this situation in panel (a) of figure 2.5.

For the PETS with an operator inserted during the euclidean evolution, we need to glue two of locally TFD solutions along the world line of the bulk particle as shown in panel (b). As reviewed in Appendix 2.7 each side of the circles have a definite $SL(2,\mathbf{R})$ charge. Charge conservation implies that the dilaton is continuous along the bulk brane when the two halves are glued [7]. As expected from the equations of motion, the slope of the dilaton is discontinuous with a jump proportional to the mass ℓ of the boundary particle $\nabla\phi_L - \nabla\phi_R \sim \ell$.

The dilaton inside of the cut-off surface stays always below the UV cut-off value fixed by $\phi_{\rm bdy}$. Then the bulk space between the cut-off surface and the singularity can be trusted. As the mass of the bulk brane is increased the gradient $\nabla\phi$ grows without bound, $\nabla\phi \to \infty$ for $\ell \to \infty$. This implies that there is a critical value $\ell_{\rm cr}$ of the mass such that for $\ell > \ell_{\rm cr}$ the low energy approximation that gives JT gravity breaks down. The geometry inside the causal future

[7] To see this simply start from charge conservation $Q_L = Q_R + Q_m$ (these are three component vectors living in embedding space, see Appendix 2.7 for notation). Then take the inner product with Y (coordinate in embedding space describing EAdS_2). Along the worldline of the particle $Q_m \cdot Y = 0$ so $\phi_L = \phi_R$.

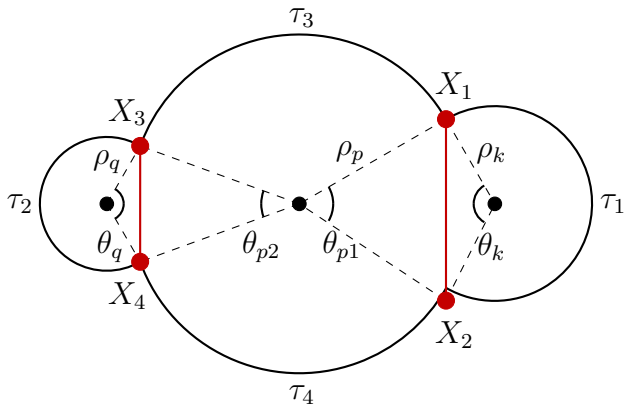

Figure 2.6: The boundary curve that maximizes the Schwarzian action with two pairwise operator insertions.

of the particle position at $t = 0$ (V-shaped region in panel (c) of figure 2.5) describes a strongly coupled region. The answer for what happens inside this region might depend on fine-grained details of the operator and of the SYK dynamics. If the operator is a projection that acts on all fermions such that $\ell \sim N$, it was argued in [51] that the region inside the V-shaped region must be removed.

2.2.3 Multiple Insertions

In this subsection we will comment on the generalization of PETS produced by multiple operator insertions. In the leading large N limit and low energy limit of the SYK model, we can then compute the relevant correlation functions using the results of [24].[8]

Using the same procedure as described above for the two-point function, we derive that the $2n$-point functions is determined by a semiclassical action which has the form

$$I = \sum_{\text{prop.}} \frac{k_i^2}{2C}\tau_i + \sum_{i,j \text{ paired}} \left(\ell \log \left(\cos\frac{\theta_i}{2} + \cos\frac{\theta_j}{2} \right)^2 + \theta_i k_i + \theta_j k_j \right) - \sum_i 2\pi k_i. \tag{2.46}$$

In the first term the sum is over propagators over times τ_i with an intermediate state energy $k_i^2/2C$. The second term is a sum over pairs of insertions into a bilocal field. Finally the third

[8]For our purpose, it will be sufficient to focus on channels where bulk propagators do not cross and therefore do not involve the R-matrix of [24].

term is a sum over momenta k that are different off-shell. From this action one can obtain the saddle point equations and bulk geometry by a gluing procedure similar to the case of two operators.

Example: Four-Point Function

As a concrete exercise we will apply the ideas above to the four-point function. This shares some general features with the case of an arbitrary number of insertions. We will use the results in section 2.5.

In figure 2.6 we show the geometry backreacted by the two bilocal insertions. We determine the shape of the geometry from the semi-classical expression of the time-ordered four point function[9]

$$\langle \mathcal{O}_{\ell_1}(X_1)\mathcal{O}_{\ell_1}(X_2)\mathcal{O}_{\ell_2}(X_3)\mathcal{O}_{\ell_2}(X_4)\rangle.$$

Applying the rules of the previous section the effective action computing this correlator is given by

$$\begin{aligned} I &= \frac{k^2}{2C}\tau_1 + \frac{q^2}{2C}\tau_2 + \frac{p^2}{2C}\tau_3 + \frac{p^2}{2C}\tau_4 \\ &\quad +\ell_1 \log\left(\cos\frac{\theta_k}{2} + \cos\frac{\theta_{p1}}{2}\right)^2 + \theta_k k + \theta_{p1} p + \ell_2 \log\left(\cos\frac{\theta_q}{2} + \cos\frac{\theta_{p2}}{2}\right)^2 + \theta_q q + \theta_{p2} p \\ &\quad -2\pi p - 2\pi q - 2\pi k. \end{aligned} \tag{2.47}$$

where $\sum_i \tau_i = \beta$. The geometric role of each variable is shown in figure 2.6. The first line corresponds to a sum over each propagator over a time τ_i. There are four of them contributing, although only three different ones (off-shell) due to a conservation law. In the second line we sum over both pairings. Finally the third line has a sum over channels coming from the density of states. Note that, since off-shell only three momenta differ, p contributes as $2\pi p$ and not $4\pi p$.

Since we will use the results in this section later we will write down the saddle-point equations

[9] If the four operators were identical we should sum over all channels. Here we assume that they are only pairwise identical.

in detail. From varying the momenta k, p, q we obtain

$$2\pi - \theta_k = \frac{k\tau_1}{C}, \quad 2\pi - \theta_q = \frac{q\tau_2}{C}, \quad 2\pi - \theta_{p1} - \theta_{p2} = \frac{p(\tau_3 + \tau_4)}{C}. \tag{2.48}$$

From varying the opening angles θ's we obtain the equations

$$\begin{aligned} \frac{k}{\sin\frac{\theta_k}{2}} &= \frac{p}{\sin\frac{\theta_{p1}}{2}} = \frac{\ell_1}{\cos\frac{\theta_k}{2} + \cos\frac{\theta_{p1}}{2}}, \\ \frac{q}{\sin\frac{\theta_q}{2}} &= \frac{p}{\sin\frac{\theta_{p2}}{2}} = \frac{\ell_2}{\cos\frac{\theta_q}{2} + \cos\frac{\theta_{p2}}{2}}. \end{aligned} \tag{2.49}$$

By eliminating the angles θ can obtain an equation for p, k and q.

2.3 Entanglement Entropy of PETS

In this section we will combine the results of the previous section (and Appendix 2.7) to compute from first principles the entanglement entropy of the partially entangled thermal states using the replica trick. We will begin by reviewing the case of the TFD. Then we will consider operators without backreaction and finally the most general case. The upshot of the calculation will be that the entanglement entropy is determined by the global minimum of the dilaton. This is consistent with the holographic entropy prescription [30].

We will consider a bipartite PETS defined in the introduction. In this section we will study the $\mathrm{QM_R}$ density matrix $\rho = \mathrm{Tr}_L|\Psi\rangle\langle\Psi|$ after performing a partial trace over the left QM. We will compute the Renyi entropy of these states and from it deduce the entanglement entropy. The Renyi entropy is defined as

$$\mathcal{S}_n = \frac{1}{1-n}\log\frac{\mathrm{Tr}\rho^n}{(\mathrm{Tr}\rho)^n}. \tag{2.50}$$

where n indicates the replica index and the limit $n \to 1$ gives the entanglement entropy. Another

observable with this properties is the modular entropy defined as

$$S_n = -n^2 \frac{\partial}{\partial n} \left[\frac{1}{n} \log \mathrm{Tr} \rho^n \right]. \tag{2.51}$$

This is a more natural candidate for an entropy associated to the system of n replicas. By using our methods we could in principle compute both. Nevertheless, only the modular entropy S_n has a clear holographic interpretation, as found in [57] building upon [58] [10].

For these reasons explained above, in this section we will focus on S_n which, with slight abuse of terminology, we will still refer to as Renyi entropy.

As a brief warm up, we will begin by analyzing the TFD state

$$|\mathrm{TFD}\rangle = \tag{2.52}$$

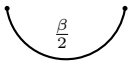

Its partition function $Z(\beta)$ is a path integral over thermal circle of length β, as shown in figure 2.2. In the semiclassical limit, large C, it is given by

$$\begin{aligned} \log Z &= \log \int [df]\ e^{C \int d\tau \{\tan \frac{1}{2} f(\tau), \tau\}}, \\ &= S_0 + \beta E_0 + \frac{2\pi^2 C}{\beta} + \ldots, \end{aligned} \tag{2.53}$$

where the dots indicate subleading terms. From the point of view of the Schwarzian theory the extremal zero-point values of entropy and energy S_0 and E_0 are undetermined but large [11]. In the case of SYK $S_0, E_0 \sim N$ while near extremal corrections are subleading $S - S_0 \sim N/(\beta J)$. The value of the dilaton at the horizon of a black hole geometry is given by $\phi_h = \frac{2\pi}{\beta}\phi_r = G_N \frac{16\pi^2 C}{\beta}$ and fixed by the temperature.

Using the replica trick, the trace of ρ^n is equivalent to the partition function of a circle of

[10] Another advantage is the fact that one can compute S_n without worrying about the normalization of the density matrix. An attempt to divide by $(\mathrm{Tr}\rho)^n$ in equation (2.51) will give the same S_n after taking the derivative with respect to n.

[11] S_0 is a zero-point entropy while S_n denotes the n-th modular entropy. We hope this will not cause confusion since we will never take the $n \to 0$ limit of the modular entropy in this thesis.

size $n\beta$. This is a simple extension of the result above

$$S_n \;=\; -n^2 \frac{\partial}{\partial n}\left[\frac{1}{n}\log Z(n\beta)\right] = (1-n\partial_n)\log Z(n\beta) = S_0 + \frac{4\pi^2 C}{n\beta}. \tag{2.54}$$

We can rewrite this result as

$$S_n \;=\; S_0 + \frac{\phi_h(n)}{4G_N}, \tag{2.55}$$

where $\phi_h(n)$ is the dilaton at the horizon of a black hole of size $n\beta$. This is the minimal value and also lies at the fix point of the replica $\mathbf{Z}_n$ symmetry [12]. The entanglement entropy $S = \lim_{n\to 1} S_n = -\mathrm{Tr}\rho\log\rho$ is given by $S = S_0 + \frac{4\pi^2 C}{\beta}$. Of course since $\rho \sim e^{-\beta H}$ we could have directly guessed this thermodynamic relation between entropy and free energy. This thermodynamic relation will no longer be true for PETS. [13]

We can repeat this entropy calculation for the PETS described in the introduction. In particular we will consider

$$|\,\Psi\rangle \;\cong\; e^{-\frac{1}{2}\beta_L H}\,\mathcal{O}_\ell\, e^{-\frac{1}{2}\beta_R H} \;=\; \tag{2.56}$$

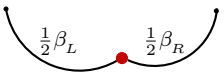

To simplify some formulas below we will parametrize this state by $\tau = \beta_R/2$ and $\beta = \beta_L + \beta_R$ or equivalently $\frac{1}{2}\beta_L = \frac{1}{2}\beta - \tau$. For reasons that will be clear below we will focus on $\beta_R \neq \beta_L$ or $\tau \neq \beta/4$. We will later generalize this state to multiple insertions in section 2.5.

The procedure, similarly to the previous computation, is to consider a thermal circle of size $n\beta$ for n replicas, with $2n$ operator insertions. Then the trace of the replicas is given, in terms

[12] This is not true for the more standard definition $\mathcal{S}_n$ since $\mathcal{S}_n = S_0 + (1+n)2\pi^2 C/n\beta = S_0 + \frac{n+1}{2}\frac{\phi_h(n)}{4G_N}$. The right-hand side is not given by $\phi_h(n)/4G_N$ unless $n = 1$, and we can see even in this simple example the advantage of the modular entropy (2.51).

[13] From the 4d perspective, the derivation of the Jackiw-Teitelboim model reduces a near extremal black hole to the near horizon region $AdS_2 \times S^2$ (see for example [59]). The dilaton then is the perturbation from extremality of the size of the horizon $A_h = \phi_0 + \phi_h$. The entanglement entropy above is therefore the usual Bekenstein entropy of a near extremal black hole since $S_0 = \phi_0/4G_N$ is related to the extremal dilaton in the same way.

of β and τ, by the following correlator

$$\begin{aligned} \mathrm{Tr}\rho^n &= Z_0(n\beta)\langle \mathcal{O}(-\tau)\mathcal{O}(\tau)\mathcal{O}(\beta-\tau)\mathcal{O}(\beta+\tau)\mathcal{O}(2\beta-\tau)\mathcal{O}(2\beta+\tau)\ldots\rangle_{n\beta}, \\ &\equiv G_n(\tau,\beta), \end{aligned} \tag{2.57}$$

where the dots indicate the remaining of the $2n$ operators and the unperturbed TFD partition function we reviewed above is $\log Z_0(n\beta) = S_0 + n\beta E_0 + \frac{2\pi^2 C}{n\beta}$. In the equation above we added the partition function since, following the notation of [24], we defined correlators to be normalized to 1 for $\mathcal{O} = \mathbb{1}$. Then the Renyi entropy we focus on in this section (2.51) is given in terms of correlation functions of the Schwarzian theory

$$S_n \;=\; -n^2\partial_n\left[\frac{1}{n}\log G_n(\tau,\beta)\right]. \tag{2.58}$$

The expression in equation (2.58) is naturally divided into the sum of two terms. The logarithm of the correlator always involves $S_0 + n\beta E_0 + \ldots$. This gives a contribution of the order N zero-point entropy $S_n = S_0 + \ldots$. The goal will be to compute the leading near-extremal correction $S_n - S_0 \sim C$ contribution to the entropy, when C is large with ℓ/C fixed [14].

2.3.1 Warm-up: Light Operators

We will begin as a warm-up by analyzing the limit $1 \ll \ell \ll C$ [15]. Correlators satisfy large N factorization and the building blocks are given by the semiclassical answer of equation (2.29), $\langle \mathcal{O}(\tau)\mathcal{O}(0)\rangle = (\pi/\beta \sin(\pi\tau/\beta))^{2\ell}$, without backreaction.

Before writing down the general answer let us begin by taking $n = 2$. Using factorization, the

[14] As mentioned in section 2.2, the dimensionless ℓ should be compared with a dimensionless ratio such as $2\pi C/(\beta_{_R} + \beta_{_L})$. Since we will use units in which β is of order one we will simply compare ℓ with C.

[15] For $\ell \ll 1$ one can apply entanglement entropy perturbation theory.

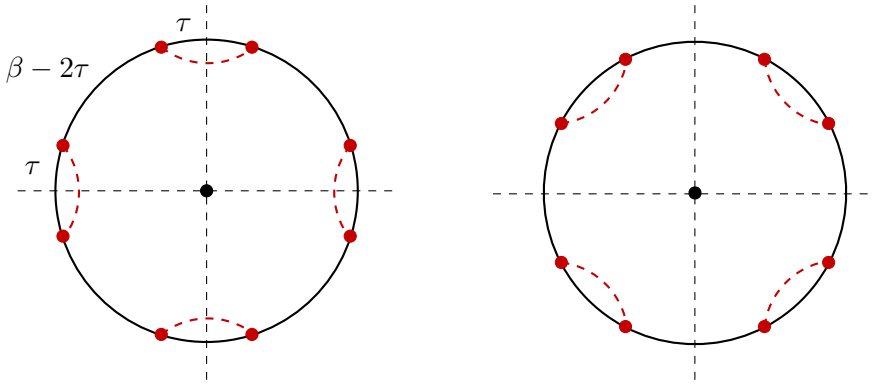

Figure 2.7: Replica Geometry for $1 \ll \ell \ll C$ with $n = 4$. We indicate the channel that dominates when $0 < \tau < \beta/4$ (left) and $\beta/4 < \tau < \beta/2$ (right). The central black dot indicates the $\mathbf{Z}_n$ symmetric horizon with minimal dilaton.

fact that all four operators are identical and the negligible backreaction gives a simple answer

$$\mathrm{Tr}\rho^2 = e^{S_0+2\beta E_0+\frac{2\pi^2 C}{2\beta}}\left[\left(\frac{\pi}{2\beta\sin\frac{\pi\tau}{\beta}}\right)^{4\ell}+\left(\frac{\pi}{2\beta\cos\frac{\pi\tau}{\beta}}\right)^{4\ell}+\left(\frac{\pi}{2\beta}\right)^{4\ell}\right], \tag{2.59}$$

The channel combinatorics makes it hard to extend to arbitrary n. But for $1 \ll \ell \ll C$ one can simplify this considerably. To be concrete assume first that $0 < \tau < \beta/4$. We can rewrite the previous expression in a convenient way as

$$\begin{aligned}\mathrm{Tr}\rho^2 &= e^{S_0+2\beta E_0+\frac{2\pi^2 C}{2\beta}}\left(\frac{\pi}{2\beta\sin\frac{\pi\tau}{\beta}}\right)^{4\ell}\left[1+\left(\tan\frac{\pi\tau}{\beta}\right)^{4\ell}+\left(\sin\frac{\pi\tau}{\beta}\right)^{4\ell}\right], \\ &\approx e^{S_0+2\beta E_0+\frac{2\pi^2 C}{2\beta}}\left(\frac{\pi}{2\beta\sin\frac{\pi\tau}{\beta}}\right)^{4\ell}[1+\mathcal{O}(e^{-\ell})].\end{aligned} \tag{2.60}$$

If we assume $\ell \gg 1$ then the second and third term are negligible regardless of τ (the tangent is smaller than one only for $\tau < \beta/4$). If $\tau > \beta/4$ then the channel contracting operators separated by $\beta - 2\tau$ (term with cosine above) dominates. Using this we can run the same argument for arbitrary n and τ. In figure 2.7 we show the situation for $n = 4$ as an example. The general

answer can be written in each case as

$$\mathrm{Tr}\rho^n \approx \begin{cases} e^{S_0+n\beta E_0+\frac{2\pi^2 C}{n\beta}} \left(\frac{\pi}{n\beta \sin\frac{\pi 2\tau}{n\beta}}\right)^{2n\ell}, & 0<\tau<\beta/4, \\ e^{S_0+n\beta E_0+\frac{2\pi^2 C}{n\beta}} \left(\frac{\pi}{n\beta \sin\frac{\pi(\beta-2\tau)}{n\beta}}\right)^{2n\ell}, & \beta/4<\tau<\beta/2. \end{cases} \tag{2.61}$$

Note that we are not using a properly normalized density matrix. This is not a problem for computing S_n (2.51) (although $\mathcal{S}_n$ is sensitive to normalization). Using this result the Renyi entropy is given by

$$S_n = S_0 + \frac{4\pi^2 C}{n\beta} + 2\ell\left(n - \frac{2\pi x}{\beta}\cot\frac{2\pi x}{n\beta}\right), \qquad x = \min\left(\tau, \frac{\beta}{2}-\tau\right). \tag{2.62}$$

From this expressions taking the limit $n \to 1$ is straightforward. The corrections to these expressions are of order $\mathcal{O}(1/\ell)$ and $\mathcal{O}(1/C)$ so that for $1 \ll \ell \ll C$ this is well justified. The only subtelty occurs at precisely $\tau = \beta/4$. For this choice there is a phase transition where the Renyi (or entanglement) entropy is continuous but with a jump in the first derivative. Another feature is the symmetry under $\tau \to \beta/2 - \tau$ ($\beta_{_L} \leftrightarrow \beta_{_R}$) due to the fact that $|\Psi\rangle \in \mathcal{H}_L \otimes \mathcal{H}_R$ is a pure state and therefore $S_{\mathrm{L}} = S_{\mathrm{R}}$.

2.3.2 Heavy Operators

The main issues appearing when attempting to compute S_n is the channel combinatorics and the presence of contractions with crossing legs that imply non-trivial gravitational interactions (the appearance of the R-matrix from [24]). Both these problems can be avoided in the semiclassical limit of large C and large $\ell \sim C$ in a way similar to the previous case. Correlators of an arbitrary number of operators, as reviewed in section 2.2, are exponential in C meaning that

$$G_n(\tau,\beta) = \sum_{\text{channel } k} e^{CI_k(\tau,\beta,\ell/C)} \approx e^{CI_{\max}(\tau,\beta,\ell/C)}[1+\mathcal{O}(e^{-C})]. \tag{2.63}$$

Therefore to exponential accuracy in C, the correlator is dominated by the channel which minimizes the classical action $I_{\rm k}$ appearing in the exponent. This is similar to the situation in higher dimensions where large N ensures that one picks the saddle-point of minimal action as long as there are no degeneracies.

This solves both problems since a single channel dominates and moreover channels with crossing legs never win (the reason is analogous to the statement in Lorenzian time that OTOC cannot be bigger than time ordered ones). For the calculation of the Renyi entropy of the state defined above there are two cases in which different channels dominate (1) $0 < \tau < \beta/4$ and (2) $\beta/4 < \tau < \beta/2$.

Case I: $0 < \tau < \beta/4$ ($\beta_{_R} < \beta_{_L}$)

We need the correlator of $2n$ operators placed periodically at a distance alternating between 2τ and $\beta - 2\tau$. For case I the channel that dominates has a contraction between operators separated a distance 2τ. We show this channel in figure 2.8, where we define the intermediate channel momenta k_i and p.

The configuration has a $\mathbf{Z}_n$ symmetry of permuting the replicas and a $\mathbf{Z}_2$ symmetry of time reversal. This is important for finding the saddle-point of the classical action giving this correlator (momenta running along outer circles k_i are different off-shell but coincide on-shell $k_i \equiv k$ thanks to the $\mathbf{Z}_n$ symmetry). In general the correlator is given semiclassically as

$$\log G_n(\tau,\beta) = S_0 + n\beta E_0 + 2\pi p + \sum_{i=1}^{n} 2\pi k_i + \sum_{i=1}^{n} \tilde{I}_i(p, k_i, \ell, \tau, \beta) \tag{2.64}$$

the explicit formula for the terms $\tilde{I}_i$ and the saddle-point equations can be obtained from the general methods explain in section 2.2. Using that $k_i \equiv k$ the correlator simplifies to

$$\log G_n(\tau,\beta) = S_0 + n\beta E_0 + 2\pi p + n\left[2\pi k + \tilde{I}(p, k, \ell, \tau, \beta)\right] \tag{2.65}$$

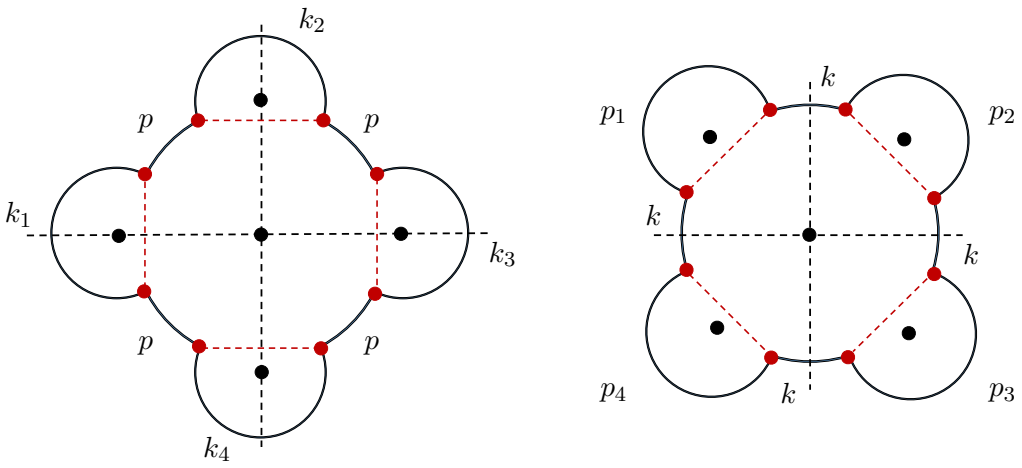

(I) $0 < \tau < \beta/4$ $(p < k)$ (II) $\beta/4 < \tau < \beta/2$ $(k < p)$

Figure 2.8: Geometry generated by the insertion of heavy operators (red dots) for $n = 4$ (replicas are separated by dashed lines). Case I: Four local dilaton local minima at the horizons (black dots) with $\phi_i \propto k_i(n) \equiv k(n)$ and at the central, (global) minimum $\mathbf{Z}_n$ symmetric, horizon with $\phi_{\min} \propto p(n) < k(n)$. Case II: Four local minima at the horizons (black dots) with $\phi_i \propto p_i(n) = p(n)$ and at the $\mathbf{Z}_n$ symmetric horizon with $\phi_{\min} \propto k(n) < p(n)$.

Using this we can compute the Renyi entropy S_n as

$$S_n = -n^2 \partial_n \frac{1}{n} \log Z_n = S_0 - n^2 \frac{\partial}{\partial n} \frac{1}{n} \left(2\pi p + n \left[2\pi k + \tilde{I}(p, k, \ell, \tau, \beta) \right] \right) \tag{2.66}$$

Now we can see the advantage of this definition of the Renyi entropy. When taking the derivative with respect to n one has the explicit n depence and the implicit dependence through the saddle-point value of $p(n)$ and $k(n)$. When evaluated on the saddle-point solution, the derivative with respect to the implicit dependence on n vanishes exactly. Taking derivatives only to the explicit factors of n simplifies considerably

$$\begin{aligned} S_n^{\text{Renyi}} &= S_0 + 2\pi p(n) = S_0 + \frac{\phi_h(n)}{4G_N}, \\ &= S_0 + \min_{Y \in \text{ Bulk}} \frac{\phi(Y)}{4G_N}, \end{aligned} \tag{2.67}$$

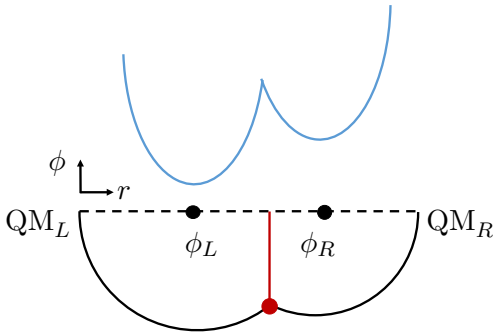

Figure 2.9: Dilaton profile (blue curve) at time $\tau = 0$ as a function of the radial direction. Below we show the Euclidean evolution that creates the state with an insertion of $\mathcal{O}_\ell$ (red dot). The profile has two local minima at the horizons $\phi_{L/R}$ at the left/right horizons. We show the case $\tau < \beta/4$ for which $\phi_L < \phi_R$, then the microscopic entanglement entropy is given by ϕ_L.

where the saddle-point equation defining $p(n)$ and $k(n)$ is given by

$$\frac{k}{C} 2\tau + 2\arctan\frac{k+p}{\ell} + 2\arctan\frac{k-p}{\ell} = 2\pi, \tag{2.68}$$

$$\frac{p}{C}(\beta - 2\tau) + 2\arctan\frac{k+p}{\ell} - 2\arctan\frac{k-p}{\ell} = \frac{2\pi}{n}. \tag{2.69}$$

Y is the position in embedding space parametrizing the bulk dual to the boundary with n replicas. As we see in figure 2.8, there are several local minima of the dilaton (only two are different due to $\mathbf{Z}_n$ symmetry). The Renyi entropy is given by the global minimum which corresponds to the value $\phi_h(n)$ at the $\mathbf{Z}_n$ symmetric central horizon in the figure. Indeed for $0 < \tau < \beta/4$ and any ℓ the condition $p(n) < k(n)$ is always satisfied.

This is consistent with the holographic prescription derived in higher dimensions in [57]. The standard Renyi entropy $\mathcal{S}_n$ does not have such a simple formula but it is still computable using the explicit expressions of the semiclassical action.

Now we can take the $n \to 1$ limit. The local minimal values of the dilaton at the left and right horizons are

$$\frac{\phi_L}{4G_N} = 2\pi p(n=1) \quad \text{and} \quad \frac{\phi_R}{4G_N} = 2\pi k(n=1), \tag{2.70}$$

we show this in terms of the black hole bulk geometry in figure 2.9. We explained in section 2.2 that one of the horizons might be hidden and would not be part of the geometry for a range of

ℓ. It is easy to see that from the two horizons the one with minimal horizon dilaton is always visible.

Case II: $\beta/4 < \tau < \beta/2$ ($\beta_{_L} < \beta_{_R}$)

After case I, deriving the results for case II is straightforward. The channel that dominates now has contractions between nearest neighboring operators separated by $\beta_{_L} = \beta - 2\tau$. The Renyi entropy is given by the momentum which does not appear with a factor of n in the semiclassical action. For case I this was p and for case II it is k instead (see right panel of figure 2.8). This gives

$$S_n = S_0 + 2\pi k(n) = S_0 + \min_{Y\in \text{ Bulk}} \frac{\phi(Y)}{4G_N}. \tag{2.71}$$

Then the holographic prescription is still valid for case II. The saddle-point equations are different though and now become

$$\frac{k}{C}2\tau + 2\arctan\frac{k+p}{\ell} + 2\arctan\frac{k-p}{\ell} = \frac{2\pi}{n}, \tag{2.72}$$

$$\frac{p}{C}(\beta - 2\tau) + 2\arctan\frac{k+p}{\ell} - 2\arctan\frac{k-p}{\ell} = 2\pi, \tag{2.73}$$

which coincides with the previous case for $n = 1$ but in general might be different. In this case now $k(n) < p(n)$ for any choice. The situation for $n = 1$ also gets reversed with respect to the previous case. The prescription of choosing the minimal value of the dilaton still gives the right answer

2.3.3 Summary

Putting everything together we can write the general result valid as long as $\tau \neq \beta/4$ ($\beta_{_L} \neq \beta_{_R}$). Looking at figure 2.9 we see that the dilaton profile has two potential local minima given by the horizons value $\phi_L = \phi(Y_{H_L})$ and $\phi_R = \phi(Y_{H_R})$, which are proportional to p and k respectively. For arbitrary n the minima occurs in the $\mathbf{Z}_n$ invariant point which is always given by $\min(p, k)$. Therefore the entanglement entropy for these partially entangled states labeled by the operator

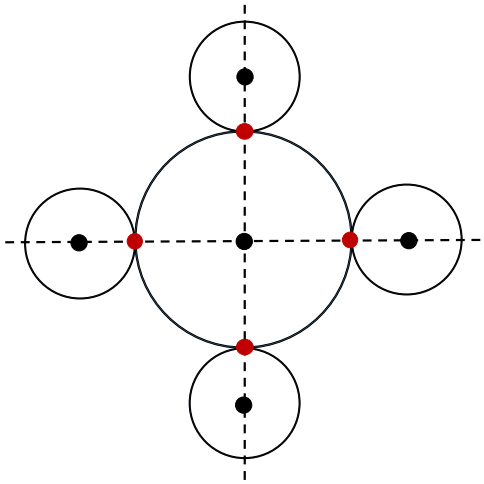

Figure 2.10: Clover diagram for $\ell/C \gg 1$, $\tau < \beta/4$ and $n = 4$. Dashed lines separate replicas and the dots indicate the local horizons of each part of the geometry.

insertion ℓ and τ is given by

$$\begin{aligned} S &= S_0 + 2\pi \, \min(p, k), \\ &= S_0 + \min_{Y \in \text{ Bulk}} \frac{\phi(Y)}{4G_N}, \end{aligned} \tag{2.74}$$

where the choice of p or k is equivalent to finding the minimum between the local minima ϕ_L and ϕ_R. The dependence of the entanglement entropy on the PETS parameters ℓ and τ is given implicitly by the saddle point equation

$$\frac{k}{C} 2\tau + 2 \arctan \frac{k+p}{\ell} + 2 \arctan \frac{k-p}{\ell} = 2\pi, \tag{2.75}$$

$$\frac{p}{C}(\beta - 2\tau) + 2 \arctan \frac{k+p}{\ell} - 2 \arctan \frac{k-p}{\ell} = 2\pi, \tag{2.76}$$

taken from the previous section for $n = 1$. This can be easily rewritten in terms of ϕ_L and ϕ_R.

In general this system of equations needs to be solved numerically. In practice we can derive analytic formulas in two cases. First when $\ell/C \ll 1$. This was studied above as a warm-up using a different approach but the same answer can be derived from equations (2.75) and (2.76). This

gives (for $\tau < \beta/4$) the approximation

$$k(n) \approx \frac{2\pi C}{n\beta} + 2\ell\left(n + \frac{2\pi\tau}{\beta}\cot\frac{2\pi\tau}{n\beta}\right), \quad p(n) \approx \frac{2\pi C}{n\beta} + 2\ell\left(n - \frac{2\pi\tau}{\beta}\cot\frac{2\pi\tau}{n\beta}\right). \tag{2.77}$$

This corresponds to a small perturbation to the TFD value of the dilaton due to the operator backreaction, since the correction is of order $\delta S \sim \ell \sim \mathcal{O}(1)$. We see that since $\tau < \beta/4$ the global dilaton minimum is indeed given by $p(n)$.

On the other extreme we can take $\ell/C \gg 1$. Then the 'clover' diagram describing the backreaction (see figure 2.10) gives a graphical representation that gives the approximation (for the $\tau < \beta/4$ case, $\beta_{_R} < \beta_{_L}$)

$$k(n) \approx \frac{2\pi C}{2\tau} = \frac{2\pi C}{\beta_{_R}}, \quad p(n) \approx \frac{2\pi C}{n(\beta - 2\tau)} = \frac{2\pi C}{n\beta_{_L}}. \tag{2.78}$$

When $\tau > \beta/4$ the roles of p and k are replaced. In this case the correction is of order $\delta S \sim \mathcal{O}(C)$ due to the semiclassical backreaction. We also see that indeed the global minimum of the dilaton corresponds to p for $\tau < \beta/4$ (and k in the other extreme).

For general values of ℓ/C the parameter p and k interpolate between these limits. As a summary of this discussion the Renyi entropies are given in each limit by the approximations

$$S_n = \begin{cases} S_0 + \frac{4\pi^2 C}{n\beta} + 2\ell\left(n - \frac{\pi x}{\beta}\cot\frac{\pi x}{n\beta}\right), & \text{for } \ell/C \ll 1, \\ S_0 + \frac{4\pi^2 C}{n\ (\beta - x)}, & \text{for } \ell/C \gg 1. \end{cases} \tag{2.79}$$

which is valid for any τ and again we used $x = \min(2\tau, \beta - 2\tau)$. A numerical solution of the saddle point equations shows that $p(n)$ (or ϕ_L) and $k(n)$ (or ϕ_R) interpolate smoothly and monotonically from the $\ell \to 0$ to the $\ell \to \infty$ limits that we derived above.

One could ask in what sense are these states partially entangled since the entropy seems to increase with ℓ. Consider the case such that $p < k$ and therefore $\phi_L < \phi_R$. The TFD corresponds to the state of maximal entropy with the constrain of a fixed average energy E_R. The energy of

the right QM in the PETS can be easily computed to be exactly $E_R = E_0 + k^2/2C$. The state that maximizes the entropy is the thermal one with an inverse temperature chosen such that $\langle H_R \rangle = E_0 + k^2/2C$. This can be purified as a TFD living in a tensor product of left- and right QM, with entropy $S_{\rm TFD} = S_0 + 2\pi k$. This should be compared with the actual entropy which is $S_{\rm PETS} = S_0 + 2\pi p$. Since $p < k$ we see that $S_{\rm PETS} < S_{\rm TFD} = S_{\rm max}$. It is in this sense that our states are partially entangled.

The entropy $2\pi k$ has another interpretation. In the case that the bulk brane falls behind the right horizon an observer in QM_R cannot notice the state not being thermal, unless one measures complicated observables that are able to see behind the horizon (see figure 2.11 below, we still take $\phi_L < \phi_R$). In the usual statistical mechanical sense, a coarse-grained observer will believe he or she is outside a TFD with temperature associated to the right horizon $\phi_R/4G_N = 2\pi k$. The coarse-grained energy will be correct, $E_R = E_0 + k^2/2C$ but the entropy $S_{\rm c.g.} = S_0 + 2\pi k$ will be off with respect to the microscopic one $S = S_0 + 2\pi p$.

Finally, another measure one can take to characterize the loss of entanglement from a bulk perspective is the decay of left-right correlators at time $t = 0$. In the TFD state they are given by

$$\langle \mathcal{O}_L(0)\mathcal{O}_R(0)\rangle_{\rm TFD} = (\pi/\beta)^{2\ell_P}, \tag{2.80}$$

where ℓ_P is the dimension of the probe operators, not related to the one of the operator insertion that created the PETS. For the PETS we are considering the left-right correlator is difficult to compute. Nevertheless for $\ell_P \gg 1$ we can approximate it by a renormalized geodesic distance. This gives

$$\langle \mathcal{O}_L\mathcal{O}_R\rangle_{\rm PETS} = \left(\tan\frac{\theta_k}{4}\tan\frac{\theta_p}{4}\right)^{\ell_P}\langle \mathcal{O}_L\mathcal{O}_R\rangle_{{\rm TFD},\beta} \tag{2.81}$$

This prefactor goes from 1 when ℓ is small (since for small backreaction $\theta \approx \pi$). For a large perturbation of the TFD $\ell \gg C$ and $\theta \approx 0$ giving $\langle \mathcal{O}_L\mathcal{O}_R\rangle_{\rm PETS} \to 0$. When the left-right correlator becomes smaller than e^{-S} where S is the entanglement-entropy, one can say the two QM are not connected by a smooth semiclassical wormhole (firewall instead?). For $\ell \gg C$

the correlator behaves as $\left(\tan\frac{\theta_k}{4}\tan\frac{\theta_p}{4}\right)^{\ell_P} \approx \left(\frac{kp}{\ell^2}\right)^{\ell_P}$ where $pk \approx \frac{4\pi^2C^2}{\beta_R\beta_L}$ and therefore the ratio between the PETS correlator and the TFD decays as $\exp(-2\ell_P \log\frac{\ell}{C})$, controlled by the distance between horizons.

2.4 Bulk Reconstruction

In this section we will comment about bulk reconstruction of PETS. We will focus on the case in which the operator $\mathcal{O}_\ell$ has dimension $\ell \sim C \sim N/\beta J$, so that the bulk geometry is the one shown in figure 2.11. We will argue in this section that the regions that can be reconstructed from either side are as shown in the right panel of figure 2.11. We will give two separate arguments in support of this proposal, one using entanglement wedge reconstruction [60] and one using a tensor network representation of the bulk state [16].

2.4.1 Entanglement wedge reconstruction

To put this discussion in context, we first take a step back to a pure higher dimensional AdS bulk space-time. Pick a region $\mathcal{A}$ included in the boundary of AdS. A natural question to ask is to what extent can we reconstruct bulk operators using CFT operators living on this region $\mathcal{A}$. Semiclassically, one can apply the BDHM/HKLL prescription to reconstruct local operators included in the bulk causal wedge $\mathcal{C}_\mathcal{A}$ of $\mathcal{A}$ [62–64]. In contrast, it is believed that from operators in region $\mathcal{A}$ one should be able to reconstruct operators inside the entanglement wedge $\mathcal{E}_\mathcal{A}$ of $\mathcal{A}$, defined as the bulk domain of dependence of the region between $\mathcal{A}$ and its extremal RT surface [60, 65, 66, 53, 67]. Since the entanglement wedge can in general be bigger than the causal wedge, $\mathcal{C}_\mathcal{A} \subset \mathcal{E}_\mathcal{A}$, it is an interesting problem to find natural ways to represent local operators ϕ such that ϕ lives in the algebra of operators associated to $\mathcal{E}_\mathcal{A}$ but not on $\mathcal{C}$.

In [68] the authors propose a concrete way to construct operators in the entanglement wedge

[16] In [24] the correlators of the Schwarzian theory were related to local insertions in 2D Liouville between ZZ-branes. It would be interesting to study bulk reconstruction using the insertion of cross-caps as in [61]. We leave this for future work.

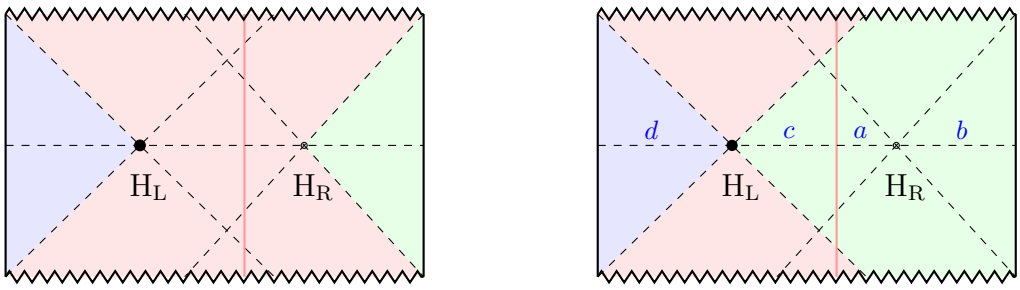

(a) Naive: CW (b) Correct: EW

Figure 2.11: Dual geometry to a PETS created by acting with a heavy operator during euclidean evolution. We indicate the region reconstructed by the left QM by blue and by the right QM by green. The reconstruction of the red region requires both sides. Naively, each side can only see its causal wedge (CW). Instead, we argue below that each side can in principle reconstruct the full entanglement wedge (EW). The right EW includes regions a, b and c.

(see also [69] and [70]). Their construction involves defining the zero-mode of a CFT operator $\mathcal{O}$ under modular flow associated to the modular Hamiltonian $K_{\mathcal{A}}$, defined via $\rho_{\mathcal{A}} = e^{-K_{\mathcal{A}}}$ with $\rho_{\mathcal{A}}$ the density matrix associated to region $\mathcal{A}$. The modular zero-mode is given by (a properly regulated version of)

$$\mathcal{O}_0 = \int ds\ e^{iK_{\mathcal{A}}s}\ \mathcal{O}\ e^{-iK_{\mathcal{A}}s}. \tag{2.82}$$

It is argued in [68] that this highly non-local CFT operator, that lives in the algebra of operators of inside the region $\mathcal{A}$, is dual to an operator that lives on the RT surface

$$\mathcal{O}_0 = \int_{\text{RT}} d\mu(Y_{\text{RT}})\ \phi(Y_{\text{RT}}). \tag{2.83}$$

Here Y labels a point in AdS restricted to the RT surface. In this expression the integral is over the RT surface associated to $\mathcal{A}$, namely the boundary (in the bulk) of the entanglement wedge, and $\phi(Y_{\text{RT}})$ is a local bulk operator. The measure $d\mu(Y)$ of the integral over Y is given by a bulk boundary propagator. We will not need its explicit form here. The proposal gives a concrete construction of (non-local) bulk operators outside of the causal wedge, at the edge of the entanglement wedge.

Let us apply this construction to the geometry of figure 2.11. We pick parameters such

that the left horizon H_L is the horizon with minimal dilaton and therefore the extremal surface. According to the result of our previous section, its area fixes the entanglement between left- and the right QM systems. In the panel (a) of figure 2.11 we show the causal wedges of QM_L (region in red) and QM_R (region in blue). A naive intuition would be that observables in QM_R can only reconstruct operators in the green region and operators in QM_L can only reconstruct operators in the blue region. The red region is outside the causal wedges and naively would require a two-sided reconstruction in terms of operators that act in both QM_L and QM_R.

The construction of [68] provides an example showing that the naive expectation is not correct. Instead one should consider the full entanglement wedges. The entanglement wedge associated to the left QM coincides with its causal wedge and its shown in blue in figure 2.11. In this low dimensional setting, the RT surface becomes a point namely

$$\text{RT surface} = \text{left horizon } \mathrm{H_L}. \tag{2.84}$$

The entanglement wedge of the right QM becomes therefore the green region in panel (b) of figure 2.11 which includes the interior spatial regions a and c. Therefore we propose that this picture is the correct one describing the bulk reconstruction in this PETS. We will motivate this proposal in two ways.

As a first motivation, we can use the construction in [68] as explained above. Our setup has two advantages. First by construction the Hilbert space factorizes $\mathcal{H} = \mathcal{H}_L \otimes \mathcal{H}_R$. Secondly, the RT surface is a point. Therefore the modular flow zero-mode defined in (2.82) becomes a local insertion (2.83) located at the left horizon. We can formally define the modular Hamiltonian associated to the density matrix of the right QM written down in equation (2.91) defined as $\rho_{_R} = e^{-K_{_R}}$ with $\rho_{_R}$ the density matrix of the PETS given in eqn (2.91). Then the suggestion of [68] implies that, up to normalizations,

$$\int ds\; e^{is\,K_{_R}}\; \mathcal{O}\; e^{-is\,K_{_R}} = \phi_{\mathcal{O}}(Y_{\mathrm{H_L}}) \tag{2.85}$$

where $\mathcal{O}$ is an operator living in the right QM.

This is an interesting result for the following reason. A naive observer in the right QM would be led to believe (by doing generic measurements) that she lives in a thermal state and therefore $K_{R}^{\text{naive}} = \beta_{R} H_{R}$. We call this the coarse-grained modular hamiltonian. Then by applying the prescription of [68] she would end up reconstructing an operator in the boundary of the causal wedge, the right horizon

$$\mathcal{O}_0^{\text{naive}} = \int ds\ e^{isH_R}\ \mathcal{O}\ e^{-isH_R} = \phi_{\mathcal{O}}(Y_{\text{H}_\text{R}}). \tag{2.86}$$

Of course, upon closer inspection, if the observer is able to do fine-grained measurements and discover that her density matrix is not thermal, correcting for the modular flow will allow her to reconstruct up to the left horizon. Even though it is believed that the entanglement wedge reconstruction gives the right microscopic answer, in practice it may still be extremely hard to reconstruct operators between the two horizons H_L and H_R using the right QM alone.

2.4.2 Tensor network representation

The above conclusion is supported by the following tensor network argument, first presented in a talk at IAS by Almheiri in [71]. In [71] it was shown how the QEC property of AdS/CFT [53] can be applied to reconstruct the interior of pure SYK black holes. This section highlights and generalizes his approach and points out its equivalence with the QEC procedure for constructing the black hole interior developed in the earlier work [29].

Figure 2.12 shows a tensor network representation for the bulk reconstruction map for the thermo-field double state (left) and the thermal pure state (right) [71]. Let us first explain the former. We assume that the left and right CFT Hilbert space can be factorized into the tensor product of a (visible) bulk QFT Hilbert space $\mathcal{H}_{L,R}^{\text{qft}}$ and (hidden) horizon Hilbert space $\mathcal{H}_{L,R}^{\text{hor}}$

$$\mathcal{H}_{L}^{\text{cft}} = \mathcal{H}_{L}^{\text{qft}} \otimes \mathcal{H}_{L}^{\text{hor}}, \qquad\qquad \mathcal{H}_{R}^{\text{cft}} = \mathcal{H}_{R}^{\text{qft}} \otimes \mathcal{H}_{R}^{\text{hor}} \tag{2.87}$$

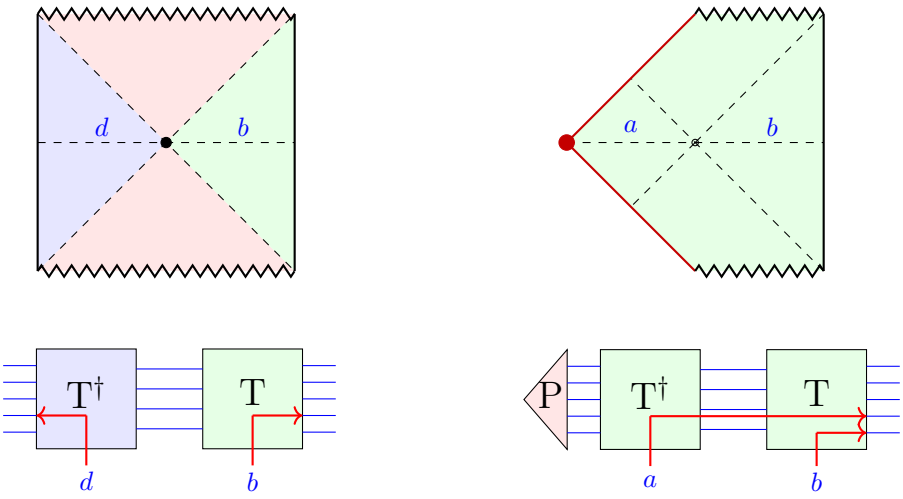

Figure 2.12: Tensor network representation of the one-sided reconstruction of interior and exterior operators for the thermo-field double state (left) and the thermal pure state (right). The reconstruction map of the bulk operators is indicated by the corresponding red arrows. Figure taken from

Each tensor T denotes the embedding of the tensor product into the respective CFT Hilbert space. The left- and right horizon Hilbert space is assumed to be in unique maximally entangled state between the two sides, and is therefore represented by the lines connecting the two tensors [71]. For the TFD state, each bulk QFT Hilbert space is reconstructed in terms of the corresponding CFT. This reconstruction map is indicated by the red arrows. Hence each side can only reconstruct its causal wedge. In this sense, the thermo-field double state has a firewall: a one-sided infalling observer (that can only use one-sided observables) cannot pass the horizon unscathed. This conclusion follows from the AMPS argument: the one-sided states are thermal mixed states, and do not encode the local entanglement that is required to ensure smoothness of the horizon.

The situation is different for the thermal pure state. Let us write the thermal pure state as

$$|\Psi\rangle_R \;=\; {}_L\langle \mathbf{s}|\mathrm{TFD}\rangle_R \tag{2.88}$$

The tensor network for the TFD state is the same as before, but it is now capped off on the left with a projection onto the left state $\langle \mathbf{s}|$, indicated by the triangle [71]. In the space-time diagram the projection is indicated by the 'end-of-the-world particle, that cuts off the left

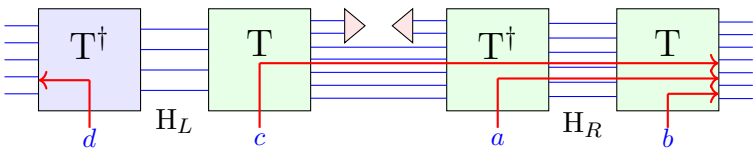

Figure 2.13: Tensor network representation of the partially entangled thermal state.

asymptotic region [51]. Since there is now only one CFT, the bulk reconstruction has to proceed towards the right. Concretely, the above figure indicates that a bulk QFT operator A inside the black hole region a with matrix elements with $A_{nm} = \langle n|A|m\rangle$ acts on the CFT Hilbert space as (c.f. [29])

$$\mathbf{A} = \sum_{m,n} A_{nm}\, \mathbf{P}\mathbf{T}^\dagger |n\rangle\langle m|\, \mathbf{T}\mathbf{P} \tag{2.89}$$

where $\mathbf{P}$ denotes the projection onto the state $|\mathbf{s}\rangle$. This tensor network is a schematic representation of the state-dependent reconstruction map of [28], or equivalently, of the general construction of the interior operators of [29] based on the application of quantum error correction technology and also works for partially mixed states. For the thermal pure state, there is no quantum information theoretic obstruction to reconstruct the black hole interior.

Finally, we turn to the tensor network representation of the partially entangled thermal states shown in figure 2.13. It is useful to think about PETS as a local operator $\mathcal{O}_\ell$ sandwiched between two thermal field double states with temperature $\beta_{_L}$ and $\beta_{_R}$. Since each TFD state is a tensor product state, this leaves a (partially) entangled state. Each TFD state is represented by a pair of tensors T and $T^\dagger$. The operator $\mathcal{O}$, viewed as an element of the tensor product of two QM Hilbert spaces, is a partially entangled state – it is partially transmitting (entangled) and partially reflecting (product of pure). In the above tensor network, this is indicated by the partial projections, depicted by the red triangles.

The number of lines between the successive tensors in figure 2.13 indicates the amount of entanglement across the corresponding interface. As indicated, the left horizon H_L supports the

minimal amount of entanglement, and thus forms the information bottleneck between the left- and right CFT. Hence the left horizon is the bifurcation between the left- and right entanglement wedge. The reconstruction of the bulk QFT modes in each region proceeds as indicated by the right arrows. The rule is that the arrow points in the direction of the nearest interface with the largest number of lines, since this is the direction that dominates entropically: the bulk modes are entangled with the largest nearby Hilbert space. This entropic argument underscores the entanglement wedge reconstruction proposal.

The QEC reconstruction procedure of [29] directly applies to region a, and with minor modification, to region c. The density matrix of the right system

$$\rho_{_R} \;=\; e^{-\frac{1}{2}\beta_{_R} H}\,\mathcal{O}_\ell\, e^{-\beta_{_L} H}\,\mathcal{O}_\ell\, e^{-\frac{1}{2}\beta_{_R} H} \tag{2.90}$$

is only partially mixed: its von Neumann entropy is strictly smaller than the thermal entropy. The operator insertions in effect restrict ρ to lie within a certain code subspace of the total Hilbert space. This enables the QEC reconstruction of the interior operators. The density matrix of the left system is maximally mixed, and the QEC procedure does not work in this case. The left entanglement wedge is equal to the left causal wedge, the outside region to the left of the horizon.

2.5 Generalizations

In this section we discuss two generalizations of partially entangled states. In the first subsection, we introduce a coarse-graining by including an incoherent sum over different operators of the same scale dimension, all inserted at the same euclidean time instant. Then we briefly discuss the case of two different operators insertions at different euclidean times.

2.5.1 Coarse graining and tripartite entanglement

Looking at figure 2.9 we have learned that the entanglement entropy is fixed by (the extremal entropy S_0 plus) the one associated to the smaller horizon ($\phi_{_L}$ in the figure). But we could ask the following question. Which physical quantity is associated to the other horizon where the dilaton attains a local minimum $\phi_{_R} > \phi_{_L}$ in the cases for which both horizons are part of the geometry? If both describe the microscopic von Neumann entropy of the corresponding QM system, the total combined state can no longer be in a pure state. This observation makes it natural to wonder if one should also associate an entropy with the operator insertion itself, and consider the PETS as a tripartite state.

Specifically, instead of the density matrix $\rho = e^{-\frac{1}{2}\beta_{_R} H}\mathcal{O}e^{-\beta_{_L} H}\mathcal{O}e^{-\frac{1}{2}\beta_{_R} H}$ of the right QM system, we study instead consider the following class of mixed states

$$\rho \;=\; \sum_{i=1}^{K} e^{-\frac{1}{2}\beta_{_R} H}\mathcal{O}_i e^{-\beta_{_L} H}\mathcal{O}_i e^{-\frac{1}{2}\beta_{_R} H} \;\;=\;\; \sum_{i=1}^{K}$$

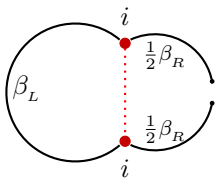

(2.91)

where we sum over $K \gg 1$ operators with dimensions $\ell_i \approx \ell$ constant. Since we assume that $\ell \sim N/\beta J \gg 1$, the scaling dimension is large and it is natural to expect a correspondingly large degeneracy K of operators with dimension close to ℓ. The density matrix (2.91) does not correspond to tracing out the left QM in a pure state in $\mathcal{H}_R \otimes \mathcal{H}_L$. In particular, the entropy is not the same for the right-QM or left-QM, $S_L \neq S_R$. One can add a Hilbert space associated to the operator $\mathcal{H}_{\rm op}$, with one basis element for each value of the index $i = 1, \ldots, K$. Then the state can be purified in the tensor product $\mathcal{H}_R \otimes \mathcal{H}_L \otimes \mathcal{H}_{\rm op}$. We will comment below on this tripartite structure of entanglement.

This generalization has a few motivations. First, taking K large makes it more straightforward to decide which contraction channel dominates in the correlator involved in the computation of the nth Renyi entropy. Take the entropy for the right CFT. In the large K limit one can see that the channel in the left panel of figure 2.8 dominates. This is true independently of $\beta_{_L}$ and

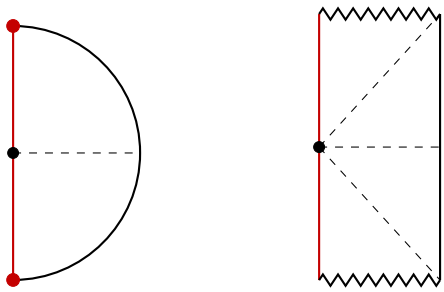

Figure 2.14: The euclidean and lorentzian space-time dual to the extremal partially entangled state (2.5) with $\beta_{_L} \to \infty$ and $\ell = k_{_R}$.

$\beta_{_R}$ as long as K is taken to be sufficiently large (but not larger than N). In this way we obtain

$$S_R \;=\; S_0 + 2\pi k = S_0 + \frac{\phi_R}{4G_N}. \tag{2.92}$$

Here $\phi_{_R}$ is a local minimum of the dilaton, but not necessarily the global minimum. On the other hand, repeating this analysis for the left QM gives

$$S_L \;=\; S_0 + 2\pi p = S_0 + \frac{\phi_L}{4G_N} \tag{2.93}$$

since now the opposite channel dominates. This should be contrasted with the entropy of pure PETS in which case the entanglement entropy in both cases is equal to the minimum between S_L and S_R.

In the type of states discussed in this section we have computed S_L and S_R. What is the maximal value of S_{LR}, the entropy of the left- and right system combined? Since the tripartite state living in the enlarged Hilbert space $\mathcal{H}_R \otimes \mathcal{H}_L \otimes \mathcal{H}_{\rm op}$ is pure, the entropy of the reduced density matrix on $\mathcal{H}_R \otimes \mathcal{H}_L$ is equal to the entropy of the density matrix on $\mathcal{H}_{\rm op}$, which in turn is bounded by the degeneracy of operators with scaling dimensions in the neighborhood of ℓ. We will call the log of this level density the spectral entropy S_ℓ. We will now argue in favor of the following inequality and equality

$$S_{LR} \leq S_\ell \qquad \text{with} \qquad S_\ell \;=\; 2\pi\ell. \tag{2.94}$$

To motivate this proposal, consider a PETS with a fixed $\beta_{_R}$ and take the limit $\beta_{_L} \to \infty$. In this limit $k_L \to 0$ and the left QM gets frozen to its ground state [17]. From the discussion in section 2.2 it is clear that if one takes $k_R = \ell$ then the end of the world brane sits on top of the right horizon as shown in figure (2.14). In this special situation, it is natural to associate an entropy to the object right at the horizon, the massive bulk particle, an entropy that is equal to the RT entropy. This leads to the formula $S_\ell = 2\pi k_R = 2\pi\ell$. A similar argument that motivates this proposal can be made using the results of [72].

We conjecture that the relation in equation (2.94) is also true for general values of $\beta_{_R}$ and $\beta_{_L}$. It would be indeed interesting to verify this conjecture, that (in the regime of large scaling dimension $\ell \simeq N/\beta J$) the SYK model has a universal level density of operators given by (2.94), from a microscopic viewpoint.

Note that this assignment is consistent with subadditivity and the Araki-Lieb inequality

$$|S_L - S_R| \leq S_{LR} \leq S_L + S_R. \tag{2.95}$$

Subadditivity is satisfied since $S_L + S_R \sim S_0$ which is trivially larger than $2\pi\ell$. One can check that strong subadditivity is also satisfied.

Using the quantities S_L, S_R and setting $S_{LR} = S_\ell = 2\pi\ell$, we can write the length of the throat (the distance between left- and right horizon) in terms of entropies

$$\cosh D_H \;=\; \frac{S_{LR}^2 + \tilde{S}_L^2 + \tilde{S}_R^2}{2\tilde{S}_L\tilde{S}_R}, \tag{2.96}$$

where we defined $\tilde{S} = S - S_0$. Similarly we can write the distance between the trajectory of the bulk particle and the right horizon as

$$\sinh D_2 \;=\; \frac{S_{LR}^2 + \tilde{S}_L^2 - \tilde{S}_R^2}{2S_\ell\tilde{S}_R} \tag{2.97}$$

[17] This is a slightly subtle argument since the SYK model has a large number of approximate ground states of order $e^{S_0} \sim e^N$. In any case we assume the dynamics of the left QM to freeze to one of its ground states.

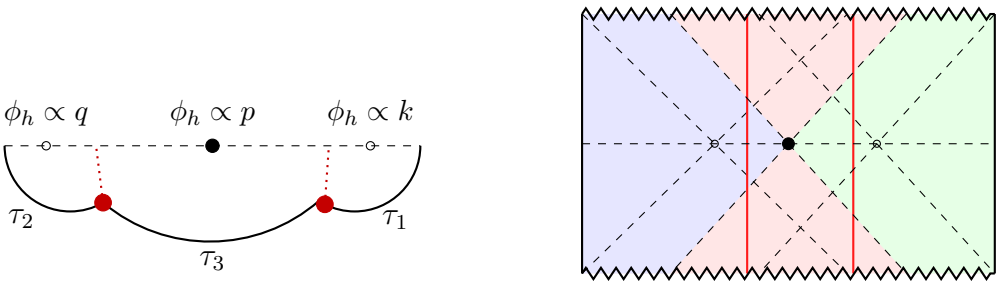

Figure 2.15: Backreaction by two operator insertions (red dots) with three local horizons (black circles and black dot). Assuming that $p < k, q$, the middle horizon is the extremal RT surface that separates the left- and right entanglement wedges, indicated by the blue and green regions on the right.

Requiring the $D_2 > 0$ implies that S_{LR} is always larger than the geometric mean of $S_L - S_R$ and $\tilde{S}_L + \tilde{S}_R$. This implies the Araki-Lieb inequality, which only becomes an equality in the case that $\tilde{S}_L = 2\pi k_L = 0$ and $S_R = 2\pi k_R = 2\pi\ell = S_\ell$.

As a final comment one can study bulk reconstruction in for these states, as in the previous section. Then if $\phi_L < \phi_R$ the right QM can only reconstruct its causal wedge (outside of the right horizon), which coincides with its entanglement wedge for these states. If one wants to reconstruct up to the left horizon using the right QM one needs to add the knowledge of the degrees of freedom creating the state, associated to the bulk brane. For the system $\mathcal{H}_R \otimes \mathcal{H}_{\text{op}}$ the entanglement wedge reaches the left horizon past the right interior, just like for the pure PETS considered above.

2.5.2 Mulitple operators

In this section we will generalize the previous analysis of PETS to multiple insertions. For simplicity we will begin with two insertions. Generalization to more operators is straight-forward.

We show the Euclidean part that produces the state in figure 2.15. To create this state we insert two operators of dimensions ℓ_1 at τ_1 and ℓ_2 at $\tau_1 + \tau_3$ and we define τ_2 such that $\tau_1 + \tau_2 + \tau_3 = \beta/2$. To each propagator for time τ_1, τ_2 or τ_3 we associate a momentum (horizon dilaton) $\tau_1 \to k$, $\tau_2 \to q$ and $\tau_3 \to p$ as shown in figure 2.15.

These dilaton values p, k, q are fixed by the saddle point equations describing the backreaction of JT gravity as explained in section 2.2. Repeating the analysis of the previous sections, or

equivalently applying the holographic prescription, we can compute the entanglement entropy of this state by

$$S = S_0 + 2\pi \, \min(p, q, k). \tag{2.98}$$

Depending on the choice of parameters different choices of horizon dilaton dominates. For the case of a single insertion this choice was simply determined by whether $\tau < \beta/4$ or $\tau > \beta/4$. In the two operator case we show a phase diagram as a function of time insertions τ_1 vs τ_2 in figure 2.16. This has an interesting behavior in terms of the 'tricritical' point that divides the three different regions. The location of the tricritical point can be found in terms of a transcendental equation derived from the saddle point relations, which should be solved numerically. In figure 2.16 we show the cases $\ell \to 0$ (left panel) and $\ell \to \infty$ (right panel) which can be analytically found. The phase diagram for intermediate ℓ interpolates between these extreme cases.

We can also consider 'multi'-partite states for which one averages over the microscopic choice of operators possible such that their dimensions are approximately ℓ_1 and ℓ_2. Following section 2.5.1 we imagine having a large number K of operators with dimensions $\ell_i \approx \ell$ for $i = 1, \ldots, K$. In a large K limit this controls the factorization channel that dominates the Renyi entropy calculation and gives

$$S_L = S_0 + 2\pi q, \qquad\qquad S_R = S_0 + 2\pi k. \tag{2.99}$$

We can compare these quantities with the entanglement entropy by looking at figure 2.16.

Another interesting feature of this kind of composite PETS is the following. Let us choose parameters such that the global minimum of the dilaton is located at the middle horizon, so that the entanglement entropy equals $S = S_0 + 2\pi p$. We choose ℓ large enough such that the two bulk particles are hidden behind the left and right horizons. Then, as opposed to figure 2.11, the extremal RT surface is outside the right and left causal wedges and has no overlap with it. This situation is shown on the right in figure 2.15. Still, following the discussion in section 2.4, left- or right observers with sufficient detailed understanding of the microscopic wave function would

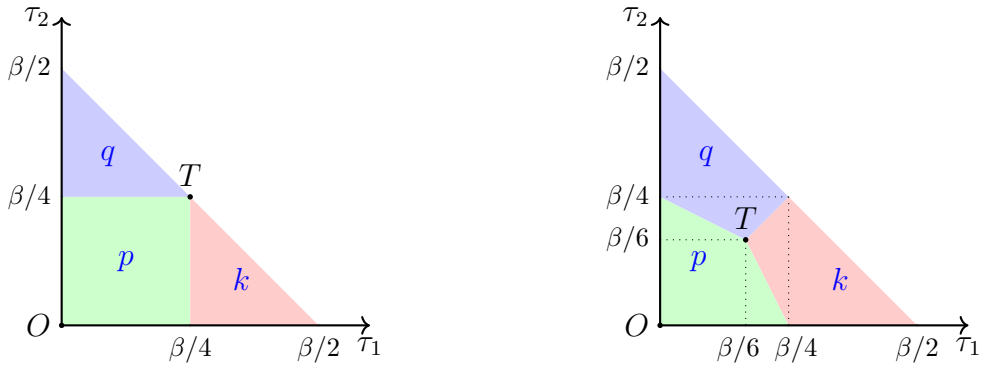

Figure 2.16: Left: Phase diagram near $\ell = 0$. T denotes the 'tri-critical' point. Right: Phase diagram near $\ell = \infty$. We see that the tri-critical point moves towards the origin.

be able to perform a one-sided bulk reconstruction of their full entanglement wedge, indicated by the green and blue regions in figure 2.15.

2.6 Appendix A : A Complete Basis of Partially Entangled States

In this Appendix we discuss a general class of partially entangled thermal states in SYK whose one-sided correlation functions coincide with their thermal expectation value while the two-side correlation functions and entanglement entropy can be different.

Consider $4N$ Majorana variables ψ^i spanning a 2^{2N} dimensonal Hilbert space. Introduce the basis of 2^{2N} states $|\mathbf{s}\rangle$ defined by

$$\left(\psi^{2k-1} - is_k\psi^{2k}\right)|\mathbf{s}\rangle = 0 \;\Leftrightarrow\; S_k|\mathbf{s}\rangle \equiv 2i\psi^{2k-1}\psi^{2k}|\mathbf{s}\rangle \;=\; s_k|\mathbf{s}\rangle\,. \tag{2.100}$$

We partition the $4N$ Majorana fermions into two groups of $2N$ Majorana fermions $\{\psi_{L,R}\}$, from which, two sub-Hilbert space $\mathcal{H}_{L,R}$ of dimension 2^N can be built. We consider a class of states

$$|\Psi\rangle \;=\; |\mathbf{s};\beta_{_L},\beta_{_R}\rangle = e^{-\frac{1}{2}\beta_{_L}H_{_L}}\otimes e^{-\frac{1}{2}\beta_{_R}H_{_R}}|\mathbf{s}\rangle\,, \tag{2.101}$$

where $H_{_{L,R}}$ are Hamiltonian of the same form acting on $\mathcal{H}_{_{L,R}}$ respectively. By choosing different

partitions, we can obtain a class of states. with different amount of entanglement between $\mathcal{H}_{_L}$ and $\mathcal{H}_{_R}$. The thermo-field double is the state for which everything is transmitted and for which all $s_k = 1$. There are 2^N other states with the same amount of entanglement as the TFD state. For generic states (2.101), K fermion pairs are reflected back and $N - K$ fermion pairs are transmitted from the left to the right system. These states are all partially entangled thermal states with entanglement entropy between zero (product states) and the thermal entropy (TFD type states).

We denote the operator that flips the sign of ψ_k by σ_k. Note that $\sigma_k H_{_{L,R}} \sigma_k^{-1} = H_{_{L,R}}$ after averaging over the random SYK couplings. The inner products of these PETS do not depend on the partition

$$\begin{aligned}\langle\Psi|\Psi\rangle &= 2^{-2N}\sum_k \langle \mathbf{s}|\sigma_k^{-1} e^{-\frac{1}{2}\beta_{_L} H_{_L} - \frac{1}{2}\beta_{_R} H_{_R}} \sigma_k \sigma_k^{-1} e^{-\frac{1}{2}\beta_{_L} H_{_L} - \frac{1}{2}\beta_{_R} H_{_R}} \sigma_k |\mathbf{s}\rangle \\ &= \mathrm{Tr}[e^{-\beta_{_L} H_{_L}} \otimes e^{-\beta_{_R} H_{_R}}] \;=\; Z(\beta_L) Z(\beta_{_R})\,. \end{aligned} \tag{2.102}$$

The one-sided two-point correlators are

$$G_{\rm diag}(\tau_1,\tau_2) \;\equiv\; \frac{\langle\Psi|\psi^i(\tau_1)\psi^i(\tau_2)|\Psi\rangle}{\langle\Psi|\Psi\rangle} = G_{\beta_{_{L,R}}}(\tau_1-\tau_2), \qquad \text{if } \psi^i \in \{\psi_{_{L,R}}\}\,, \tag{2.103}$$

which is the same as the thermal expectation value of the temperature associated to the subsystem and does not depend on the details of the partition. The temperature can be different in general. We can also compute off-diagonal two-point functions. Only the combination $s_k\psi^{2k-1}\psi^{2k}$ has nontrivial expectation value at leading order. Using that it is flip invariant, we compute

$$G_{\rm off}(\tau_1,\tau_2) \equiv s_k \frac{\langle\Psi|\psi^{2k-1}(\tau_1)\psi^{2k}(\tau_2)|\Psi\rangle}{\langle\Psi|\Psi\rangle} \;=\; -2iG_{\beta_{_L}}(\tau_1+\tfrac{1}{2}\beta_{_L})G_{\beta_{_R}}(\tau_2+\tfrac{1}{2}\beta_{_R})\,. \tag{2.104}$$

If ψ^{2k-1}, ψ^{2k} belong to the same partition, the correlation function can be interpreted as one-sided off-diagonal correlation function. If they belong to different partition, the correlation function can be interpreted as a two-side correlation function and ψ^{2k-1} is the counterpart of ψ^{2k} at the

other side.

2.7 Appendix B : Bulk Kinematics and Dynamics

2.7.1 Kinematics

We will summarize the coordinate systems we use to describe AdS_2. It is useful to work in embedding space $Y = (Y^{-1}, Y^0, Y^1)$. The metric is $ds^2 = \eta_{AB} dY^A dY^B$ with the inner product $Y_1 \cdot Y_2 = \eta_{AB} Y_1^A Y_2^B$. Then by restricting to $Y \cdot Y = -1$ we obtain Euclidean AdS_2 if $\eta = \mathrm{diag}(-1, 1, 1)$ or Lorenzian AdS_2 if $\eta = \mathrm{diag}(-1, -1, 1)$. For definiteness we will focus in Euclidean signature.

A first set of convenient coordinates are (ρ, τ) such that

$$Y = \pm(\cosh\rho, \sinh\rho\sin\tau, \sinh\rho\cos\tau) \tag{2.105}$$

In these coordinates the metric of AdS_2 is

$$ds^2 = d\rho^2 + \sinh^2\rho\, d\tau^2. \tag{2.106}$$

This covers the Rindler patch when analytically continued to Lorenzian signature $\tau \to it_R$. Another choice of coordinates parametrizes the hyperboloid as

$$Y = \pm\left(\frac{1+x^2+y^2}{1-x^2-y^2}, \frac{2x}{1-x^2-y^2}, \frac{2y}{1-x^2-y^2}\right) \tag{2.107}$$

This gives polar coordinate for the plane $(x, y) = (r\cos\theta, r\sin\theta)$. The metric is

$$ds^2 = \frac{dx^2+dy^2}{1-x^2-y^2} \tag{2.108}$$

Then AdS_2 is mapped to the Poincare disk $x^2+y^2 < 1$. To compare with the Rindler parametriza-

tion one can take $\theta = \tau$ and $r \equiv \sqrt{x^2 + y^2} = \tanh \rho/2$.

Finally one can define coordinates giving the Poincare patch of AdS as

$$Y = \pm \left(\frac{1 + t^2 + z^2}{2z}, \frac{t}{z}, \frac{1 - t^2 - z^2}{2z} \right) \tag{2.109}$$

this gives the metric $ds^2 = z^{-2}(dt^2 + dz^2)$.

In any coordinate system, geodesic distance between two points can be computed as $\cosh D_{12} = -Y_1 \cdot Y_2$. This can be rewritten in any of the coordinates above. Geodesics in this geometry are parametrized by a ray X in embedding space and is given by Y such that

$$X \cdot Y = 0. \tag{2.110}$$

2.7.2 Dynamics

We summarize the classical solutions of JT gravity in terms of embedding coordinates following and using the notation of [13]. It is then straightforward to translate results to any coordinate system described in the previous section according to convenience. Since the effective coupling is proportional to the combination ϕ_b/G_N involving the boundary dilaton we will take a dilaton normalization such that $8\pi G_N = 1$ without loss of generality (since in 2D G_N is dimensionless).

The dilaton in regions without matter behaves as [12] [13] [15]

$$\phi(Y) = Z \cdot Y, \quad \text{for } Y^2 = -1 \tag{2.111}$$

where Z is an arbitrary vector in embedding space. Natural boundary conditions for JT gravity giving boundary gravitons described by the Schwarzian action fixes metric and dilaton. Then the boundary is described by $Z \cdot Y = \phi_b = \phi_r/\epsilon$, where ϵ denotes the cut-off. This describes a circle (set of points at fixed geodesic distance from a center) in AdS_2. The center of this circle coincides to the horizon, where the value of the dilaton is minimal. It is easy to find this location

as

$$Y_h = (-Z \cdot Z)^{-1/2} Z, \qquad \phi_h = (-Z \cdot Z)^{1/2}. \tag{2.112}$$

To summarize, the sourceless solution is fixed by a three-component vector in embedding space $\mathbb{R}^{2,1}$. Its direction fixed the location of the horizon and its magnitude fixes the horizon dilaton. Moreover for a fixed Z the boundary curve has length β/ϵ (where ϵ denotes the cut-off) with inverse temperature β related to the magnitude of Z (or equivalently ϕ_h) as $\phi_h = \frac{2\pi}{\beta}\phi_r$. In this units, the Bekenstein-Hawking entropy of this geometry is $S = 2\pi\phi_h$. Finally, the ADM energy is $E = \phi_h^2/(2\phi_r)$. By adding a topological term to the action $\int d^2x\ \phi_0 R$, with ϕ_0 constant, one can account for a possible zero-point entropy S_0.

These boundary trajectories of constant $Z \cdot Y$ correspond to circles in the Poincare disk coordinates (x, y). Therefore it is natural to draw the backreacted boundary in the Poincare disk coordinates such as figure 2.3 or 2.6 (nevertheless these coordinates distort the size and location of the origin with respect to the flat (x, y) plane).

From the 2D Liouville perspective of the Schwarzian theory [24] (see [25] for more details) the horizon dilaton ϕ_h corresponds to the momentum $k = \phi_h$ associated to a primary state of Liouville with energy $E = k^2/(2C)$, with $C = \phi_r$ in units with $8\pi G_N = 1$. This is a natural variable to label intermediate states.

Using these identifications and coordinates defined above it is a straightforward exercise to get the equations and relations presented in section 2.2.

The $SL(2, R)$ charge of a given solution is also fixed by the vector Z as $Q = 2Z$ [13]. Then one can interpret the boundary trajectory as a particle in a magnetic field [54]. More importantly this allows to add matter in a straightforward way. Within the JT approximation of free matter bulk particles propagate along geodesics $Q_{\rm m} \cdot Y = 0$ with the space-like vector $Q_{\rm m}$ giving the $SL(2, R)$ charge of the particle, normalized by the mass square $Q_m^2 = \mu^2$. Then one can glue bulk solutions labeled by $Z = Q_L/2$ and $Z = Q_R/2$ along the particle geodesic with the singlet constrain

$$Q_L + Q_R + Q_m = 0. \tag{2.113}$$

This charge conservation constrain has the nice property of making the dilaton ϕ continuous along the matter geodesic. But the dilaton slope jumps proportional to its mass

$$\frac{\partial\phi}{\partial s}\Big|_L - \frac{\partial\phi}{\partial s}\Big|_R = 2\mu, \tag{2.114}$$

in a particle's rest frame where $Q_{\text{matter}} = (0, 0, \mu)$. In this notation, the mass of the particle $\mu = \ell$ (for large ℓ), the dimension of the dual operator. s is a geodesic length in the direction perpendicular to the particle's geodesic. This is consistent with the equations of motion that come from varying the metric which relates the matter stress tensor with the second derivative of the dilaton.

Chapter 3

Classifying Boundary Conditions in JT Gravity

In recent years, two-dimensional Jackiw-Teitelboim (JT) gravity has emerged as an important toy model for quantum gravity and near-horizon physics [19, 18, 10, 12, 14, 56, 13, 15, 33]. As we have discussed in the introduction, the simplicity of this model allows for a detailed analytic analysis, which covers not only perturbative features of gravity [13], but also non-perturbative ones, such as the sum over topologies [33]. However, most of these discussions focused on a particular set of boundary conditions that fix the asymptotic value of the dilaton and metric. Such boundary conditions can be taken to be part of the definition of the theory, and one might wonder whether there are other boundary conditions that one can impose and explore what new features they exhibit.

The analysis of different boundary conditions in gravity is, of course, not new. In the past, it has been the subject of various studies [73, 74]. Nevertheless, the focus there was mostly on gravity theories in three or more space-time dimensions where the full quantization of the theory is not well understood. The purpose of this chapter is to understand the role of boundary conditions in two-dimensional gravity and, in particular, in JT gravity, where the quantization of the theory is possible at the level of the path integral. The study of these different boundary

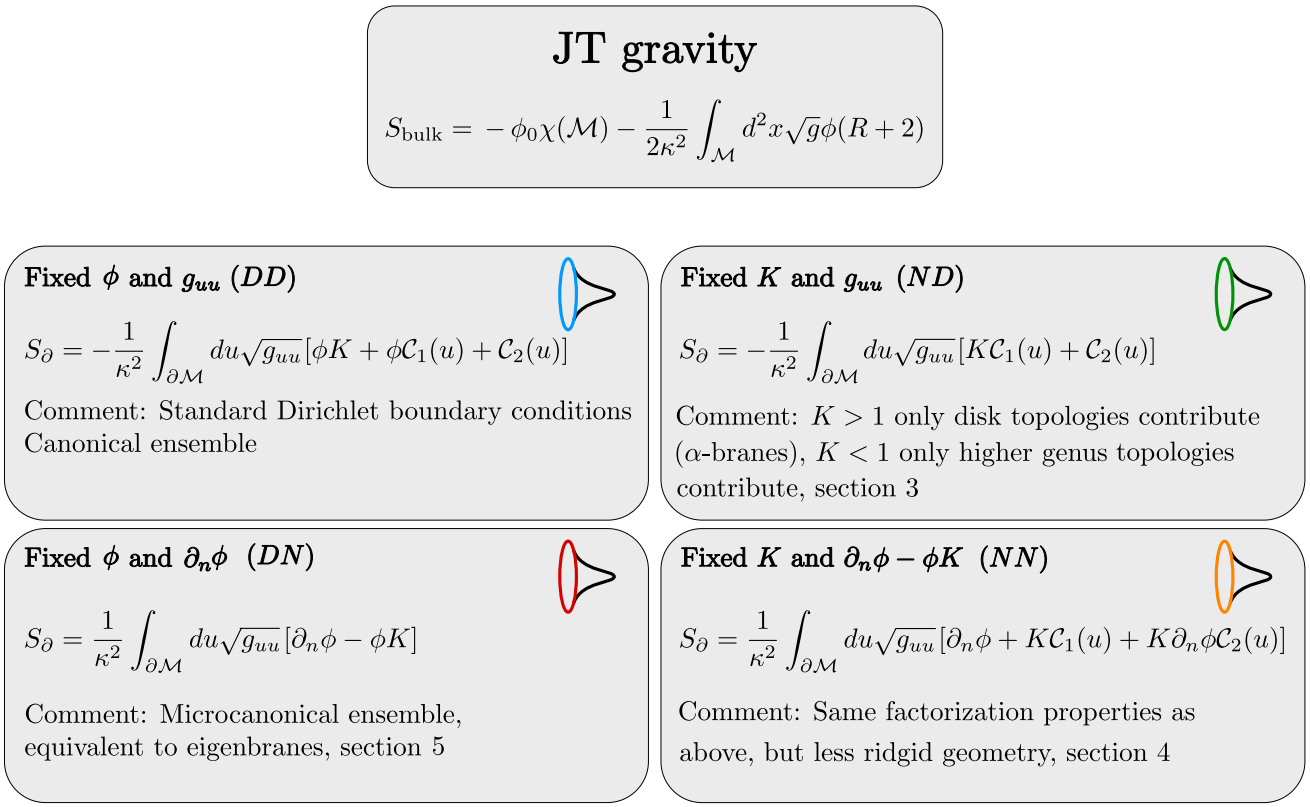

Figure 3.1: Summary of the boundary conditions considered in this chapter. On the left column, one can see the boundary conditions for fixed dilaton ϕ (D) on the boundary, whereas the right column is for fixed K, i.e., Neumann boundary conditions on the dilaton (N). This is indicated by the first letter of the two letters in brackets. The rows are analogous, but then for the boundary metric g_{uu} and is specified in the second letter in brackets.

conditions can reveal various aspects of the theory that are hard, or even impossible, to study in the (by now standard) Dirichlet boundary conditions for the metric and dilaton.

As we will explain, JT gravity admits four inequivalent boundary conditions obtained by fixing combinations between the dilaton ϕ and boundary metric g_{uu} or their canonical momenta, schematically given by the extrinsic curvature K and the derivative of the dilaton $\partial_n\phi$ normal to the boundary, respectively. The properties and features of these boundary conditions are summarized in figure 3.1.

To exemplify and compare many of these features, we start by reviewing past results in the standard Dirichlet-Dirichlet (DD) boundary condition where the dilaton ϕ and the boundary metric g_{uu} are fixed, when the cosmological constant in JT gravity is set to be negative. In the

limit in which the value of the dilaton and the proper length of the boundary is large (the so-called Schwarzian limit), such boundary conditions correspond to the thermal canonical ensemble for the near-extremal black holes whose dynamics can be captured by JT gravity [13, 75, 59, 76–79]. [1] Consequently, one might wonder what role other boundary conditions in JT gravity play when describing the near-horizon physics of near-extremal black holes. The other boundary condition whose meaning is clear fixes $\partial_n\phi$ instead of g_{uu} (DN). Such a boundary condition corresponds to the micro-canonical ensemble for the near-extremal black holes: instead of fixing the temperature of the system (which is the case when fixing g_{uu}) we fix the ADM mass of the black hole (which in dilaton gravity is given by $\partial_n\phi$). When setting K instead of ϕ (ND or NN), the black hole interpretation is somewhat unclear. In such a case, we find that the dilaton solution cannot be fully fixed.[2] Therefore, the classical solutions do not exhibit the presence of a horizon and, consequently, such boundary conditions do not have any thermodynamical interpretation.

When accounting for corrections from manifolds with other topologies, the partition function with the standard boundary conditions is reproduced by the insertion of the "partition function" operator $\mathrm{Tr}e^{-\beta H}$ in a specific double-scaled matrix integral which averages over the "Hamiltonians" H [33, 80, 81]. Because of this interpretation as an ensemble average, or equivalently, due to the contribution from geometries that connect different boundaries, the partition function of the gravitational theory does not factorize when studying configurations with multiple boundaries. To improve the dictionary between gravity and its matrix integral "dual", we should determine what operator insertion on the matrix integral side corresponds to studying the three other previously mentioned boundary conditions in JT gravity. For instance, if instead of fixing g_{uu}, we fix $\partial_n\phi$, we find that the matrix operator insertion required for considering such boundaries is equivalent to the energy-eigenbranes (i.e. for n boundaries, we fix n eigenvalues of the random matrix H to the ADM masses specified by $\partial_n\phi$ on each border) recently studied in [82]. Once

[1] Such black holes have their horizon located where the value of the dilaton (which captures the volume of the transverse space) is minimized.

[2] As we shall explain, the classical dilaton solution is fixed up to three undetermined constants. For DD or DN boundary conditions, these constants are fixed by the fact that ϕ is fixed on the boundary. For ND and NN boundary conditions, all three constants cannot be fixed.

again, we find that the partition function of the theory with such boundary conditions does not factorize.

Since both the DD and DN boundary conditions exhibit this feature, we can consequently ask whether there are other boundary conditions in JT gravity for which we instead have a factorizable multi-boundary partition function. As we shall explain shortly, when appropriately fixing K (instead of the boundary value of the dilaton ϕ), we will show that the multi-boundary partition function factorizes. Specifically, when setting $K > 1$, we find that the multi-boundary partition function only receives contributions from geometries with disk topology and, therefore, factorizes.[3] In the context of the baby universe Hilbert space discussed in [86–89], such boundaries can naturally be called α-eigenbranes; i.e. states that have a clear geometric meaning, such as the Hartle-Hawking state, are eigenfunctions of the operators corresponding to such boundary insertions. This should be contrasted with the case of the DD or DN boundary conditions for which the α-states are an infinite linear combination of geometric states which can have an arbitrary number of boundaries. As opposed to $K > 1$, for $K < 1$, we find that the partition function receives no contribution from disk topologies, and only higher genus or connected multi-boundary geometries contribute.[4]

Another related direction that we study concerns the definition and quantization at finite cutoff. For the standard Dirichlet-Dirichlet boundary condition the quantization of the theory with finite proper length and dilaton value was studied in [90, 91]. However, the exact quantization of the theory for all values of the proper length remains ambiguous: in [90] non-perturbative corrections in the proper length to the partition function could not be fixed, while in [91] it was found that for small enough proper lengths, there is no effective theory which can describe the dynamics of the boundary. Furthermore, neither of these works fully accounted for the

[3]When coupling the theory to matter (which we can take to couple solely to the metric, and not to the dilaton), our conclusions regarding the factorization of the multi-boundary partition functions for $|K| > 1$ remains unchanged. In the context of black holes and in the presence of matter, the existence of Euclidean wormholes that connect different boundaries has been crucial to reproducing the Page curve predicted by requirements of unitarity [83–85]. Nonetheless, since the ND or NN boundary conditions do not have solutions that contain a clear horizon, the interpretation of the gravitational theory in terms of black hole physics is now unclear.

[4]Throughout this chapter, we shall focus on the case with $K > 0$.

contributions from higher genus geometries. As we shall explain shortly, due to the rigidity of two-dimensional hyperbolic space, by fixing K instead of ϕ, the theory is easy to define at finite cutoff, and its partition function can be computed in a genus expansion.

JT gravity, this time with a positive cosmological constant, has recently been used as a cosmological toy model [92–94]. When computing expectation values of operators within this setting, one could use the path integral in the gravitational theory to prepare the density matrix of the system [92, 84, 94, 95]. Thus, one is typically interested in computing the path integral for both connected and disconnected geometries in the presence of two or more boundaries. If one fixes the standard Dirichlet-Dirichlet boundary condition, the contribution of connected geometries, some of which are called bra-ket wormholes, resolves an inconsistency in the entropy of the theory when coupled to matter [84, 94]. Since the connected geometries play such an important role, one can ask, just like in the case of AdS_2, whether there exist boundary conditions which disallow the existence of such connected manifolds with multiple boundaries. Once again, we find that by appropriately fixing K (this time, $K < 1$) the path integral which prepares the density matrix in the gravitational theory does not receive contributions from connected geometries, and, in particular, from the bra-ket wormhole geometries. Such boundary conditions, where one fixes g_{uu} in addition to K, are in fact, quite natural in higher-dimensional models of cosmology [96]; in such a case, one fixes the trace of the extrinsic curvature K and the conformal metric. K can then be taken to be a clock (called York time) that parametrises the slices in the bulk.

3.1 A classification of boundary conditions

We reviewed the results for the Dirichlet-Dirichlet boundary conditions in Section 1.2, we will now consider JT gravity with alternative boundary conditions. For each case, we will conduct both a classical and quantum analysis similar to the Dirichlet-Dirichlet case, briefly discussed above. However, as opposed to the Dirichlet case, for several boundary conditions that we study,

we will easily be able to go beyond the nearly-AdS_2 limit, to a finite patch of AdS_2.

To start our analysis, we first review the variation of the bulk action (see also appendix 3.6 for details) and map out all different boundary conditions consistent with a well-defined variational problem together with the appropriate boundary terms. We point out that there are two different sets of conjugate variables that are natural to consider, giving, in total 6 different type of boundary conditions, of which only 4 are physically inequivalent. In subsequent sections we will then discuss these boundary conditions (excluding the standard Dirichlet case) in more detail, not only classically, but also quantum mechanically.

The bulk action for JT gravity was given in (1.14) and in appendix 3.6 we review its variation. The variation of this bulk term is given by,

$$\delta S_{\text{bulk}} = -\text{EOM} - \int_{\partial\mathcal{M}} du\sqrt{h}\left([(\partial_n\phi)h^{\mu\nu} - \phi K^{\mu\nu}]\,\delta h_{\mu\nu} - 2\phi\delta K\right)\,, \tag{3.1}$$

where EOM refers to the equations of motion in (1.15), $h_{\mu\nu}$ is the induced boundary metric and K is the trace of the extrinsic curvature. We can reduce to two dimensions $K^{\mu\nu} = Kh^{\mu\nu}$ and express the boundary metric in terms of the variable g_{uu}

$$g_{uu} = h_{\mu\nu}t^\mu t^\nu \qquad \Leftrightarrow \qquad ds^2 = h_{\mu\nu}dx^\mu dx^\nu = g_{uu}du^2\,, \tag{3.2}$$

with t^μ a tangent vector to the boundary of $\mathcal{M}$. This results in

$$\delta S_{bulk} = -\text{EOM} - \int_{\partial\mathcal{M}} du\left([2\left(\partial_n\phi - \phi K\right)]\,\delta\left(\sqrt{g_{uu}}\right) - [2\phi\sqrt{g_{uu}}]\,\delta K\right)\,. \tag{3.3}$$

From this we immediately recognize the following canonically conjugate pairs

$$\begin{aligned}\phi\sqrt{g_{uu}} \quad &\leftrightarrow \quad K\,,\\ \sqrt{g_{uu}} \quad &\leftrightarrow \quad \partial_n\phi - \phi K\,,\end{aligned} \tag{3.4}$$

Our convention is to denote the left side of the pairs in (3.4) to be associated to the coordinates while the right side are the canonical momenta. Fixing the coordinate means a Dirichlet boundary condition, which we will abbreviate with D, whereas for fixing the canonical momentum, we will use N to denote a Neumann boundary condition. As we will discuss below the choice of canonical conjugates pairs is not unique and it is interesting to study the spectrum of choices.

At the level of the path integral it is natural to study the case in which one fixes on the boundary either one of the two sides of the two canonical pairs in (3.4). This allows us to study the following four possible boundary conditions and the boundary terms required in order for the problem to have a well defined variational principle:

DD : Fixed ϕ and g_{uu}

This is the standard JT gravity theory with Dirichlet boundary conditions. In this case, we require the addition of a boundary term [5]

$$S_{DD} = S_{\text{bulk}} - 2\int du\,\sqrt{g_{uu}}\,[\phi K + \mathcal{M}_1(u)\phi + \mathcal{M}_2(u)]\ . \tag{3.5}$$

Here, $\mathcal{M}_1(u)$ and $\mathcal{M}_2(u)$ are arbitrarily fixed functions that do not affect the equation of motion. Thus, they serve as possible counter-terms to be added to the Euclidean path integral. In the usual JT gravity literature it is customary to take these to be $\mathcal{M}_1(u) = -1$ and $\mathcal{M}_2(u) = 0$ which fixes the vacuum energy of the equivalent boundary Schwarzian theory to be 0 and renders the on-shell action finite.

[5]Below, when writing $S_{DD/ND/DN/NN}$ we are not including the topological term in (1.12). The variational problem for this term will be discussed at the end of this section.

ND : Fixed K and g_{uu}

In this case one does not require an additional boundary terms. possible counterterms which do not affect the equations of motion are given by

$$S_{ND} = S_{\text{bulk}} - 2\int du\,\sqrt{g_{uu}}\,(K\mathcal{M}_1(u) + \mathcal{M}_2(u))\ . \tag{3.6}$$

When both $\mathcal{M}_1(u) = 0$ and $\mathcal{M}_2(u) = 0$ the equivalent $\mathfrak{sl}(2,\mathbb{R})$ gauge theory is purely topological.

NN : Fixed K and $(\partial_n\phi - \phi K)$

In this case the additional boundary term is

$$S_{NN} = S_{\text{bulk}} + 2\int du\,\sqrt{g_{uu}}\,(\partial_n\phi - \phi K)\ . \tag{3.7}$$

If we again specialise to $(\partial_n\phi - \phi K)$ constant, the boundary action is proportional to the length of the boundary. However, since we are not fixing the boundary metric $\sqrt{g_{uu}}$, if we do choose $(\partial_n\phi - \phi K)$ and $K(u)$ to not be a constant (but rather depend on u) we have to specify how to choose the parametrization of the boundary time. One can for instance choose to fix a boundary diffeomorphism gauge in which $\sqrt{g_{uu}} =$ constant and $u \to [0, 2\pi]$, without fixing the diffeomorphism invariant proper length. In such a case the boundary observer specifies the 2π periodic functions $(\partial_n\phi - \phi K)$ and $K(u)$.[6]

[6]Alternatively, if we do not fix a boundary diffeomorphism gauge we can specify the values of $K(u)$ and $(\partial_n\phi - \phi K)(u)$ according to the boundary proper length from a given boundary point. While this makes sense in Lorentzian signature, in Euclidean signature where the boundary is periodic, the proper boundary length is no longer fixed and therefore we do not know the periodicity of the functions $K(u)$ and $(\partial_n\phi - \phi K)(u)$. Furthermore, if we do not choose to fix boundary diffeomorphisms we see that there is no consistent diffeomorphism invariant counter-term that could be added to the action.

DN : Fixed* $\phi\sqrt{g_{uu}}$ *and* $(\partial_n\phi - \phi K)$

In this case, both the boundary terms need to be added

$$S_{DN} = S_{\rm bulk} + 2\int \sqrt{g_{uu}}\,(\partial_n\phi - 2\phi K + \phi\,\mathcal{M}_1(u) + (\partial_n\phi - \phi K)\phi\,\mathcal{M}_2(u))\ . \tag{3.8}$$

where $\mathcal{M}_1(u)$ and $\mathcal{M}_2(u)$ represent the possible counter-term whose variation vanishes.

An alternate set of conjugate variables can be obtained by rewriting (3.3) as,

$$\delta S_{\rm bulk} = \int du\,([2\phi]\,\delta\,(\sqrt{g_{uu}}K) - [2\,(\partial_n\phi)]\,\delta\,(\sqrt{g_{uu}}))\ . \tag{3.9}$$

With this choice, the pair of canonical conjugates pairs are given by

$$\begin{aligned} \phi &\leftrightarrow \sqrt{g_{uu}}K\,, \\ \sqrt{g_{uu}} &\leftrightarrow \partial_n\phi\,. \end{aligned} \tag{3.10}$$

Using this pair of canoncial variables two alternative boundary conditions follow:

NN: Fixed* $\sqrt{g_{uu}}K$ *and* $(\partial_n\phi)$

In this case the additional boundary term is

$$S_{NN^*} = S_{bulk} + 2\int du\,\sqrt{g_{uu}}\,[\partial_n\phi + \mathcal{M}_1(u)K + (K\partial_n\phi)\mathcal{M}_2(u)]\ . \tag{3.11}$$

Again, $\mathcal{M}_1(u)$ and $\mathcal{M}_2(u)$ represent the possible counter-terms.

DN: Fixed ϕ and $(\partial_n\phi)$

In this case, two boundary terms need to be added in order to cancel the variation in (3.9)

$$S_{DN^*} = S_{bulk} + 2\int du\sqrt{g_{uu}}\left(\partial_n\phi - \phi K\right) . \tag{3.12}$$

As in the case of NN boundary conditions there are no possible counter-terms which are invariant under boundary diffeomorphisms.

We can also analyze the variation of the topological term in (1.12). On the one hand, because the bulk plus boundary terms in the action is invariant under metric fluctuations (since the action solely depends on the Euler characteristic of the manifold), it is clear that the variation should vanish regardless of the boundary conditions that we imposed. On the other hand, explicitly checking that the boundary term of the topological term arises from consistency with the variational principle serves as a non-trivial consistency check. Following 3.3, the variation of the bulk topological term is

$$\delta S_{\text{top, bulk}} = -\text{EOM} + \int_{\partial\mathcal{M}} du\left[2\phi_0 K\delta\left(\sqrt{g_{uu}}\right) + 2\phi_0\sqrt{g_{uu}}\delta K\right] . \tag{3.13}$$

With the addition of the boundary topological term the variation of S_{top} always vanishes regardless of whether we set $\delta K = 0$, $\delta\sqrt{g_{uu}} = 0$ or $\delta(\sqrt{g_{uu}}K) = 0$.

In summary, we have listed 6 boundary conditions for JT gravity, which, in fact are also valid for any other dilaton gravity. However, since we only have two pairs of conjugate variables, it suffices to study four of them or three actually as we will not consider the standard Dirichlet case here. Below we will therefore consider the boundary conditions ND, NN and DN in more detail. We will study the associated classical solutions space, the quantum theory, coupling to matter and comment on the physical aspects of the boundary conditions and what properties of JT gravity they probe.

3.2 Fixing K and g_{uu}: towards factorization

The fixed K boundary conditions have a less clear interpretation from the "boundary dual" point of view.[7] Still, JT gravity with these boundary conditions is a rich theory that allows us, as we will show, to turn on (leading to factorization) or off (leading to an ensemble average) the sum over topologies depending on the value of the extrinsic curvature. As we shall explain below, in the particular case when $K = 0$, the partition function of JT gravity is given by the Weil-Peterson volumes whose recursion relation was determined by Mirzakhani [37, 97]. Thus, the results for the partition function with boundaries given by different values of K and g_{uu} can be viewed as a generalization of the results previously obtained in the mathematical literature.

3.2.1 Classics

Before we begin our classical analysis, we emphasize that, as opposed to the Dirichlet boundary conditions reviewed in section 3.1, or to the micro-canonical boundary conditions which we will study in section 3.4 [33], the fixed K and g_{uu} boundary conditions allow for the existence of richer on-shell higher topology or multi-boundary solutions.[8]

With this in mind, we start by studying solutions when $K \equiv k$ is fixed to a constant. To understand such solutions we provide three different perspectives. The first is purely geometric and reviews the classification of constant K curves on the Poincaré plane or disk and on its quotients. The second explicitly solves for fixed K curves by working in the Fefferman-Graham gauge for the metric. Using this metric, it becomes clear why fixing $|k| > 1$ solely isolates disk topologies while $|k| < 1$ isolates topologies with a higher genus or a higher number of boundaries. Finally, in our third approach we will again solve for curves of constant K, this time reformulating JT gravity as a $PSL(2, \mathbb{R})$ BF theory. This latter perspective allows us to

[7] Such boundary conditions are however very natural to consider in the context of cosmology, where one can take K to be a clock (called York time) that parametrises slices in the bulk. In the current context, however, we have a time-like boundary and we cannot use this intuition.

[8] This is because in the previously studied cases the problem with the existence of such solutions stemmed from imposing a boundary value of the dilaton and from imposing the dilaton equation of motion in the bulk. In this section, since we do not fix the boundary value of the dilaton, we can always study the trivial (but not necessarily unique) solution $\phi(x) = 0$.

study the case with varying $K \equiv k(u)$. In particular, we show that such solutions can in turn be mapped to solutions of the Hill equation whose classification has been extensively studied.

A geometric construction

Before explicitly solving for curves of constant $K = k$ on the hyperbolic plane, it is useful to develop a geometric intuition that will be made concrete through the explicit computations in the next subsection. Just as in flatspace, curves with constant k are circles in the Poincaré half-plane or disk. The circles in the Poincaré half-plane can be classified by their relation to the axis that bounds the half-plane (or on the Poincaré disk by their relation to the boundary of the disk):

- **Geodesics** ($k = 0$). As is well known the geodesics of hyperbolic space are the semi-circles perpendicular to the axis (or the boundary circle of the Poincaré disk).
- **Hypercycles** ($|k| < 1$) are the circles that intersect the boundary at exactly two points. An alternative definition that we will make use of is that it is the locus whose points have the same orthogonal distance from a given geodesic.
- **Horocycles** ($|k| = 1$) are the circles which are tangent to the boundary of the Poincaré half-plane or disk.
- **Curves of interest.** ($|k| > 1$) are the circles which are fully contained in the Poincaré half-plane or in the disk.

We show examples of such curves in figure 3.2. We will for now focus on $k \geq 0$. Since curves with $k < 1$ always intersect the boundary of hyperbolic space we can therefore never have a disk geometry whose boundary has $k < 1$ at every point. Therefore, solutions with disk topology only exist for $k > 1$.

We now explain why a stronger statement also follows from the above classification: when $0 \leq k < 1$, solely higher topology or multi-boundary geometries contribute, while if $k > 1$ only

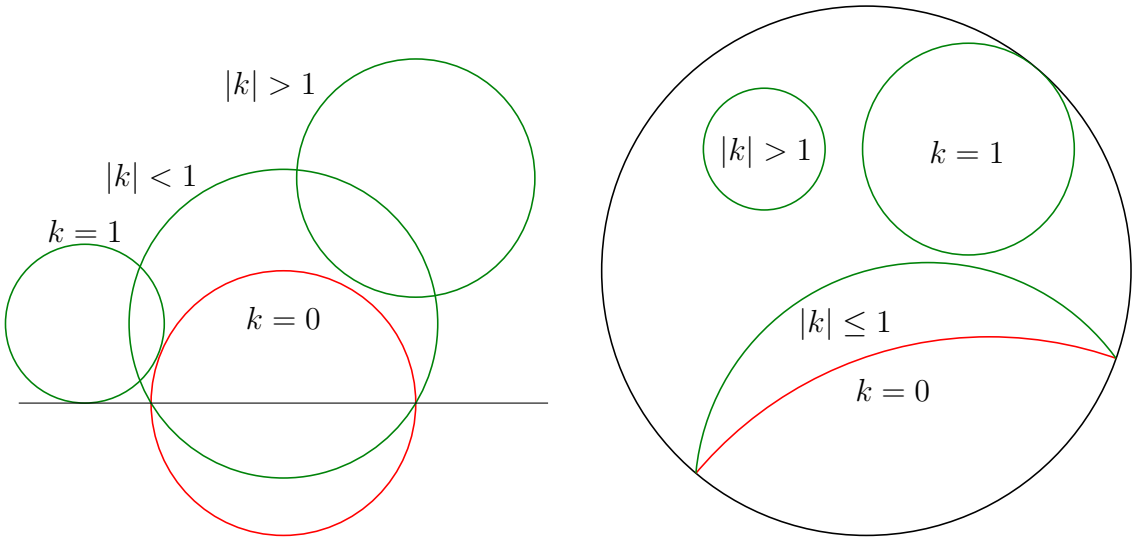

Figure 3.2: Figure showing the different curves of constant k in the Poincaré plane and disk. The sign of k is dependent on the direction of the normal vector perpendicular to the boundary; for instance, for $|k| > 1$, $k > 1$ is the boundary of the compact space (the disk), and $k < -1$ is the boundary of the non-compact space (the outside of the disk). In this chapter, we will focus on $k > 0$ to simplify our higher genus analysis.

the disk topology contributes. To do this, we first note that in order to construct higher genus or multi-boundary surfaces we need to glue a bordered higher genus Riemann surface whose boundaries are all closed geodesics to "trumpets". Such "trumpets" on one side have a closed geodesic, while on the other they have the fixed K and g_{uu} boundary that we are interested in. Thus, in order to understand the higher genera or multi-boundary case we need to study the possible boundaries that can be present on one end of the trumpet. To construct the trumpet, we consider the $\mathbb{Z}$ quotient of hyperbolic space by identifying two geodesics (for instance G_1 and G_2 in Figure 3.3). Then, the trumpet is identified as the (top) patch separated by the three geodesics G_0, G_1, and G_2, where G_0 is perpendicular to both G_1 and G_2. Thus, on the trumpet, G_0 is the closed geodesic whose length, b, is the distance between the geodesics G_1 and G_2. To construct the other boundary of the trumpet, we need to consider a fixed $K = k$ curve that intersects G_1 and G_2 at an equal distance from the intersection points between these two geodesics and G_0 (the red points in figure 3.3). Furthermore, in order for the fixed $K = k$ curve to be smooth when taking the $\mathbb{Z}_2$ quotient, the curve of fixed $K = k$ should be perpendicular

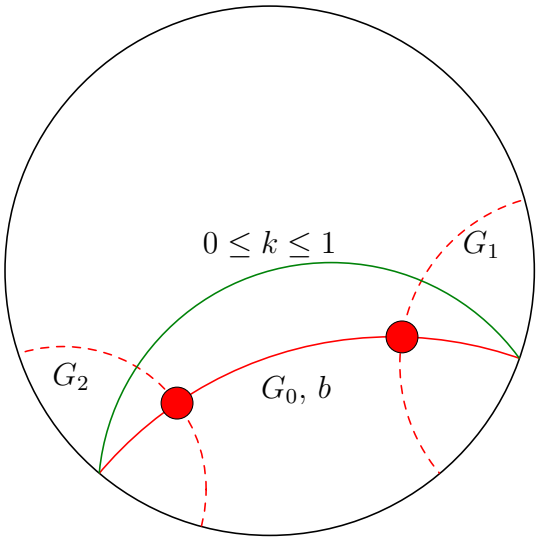

Figure 3.3: Figure showing a region of a trumpet which ends on a single geodesic boundary G_0 of length b. The red curves represent geodesics on the Poincaré disk and the two geodesics G_1 and G_2 which are dotted are identified ($G_1 = G_2$). In order to be able to identify such two geodesics we require them to be perpendicular to the closed geodesic containing the segment of length b. To construct boundaries with constant K in the same homotopy class as the geodesic boundary with length b we construct hypercycles (shown in green) which, by definition, intersect the two geodesics G_1 and G_2 at equal distances. Note that because the hypercycles need to pass through the points where G_0 intersects the boundary, the hypercycles can never be fully contained on the Poincaré disk and always have $k < 1$.

to the two geodesics. Consequently, we are precisely replicating the definition of a hypercycle which we have reviewed earlier, where this hypercycle has a constant distance from the geodesic G_0. Therefore, only hypercycles (with $k < 1$) can serve as the other boundary of the trumpet and, consequently, higher genus or multi-boundary surfaces can all only have boundaries with $k < 1$. Next, we explicitly solve for such solutions and show that fixing k uniquely fixes the proper length of the boundary.

Finding the boundary curve

Let us focus on Euclidean signature. To fix $K = k$ in the usual Poincaré metric where we cut out an arbitary shape parametrized by $(t(u), z(u))$ is non-trivial, since the expression for K is rather cumbersome. We would therefore like to study the fixed K boundary conditions with a different metric. A convenient metric, which has a more manageable expression for K and that

solves $R+2=0$ is one in Fefferman-Graham gauge

$$ds^2 = \frac{dr^2}{r^2} + \left(r - \frac{b(u)}{r}\right)^2 du^2. \tag{3.14}$$

This is a solution for any (smooth) $b(u)$. We will normalise the coordinate u such that $u \sim u+2\pi$ and hence, $b(u)$ needs to be 2π periodic. However it is important to note that not every $b(u)$ gives rise to a smooth geometry.

For this metric, the extrinsic curvature on constant r slices and their length is,

$$K(u) \equiv k(u) = \frac{1+\tilde{K}(u)}{1-\tilde{K}(u)}, \quad \tilde{K}(u) = \frac{b(u)}{r^2}, \quad L = \int_0^{2\pi} du \left| r - \frac{b(u)}{r} \right| \tag{3.15}$$

where we have defined $\tilde{K}$ for later convenience. From this, the advantage of using Fefferman-Graham gauge for these boundary conditions is also clear, since $K(u)$ is so simple. In order to gain some intuition for this metric, let us again first focus on u-independent metrics: $k(u)=k$ and so $b(u) \equiv b_0$.[9] The time-dependent solutions are more intricate to consider and will be done below.

For $b_0 = 0$ this metric is the Poincaré patch of AdS_2, with (non-compact) boundary at $r=\infty$ and the Poincaré horizon at $r=0$. When $b_0 > 0$ the metric has a conical singularity at $r=\sqrt{b_0}$. This singularity is avoided when we pick $b_0 = 1/4$. For a smooth geometry, the value of b_0 is thus fixed,[10] and take $r > 1/2$ as our space-time with the boundary located at $r=\infty$.[11]

In the case of $b_0 < 0$, the metric is completely smooth. In fact, this geometry has two boundaries, one at $r=0$ and another at $r=\infty$. Furthermore, the thermal circle takes a minimum value for g_{uu} at $r=\sqrt{-b_0}$. This is precisely the double trumpet with the size of the

[9] In embedding coordinates Y_i the geometry is given by

$$Y_0 = \frac{\sqrt{b_0}}{2r}\left(1+\frac{r^2}{b_0}\right), \quad Y_1 = \frac{1}{2\sqrt{b_0}}\left(r-\frac{b_0}{r}\right)\cos(2\sqrt{b_0}u), \quad Y_2 = \frac{1}{2\sqrt{b_0}}\left(r-\frac{b_0}{r}\right)\sin(2\sqrt{b_0}u). \tag{3.16}$$

[10] If we allow a different periodicity for u, say $u \sim u+\beta$, b_0 will be fixed to π^2/β^2.

[11] One could also take $r < 1/2$, but that patch can be mapped to the $r > 1/2$ patch through the diffeomorphism $r \to \frac{1}{4r}$.

neck set by b_0. One can readily check that $K = 0$ at the neck. Finally, let us make the following important remark. The geometries with $b_0 < 0$ are all diffeomorphic to the $b_0 = -1$ solution as can be seen by rescaling r and u as $r \to \sqrt{-b_0}r$ and $u \to u/\sqrt{-b_0}$. Notice that for $b_0 > 0$ the geometry was already fixed at a particular value for b_0 (if fixing the periodicity of u) and so we cannot do this rescaling. This is not true for the Lorentzian geometries, where we can do the rescaling for any sign of b_0.

Our primary focus in what follows will be boundaries at large, constant r and we want to fix the extrinsic curvature on those slices.[12] At constant $r = r_0$ slices, we have

$$k = \frac{r_0^2 + b_0}{r_0^2 - b_0}. \tag{3.17}$$

As we will see this greatly simplifies some of the analysis below. An important relation that we will use throughout this chapter is that for $b_0 > 0$ and $r_0 > \sqrt{b_0}$ (or $r_0 < \sqrt{b_0}$) we have that $k > 1$, while for $b_0 < 0$ we find $k < 1$.

The geometries at $b_0 > 0$ (and so $b_0 = 1/4$) or $b_0 < 0$ or, equivalently, $k > 1$ or $k < 1$, respectively, can also be brought in more conventional form through the following coordinate transformations,

$$b_0 = \frac{1}{4}: \quad r = \frac{1}{2}\coth\frac{\rho}{2} \quad \Rightarrow \quad ds^2 = \frac{d\rho^2 + du^2}{\sinh^2\rho}, \tag{3.18}$$

$$b_0 < 0: \quad r = \frac{\sqrt{-b_0}}{2}\tan\frac{\rho}{2}, \quad \widehat{u} = u\sqrt{-b_0} \quad \Rightarrow \quad ds^2 = \frac{d\rho^2 + d\widehat{u}^2}{\sin^2\rho}, \tag{3.19}$$

where in the second case $\rho \in [0, \pi)$. In the first case one can do another coordinate transformation to bring the geometry the form,

$$ds^2 = (r^2 - 1)d\tau^2 + \frac{dr^2}{r^2 - 1}. \tag{3.20}$$

[12] In the standard Dirichlet case, this metric can also be used to get the boundary Schwarzian action, see for instance [98, 99]

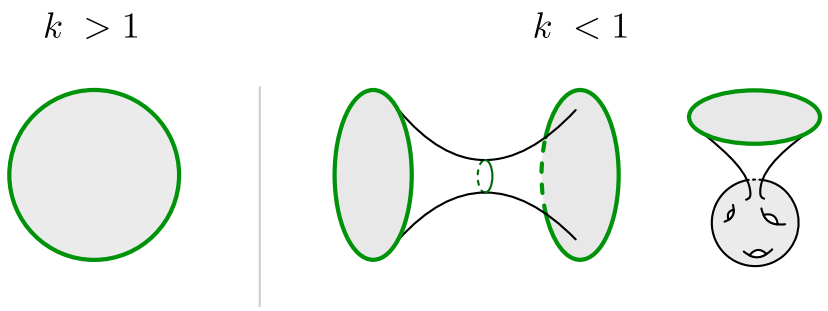

Figure 3.4: Summary of the classical Euclidean geometries for fixed K and g_{uu} boundary conditions. For $k > 1$ we can have a smooth bulk geometry, the disk. For $k < 1$ the geometry is cylindrical and we have drawn (in slightly darker green) another fixed K and g_{uu} boundary in the middle and cutting the geometry there gives the trumpet geometry.

This looks like the familiar Euclidean black hole solution, but we will see below that such an interpretation is misleading.

Having discussed the solution to the equations of motion, let us now impose the various boundary conditions. Let us first consider the Euclidean theory. We want to fix K and $\int du\sqrt{g_{uu}}$ at some radial slice $r = r_0$:

$$K|_{r=r_0} = k, \quad \int_{r=r_0} du\sqrt{g_{uu}} = L\,. \tag{3.21}$$

Notice that with these boundary conditions we cannot fix b_0 (in case it is negative) to -1, since such rescalings would change the boundary length. Solving this for b_0 and r_0, we find

$$r_0 = \frac{L(k+1)}{4\pi}, \quad b_0 = \frac{L^2(k^2-1)}{16\pi^2}\,. \tag{3.22}$$

For $k > 1$ we have $b_0 > 0$ and hence $b_0 = 1/4$, which means that L and k are not independent:

$$\text{For disk:} \qquad L = \frac{2\pi}{\sqrt{k^2-1}}. \tag{3.23}$$

On the other hand, for $k < 1$ only $b_0 < 0$ is a consistent bulk geometry. At this point we can reiterate the important observation that we have made in the previous subsection. We know that for $b_0 > 0$ the geometry has the disk topology, but for $b_0 < 0$ it is cylindrical. So depending

on $k > 1$ or $k < 1$ we either get a disk or cylinder geometry. In fact, we can also construct the trumpet geometry with the metric (3.14) by cutting the geometry at that radial location where the thermal circle becomes geodesic. This happens at $r = \sqrt{-b_0}$. The trumpet geometry is thus (3.14) with $r \geq \sqrt{-b_0}$ and conventionally we set the boundary length of the geodesic boundary to b,[13] which we can then relate to b_0 as

$$b = 4\pi\sqrt{-b_0}\,, \tag{3.24}$$

and, hence, for the trumpet geometry we get a relation between L, k and b:

$$\text{For trumpet:} \qquad L = \frac{b}{\sqrt{1-k^2}}. \tag{3.25}$$

Thus, we conclude that only for $k < 1$ the trumpet is an allowed (by the boundary conditions) bulk geometry and so only for those values of k higher topologies contribute to the partition function. Such geometries do not contribute when $k > 1$. In that case only disks contribute.

Finally, it is also interesting to consider the case when the manifold has a conical defect, which, for convenience, we can place at $r = \sqrt{b_0}$, which is real since $b_0 > 0$ now. In this case, we want $4b_0 = \Theta^2$ where the angular deficit is $2\pi(1-\Theta)$. In such a case we find, using (3.22), that

$$L = \frac{2\pi|\Theta|}{\sqrt{k^2-1}}\,. \tag{3.26}$$

which is analogous to (3.25) with the geodesic length b identified with the the deficit angle Θ – this makes sense since we can understand this geometry as an analytic continuation of the trumpet geometry.

Before moving on to studying the solution of the dilaton, let us briefly mention the Lorentzian

[13] This should not be confused with the function $b(u)$ in the Fefferman-Graham metric (3.14).

theory. The Lorentzian geometries take the form (again for constant $b(u)$)

$$ds^2 = \frac{dr^2}{r^2} - \left(r - \frac{b_0}{r}\right)^2 dt^2, \tag{3.27}$$

which, by the rescaling mentioned above, are diffeomorphic to the geometry with $b_0 = 1$ when $b_0 > 0$ and diffeomorphic to the geometry with $b_0 = -1$ whenever $b_0 < 0$. This is possible since the time direction covers the entire real line. Through analytic continuation $u = it$ (or $\widehat{u} = it$) we can map the Euclidean solutions to Lorentzian ones. For $k > 1$ we get the Lorentzian black hole solution, but as we mentioned before such an interpretation is subtle, whereas for $k < 1$ we get global AdS_2. To impose the boundary conditions we fix the boundary metric and not the fixed length (because that is infinite). This is morally the same and gives the same values for r_0 and b_0 as in (3.22), but with $L \to 2\pi\alpha$ if we fix $g_{uu} = \alpha^2$ at $r = r_0$.

In both the Lorentzian and Euclidean case, the geometry is completely fixed by the boundary conditions. The opposite is true for the dilaton. For these particular boundary conditions, we do not impose any constraint on the dilaton. To gain some intuition of what this means, we can solve the Euclidean bulk equations of motion for the dilaton in the coordinates (3.14). For constant $b(u)$ we have

$$\phi = \frac{A}{r}\left(1 + \frac{r^2}{b_0}\right) + \left(r - \frac{b_0}{r}\right)\left(B\cos(2\sqrt{b_0}u) + C\sin(2\sqrt{b_0}u)\right). \tag{3.28}$$

where the constants A, B, and C are arbitrary constants. Since A, B, and C cannot be fixed from the boundary conditions, we cannot say whether ϕ has a minimum, maximum or no local extremum at all. Therefore, since the location at which ϕ is at its local minimum is typically interpreted as the location of a 2D black hole horizon, when fixing $K = k$ and $\int du\,\sqrt{g_{uu}} = L$ we cannot specify whether the geometries under consideration contain a black hole or not. We will briefly come back to this issue in section 3.5.

Next, we proceed by studying the classical solutions from a different perspective, by reformulating JT gravity as a $PSL(2,\mathbb{R})$ gauge theory.

Connections to the BF formulation of JT gravity and varying $K(u)$

It is also useful to think about the classical geometries in the gauge theory formulation of JT gravity, in particular when we want to study boundaries with a varying, i.e. time-dependent extrinsic curvature. For the present boundary conditions, there are no boundary terms,[14] and so the JT action is that of an pure $PSL(2,\mathbb{R})$ BF gauge theory with action [100, 101, 36, 25, 33, 35]

$$S = -i \int \mathrm{Tr} BF \tag{3.29}$$

with B an adjoint scalar and $F = dA + A \wedge A$ the field strength of an $\mathfrak{sl}(2)$ gauge field. These variables are given in terms of the gravitational variables as (see for instance [33])

$$A = \frac{1}{2}\begin{pmatrix} -e^1 & e^2 - \omega \\ e^2 + \omega & e^1 \end{pmatrix} = \begin{pmatrix} -\frac{dr}{2r} & rdu \\ -\frac{b(u)}{r}du & \frac{dr}{2r} \end{pmatrix}, \qquad B = -i\begin{pmatrix} \phi^1 & \phi^2 + \phi \\ \phi^2 - \phi & -\phi^1 \end{pmatrix} \tag{3.30}$$

Here the e^i are the tweibeins of the $2d$ metric and ω the spin connection,

$$e^1 = \frac{dr}{r}, \qquad e^2 = \left(r - \frac{b(u)}{r}\right)du, \qquad \omega = -\left(r + \frac{b(u)}{r}\right)du\,. \tag{3.31}$$

The fields ϕ^i are additional Lagrange multiplier fields necessary to enforce torsionlessness of the metric. In the second equality we have put in the explicit metric einbeins in the Fefferman-Graham gauge (3.14). The equations of motion for B give us flatness of the $\mathfrak{sl}(2,\mathbb{R})$ connection and is the analogue of the $R + 2 = 0$ equation. There is a beautiful way to solve such flatness conditions: $A = g^{-1}dg$. Let us directly study the general case of time-dependent $b(u)$ and consider,

$$g = \begin{pmatrix} r^{-1/2}\psi_1'(u) & r^{1/2}\psi_1(u) \\ r^{-1/2}\psi_2'(u) & r^{1/2}\psi_2(u) \end{pmatrix}. \tag{3.32}$$

[14] Apart from counter terms which we can set to zero.

The flatness of the connection then tells us that

$$\psi''_{1,2}(u) + b(u)\psi_{1,2}(u) = 0. \tag{3.33}$$

This differential equation is known as Hill's equation and is a central object in the study of Schrodinger operators with a periodic potential (recall $b(u)$ is periodic) and coadjoint orbit theory [102]. Next, we need to make sure that g is an $PSL(2,\mathbb{R})$ element, which is nothing but a normalisation of the Wronskian,

$$\det g = 1 \quad \Leftrightarrow \quad \psi'_1\psi_2 - \psi_1\psi'_2 = 1. \tag{3.34}$$

Thus $\psi_{1,2}$ need to be linearly independent solution to the Hill equation such that the Wronskian is normalised to unity. Finally, to ensure that the connection corresponds to a smooth bulk geometry, meaning that for the disk topology the boundary is contractible, the holonomy of the gauge field A needs to be trivial. We define the holonomy U to be

$$U = \mathcal{P}\exp\left(-\oint A\right) = g^{-1}(2\pi)g(0), \tag{3.35}$$

where in the second equality we used flatness of $A = g^{-1}dg$. Triviality of U thus means $g(0) = \pm g(2\pi)$ (recall we are working with $PSL(2,\mathbb{R})$ here). Other geometries with a different topology can be obtained by considering a different value for the holonomy.

Let us exemplify this method of finding smooth geometries by taking constant b. It is straightforward to check that the holonomy is given by (at some radius r)

$$U = \begin{pmatrix} \cos(2\pi\sqrt{b_0}) & -\frac{r}{\sqrt{b_0}}\sin(2\pi\sqrt{b_0}) \\ \frac{\sqrt{b_0}}{r}\sin(2\pi\sqrt{b_0}) & \cos(2\pi\sqrt{b_0}) \end{pmatrix}. \tag{3.36}$$

So, when $\sqrt{b_0} = n/2$ for $n \in \mathbb{N}$, $U = \pm\mathbf{1}$ and we have as smooth disk geometry. Furthermore, we know that $\sqrt{b_0}$ is related to k and L as given in (3.22) and so one can easily see that this

integer n corresponds to a geometry with a 'boundary' that winds n times. This is not a smooth orientable geometry and is therefore not present in the gravity path integral and as a result only $n = 0, 1$ are relevant here. In fact, for $n = 0$ we are dealing with the Poincaré patch, which has a real line as its boundary and so clearly does not have the topology of a disk. This case is therefore excluded as well. The only relevant geometry is thus $n = 1$.

We can also extract the other geometries we found before. For the three different geometries, disk, defect and wormhole, we found the three different conjugacy classes U can be in. To determine them, we simply look at the trace of U:

$$\mathrm{Tr}\, U = 2\cos(2\pi\sqrt{b_0}). \tag{3.37}$$

The conjugacy classes are then determined as follows,

$$\mathrm{Tr}\, U = \begin{cases} < 2 & b_0 > 0, b_0 \neq n^2/4 \quad \text{Elliptic} \\ = 2 & b_0 = n^2/4 \quad \text{Parabolic} \\ > 2 & b_0 < 0 \quad \text{Hyperbolic} \end{cases} . \tag{3.38}$$

An elliptic U thus corresponds to the defect geometry, a parabolic one to the disk and the wormhole is realised by an holonomy in the hyperbolic conjugacy class. This concludes our discussion of the constant $b(u) = b_0$ solutions. For varying $b(u)$ it is much more complicated to find solutions, in particular due to the path ordering involved in the definition of U. However, for the disk topologies, we need to find periodic/anti-periodic solutions to Hill's equatin and we can ask about the existence of such solutions.

For a generic potential $b(u) = r^2\tilde{K}(u)$, the Hill equation does not have such solutions. However, so far, we have not fixed the value of r at which the boundary is located; therefore, we wish to understand whether there exist values of r such that the Hill equation $\psi''_{1,2} + r^2\tilde{K}(u)\,\psi_{1,2} = 0$ has periodic/anti-periodic solutions. In turn, if there exists a value of r for which such a solution exists, then this in turn fixes the values of the proper length L. Following the intuition developed

for the case with constant $K = k$ where only configurations with $k > 1$ exist on the disk, we will first focus on the case $k(u) > 1$ and consequently, $\tilde{K}(u) > 0$. For such a case, assuming that $\tilde{K}(u)$ is sufficiently differentiable, Lyapunov [103] proved that there exist an infinite series of values of r for which the Hill equation has a periodic/anti-periodic solution. The proof relies on the Liouville transformation; i.e. solutions of $\psi''_{1,2} + r^2\tilde{K}(u)\,\psi_{1,2} = 0$ can be mapped to solutions of

$$\frac{d^2\xi_{1,2}}{dx^2} + (r^2\gamma^2 + Q(x))\xi_{1,2} = 0\,, \tag{3.39}$$

via the map

$$x = \frac{1}{\gamma}\int_0^u \tilde{K}^{1/2}(\tilde{u})d\tilde{u}\,, \qquad \gamma = \frac{1}{\pi}\int_0^{2\pi} K^{1/2}(\tilde{u})d\tilde{u}\,, \qquad \xi(x) = \tilde{K}^{\frac{1}{4}}(u)\psi(u)\,, \tag{3.40}$$

and

$$Q(x) = (\tilde{K}(u))^{-\frac{1}{4}}\frac{d^2(\tilde{K}(u))^{\frac{1}{4}}}{dx^2}\,. \tag{3.41}$$

Eq. (3.39) can be viewed as an eigenvalue equation for the differential operator $\frac{d^2}{dx^2} + Q(x)$ with eigenvalue $-r^2\gamma^2$. Since, when $Q(x)$ and γ are real, such an operator has an infinite number of real eigenvalue when imposing periodic or anti-periodic solutions and it then follows that there are an infinite number of values of r that yield a manifold which is smooth. As can be seen from the case of constant k, different values of r correspond to different windings of the boundary. Since we are interested in surfaces that have a boundary which is not self-intersecting we will solely be interested in a single value (out of the infinite series) of r, which we call r_s. Consequently, the proper length is fixed to

$$L = r_s\int_0^{2\pi} du\,|1 - \tilde{K}(u)|\,. \tag{3.42}$$

One can similarly prove that when $0 < k(u) < 1$ ($\tilde{K}(u) < 0$) then the Hill equation does not have any periodic or anti-periodic solutions. Therefore, in that case the boundary conditions exclude all surfaces with the topology of a disk.

To summarize, while we have not found the analytic constraint that relates $k(u)$ to L (since we have not explicitly determined r_s in (3.42)) we have proven that given $k(u) > 1$, there always exists a single value of L for which a hyperbolic surface with disk topology exists. For $-1 < k(u) < 1$ the disk topology never exists, therefore generalizing the results found for constant k.

3.2.2 Quantum theory

The disk topology

Let us now compute the partition function for fixed $K = k$ and g_{uu} boundary conditions. We have seen that with these boundary conditions no boundary terms are necessary and when setting the counter terms $\mathcal{M}_i$ to zero, we just need to path integrate over the bulk action. We thus wish to calculate (in Euclidean signature),

$$Z_{ND}[k,\ell] = \int \frac{\mathcal{D}\phi\mathcal{D}g}{\text{Vol(diff)}}\, e^{\phi_0\chi(\mathcal{M})} e^{\int_{\mathcal{M}} d^2x\sqrt{g}\,\phi(R+2)}. \tag{3.43}$$

The manifolds we sum over in this path integral are denoted by $\mathcal{M}$. For now will restrict our attention to orientable manifolds with a single boundary and discuss multiple boundaries below. Here the contour of ϕ is chosen to be along the imaginary axis, in which case the path integral over ϕ gives a delta functional $\delta(R+2)$ and our path integral simply counts the number of hyperbolic metrics having a boundary with fixed k and ℓ modulo diffeomorphisms:

$$Z_{ND}[k,\ell] = \int \frac{\mathcal{D}g}{\text{Vol(diff)}}\, e^{\phi_0\chi(\mathcal{M})}\ \delta(R+2). \tag{3.44}$$

The easiest way to compute this partition function is by going to a BF theory formulation of JT gravity that reviewed above.[15] The path integral is then just a function of the holonomy U of the gauge field A around the boundary circle, The partition function of the $PSL(2,\mathbb{R})$ gauge

[15] In [33] this was done for closed manifolds, which then also has no boundary terms, but the boundary conditions are different, so we cannot directly apply their formulae to the current case.

theory is [33]

$$Z_{ND}[U] = \int \frac{\mathcal{D}A\mathcal{D}B}{\text{Vol(gauge)}}\, e^{\phi_0 \chi(\mathcal{M})} e^{i\int \text{Tr}BF} = \int \frac{\mathcal{D}A}{\text{Vol(gauge)}} e^{\phi_0\chi(\mathcal{M})}\delta(F), \tag{3.45}$$

with $\chi(\mathcal{M} = D_2) = 1$. This partition function thus computes the number of flat connections modulo gauge transformations, but with one important caveat. In the gauge theory only connections A that are not related by smooth gauge transformations are counted seperately, whereas in the gauge theory variables such connections might be related by large diffeomorphisms, i.e. elements on the mapping class group of the underlying manifold. In the gravity theory metrics related by the mapping class group are not counted separately and in the gauge theory we need to account for that. This imposes no subtleties in the disk for which the mapping class group is trivial, but does so for the cylinder or higher topologies as the mapping class group is non-trivial in those cases. The disk partition function $Z_{\text{Disk}}[k, L]$ for constant k ($b(u) = b_0$) can thus be computed rather directly in the $PSL(2,\mathbb{R})$ gauge theory. In fact, there is only one flat $PSL(2,\mathbb{R})$ connection (modulo gauge transformations) on the disk and the partition function is

$$Z_{ND}^{(\text{Disk})}[U] = e^{\phi_0}\delta(U - \mathbf{1}). \tag{3.46}$$

To write this in terms of the diffeomorphism invariant gravity variables k and ℓ, we need to express the holonomy U in terms of k and ℓ. The holonomy was given in (3.36) and so the remaining step is to rewrite the δ-function on the $PSL(2,\mathbb{R})$ group manifold in terms of Dirac-delta functions solely dependent on L and k. There are two possible ways in which one can rewrite the δ-function on the group manifold, dependent on the space of test-functions which we plan to integrate the test function against. The first, (a) are general functions on the group manifold, while the second (b) are trace-class functions. If we fix $PSL(2,\mathbb{R})$ gauge transformations on the boundary (or, equivalently, fixing gravitational diffeomorphisms), then, in order to get some generic observable, one can integrate the partition function against a general function on the group manifold, while if one does not fix gauge transformations on the boundary, the holonomy is

not gauge invariant but its conjugacy class is. To summarize, the interpretation of the δ-function on the group as a distribution in L and K depends on whether we fix diffeomorphisms on the boundary.

In appendix 3.8 we give a detailed account about the difference between the resulting conversion for the δ-function on the group manifold. When studying the distribution (a) we find that (3.46) becomes

$$Z_{ND}^{(\text{Disk})}[k,\ell] = \frac{e^{\phi_0}}{2\pi}\delta^2(0)\delta\left(\sqrt{b_0}-\frac{1}{2}\right) = \frac{2e^{\phi_0}}{\sqrt{k^2-1}}\delta^2(0)\delta\left(L-\frac{2\pi}{\sqrt{k^2-1}}\right), \tag{3.47}$$

where we used (3.22). When studying the distribution (b) that acts on the space of trace-class functions, we instead find

$$Z_{ND}^{(\text{Disk})}[k,\ell] = \frac{e^{\phi_0}}{2\pi}\delta''\left(\sqrt{b_0}-\frac{1}{2}\right) = \frac{e^{\phi_0}}{2\pi}\delta''\left(\frac{L\sqrt{k^2-1}}{4\pi}-\frac{1}{2}\right). \tag{3.48}$$

We can perform a further check of this result by going in between Dirichlet-Dirichlet and Dirichlet-Neumann boundary conditions using a Laplace transform on the boundary value of the dilaton field $\phi_r(u)$. In the limit in which the proper length of the boundary L is large (i.e. the Schwarzian limit when studying Dirichlet-Dirichlet boundary conditions) the path integral that we need to evaluate is (omitting the topological term)

$$\begin{aligned} Z_{ND}^{(\text{Disk})} &= \int D\phi_b(u) e^{-2\int_0^\beta du\sqrt{g_{uu}}\phi_b(u)k} \sim \int D\phi_r(u)\int Df(u) e^{\int_0^\beta du\phi_r(u)(\text{Sch}(f,u)-\kappa)} \\ &\sim \int Df(u)\delta(\text{Sch}(f,u)-\kappa) \end{aligned} \tag{3.49}$$

where the "$\sim$" means equality up to counterterms which have the role to eliminate an overall divergent constant multiplying the partition function. Furthermore, above, we define the renormalized quantities $k = 1+\varepsilon^2\kappa$ and $\phi_r(u) = \phi_b(u)/\varepsilon$. In appendix 3.7 we compute the path integral (3.49) explicitly and show that the result agrees with the BF computation from (3.47).

This concludes our brief discussion of the disk partition function with fixed k and L boundary

conditions. For varying $K_{r=r_s} = k(u)$ we can use the results about the Hill equation with general potential we discussed above, in particular (3.42) and we get a δ-function that activates when $L - \int_0^{2\pi} du \left| r_s - \frac{k(u)}{r_s} \right| = 0$. As previously mentioned, for a given $k(u)$, we cannot determine r_s analytically; rather as described in section 3.2.1, it is determined by the solution of the Hill equation.

The trumpet and cylinder with fixed K

We can compute the partition function on the trumpet or cylinder, again, in two different ways.

In the first, we again rely on the BF formulation of JT gravity and need to glue the opposite sides of the gravitational theory when placed on a manifold with the topology of a square. This is very similar to the computation of the partition function of the conventional BF theory on a cylinder with one important distinction. This is that in the gravitational theory we should also quotient by the mapping class group of the cylinder (given by $\mathbb{Z}$) while in conventional BF theory this is not necessary. As we will see, considering this quotient is important in obtaining a convergent partition function.

In the second approach, we will again transform the partition function with DD boundary conditions to that with ND boundary conditions via a Laplace transform. This amount to evaluating the Schwarzian path integral (3.49) on a different orbit than we did in the subsection above; i.e. $\text{Diff}(S^1)/U(1)$ instead of $\text{Diff}(S^1)/SL(2,\mathbb{R})$.

We begin by presenting the first approach. Formally we want to compute

$$Z_{ND}^{(\text{Cylinder})}(U_L, U_R) = \int_{PSL(2,\mathbb{R})/\mathbb{Z}} dh\, \delta(U_L h^{-1} U_R^{-1} h)\,, \tag{3.50}$$

where U_1 and U_2 are the holonomies along the edges of the cylinder and h is the holonomy along a line uniting the two sides. The difficulty in computing this partition function is partly due to the quotient and in particular in explaining what quotient of $PSL(2,\mathbb{R})$ we need to consider. To figure this out, we will consider a particular on-shell metric solution, convert it to the gauge

theory variables, and compute the holonomies around the non-contractible cycle and along the gluing curve. From the metric variables, it will be clear what identifications we need to make in order to quotient out the mapping class group and the above procedure will tell us what part of the gauge theory variables, in particular the group element, needs to be identified.

To that end, it is first useful to consider an on-shell hyperbolic configuration which has the following metric [33]

$$ds^2 = d\rho^2 + \cosh(\rho)^2[bdx + \tau\delta(\rho)d\rho]^2\,, \qquad x \sim x + 1\,. \tag{3.51}$$

The variable τ represents the distance of a twist made along the closed geodesic at $\rho = 0$. To see that the metric (3.51) is equivalent to a purely hyperbolic metric one can introduce the coordinate y:

$$y = bx + \tau\theta(\rho)\,, \qquad dy = bdx + \tau\delta(\rho)d\rho\,. \tag{3.52}$$

In such a case, it is clear that τ should be identified up $\tau \sim \tau + b$ since the coordinate x is compact and periodically identified. In fact, shifts of τ by b are precisely identified with the Dehn twists which generate the mapping class group $\mathbb{Z}$ of the cylinder. Therefore, in our computation of the cylinder partition function we will need to identify holonomies for which τ is shifted by b.

To achieve this we start by writing the frame and spin-connection for the metric (3.51),

$$\begin{gathered} e^1 = d\rho\,, \qquad e^2 = b\cosh(\rho)dx + \tau\cosh(\rho)\delta(\rho)d\rho, \qquad \omega = -\sinh(\rho)(bdx + \tau\delta(\rho)d\rho), \\ A = \frac{1}{2}\begin{pmatrix} -d\rho & be^{\rho}dx + \tau e^{\rho}\delta(\rho)d\rho \\ be^{-\rho}dx + \tau e^{-\rho}\delta(\rho)d\rho & d\rho \end{pmatrix}. \end{gathered} \tag{3.53}$$

and consider the holonomy around the closed cycle of the cylinder at the left and right boundary,

$$U_{L,R} = \mathcal{P}\exp\left(-\oint_{\rho=\text{const}} A\right) = \begin{pmatrix} \cosh(b/2) & -e^{\rho_{\text{bdy}_{L,R}}}\sinh(b/2) \\ -e^{-\rho_{\text{bdy}_{L,R}}}\sinh(b/2) & \cosh(b/2) \end{pmatrix} \tag{3.54}$$

whose eigenvalues are $(e^{b/2},\, e^{-b/2})$ for all ρ. Thus, we see that the conjugacy class of the holonomy around the closed cycle of the cylinder is independent of the location at which the holonomy is evaluated. This of course follows from the fact that the connection is flat and from the gluing formula (3.50) we clearly see that the δ-function only activates when U_L and U_R are in the same conjugacy class, regardless of the integration space for h. To understand the quotienting procedure we consider the Wilson line along a curve with constant x, from one end of the cylinder to the other. In such a case,

$$h = \mathcal{P}\exp\left(-\int_{\rho=\rho_{\mathrm{bdy}_L}}^{\rho=\rho_{\mathrm{bdy}_R}} A\right) = \begin{pmatrix} e^{\frac{\rho_{\mathrm{bdy}_R}-\rho_{\mathrm{bdy}_L}}{2}}\cosh(\tau/2) & -e^{\frac{\rho_{\mathrm{bdy}_R}+\rho_{\mathrm{bdy}_L}}{2}}\sinh(\tau/2) \\ -e^{-\frac{\rho_{\mathrm{bdy}_R}+\rho_{\mathrm{bdy}_L}}{2}}\sinh(\tau/2) & e^{\frac{\rho_{\mathrm{bdy}_L}-\rho_{\mathrm{bdy}_R}}{2}}\cosh(\tau/2) \end{pmatrix} \tag{3.55}$$

where we assume $\rho_{\mathrm{bdy}_L} < 0$ and $\rho_{\mathrm{bdy}_R} > 0$.[16] We will thus assume that the holonomy along the two-sides of the cylinder take the form (3.54) where b is determined by the proper length and extrinsic curvature on each side while the "gluing" holonomy is given by (3.55) up to a $\mathbb{Z}$ identification. It is convenient to re-express (3.50) in terms of the conjugacy classes of U_L and U_R. To diagonalize U_L and U_R we have that

$$Z_{ND}^{(\mathrm{Cylinder})}(U_L, U_R) = \int dh\delta(\tilde{U}_L A_L h^{-1} A_R^{-1}\tilde{U}_R^{-1}A_R^{-1}hA_L^{-1}), \tag{3.56}$$

where $U_{L,R} = A_{L,R}^{-1}\tilde{U}_{L,R}A_{L,R}$

$$A_{1,2} = \frac{1}{\sqrt{2}}\begin{pmatrix} -e^{-\rho_{L,R}/2} & e^{\rho_{L,R}/2} \\ -e^{-\rho_{L,R}/2} & e^{\rho_{L,R}/2} \end{pmatrix}, \tag{3.57}$$

and where we can change integration variables to $\tilde{h} = A_L h^{-1} A_R^{-1}$,

$$Z_{ND}^{(\mathrm{Cylinder})}(U_L, U_R) = \int d\tilde{h}\delta(\tilde{U}_L\tilde{h}\tilde{U}_R\tilde{h}^{-1})\,. \tag{3.58}$$

[16] This assumption is unimportant since one can always perform a diffeomorphism which places the δ-function in (3.51) at any ρ-location.

For the on-shell configuration studied above $\tilde{h}$ can be expressed as

$$\tilde{h} = e^{-\tau\sigma_3/2}\,, \tag{3.59}$$

and thus (since we are studying an on-shell configuration) for these values of $\tilde{U}_L$, $\tilde{U}_R$ and $\tilde{h}$ the δ-function activates.

Nevertheless, this computation allows us to see which elements h or $\tilde{h}$ are related by a large diffeomorphism. Namely, we have learned that the quotient we want to do is on elements in $PSL(2,\mathbb{R})$ which are related by multiplication by a hyperbolic diagonal group element. To be more specific, given two elements h_1 and h_2, we want to identify them when they are related by a right multiplication by the element $e^{-b\sigma_3/2}$. Concretely, let us consider the KNA decomposition of a general element of $PSL(2,\mathbb{R})$,

$$\tilde{h} = KNA\,, \qquad K = \begin{pmatrix} \cos(\theta) & \sin(\theta) \\ -\sin(\theta) & \cos(\theta) \end{pmatrix}\,, \qquad N = \begin{pmatrix} 1 & n \\ 0 & 1 \end{pmatrix}\,, \qquad A = \begin{pmatrix} e^{a} & 0 \\ 0 & e^{-a} \end{pmatrix}\,, \tag{3.60}$$

for which the Haar measure can be written as $d\tilde{h} = d\theta\, dn\, da$. Thus our identification is a restriction on the range of a, which we take to be from 0 to $b/2$ (while in $PSL(2,\mathbb{R})$ this range is non-compact).

Let us now return to the general problem, i.e. evaluating (3.58). Using the above decomposition the delta function of a group element in the KNA decomposition is given by $\delta(U) = \delta(\theta)\delta(n)\delta(a)$. We take $U = \tilde{U}_L\tilde{h}\tilde{U}_R\tilde{h}^{-1}$ with $\tilde{h}$ written in the KNA decomposition and consider (the possibly off-shell configuration) $\tilde{U}_{L,R} = \exp(\sigma_3\lambda_{L,R}/2)$. The only thing left to do is to evaluate the one-loop factor, which can be done straightforwardly by expanding the argument of the delta function close to $\theta = 0$ and $n = 0$, since the delta function only fires when

$\tilde{h}$ is diagonal

$$\delta(\tilde{U}_L\tilde{h}\tilde{U}_R\tilde{h}^{-1}) = \delta\begin{pmatrix} e^{(\lambda_1-\lambda_2)/2} & 2e^{\lambda_1/2}(n+\theta)\sinh(\lambda_2/2) \\ 2e^{-\lambda_1/2}\theta\sinh(\lambda_2/2) & e^{-(\lambda_1-\lambda_2)/2}\end{pmatrix} + \mathcal{O}\left(n\theta,\, n^2,\, \theta^2\right) \tag{3.61}$$

The coordinate a does not appear in the integrand and directly gives a factor of $b/2 = \lambda_L/2 = \lambda_R/2$. The cylinder partition function is thus,

$$Z_{ND}^{(\text{Cylinder})}(\lambda_L, \lambda_R) = \lambda_L \frac{\delta(\lambda_L - \lambda_R)}{4\sinh^2\lambda_L/2}\,, \tag{3.62}$$

where $e^{\pm\lambda_L/2}$ and $e^{\pm\lambda_R/2}$ are the eigenvalues of the holonomies $\tilde{g}_L$ and $\tilde{g}_R$.

Naively, the trumpet partition function would be defined by taking $\lambda_L = b$, i.e. the geodesic boundary has a holonomy determined by b. However, this is too quick, because the cylinder is obtained by gluing two trumpets and there can be a non-trivial measure factor appearing in the gluing depending on how we define the trumpet. In fact, since here we have expressed the partition function as a delta function on the conjugacy classes of the boundary holonomies, there is indeed a non-trivial measure as can be seen from the Weyl integration formula for $PSL(2,\mathbb{R})$, see appendix 3.8. Furthermore, if we would have constructed two trumpets from (3.62), we would have implicitly taken two twist integrals (the integrals over a that gave us a factor of $b/2$) into account, whereas we need only one. To account for that, we divide by $b/2$ in the gluing of two trumpets. We thus get

$$Z_{ND}^{(\text{Cylinder})}(\lambda_L, \lambda_R) = \int_0^\infty db\left(2\sinh^2 b/2\right)\left(b\frac{\delta(b-\lambda_L)}{4\sinh^2\lambda_L/2}\right)\left(b\frac{\delta(b-\lambda_R)}{4\sinh^2\lambda_R/2}\right)\left(\frac{2}{b}\right), \tag{3.63}$$

where each term in brackets corresponds to the measure obtained from the Weyl integration formula,[17] the two cylinders, and the division by b to account for overcounting, respectively. From this, we define the trumpet partition function by distributing the measure (the first term

[17]Here we picked a particular normalisation ($\alpha = 1$) of the measure instead of keeping it around as was done in [33].

in round brackets) in the definition of the trumpet,

$$Z_{ND}^{(\text{Trumpet})}(b,\lambda_L)=\frac{\delta(b-\lambda_L)}{2\sinh b/2}, \tag{3.64}$$

and the gluing measure is just the Weil-Petersson measure $b\,db$.

In appendix 3.7 we confirm this way of defining the trumpet and cylinder partition function by doing the path integral directly using the boundary Schwarzian mode. The main difference between the computation in for the trumpet as opposed to the disk (3.49) is the number of zero modes for the Schwarzian field $F(u)$ (since we are integrating over different orbits). Because of this difference the divergent factor $\delta^2(0)$ present on the disk in (3.47) is no longer present in the case of the trumpet or cylinder.

To complete our analysis we solely need to use the relation between the conjugacy class of the holonomy for the Neumann-Dirichlet boundary and the extrinsic curvature K together with the proper length L. We will take the λ_L to be the eigenvalue of this holonomy while $\lambda_R=b$ is the eigenvalue of the holonomy on the closed geodesic boundary. This is given by

$$Z_{ND}^{(\text{Trumpet})}(b;L,k)=\frac{\delta\left(L\sqrt{1-k^2}-b\right)}{2\sinh b/2}. \tag{3.65}$$

The cylinder partition function then becomes,

$$Z_{ND}^{(\text{Cylinder})}(L_1,k_1;L_2,k_2)=\frac{L_1\sqrt{1-k_1^2}}{4\sinh^2\left(\frac{L_1\sqrt{1-k_1^2}}{2}\right)}\delta\left(L_1\sqrt{1-k_1^2}-L_2\sqrt{1-k_2^2}\right). \tag{3.66}$$

Putting it all together

We can now consider the general genus expansion of the partition function of JT gravity with ND b.c. We have already seen that boundaries which have $K > 1$ lead to factorization:

$$\begin{aligned}\langle Z_{ND}(k_1 > 1, L_1) \dots Z_{ND}(k_i > 1, L_i]) Z_{ND}(k_{i+1} < 1, L_{i+1}) \dots Z_{ND}(k_n < 1, L_n)\rangle = \\ = \langle Z_{ND}(k_1 > 1, L_1)\rangle \dots \langle Z_{ND}(k_i > 1, L_i)\rangle \langle Z_{ND}(k_{i+1} < 1, L_{i+1}) \dots Z_{ND}(k_n < 1, L_n)\rangle\end{aligned} \tag{3.67}$$

with

$$\langle Z_{ND}(K_1 > 1, L_1)\rangle = \frac{e^{\phi_0}}{2\pi}\delta''\left(\frac{L\sqrt{k^2-1}}{4\pi} - \frac{1}{2}\right) \tag{3.68}$$

Thus, we simply want to discuss the genus expansion of $\langle Z_{ND}(K_1 < 1, L_{i+1}) \dots Z_{ND}(K_n < 1, L_n)\rangle$. As previously specified, we simply have to integrate the partition function the trumpet against the Weil-Petersson volumes (denoted here by $\mathrm{Vol}_{g,n}(b_1, \dots, b_n)$ for a manifold of genus g and with n geodesic boundaries with lengths $b_1, \dots\ b_n$) using the Weil-Petersson measure. This yields,

$$\begin{aligned}& \langle Z_{ND}(K_1 < 1, L_1) \dots Z_{ND}(K_n < 1, L_n)\rangle \\ \sim\ & \sum_{g=0}^{\infty} e^{\phi_0 \chi_{g,n}} \int db_1 b_1 \cdots \int db_n b_n \, \frac{\delta(L_1\sqrt{1-K_1^2} - b_1)}{2\sinh b_1/2} \cdots \frac{\delta(L_n\sqrt{1-K_n^2} - b_n)}{2\sinh b_n/2} \\ & \qquad \times \mathrm{Vol}_{g,n}(b_1, \dots, b_n) \\ =\ & \frac{\left(L_1\sqrt{1-K_1^2} \cdots L_n\sqrt{1-K_n^2}\right)}{2^n \sinh\frac{L_1\sqrt{1-K_1^2}}{2} \cdots \sinh\frac{L_n\sqrt{1-K_n^2}}{2}} \sum_{g=0}^{\infty} e^{\phi_0\chi_{g,n}} \mathrm{Vol}_{g,n}(L_1\sqrt{1-K_1^2}, \dots, L_n\sqrt{1-K_n^2})\end{aligned}$$

where we formally define $\mathrm{Vol}_{0,1}(b) \equiv 0$ and $\mathrm{Vol}_{0,2}(b_1, b_2) \equiv \delta(b_1 - b_2)/b_1$.[18] Thus, up to overall constants the partition function for boundaries with $K_i < 1$ simply yields a sum over the Weil-Petersson volumes. We will use the simplicity of this result to determine the matrix integral interpretation for the insertion of an ND boundary in the JT gravity path integral.

[18] This corresponds to the Laplace transforms of the volumes $W_{g,n}(z_1, \dots, z_n)$ to have $W_{0,1}(z) = 0$ and $W_{0,2}(z_1, z_2) = \frac{1}{(z_1 - z_2)^2}$.

3.2.3 Matrix integral interpretation

With the geometric result for the partition function in mind, we now wish to find the operator insertion in the JT gravity matrix integral which reproduce the results above. To do this, we will first attempt to understand this matrix integral interpretation by performing a path integral for the boundary valued dilaton $\phi_b(u)$ for the matrix integral result with Dirichlet-Dirichlet boundary conditions. While we shall not be able to perform this path integral exactly, we will still be able to determine an integral kernel which when applied to the Dirichlet-Dirichlet partition function reproduces the factorization properties observed in the previous subsection. Using this kernel, we will be able to finally determine the correct operator insertion in the matrix integral to reproduce (3.67)–(3.69).

A Transformation Kernel

As previously mentioned, $\phi_b(u)$ and $K(u)$ are canonical conjugates. Thus, to obtain Z_{ND} from Z_{DD}, we need to perform the path integral

$$Z_{ND}[k, L] = \int D\phi_r(u) e^{\frac{1}{\epsilon^2}\int_0^\beta du \phi_r(u)(1-k(u))} Z_{DD}[\phi_b(u), L]. \tag{3.69}$$

To continue, we will use the formula for $Z_{DD}[\phi_b(u), L]$ for varying $\phi_b(u) = \phi_r(u)/\varepsilon$, obtained in the Schwarzian nearly-AdS$_2$ limit ($L = \beta/\varepsilon \to \infty$) by interpreting the results in appendix C of [81] or the results reviewed in more detail in appendix A in [90]: [19]

$$Z_{DD}^{(\text{Schw})}[\phi_b(u), L] = e^{\int_0^\beta du \frac{\phi_r'(u)^2}{2\phi_r(u)}} \left\langle \operatorname{Tr} e^{-H\int_0^\beta du/\phi_r(u)} \right\rangle_{\text{MI}}, \tag{3.70}$$

[19] In this subsection we fix the normalization of the matrix integral over H following the convention of [33] with $\gamma = 1$.

where $\left\langle \mathrm{Tr} e^{-H\int_0^L du/\phi_r(u)} \right\rangle_{\mathrm{MI}}$ is the expectation value of the "partition function operator" with the effective temperature $\beta_{\mathrm{eff}}[\phi_r(u)] = \int_0^\beta du/\phi_r(u)$. Thus, we would like to evaluate

$$Z_{ND}[k(u), L] = \int d\tilde{L} \left\langle e^{-H\tilde{L}} \right\rangle_{\mathrm{MI}} \times \underbrace{\int_{-i\infty}^{i\infty} d\sigma \int D\phi_r(u) e^{\sigma\left(\tilde{L} - \int_0^\beta \frac{du}{\phi_r(u)}\right)} e^{\int_0^\beta du \frac{\phi_r'(u)^2}{2\phi_r(u)}} e^{\frac{1}{\epsilon^2}\int_0^\beta du \phi_r(u)(1-k)}}_{\mathcal{F}_k(\tilde{L}, L)}, \tag{3.71}$$

where we have introduced the Lagrange multiplier σ to emphasize that one can obtain the ND partition function by performing an integral over L (instead of a path integral over $\phi_r(u)$) with the appropriate kernel $\mathcal{F}_k(\tilde{L}, L)$. This allows us to give an exact definition of the kernel in the Schwarzian lmit. However, the path integral over $\phi_b(u)$ in the last line of (3.71) is difficult to perform exactly. Nevertheless, a naive semi-classical evaluation of this path integral in the Schwarzian limit yields (integrating solely over configurations for which $\phi_r(u)$ varies only very slowly with u)

$$\mathcal{F}_k^{\text{semi-classical}}(\tilde{L}, L) \sim \frac{1}{\tilde{L}^{3/2}} e^{L^2 \frac{(1-k)}{\tilde{L}}} . \tag{3.72}$$

It is tempting to guess that the factorisation properties required of the kernel can be reproduced by a simple modification of the approximate semi-classical kernel (3.72). In what follows, we will show that this is the case. Moreover, we will see that this kernel can also be applied away from the Schwarzian regime ($k \approx 1$, $L \to \infty$).

The modification of the kernel which we propose is:

$$\mathcal{F}_K(\tilde{L}, L) = \sqrt{2\pi} \frac{e^{\frac{\lambda^2}{2\tilde{L}}}}{\tilde{L}^{3/2}} \mu(\lambda) \qquad \mu(\lambda) = \left(\frac{\lambda}{2 \sinh \frac{\lambda}{2}} \right) \tag{3.73}$$

where we have defined

$$\lambda \equiv L\sqrt{1-k^2} . \tag{3.74}$$

In the Schwarzian limit, $k = 1 + O(\varepsilon^2)$ we may also replace $1 - k^2 \sim 2(1-k)$ in this expression to recover the approximate kernel (3.72).

From the BF perspective, λ is the eigenvalue of the holonomy along the corresponding boundary. When $k < 1$, λ is real, otherwise it is purely imaginary. We will demonstrate that this kernel satisfies the desired properties. This allows us to define the ND partition function as a simple integral transform of the DD partition function,

$$Z_{ND}(k, L) = \int_{\mathcal{C}} d\tilde{L}\ Z_{DD}^{(g)}(\tilde{L}) \mathcal{F}_K(\tilde{L}, L). \tag{3.75}$$

where $\mathcal{C}$ is a contour to be specified. Here, it is useful to think of the perturbative (in $e^{-\phi_0}$) part of the decomposition of the Dirichlet partition function into contributions from different genera

$$\langle Z_{DD}(\tilde{L}) \rangle = e^{\phi_0} Z_{DD}^{(\text{Disk})}(\tilde{L}) + \sum_{g=1}^{\infty} e^{(1-2g)\phi_0} \int_0^{\infty} db\, b\, V_{g,1}(b) Z_{DD}^{(\text{Trumpet})}(b;\, \tilde{L}) \tag{3.76}$$

where we have the explicit expressions for the disk and trumpet [33, 81]

$$Z_{DD}^{(\text{Disk})}(\tilde{L}) = \frac{1}{\sqrt{2\pi}} \frac{e^{\frac{2\pi^2}{\tilde{L}}}}{\tilde{L}^{3/2}} \qquad Z_{DD}^{(\text{Trumpet})}(b;\, \tilde{L}) = \frac{1}{\sqrt{2\pi}} \frac{e^{-\frac{b^2}{2\tilde{L}}}}{\tilde{L}^{1/2}}. \tag{3.77}$$

where we are studying the theory with the effective temperature, $\tilde{L} = \beta/\phi_r$, and where b is the proper length of the closed geodesic that separates the trumpet from the rest of the bordered higher genus Riemann surface.

In order to study the properties of (3.75), let us first consider the trumpet contribution. In order to specify the contour of integration for the kernel, it is useful to introduce the variable $z = \tilde{L}^{-1}$. We then chose the integration contour for z along the imaginary axis

$$\begin{aligned} \frac{Z_{ND}^{(\text{Trumpet})}(k, L)}{\mu(\lambda)} &= \int_{-i\infty}^{i\infty} \frac{dz}{z^2} \left(z^{1/2} e^{-\frac{b^2}{2} z} \right) \left(z^{3/2} e^{\frac{\lambda^2}{2} z} \right) = \int_{-i\infty}^{i\infty} dz\, e^{\frac{z}{2}\left(-b^2 + L^2(1-k^2)\right)} \\ &= \begin{cases} 2\delta\left(b^2 - \lambda^2\right) = \frac{1}{\lambda}\delta\left(b - \lambda\right) & \text{for } k < 1 \\ 0 & \text{for } k > 1 \end{cases} . \end{aligned} \tag{3.78}$$

When $k \geq 1$, the integral contour for z can be closed on the right half plane $\mathrm{Re}(z) > 0$ and hence vanishes. Thus, the trumpet does not contribute for an ND boundary with $k > 1$. In the opposite case, $k < 1$, we have the second line which reproduces (3.64) derived from other methods. Thus, the trumpet result

$$Z_{ND}^{(\mathrm{Trumpet})}(k, L) = \frac{\delta(b - L\sqrt{1-k^2})}{2\sinh\frac{b}{2}}, \tag{3.79}$$

agrees with (3.64) obtained from BF theory or by considering the Laplace transform of the Dirichlet-Dirichlet partition function. Therefore, applying the kernel (3.75) to (3.78) we obtain the sum over Weil-Peterson volumes from (3.69).

The final step needed to compare the matrix integral and geometric results is to understand the effect of the kernel on manifolds with disk topology. The disk contribution to (3.75) is given by

$$\frac{Z_{ND}^{(\mathrm{Disk})}(k, L)}{\mu(\lambda)} = \int_{-i\infty}^{i\infty} \frac{dz}{z^2} \left(z^{3/2} e^{2\pi^2 z}\right) \left(z^{3/2} e^{\frac{\lambda^2}{2} z}\right) = \int_{-i\infty}^{i\infty} dz\, z\, e^{z\left(2\pi^2 + \frac{L^2}{2}(1-k^2)\right)} \tag{3.80}$$

In this case, when $k \leq 1$, the integral contour for z can be closed on the left half plane $\mathrm{Re}(z) < 0$ and hence vanishes. Thus the disk topology does not contribute to the partition sum in this case. When $k > 1$, the integral can be evaluated exactly and yields the same type of divergence as in (3.68). Therefore, we find that the integral kernel (3.73) reproduces the ND partition function computed in section 3.2.2.

Operator Insertion in Matrix Integral

Given that we see that the kernel applied to the DD partition functions reproduces the correct ND partition function we can now ask what operator in the matrix integral directly reproduces the insertion of this latter boundary in the gravitational path integral. This is simply given by

considering the action of the kernel on the partition function operator:

$$e^{-\tilde{L}H} \to \int_{-i\infty}^{+i\infty} \frac{dz}{z^{1/2}}\, \mu(\lambda)\, e^{L^2 \frac{(1-K^2)}{2} z} e^{-\frac{H}{z}} \sim \begin{cases} \frac{\cos(L\sqrt{1-K^2}\sqrt{2H})}{\sinh\left(\frac{L}{2}\sqrt{1-K^2}\right)} & K<1, \\ \frac{\cosh(L\sqrt{K^2-1}\sqrt{2H})}{\sin\left(\frac{L}{2}\sqrt{K^2-1}\right)} & K>1 \end{cases} . \tag{3.81}$$

Thus, we conclude that

$$Z_{ND}[K,L] \sim \langle \text{Tr } \cos(\lambda\sqrt{2H}) \rangle_{MI}, \tag{3.82}$$

which has the same properties as the ones discussed above.

It is important to note however, that one needs to keep careful track of the integration contour when evaluating this operator via analytic continuation in the matrix integral. For instance, when integrating the $K<1$ operator against the trumpet, the "energy of the Hamiltonian" H should be integrated along the imaginary axis.

3.3 Fixing K and $\partial_n\phi - \phi K$: a less rigid geometry

The study the partition function with fixed $K \equiv k(u)$ and $\partial_n\phi - \phi K \equiv -\phi_b'(u)/2$ (NN boundary conditions)[20] is similar, yet less rigid than that for fixed K and g_{uu}. To emphasize this point we start by re-analyzing the classical behavior discussed in the previous section. While fixing K completely fixes the geometry of the manifold, by setting the location and proper length of the boundary, when fixing g_{uu} the arbitrary constants in the classical dilaton solution (3.28) could not be fixed from the ND boundary condition. For the NN boundary condition however, fixing $\partial_n\phi - \phi K$ fixes the constant A in (3.28), however the constants B and C are still unfixed in the classical solution. Thus, B and C are zero modes for the dilaton solution. In such a case, the classical dilaton solution in Euclidean or Lorentzian signature (3.28) is set (in the

[20]The function $\phi_b'(u)$ should not be confused with the derivative of the boundary value of the dilaton which is not specified for these boundary conditions.

Fefferman-Graham gauge (3.14)) to be:

$$
\begin{aligned}
r_0 &= \sqrt{b_0 \frac{k+1}{k-1}}\,, \\
\phi(r,u) &= \frac{\phi_b'}{2r\sqrt{k^2-1}} \left(1 + \frac{r^2}{b_0}\right) + \left(r - \frac{b_0}{r}\right) \left(B\cos(2\sqrt{b_0}u) + C\sin(2\sqrt{b_0}u)\right)\,,
\end{aligned}
\tag{3.83}
$$

with the boundary located at r_0. Nevertheless, as for the ND b.c. , for $k > 1$ we again only have the disk contribution, and $b_0 = 1/4$ in order for the Euclidean geometry to be smooth. For $k < 1$ and, consequently, $b_0 < 0$, we only have contributions from higher genus or multi-boundary geometries.

Finally, in order to compare the classical results to the partition function which we shall obtain shortly, it is useful to compute the on-shell action (for disk topologies) coming from boundary term in (3.7):

$$
S_{NN}^{\text{on-shell}} = -L\phi_b' = -\frac{2\pi}{\sqrt{k^2-1}}\phi_b'\,. \tag{3.84}
$$

where we have used the fact that fixing $K = k$ also fixes the proper length of the boundary L, according to (3.23).

We now discuss the quantization of the gravitational theory with the NN boundary conditions. We have seen in the previous section that fixing $k > 1$ completely fixes the topology of the manifold and the proper length of its boundary. Therefore, since the proper length of the boundary is not fixed by the boundary conditions, the partition function on the disk will no longer yield a δ-function even though the geometry is fixed. Similarly, for $k < 1$ we again only receive contributions from higher genus or multi-boundary manifolds. Thus, we again have that

$$
\begin{aligned}
&\langle Z_{NN}(k_1 > 1, \phi_{b,1}') \dots Z_{NN}(k_i > 1, \phi_{b,i}') Z_{NN}(k_{i+1} < 1, \phi_{b,i+1}') \dots Z_{NN}(k_n < 1, \phi_{b,n}')\rangle = \\
&= \langle Z_{NN}(k_1 > 1, \phi_{b,1}')\rangle \dots \langle Z_{NN}(k_i > 1, \phi_{b,i}')\rangle \langle Z_{NN}(k_{i+1} < 1, \phi_{b,i+1}') \dots Z_{NN}(k_n < 1, \phi_{b,n}')\rangle.
\end{aligned}
\tag{3.85}
$$

However, while in the previous section, fixing g_{uu} on the boundary completely fixes the length b

of the closed geodesic homotopic to the boundary, in this section, since the proper length of the boundary is not fixed, b is also, consequently, not fixed.

To make things concrete and obtain the partition function, Z_{NN}, we can go between Dirichlet-Dirichlet and Neumann-Dirichlet boundary conditions using a Laplace transform and integrating over the boundary metric. Schematically this is given by[21]

$$Z_{NN}[k(u),\phi_b'] = \int \frac{\mathcal{D}g_{uu}}{\text{Diff}(S^1)} e^{2\int du\sqrt{g_{uu}}(\phi K - \partial_n\phi)} Z_{ND}\left[k(u), \int du\sqrt{g_{uu}}\right]. \tag{3.86}$$

The ND system has boundary diffeomorphism symmetry which has been mode out to get a finite result. Just like in the case of path integral of a relativistic particle, the integration over the boundary metric can be simplified by going to the gauge where $\sqrt{g_{uu}}$ is equal to a constant. Then the functional integral of $\sqrt{g_{uu}}$ can be reduced to an integral over the proper length L.[22] With the existence of a marked (for instance, at $u = 0$) point at the boundary, we have[23]

$$Z_{NN}[k(u),\phi_b'] = \int dL e^{2\int du\sqrt{g_{uu}}(\phi K - \partial_n\phi)} Z_{ND}[k(u), L]. \tag{3.87}$$

For simplicity, we will assume that $k(u) = k$ and $\phi_b'(u) = \phi_b'$ are constant. In such a case, we find that for the disk:

$$\begin{aligned} Z_{NN}^{(\text{Disk})}(k>1,\phi_b') &= \int dL e^{L\phi_b'} Z_{ND}^{(\text{Disk})}(k>1, L) \\ &= \frac{e^{\phi_0}}{2\pi}\int dL e^{L\phi_b'}\delta''\left(\frac{L\sqrt{k^2-1}}{4\pi} - \frac{1}{2}\right), \end{aligned} \tag{3.88}$$

where we have used (3.48) for the ND disk partition function, acting on the space of trace-class

[21] Below, for the NN boundary conditions we are no longer fixing g_{uu}. Therefore, we need to fix $k(u)$ in a diffeomorphism invariant fashion. This can be done by going to a diffeomorphism gauge where g_{uu} is constant and where the periodicity of u is fixed. Thus, when one fixes $k(u)$ for the ND and NN boundary conditions in (3.86), it should be understood that u is specified in this gauge.

[22] See section 9.2 of [104] for discussion about the procedure of fixing boundary diffeomorphism symmetry.

[23] If we don't have a marked point, there will be an additional $\frac{1}{\beta}$ factor coming from the time translation symmetry.

functions. Consequently,

$$\langle Z_{NN}(k>1,\phi_b')\rangle = \frac{8\pi e^{\phi_0} e^{\frac{2\pi\phi_b'}{\sqrt{k^2-1}}}}{(k^2-1)^2}\,. \tag{3.89}$$

This matches with the classical saddle-point obtained in (3.84). Similarly, for the trumpet we find

$$\begin{aligned} Z_{NN}^{(\text{Trumpet})}(k<1,\,\phi_b') &= \int dL e^{L\phi_b'}\frac{\delta(L\sqrt{1-k^2}-b)}{2\sinh\frac{b}{2}} \\ &= \frac{e^{\frac{b\phi_b'}{\sqrt{1-k^2}}}}{2\sqrt{1-k^2}\sinh\frac{b}{2}}\,, \end{aligned} \tag{3.90}$$

where we have used (3.65) for the ND partition function of the trumpet. Therefore, the NN partition function when summing over connected manifolds with n boundaries is

$$\begin{aligned} &\langle Z_{NN}(k_1<1,\phi_{b,1}')\dots Z_{NN}(k_n<1,\phi_{b,n}')\rangle_{\text{conn.}} \sim \\ &\sim \sum_{g\geq 0} e^{\phi_0\chi_{g,n}}\int db_1\, b_1\int db_2\, b_2\cdots\int db_n b_n \frac{e^{-\sum_{i=1}^n\frac{b_i\phi_{b,i}'}{\sqrt{1-k_i^2}}}}{2^n\left(\prod_{i=1}^n\sqrt{1-k_i^2}\sinh\frac{b_i}{2}\right)}\text{Vol}_{g,n}(b_1,\dots,b_n). \end{aligned} \tag{3.91}$$

Note that with the conventions from section 3.2.2 for the cylinder we have that $\text{Vol}_{0,2}(b_1,b_2) = \delta(b_1-b_2)/b_1$. Therefore, the NN cylinder partition function exhibits a log-divergence coming from the $\sim 1/b$ behavior in the limit $b\to 0$ of the integrand. Therefore, if we do not consider a more general UV completion of JT gravity,[24] all partition functions with $n\geq 2$ boundaries are dominated by cylindrical contributions.

Next, with the results in section 3.2.3, we can determine what operator insertion in the matrix integral description of JT gravity yields the NN results for the partition function obtained in

[24]It would however be interesting to understand whether there indeed is a UV completion of the model which leads to a convergent cylindrical partition function for the NN boundary conditions.

(3.85)–(3.91). By considering the Laplace transform of 3.81 we have that

$$Z_{NN}(k,\phi_b') \leftrightarrow \int dL e^{-L\phi_b'} \operatorname{Tr} \frac{\cos\left(L\sqrt{1-k^2}\sqrt{2H}\right)}{\sinh\left(\frac{L}{2}\sqrt{1-k^2}\right)}$$
$$= \operatorname{Tr}\left[-\frac{\mathcal{H}\left(-\frac{1}{2}+\frac{\phi_b'}{\sqrt{1-k^2}}-i\sqrt{2H}\right)+\mathcal{H}\left(-\frac{1}{2}+\frac{\phi_b'}{\sqrt{1-k^2}}+i\sqrt{2H}\right)}{\sqrt{1-k^2}}\right], \tag{3.92}$$

where $\mathcal{H}(x)$ is the analytically continued harmonic number.

3.4 Fixing ϕ and $\partial_n\phi$: microcanonical ensemble, relation with eigenbranes

In this section, we will discuss the DN boundary condition in JT gravity: fixed boundary value of dilaton field $\phi(u)|_{\partial\mathcal{M}} = \phi_b$ and its normal derivative $\partial_n\phi|_{\partial\mathcal{M}} = \phi_b'$. Let's start by discussing the classical solution with the DN boundary condition. Again, using the Fefferman-Graham gauge, we have the bulk solution of the dilaton field (3.28) on a disk:

$$\phi = \frac{A}{r}\left(1+4r^2\right) + \left(r-\frac{1}{4r}\right)\left(B\cos(u)+C\sin(u)\right). \tag{3.93}$$

Since we are fixing the boundary value of dilaton and its derivative, we can perform an $SL(2,\mathbb{R})$ coordinate transformation to set $B = C = 0$. Then the constant ϕ_b condition sets the boundary at constant r radius. Together with its normal derivative, this gives us two equations:

$$A = \frac{\sqrt{\phi_b^2-\phi_b'^2}}{4}, \qquad r_0 = \frac{1}{2}\sqrt{\frac{\phi_b+\phi_b'}{\phi_b-\phi_b'}}. \tag{3.94}$$

Notice that ϕ_b and ϕ_b' scale like $1/\varepsilon$ and their difference as ε.

The quantization of the theory is closely related to that with the standard DD boundary condition where the boundary value of dilaton ϕ_b and the boundary metric g are fixed. As we have explain previously, in Euclidean signature, the DD boundary condition with constant ϕ_b

corresponds to the canonical ensemble of the underlying gravitational theory where the inverse temperature β is the total regularized length $\varepsilon \int du \sqrt{g_{uu}}$.

The DN boundary condition, can be obtained from a Laplace transform of the DD boundary conditions. In this case we have to perform an integral of the DD partition function over the boundary metric g_{uu} with an additional weighting $e^{\varepsilon E \int du \sqrt{g_{uu}}}$:

$$Z_{DN}(\phi_b, E) = \int \frac{\mathcal{D}g_{uu}}{\text{Diff}(S^1)} e^{\varepsilon E \int du \sqrt{g_{uu}}} Z_{DD}(\phi_b, \varepsilon \int \sqrt{g_{uu}}). \tag{3.95}$$

Due to a counter term in the DD partition function, the relation between E and $\partial_n \phi$ is

$$E = \frac{2(\phi_b - \phi_b')}{\varepsilon}. \tag{3.96}$$

We will again follow the gauge fixing procedure for the boundary metric described in section 3.3 to write[25]

$$Z_{DN}(\phi_b, E) = \int d\beta e^{E\beta} Z_{DD}(\phi_b, \beta). \tag{3.97}$$

Given that in the matrix integral description we know that considering a DD boundary corresponds to inserting a partition function operator in the matrix integral, $Z_{DD}(\phi_b, \beta) \leftrightarrow \text{Tr} e^{-\beta H}$, we then can use this Laplace transform to obtain the matrix integral description of an ND boundary. This corresponds to the insertion of the density of states operator in the matrix integral,[26]

$$Z_{DN}(\phi_b, E) \qquad \leftrightarrow \qquad \rho(E) = \text{Tr}\, \delta(H - E) = \sum_i \delta(\lambda_i - E). \tag{3.98}$$

It is interesting to make connection of the DN boundary with the energy-eigenbrane dicussed in [82], which fixes one eigenvalue of the matrix H to be some fixed value E: $\delta(\lambda_1 - E)$. Using the permutation symmetry of the eigenvalues in the random matrix distribution, we see that the the DN partition function is just proportional to the eigenbrane operator. Consequently, any

[25]Here the β integration contour is along the imaginary axis.

[26]The normalization of H in the matrix integral on the RHS of (3.98) is the same as in [33] when setting $\gamma = \phi_r$.

correlator measured in JT gravity with DN boundary conditions will be equivalent to computing the same correlator in the matrix integral in the presence of eigenbranes. For this reason, we can identify the DN boundary conditions as energy-eigenbranes or energy-branes for short.

We now turn to the exact computation of the partition function for the DN boundary conditions. As in (3.76), the DD partition function can be written as a summation of Riemann surfaces [33]:

$$\langle Z_{DD}(\phi_b,\beta)\rangle = e^{\phi_0} Z_{DD}^{(\text{Disk})}(\phi_b,\beta) + \sum_{g=1}^{\infty} e^{\phi_0(1-2g)} \int_0^{\infty} bdb\, V_{g,1}(b) Z_{DD}^{(\text{Trumpet})}(b;\phi_b,\beta)\,. \tag{3.99}$$

To obtain the microcanonical (ND) partition function, one only needs to inverse laplace transform the corresponding disk and trumpet partition function:

$$Z_{DN}^{(\text{Disk})}(E) = \frac{\phi_r}{2\pi^2}\sinh 2\pi\sqrt{2\phi_r E}; \qquad Z_{DN}^{(\text{Trumpet})}(E,b) = \frac{\phi_r^{1/2}\cos b\sqrt{2\phi_r E}}{\pi\sqrt{2E}}. \tag{3.100}$$

The moduli integral and $V_{g,1}(b)$ will not change, since those are fully determined by the bulk curvature constraint and the Weil-Petersson measure. Replace these expressions in 3.99, we have the full genus expansion of the DN partition function,

$$\langle Z_{DN}(E)\rangle = e^{\phi_0} Z_{DN}^{(\text{Disk})}(E) + \sum_{g=1}^{\infty} e^{\phi_0(1-2g)} \int_0^{\infty} bdb\, V_{g,1}(b) Z_{DN}^{(\text{Trumpet})}(E,b) \tag{3.101}$$

Since we take the asymptotic limit $\phi_b \to \infty$, the integral range of b is from zero to infinity. Finally, note that non-perturbative corrections for correlators of the form (3.101) were computed in the context of energy-branes in [82]. With these results in mind we proceed to discuss the implications of these results to black hole toy models and, in particular, their relation to the microcanonical thermofield double and to fixed area states.

3.5 Applications

We can now use the results derived in sections 3.2–3.4 in the setting of black hole thermodynamics, holography, cosmology, of the minimal string, and of the baby universe Hilbert space where JT gravity has served as a toy model in the past [83, 84, 92–94].

In the case of black hole thermodynamics, we will only focus on the case of fixed ϕ and $\partial_n\phi$ in which a black hole horizon is present. We again emphasize that for fixed $K = k$, one cannot know whether the geometry has a horizon or not since the solution for ϕ cannot be fully fixed. Consequently, the factorization properties (that we point out in the previous sections) are not in tension with the Page curve analysis from [83,84] for which the contribution of connected replica wormholes is required.

Nevertheless, as we will see, the fixed $K = k$ and g_{uu} boundary condition is natural in the context of cosmological toy models, where similar factorization properties can be derived. For the convenience of the reader, it is useful to rephrase these factorization properties (both in AdS_2 and dS_2) in the baby universe Hilbert space language of Marolf and Maxfield [86]; in turn, this will motivate the renaming of the fixed K boundary conditions as α-eigenbranes, or α-branes for short.

Furthermore, it will prove informative to interpret the change of boundary conditions that we have studied throughout this chapter in the larger context of AdS/CFT. In that case, understanding the change of boundary conditions in the bulk amounts to studying the flow of the boundary theory under a multi-trace deformation. While for JT gravity, the exact boundary dual is still uncertain, it is interesting to speculate about the role of such deformations in the SYK model.

Finally, we will comment on the relation with $(2, p)$ minimal string theories. Specifically, in [33], it was shown how the spectral density of JT gravity arises from the large p limit of the $(2, p)$ minimal string. Here, we show how JT gravity's different boundary conditions can be explicitly mapped to boundary conditions in the minimal string.

3.5.1 Cosmology

So far, we have discussed mostly the anti-de Sitter case in two dimensions, but the attentive reader might have noticed that our analysis in section 3.1 applies to general dilaton potentials. In particular, it also holds for potentials with negative cosmological constant, where for instance, we have the action

$$S_{\text{top}} + S_{\text{bulk}} = -\chi(\mathcal{M})\phi_0 + \int_{\mathcal{M}} \sqrt{g}\phi(R-2) - 2\int_{\partial\mathcal{M}} \sqrt{\gamma}\phi K. \tag{3.102}$$

This theory was considered in detail in [92]. Instead of time-like asymptotic boundaries as in the AdS case, we now have space-like asymptotic boundaries, and we can ask what type of boundary conditions we can put on the phase space variables there since such variables are identical to those in AdS_2. While the variables are the same, there are a few differences. First of all, the object we compute in de Sitter is not a partition function but rather a wavefunctional. Second, in AdS, there are time-like boundaries, and so we can interpret some of the boundary conditions as different ensembles in quantum mechanics, but for dS it is not clear how to do that. For instance, fixing the normal derivative of the dilaton in the AdS case corresponded to fixing the energy of the boundary quantum mechanics, but in dS such an identification is not possible. From the gravitational path integral point of view, such boundary conditions are however well-defined.

One very natural and common boundary condition in cosmology (in 2D) fixes the metric and extrinsic curvature on the Cauchy slice. In particular, the extrinsic curvature can be used as a time coordinate conjugate to the volume of the spatial slice [96]. For JT in dS_2, these boundary conditions mean that we fix the extrinsic curvature and metric at the asymptotic past and future. This boundary condition was already discussed extensively in section 3.2, so we will be brief here and highlight the important implications for dS_2.

If we solve the equations of motion coming from varying (3.102), we find the following global

metric for dS_2 and the following profile for the dilaton:

$$ds^2 = -d\tau^2 + \cosh^2\tau\, d\varphi^2, \quad \phi = \phi_h \sinh\tau, \tag{3.103}$$

where $\varphi \sim \varphi + 2\pi$ for the Hartle-Hawking state. In the Fefferman-Graham gauge used in equation 3.14 we can write the metric solution as

$$ds^2 = -\frac{dt^2}{t^2} + \left(t + \frac{f(\tilde{\varphi})}{t}\right)^2 d\tilde{\varphi}^2. \tag{3.104}$$

Here t and τ are to be thought of as complex, representing a Euclidean section when purely imaginary and Lorentzian when real and a particular contour in the complex t or τ plane corresponds to a particular gluing of a Lorentzian section to a Euclidean one. For instance, when computing the Hartle-Hawking wavefunction we employ the no-boundary proposal and continue the metric (3.103) (at $\tau = 0$ we set $\tau = i\theta$) to a hemisphere to cap off the space-time.

As noted in [92], since $R = 2$ for these metrics, it seems, naively that we cannot have higher genus contributions. This can be overcome by taking a different contour for the metric. There the contour $\tau = i\pi/2 + \tilde{\tau}$ was used [105] and sends the metric in (3.103) to

$$ds^2 = -(d\tilde{\tau}^2 + \sinh^2\tilde{\tau} d\varphi^2), \tag{3.105}$$

which was dubbed $-$AdS for obvious reasons. This then naturally paves the way for considering geometries like the trumpet but with an overall sign in front of the metric. In this way, one can indeed have higher genus contributions to the wavefunction. From the Fefferman-Graham gauge, equation (3.104), it is also amusing to see that the usual contour would already work. If we take $t = i\tilde{\tau}$, then the metric becomes

$$ds^2 = -\left(\frac{d\tilde{\tau}^2}{\tilde{\tau}^2} + \left(\tilde{\tau} - \frac{f(\tilde{\varphi})}{\tilde{\tau}}\right)^2 d\tilde{\varphi}^2\right). \tag{3.106}$$

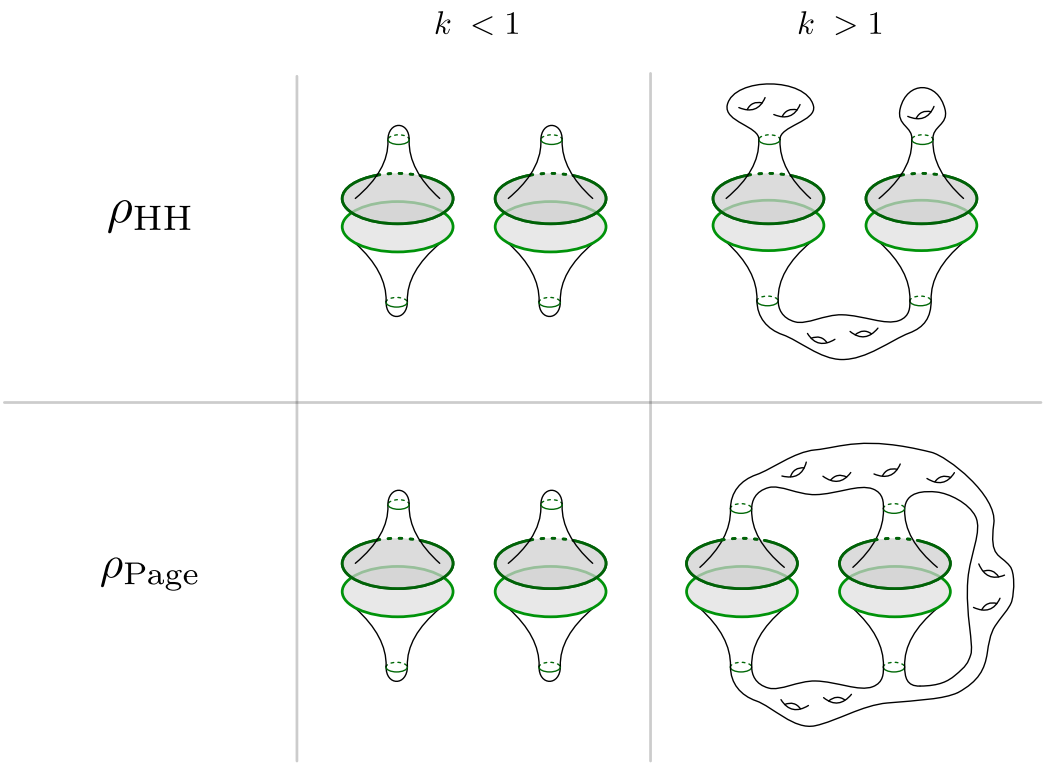

Figure 3.5: Contributions to two examples of gravitational density matrices. The lighter green boundaries indicate the ket and the darker ones the bra. In the top row we indicated the contributions to the density matrix associated to the Hartle-Hawking state ($\rho_{\text{HH}} = |\Psi_{\text{HH}}\rangle \langle\Psi_{\text{HH}}|$) for $k < 1$ and $k > 1$. In the latter case, any topology other than the disk contributes as long as there are no bra-ket wormholes (wormholes connecting the ket and bra). In the bottom row, we indicated what topologies contribute to the Page density matrix. The situation is similar in the top row; however, since the Page state allows bra-ket wormholes, there can be topologies connecting the bra and ket. Notice that $\rho_{\text{HH}} = \rho_{\text{Page}}$ for $k < 1$, whereas they are unequal for $k > 1$ due to the appearance of bra-ket wormholes. In each geometry, we have indicated the gluing of the Lorentzian with the Euclidean section with a small green curve.

This is precisely minus the metric (3.14). So the minus trumpet would be obtained by taking $f(\tilde{\varphi})$ constant and negative and cut the geometry at the minimal waist size. There we can then glue higher genus geometries.

Now that we understand how to glue higher genus topologies to an asymptotic de Sitter boundary, let us see what fixed $K|_\partial = k$ [27] and g_{uu} implies. In fact, all conclusions in the AdS case similarly go through in this case. First, for $k < 1$ (as opposed to $k > 1$ in AdS_2) we only have disk contributions and so this means that when we compute a wavefunction with a

[27] Recall that we only focus on $K > 0$.

number of future boundaries, it will just be the product of the wavefunctions for the disk for each boundary. Furthermore, if we are computing matrix elements of a gravitational density matrix, so there are a number past and future boundaries, there are no bra-ket wormholes, i.e., a geometry connecting the bra and ket boundary, [94, 95, 84]. Second, for $k > 1$, this situation is reversed as there will only be higher genus and no disk contributions. Therefore, matrix elements of the gravitational density matrix would allow for bra-ket wormholes.

A few comments are in order. As noted in [95], when computing gravitational density matrices, it is important to specify the global state in the baby universe Hilbert space $\mathcal{H}_{\text{BU}}$. If one computes the Hartle-Hawking density matrix, the matrix elements are computed by a product of two path integrals, and so no bra-ket wormholes can exist in the first place, regardless of what the extrinsic curvatures of the boundaries are. For the Page density matrix, there can be bra-ket wormholes but with these fixed k boundary conditions, they only exist for $k > 1$, leading to the non-trivial statement that for $k < 1$ the Page density matrix appears to be equivalent to the Hartle-Hawking state. We have summarized the case for the Hartle-Hawking state and Page density matrix in figure 3.5.

3.5.2 α-states in JT gravity

In section 3.2 and 3.5.1, we saw that depending on whether the extrinsic curvature is bigger or smaller than one, we allow or disallow higher genus corrections to the gravitational path integral. If such higher genus topologies (say in the case of l boundaries with $k > 1$) do not contribute, it means that the full perturbative partition function equals the disconnected contribution, i.e., it is a product of l disk partition functions. This allows us to define α-states directly. Following [86–89] we define the operator $\widehat{Z}_{ND}[k, L]$ as an operator in the baby universe Hilbert space $\mathcal{H}_{\text{BU}}$ that creates a boundary with proper length L and extrinsic curvature k. An α state is then an eigenstate of the operator $\widehat{Z}_{ND}[k, L]$.

For an l-point function of such boundary creating operators with $k > 1$, we have

$$\langle \widehat{Z}^{>}_{ND,1} \cdots \widehat{Z}^{>}_{ND,l} \rangle = \langle \widehat{Z}^{>}_{ND,1} \rangle \cdots \langle \widehat{Z}^{>}_{ND,l} \rangle = Z^{\text{Disk}}_{ND,1} \cdots Z^{\text{Disk}}_{ND,l} \,, \tag{3.107}$$

where the subscript indicates the the argument (k_i, L_i), the superscript $k > 1$ and the expectation value is in the Hartle-Hawking state. This is a curious equation, because it says that the Hartle-Hawking state is an α state for $k > 1$ boundary creating operators

$$\widehat{Z}^{>}_{ND}[k, L] \, |\text{HH}\rangle = Z^{\text{Disk}}_{ND}(k, L) \, |\text{HH}\rangle \,, \quad k > 1 \,. \tag{3.108}$$

Furthermore, it is easy to construct more α states $|\alpha_l\rangle$ by acting with $\widehat{Z}^{<}_{ND}[k, L]$ on the Hartle-Hawking state but now restricting $k < 1$,

$$|\alpha_l\rangle = \widehat{Z}^{<}_{ND,1} \cdots \widehat{Z}^{<}_{ND,l} \, |\text{HH}\rangle \tag{3.109}$$

These operators with $k < 1$ do not factorize by themselves, since higher genera do contribute in that case, but the $k > 1$ operators do again factorize out,

$$\langle \widehat{Z}^{>}_{ND,1} | \alpha_l \rangle = \langle \widehat{Z}^{>}_{ND,1} \widehat{Z}^{<}_{N,1} \cdots \widehat{Z}^{<}_{ND,l} \rangle = \langle \widehat{Z}^{>}_{ND,1} \rangle \, \langle \widehat{Z}^{<}_{ND,1} \cdots \widehat{Z}^{<}_{ND,l} \rangle \tag{3.110}$$

so

$$\widehat{Z}^{>}_{ND,1} \, |\alpha_l\rangle = Z^{\text{Disk}}_{ND,1} \, |\alpha_l\rangle \,. \tag{3.111}$$

The $|\alpha_l\rangle$ states thus constructed are, however, not orthogonal to the Hartle-Hawking state.

One of the interesting statements about the construction of a Hilbert space using these correlation functions, i.e., the GNS construction, is the existence of null states. From a gravitational perspective, these null states form a highly non-trivial relation between states with a different number of boundaries. For the fixed $k < 1$ operators $\widehat{Z}_{ND}[k < 1, L]$, the correlators are (up to multiplicative factors) the Weil-Petersson volumes, and the existence of such null states is

equivalent to the presence of a highly non-trivial relation between such volumes. Given that such volumes are polynomial in the L_i, one could choose coefficients in a superposition of states $|\alpha_l\rangle$ so that all powers of the L_i have vanishing coefficient once the inner product is taken. It would be interesting to see whether such a system of equations has a non-trivial solution.

Furthermore, although it is not true that the α-states defined with fixed K can easily give α-states in the theory defined with DD b.c., the reversed statement is true. An α-state in the DD theory, which would be the original α-states proposed by Marolf and Maxfield, does correspond to an α-state in the fixed K theory. That is because, in the DD theory, the α-state would be an eigenstate of $\widehat{Z}_{DD}[\phi, L]$ for any ϕ; thus, the Laplace transform gives an eigenstate of $\widehat{Z}_{ND}[k, L]$, but now for any k, not just $k > 1$.

3.5.3 Mixed boundary conditions and AdS/CFT

In the previous discussions, we mostly focussed on fixing either member of a canonical pair. This gave us the four different boundary conditions: DD, ND, DN and NN. In the context of AdS/CFT however, there is a standard way [106,107] to generalise this to mixed boundary conditions, which fixes a certain combination of say, the metric and stress tensor. For a well-defined variational principle, this means that one has to add a multi-trace operator to the boundary field theory, or said differently, the addition of a multi-trace operator is holographically dual to a change in boundary conditions, at least to leading order in large N. In [108] this was worked out for the case of JT gravity on the disk, assuming a putative dual quantum mechanics. In particular in that case one would start with the JT gravity action with DD boundary conditions, whose variation gives

$$\delta S = \int_{\partial \mathcal{M}} du \sqrt{g_{uu}} \left(\frac{1}{2} T_{uu} \delta g^{uu} + O \delta \phi \right) , \tag{3.112}$$

with (using the Fefferman-Graham gauge (3.14))

$$T_{uu} = (-2 r g_{uu} (1 - r \partial_r) \phi)|_\partial , \quad O = (2 r^2 (1 - K))|_\partial , \tag{3.113}$$

the Hamiltonian density of the dual quantum mechanics and the operator dual to the dilaton, respectively. The variation (3.112) of course vanishes because we have fixed the metric and dilaton on the boundary. From the putative dual quantum mechanics, (3.112) is the usual formula for how the action changes due to a change of the metric and scalar source (in this case the dilaton).

To change the DD boundary conditions, we want to add to the original action a term that can combine into something else that instead of just giving δg^{uu} or $\delta\phi$, could perhaps come from a linear combination that involves O and T_{uu}. In [108] this idea was employed to determine the term needed to impose the DD boundary conditions at finite radial coordinate (see also [109] for the original proposal). In the present context, let us for instance consider adding the following term to the action,

$$S_{\text{d.t.}} = \mu \int du \sqrt{g_{uu}} O^2 \tag{3.114}$$

The variation of this term together with (3.112) can be combined into a variation just like (3.112), but with T_{uu} and ϕ now depending on μ,

$$\delta S_{\text{tot}} = \int du \sqrt{g_{uu}} \left(\frac{1}{2}(T_{uu} - \mu g_{uu} O^2)\delta g^{uu} + O\delta(\phi + 2\mu O) \right). \tag{3.115}$$

Thus for a well-defined variational problem from the bulk point of view, we need to fix $\phi + 2\mu O$ [28] instead of ϕ, whereas we still fix g_{uu} on the boundary. Taking μ large we see that we are basically fixing (the one-point function of) O, the operator canonically conjugate to the dilaton, which in term of gravitational variables is just K_r if we scale $K = 1 + \epsilon^2 K_r$. The addition of O^2 therefore interpolates between DD and ND boundary conditions.

Let us make two comments regarding this standard way of dealing with different boundary conditions in AdS/CFT. First, the analysis done here is classical and the fate of them at the quantum level is unclear. We have analysed the problem in the $\mu = 0$ and $\mu \to \infty$ limit in which we could do the computation exactly. However, these two limits are rather special and

[28] Here we work at the classical level and one should think of fixing $\phi + 2\mu O$ as fixing its one-point function.

in particular the ND boundary conditions gave us a topological theory. By tuning μ we thus need to see this transmutation of the theory, which most likely involves a careful analysis of the quantum theory. Furthermore, as we saw in section 3.2 the sign of $1 - K$ is also important, hence the sign of μ will also have to play a crucial role. Second, in contrast to some of the higher dimensional versions of AdS/CFT, in one dimension, we only know of a theory that approximately (there are many massless modes) describes the 2d bulk, namely the Sachdev-Ye-Kitaev (SYK) model. In the IR, this model behaves as a gravitational theory, while in the UV it is a theory of disorderly interacting Majorana fermions. In the IR theory we can identify the boundary value of the dilaton with the inverse of the variance of the gaussian disorder in SYK. The question then remains what is the operator O in SYK model? If we imagine perturbing the dilaton we induce a rescaling of the couplings J_{ijkl} and the change in the action will then be the SYK Hamiltonian. A proposal for the operator O would then simply be the UV Hamiltonian of the SYK model. With this proposal one would then need to check that adding this operator in the UV and flowing to the IR has the desired effect of changing the IR action by (3.114).

3.5.4 Boundary Conditions in the Minimal String

Finally, one can consider an analogous classification of boundary conditions from the perspective of minimal gravity. The connection between JT gravity and the minimal string was first conjectured in [33], who obtained the spectral density of JT gravity from the large p limit of the $(2, p)$ minimal string. This connection was elaborated in [47]. This motivates us to extend our classification to this more general setup. We will investigate this connection from an alternate point of view using the Coulomb gas description of the matter field derived in [110,111] (see also, Appendix F of [47]). The theory considered here may then be viewed as a Coulomb gas CFT (χ) with a gravitational dressing described by a Liouville CFT (φ) resulting in a Weyl invariant

theory with action $S = S_L[\varphi, \widehat{g}] + S_M[\chi, \widehat{g}] + S_{gh}[b, c, \widehat{g}]$, [29]

$$\begin{aligned} S_L[\varphi] = & \quad \frac{1}{2}\int_{\mathcal{M}} d^2x\sqrt{\widehat{g}}\left[(\widehat{\nabla}\varphi)^2 + Q\widehat{R}\varphi + 4\pi\mu_L e^{2b\varphi}\right] + \oint_{\partial\mathcal{M}} du\sqrt{\widehat{h}}\left[Q\widehat{K}\varphi + 2\pi\mu_L^B e^{b\varphi}\right] \\ S_M[\chi] = & \quad \frac{1}{2}\int_{\mathcal{M}} d^2x\sqrt{\widehat{g}}\left[-(\widehat{\nabla}\chi)^2 - q\widehat{R}\chi + 4\pi\mu_M e^{2b\chi}\right] + \oint_{\partial\mathcal{M}} du\sqrt{\widehat{h}}\left[-q\widehat{K}\chi + 2\pi\mu_M^B e^{b\chi}\right] \end{aligned} \tag{3.116}$$

with $\widehat{g}$ a fixed background metric, worldsheet coordinates x, background charges $Q = b + b^{-1}$, $q = b^{-1} - b$ and central charges $c_L = 1 + 6Q^2$, $c_M = 1 - 6q^2$. We have also included the proper boundary terms. The first term is fixed by the Euler character that controls the string expansion and a potential FZZT boundary interaction term with fixed boundary cosmological constant. The parameter b is related to p via $b = \sqrt{\frac{2}{p}}$.

Using the field redefinitions

$$\varphi = b^{-1}\rho - b\Phi, \qquad\qquad \chi = b^{-1}\rho + b\Phi, \tag{3.117}$$

one can establish a correspondence with a 'p-deformed' version of JT gravity with a sinh potential for the dilaton [110, 47]

$$\begin{aligned} S = & \int_{\mathcal{M}} d^2x\sqrt{\widehat{g}}\left[2\Phi\cdot\widehat{\nabla}^2\rho + \widehat{R}(\rho - \Phi) - 4\pi\mu e^{2\rho}\sinh\left(2b^2\Phi\right)\right] \\ & + 2\oint_{\partial\mathcal{M}} du\sqrt{\widehat{h}}\left[\widehat{K}(\rho - \Phi) - 2\pi\mu^B e^{\rho}\sinh\left(b^2\Phi\right) - \Phi\widehat{\partial}_n\rho\right] + S_{\rm gh} \end{aligned} \tag{3.118}$$

where we also chose $\mu_L = -\mu_M = \mu$ and $\mu_L^B = -\mu_M^B = \mu^B$.

Let us express the above action in terms of a physical (dynamical) metric g which is related to the fiducial metric $\widehat{g}$ via a conformal factor which we identify with the field ρ, namely $g_{\mu\nu} = e^{2\rho}\widehat{g}_{\mu\nu}$. To express the action in terms of the physical metric, we use the Weyl transformation

[29] Notice that at the level of the action, one can obtain the matter action from the Liouville action by rotating $b \to ib$ and $\varphi \to -i\chi$ to treat both the theories as Liouville fields φ_+ and φ_- on an equal footing. The central charges are then $c_\pm = 1 + 6Q_\pm^2 = 13 \pm (b^2 + b^{-2})$ and $c_+ + c_- = 26$.

properties,

$$R = e^{-2\rho}(\widehat{R} - 2\widehat{\nabla}^2\rho), \qquad K = e^{-\rho}\left(\widehat{K} + \widehat{\partial}_n\rho\right), \tag{3.119}$$

where hatted quantities are evaluated in the background metric. The action is then given by

$$\begin{aligned} S = &-\int_{\mathcal{M}} d^2x\sqrt{g}\left[\Phi R - R\rho + 2(\nabla\rho)^2 + 4\pi\mu\sinh\left(2b^2\Phi\right)\right] \\ &- 2\oint_{\partial\mathcal{M}} du\sqrt{h}\left[K\Phi - K\rho + 2\pi\mu^B e^{\rho}\sinh\left(b^2\Phi\right)\right] + S_{\text{gh}}\,. \end{aligned} \tag{3.120}$$

In the $p \to \infty$ limit, one recovers ordinary JT with the identification of the physical metric $g_{\mu\nu} = e^{2\rho}\widehat{g}_{\mu\nu}$ in terms of the fiducial metric $\widehat{g}$ and by scaling the cosmological constant to large values such that $4\pi\mu b^2 = \Lambda_{JT} = 1$ and $2\pi\mu^B b^2 = 1$. In the strict JT limit, the conformal mode ρ is non-dynamical and kinetic term involving solely ρ may be omitted as it contributes to an overall constant in the path integral [30]

$$S \overset{b\to 0}{\approx} -\int_{\mathcal{M}} d^2x\sqrt{g}\left[\Phi(R+2)\right] - 2\oint_{\partial\mathcal{M}} du\sqrt{h}\left[\Phi(K-1)\right]. \tag{3.121}$$

Hence, we see the correspondence between the degrees of freedom in the two descriptions

$$(e^{2\rho})_{\text{Liouville}} \leftrightarrow (g_{uu})_{\text{JT}}, \qquad (\Phi)_{\text{Liouville}} \leftrightarrow (\phi)_{\text{JT}}. \tag{3.122}$$

where all the quantities refer to their boundary values.

To classify the boundary conditions, let us compute the variation of the action

$$\begin{aligned} \delta S &= \text{EOM} - 2\oint_{\partial\mathcal{M}} du\sqrt{h}\left(\delta\Phi(\widehat{\partial}_n\rho + \widehat{K}) + \delta\rho(\widehat{\partial}_n\Phi - \widehat{K}) + 2\pi\mu^B\delta\left(e^{\rho}\sinh(b^2\Phi)\right)\right) \\ &= \text{EOM} - 2\oint_{\partial\mathcal{M}} du\left[\delta\Phi e^{\rho}(K + 2\pi\mu^B b^2\cosh(b^2\Phi))\right. \\ &\qquad\qquad \left. +\delta(e^{\rho})\left(\partial_n\Phi - K + \partial_n\rho + 2\pi\mu^B\sinh(b^2\Phi)\right)\right]. \end{aligned} \tag{3.123}$$

[30] The same is also true for the ghost part of the action $S_{gh} = \int d^2z\sqrt{\widehat{g}}(b\widehat{\nabla}c + \overline{b}\widehat{\nabla}\overline{c})$, which does not depend on ρ and Φ.

where in the last equation, we took $h_{\mu\nu}dx^\mu dx^\nu = e^{2\rho}du^2$. We see that the variation vanishes when fixing ρ and Φ on the boundary. This is analogous to the DD boundary condition in JT gravity via the identification (3.122) and is consistent with the corresponding boundary term appearing in (4.28).

Hence, we see that the alternate boundary conditions involve fixing the energy in this theory or fixing the extrinsic curvature in the physical metric instead of ϕ and ρ via a Legendre transform to the corresponding conjugate variables. So to complete the mapping, we have

$$\begin{aligned}(K + 2\pi\mu^B b^2\cosh(b^2\Phi))_{\text{Liouville}} &\leftrightarrow (K)_{\text{JT}},\\ (\partial_n\Phi - K + \partial_n\rho + 2\pi\mu^B\sinh(b^2\Phi))_{\text{Liouville}} &\leftrightarrow (\partial_n\phi - \phi K)_{\text{JT}}\,,\end{aligned} \tag{3.124}$$

which leads to an analogous four-fold classification of boundary terms. We see that the conjugate variables are p-deformed by the boundary interaction. In addition, we also have extra contributions from the variation of the ρ mode that we have dropped earlier in the JT limit. This implies that one must be wary of the fact that the operations of varying the action and taking the JT limit do not commute.

So far, the analysis is exact at the level of the path integral. However, the boundary conditions implied here only match in the $b \to 0$ limit when compared to those used in [47]. This is related to the choice of normal ordering when quantizing this theory. It would be interesting to study the full quantum mechanical partition function and amplitudes in this theory and its matrix model dual. It would also be interesting to see if this theory can be directly related to the gas of defects studied in [112, 113].

3.6 Appendix A : The variation of the bulk action

In this appendix we compute the variation of the bulk action

$$S_{\text{bulk}} = -\frac{1}{2\kappa^2}\int_{\mathcal{M}} d^2x\sqrt{g}\,(\phi R - 2U(\phi)) \tag{3.125}$$

In particular, we will focus on the boundary terms, which are of prime importance in the bulk of the text. We will set $2\kappa^2 = 1$. Abstractly the variation will take the form

$$\delta S_{\text{bulk}} = -\int_{\mathcal{M}} d^2x\sqrt{g}\,(E_\phi\delta\phi + E_{\mu\nu}\delta g^{\mu\nu} + \nabla^\mu\Theta_\mu) \tag{3.126}$$

The first two terms give the equations of motion:

$$E_\phi = (R+2), \quad E_{\mu\nu} = \left(\nabla^\mu\nabla^\nu - g^{\mu\nu}\nabla^2\right)\phi - g_{\mu\nu}U(\phi), \tag{3.127}$$

whereas $\nabla^\mu\Theta_\mu$ gives rise to a boundary term in the variation. To derive the equations of motion and an explicit form for Θ_μ, we use

$$\delta R = R_{\mu\nu}\delta g^{\mu\nu} + \nabla^\rho(g^{\mu\nu}\delta\Gamma^\rho_{\nu\mu} - g^{\mu\rho}\delta\Gamma^\nu_{\nu\mu}), \tag{3.128}$$

with Γ the Christoffel symbol associated to g. Inserting its explicit form, we can write the term in brackets as

$$g^{\mu\nu}\delta\Gamma^\rho_{\nu\mu} - g^{\mu\rho}\delta\Gamma^\nu_{\nu\mu} = g^{\nu\rho}g^{\alpha\beta}(\nabla_\beta\delta g_{\alpha\nu} - \nabla_\nu\delta g_{\alpha\beta}) \tag{3.129}$$

and the variation of the bulk action becomes

$$\begin{aligned}\delta S_{\text{bulk}} = -\int_{\mathcal{M}} d^2x\sqrt{g}\,\big(&\delta\phi(R - 2U'(\phi)) - \nabla^\rho\phi(\nabla^\alpha\delta g_{\alpha\rho} - g^{\alpha\beta}\nabla_\rho\delta g_{\alpha\beta}) \\ &-U(\phi)g^{\mu\nu}\delta g_{\mu\nu}) - \int_{\partial\mathcal{M}} du\sqrt{h}\phi n^\mu(\nabla^\alpha\delta g_{\alpha\mu} - g^{\alpha\beta}\nabla_\mu\delta g_{\alpha\beta}),\end{aligned} \tag{3.130}$$

with h the induced metric on the boundary. Notice that in $2d$ we have $R_{\mu\nu} = \frac{1}{2}Rg_{\mu\nu}$, $K_{\mu\nu} = Kh_{\mu\nu} = \nabla_\alpha n^\alpha h_{\mu\nu}$ and

$$n^\mu(\nabla^\alpha \delta g_{\alpha\mu} - g^{\alpha\beta}\nabla_\mu \delta g_{\alpha\beta}) = -2\delta K + D^\nu(n_\nu n^\alpha n^\beta \delta g_{\alpha\beta}) - 2K^{\mu\nu}\delta g_{\mu\nu} - n^\nu h^{\alpha\beta}\nabla_\alpha \delta g_{\beta\nu} \quad (3.131)$$

Here D^ν is the boundary covariant derivative. After doing a couple of partial integrations it is straightforward to verify that the equations are as given above. The boundary term takes the form

$$\delta S_{\text{bulk},\partial} = -\int_{\partial\mathcal{M}} \sqrt{h}du \left[(\partial_n\phi - K\phi)\, g^{\alpha\beta}\delta g_{\alpha\beta} - 2\phi\delta K\right] \quad (3.132)$$

This term needs to cancelled by an appropriated boundary term depending on what boundary conditions are chosen in order to have a well-defined variational problem.

3.7 Appendix B : Schwarzian calculation for fixed K and g_{uu}

Here we will perform a direct Schwarzian calculation of the fixed K boundary path integral in the asymptotic limit. Let's start with the disk case first, the fixed K boundary condition can be obtained from the usual dirichlet boundary condition by doing a functional integral over $\phi_b = \frac{\phi_r}{\varepsilon}$, this gives us the following boundary integral:

$$\begin{aligned} Z_{ND} &= \int D\phi_b(u) e^{-2\int_0^\beta du\sqrt{g_{uu}}\phi_b(u)k} Z_{DD}(\phi_b(u)) = \int D\phi_r(u) \int Df(u) e^{\int_0^\beta du\phi_r(u)(\text{Sch}(f,u)-\kappa)} \\ &= \int Df(u)\delta(\text{Sch}(f,u)-\kappa), \end{aligned} \quad (3.133)$$

where $\kappa = \frac{k-1}{\varepsilon^2}$ is the regularized extrinsic curvature in the asymptotic limit. This integral can be done by perturbation theory, where we expand

$$f(u) = \tan\left(\frac{\pi}{\beta}(u+\epsilon(u))\right), \quad \epsilon(u) = \sum_{|n|\geq 2} e^{-\frac{2\pi}{\beta}inu}(\epsilon_n^{(R)} + i\epsilon_n^{(I)}), \tag{3.134}$$

and we have $\epsilon_n^{(R)} = \epsilon_{-n}^{(R)}$ and $\epsilon_n^{(I)} = -\epsilon_{-n}^{(I)}$. The integral measure for ϵ is determined by their symplectic form [33]

$$\Omega = 2\frac{(2\pi)^3}{\beta^2}\sum_{n\geq 2}(n^3-n)d\epsilon_n^{(R)} \wedge d\epsilon_n^{(I)}. \tag{3.135}$$

To the first order expansion of ϵ, the delta function of Schwarzian function is equal to

$$\begin{aligned}
&\delta\left(\frac{2\pi^2}{\beta^2} - \kappa + \sum_{n\geq 2} 2\frac{(2\pi)^3}{\beta^3}(n^3-n)(\epsilon_n^{(R)}\sin\frac{2\pi nu}{\beta} - \epsilon_n^{(I)}\cos\frac{2\pi nu}{\beta})\right) \\
&= \delta\left(\frac{2\pi^2}{\beta^2} - \kappa\right)\delta(0)^2\prod_{n\geq 2}\frac{1}{2\frac{(2\pi)^6}{\beta^6}(n^3-n)^2}\delta(\epsilon_n^{(R)})\delta(\epsilon_n^{(I)}),
\end{aligned} \tag{3.136}$$

where the additional two $\delta(0)$s come from the $n = \pm 1$ fourier modes. It is then straightforward to direct evaluate the path integral

$$Z_{ND}^{(\text{Disk})} = \delta\left(\frac{2\pi^2}{\beta^2} - \kappa\right)\delta(0)^2\prod_{n\geq 2}\frac{\beta^4}{(2\pi)^3}\frac{1}{n^3-n} = \delta\left(\frac{2\pi^2}{\beta^2} - \kappa\right)\delta^2(0), \tag{3.137}$$

where in the last equality we absorbed the regularized product (which is finite) in $\delta^2(0)$. Let's now look at the trumpet partition funciton with geodesic length b. The perturbation of the boundary wiggle is

$$f(u) = e^{-\frac{b}{\beta}(u+\epsilon(u))}; \quad \epsilon(u) = \sum_{|n|\geq 1} e^{-\frac{2\pi}{\beta}inu}(\epsilon_n^{(R)} + i\epsilon_n^{(I)}). \tag{3.138}$$

The symplectic measure for ϵ is now

$$\Omega = 2\frac{(2\pi)^3}{\beta^2}\sum_{n\geq 1}\left(n^3+\frac{b^2}{(2\pi)^2}n\right)d\epsilon_n^{(R)}\wedge d\epsilon_n^{(I)}. \tag{3.139}$$

The delta function of the Schwarzian variable to linear order in ϵ is equal to

$$\begin{aligned}&\delta\left(-\frac{b^2}{2\beta^2}-\kappa+\sum_{n\geq 1}2\frac{(2\pi)^3}{\beta^3}(n^3+\frac{b^2}{(2\pi)^2}n)(\epsilon_n^{(R)}\sin\frac{2\pi nu}{\beta}-\epsilon_n^{(I)}\cos\frac{2\pi nu}{\beta})\right)\\&=\delta\left(\frac{b^2}{2\beta^2}+\kappa\right)\prod_{n\geq 1}\frac{1}{2\frac{(2\pi)^6}{\beta^6}\left(n^3+\frac{b^2}{(2\pi)^2}n\right)^2}\delta(\epsilon_n^{(R)})\delta(\epsilon_n^{(I)}).\end{aligned} \tag{3.140}$$

Putting these together, the single trumpet partition function is given by

$$Z_{ND}^{(\text{Trumpet})}=\delta\left(\frac{b^2}{2\beta^2}+\kappa\right)\prod_{n\geq 1}\frac{\beta^4}{(2\pi)^3}\frac{1}{n^3+\frac{b^2}{(2\pi)^2}n}=\delta\left(\frac{b^2}{2\beta^2}+\kappa\right)\frac{b}{2\beta^2\sinh\frac{b}{2}}, \tag{3.141}$$

where we use the formula

$$\sum_{n\geq 1}\log(n^2+a^2)=\log\frac{2\sinh a\pi}{a}. \tag{3.142}$$

The cylinder result can be obtained by gluing two trumpets with the WP measure of b, this give us

$$\int bdbZ_{ND}^{(\text{Trumpet})}(\beta_1,\kappa_1;b)Z_{ND}^{(\text{Trumpet})}(\beta_2,\kappa_2;b)=\frac{-2\kappa_1\beta_1^2}{\sinh^2\left(\beta_1\sqrt{\frac{-\kappa_1}{2}}\right)}\delta(\kappa_1\beta_1^2-\kappa_2\beta_2^2). \tag{3.143}$$

To make comparison with formula 3.62 and 3.64, we can define the holonomy $\lambda_{1,2}=\beta_{1,2}\sqrt{-2\kappa_{1,2}}$. Then the cylinder partition function and trumpet partition function can be rewritten as:

$$Z_{ND}^{(\text{Cylinder})}=\frac{\lambda_1}{4\sinh^2\frac{\lambda_1}{2}}\delta(\lambda_1-\lambda_2),\quad Z_{ND}^{(\text{Trumpet})}=\frac{\delta(b-\lambda)}{2\sinh\frac{b}{2}}. \tag{3.144}$$

3.8 Appendix C : Delta functions and the Weyl integration formula

Here we consider the different delta functions that appeared in the main text in more detail. We will first consider the compact group case, exemplified with $SU(2)$ and move on to $PSL(2,\mathbb{R})$ afterwards. These discussions are just to gain some intuition. The more rigorous unifying framework to discuss both cases at once is the Weyl integration formula, which we discuss at the end.

3.8.1 The case for $SU(2)$

As is well known, the delta function $\delta(g)$ on a group manifold G for $g \in G$ has two different interpretations. On the one hand, we can think of the Lie group G as a manifold and locally one can pick a metric with which one can define the delta function in the usual sense. For instance, consider the group $SU(2)$. This Lie group is isomorphic to the 3-sphere. A metric on this three sphere is

$$ds^2 = d\alpha^2 + \sin^2\alpha\, d\beta^2 + \sin^2\alpha \sin^2\beta\, d\gamma^2, \quad \alpha,\beta \in (0,\pi], \gamma \in [0,2\pi), \tag{3.145}$$

with measure $d^3x = \sin^2\alpha \sin\beta \;\; d\alpha d\beta d\gamma$. In these coordinates $SU(2)$ group elements are parametrized as

$$g = \begin{pmatrix} \cos\alpha + i\cos\beta\sin\alpha & e^{i\gamma}\sin\alpha\sin\beta \\ -e^{-i\gamma}\sin\alpha\sin\beta & \cos\alpha - i\cos\beta\sin\alpha \end{pmatrix} \tag{3.146}$$

The delta function on $SU(2)$ is

$$\delta_{SU(2)}(g) = \frac{1}{\sin^2\alpha\sin\beta}\delta(\alpha)\delta(\beta)\delta(\gamma). \tag{3.147}$$

This delta function is then defined for smooth test functions f on the three sphere or equivalently on $SU(2)$. Suppose now that we restrict the space of test functions to only those that depend on the conjugacy classes of $SU(2)$, which with our parametrisation are parametrized by α. So we have $f = f(\alpha)$. On the sphere, these are spherical symmetric test functions. For such functions, the delta function is slightly different as can be seen as follows,

$$f(0) = \int dg \delta_{SU(2)}(g) f(g) = \int d^3x \frac{1}{\sin^2\alpha \sin\beta} \delta(\alpha)\delta(\beta)\delta(\gamma) f(\alpha) = \int_0^\pi d\alpha \sin^2\alpha f(\alpha) \frac{\delta(\alpha)}{\sin^2\alpha} \tag{3.148}$$

So on the 'spherically symmetric' test functions, the delta function is

$$\delta_c(g) = \frac{\delta(\alpha)}{\sin^2\alpha} \tag{3.149}$$

with the subscript c referring to 'conjugacy class'. Yet another way of thinking about the delta function $\delta(g)$ is through the character decomposition:

$$\delta(g) = \sum_R \dim R \, \chi_R(g) \tag{3.150}$$

where the sum is over all irreducible representations of G. From this expression, it is clear thet $\delta(g)$ is trace class. For $G = SU(2)$ this gives

$$\delta(g) = \sum_{l=1}^{\infty} l \, \frac{\sin l\alpha}{\sin\alpha} = -\pi \frac{\delta'(\alpha)}{\sin\alpha}. \tag{3.151}$$

This seems different from what we had obtained previously, but a closer look will reveal they are the same, up to normalisation. Again, we need to integrate this delta function against test functions that only depend on the conjugacy class of g, i.e. only depend on α and the measure is important. From the previous calculation, we know the measure is $\sin^2\alpha$, so

$$\int_0^\pi -\pi \frac{\delta'(\alpha)}{\sin\alpha} f(\alpha) \sin^2\alpha = \pi f(0)\,, \tag{3.152}$$

and hence, upto normalisation this agrees with $\delta_c(g)$.

3.8.2 The case for $PSL(2,\mathbb{R})$

Let us now consider another example that we focussed on in the main text: $G = PSL(2,\mathbb{R})$. The manifold for this group is AdS_3 with metric

$$ds^2 = da^2 - \sinh^2 a\, db^2 + \sinh^2 a \cosh^2 b\, dc^2 \tag{3.153}$$

with a, b run over the entire real line and c is between 0 and 2π. With this parametrisation we can represent hyperbolic elements of $SL(2,\mathbb{R})$ as

$$g = \begin{pmatrix} \cosh a + \cos c \cosh b \sinh a & \sinh\alpha(\cosh b \sin c + \sinh b) \\ \sinh\alpha(\cosh b \sin c - \sinh b) & \cosh a - \cos c \cosh b \sinh a \end{pmatrix} \tag{3.154}$$

In these elements a parametrizes the conjugacy class. Let us consider test functions that are just functions of a. The delta function on such functional spaces is then given by

$$\delta_c(g) = \frac{\delta(a)}{\sinh^2 a} \tag{3.155}$$

Here is a subtle difference between $SU(2)$ and $SL(2)$, in $SU(2)$ there is just elliptic elements, whereas for $PSL(2,\mathbb{R})$ we have two more conjugacy classes, so the element g above only covers the hyperbolic elements. This is saying the above coordinates are not global AdS_3 coordinates. To understand the general case for $PSL(2,\mathbb{R})$ we invoke Weyl's integration formula.

3.8.3 Weyl integration formula

Weyl's integration formula is a formula that relates the integral of a function on the group integrated over the entire group G to the integral of a slightly different function over the Cartan subgroups H_i, $i = 1, \cdots r$. Let $f(g)$ be a compactly supported function on G, then Weyl's

integration formula is the following statement, (see [114], proposition 5.27 for more details)

$$\int_G dg f(g) = \sum_{i=1}^{r} \frac{1}{|W_{H_i}|} \int_{H_i} dU |D_{H_i}(U)|^2 \left(\int_{G/H_i} d\widehat{g} f(\widehat{g} g \widehat{g}^{-1}) \right). \tag{3.156}$$

Lets unpack this formula. Here we assumed the group G having r Cartan subgroups with Weyl group W_{H_i}. The term in round brackets is an integral over the quotient G/H_i. The most important term here is $D_{H_i}(H)$, which explicitly reads

$$D_{H_i}(U) = \chi_\delta(U) \prod_{\alpha \in \Delta^+} (1 - \chi_\alpha(U)^{-1}) = \prod_{\alpha \in \Delta^+} (\chi_{\alpha/2}(U) - \chi_{\alpha/2}(U)^{-1}), \tag{3.157}$$

where χ is the character of the group H_i with the subscript indicating the representation of the Lie algebra of H_i. Explicitly, for the cases we will consider the H_i will be abelian and the characters are just exponentials,

$$\chi_\alpha(U) = e^{\alpha(u)} \tag{3.158}$$

with u the corresponding Lie algebra element to U. The product in (3.157) is over all positive roots α and δ half the sum of all positive roots.

Let us now consider out two examples $PSL(2, \mathbb{R})$ and $SU(2)$. In the latter case, there is one Cartan subgroup H given by elements $\mathrm{diag}(e^{i\theta}, e^{-i\theta})$. The roots system is well known and there is only a single positive root. We have $\chi_{\alpha/2}(U) = e^{i\theta}$. So,

$$|D_H(U)|^2 = |e^{i\theta} - e^{-i\theta}|^2 = 4 \sin^2(\theta) \tag{3.159}$$

Furthermore $W_H = 2$. If we now consider a trace-class function f we just get the volume of G/H, which is 4π. So we get,

$$\int_{SU(2)} dg f(g) = \frac{1}{2} \int_0^{2\pi} \frac{d\theta}{2\pi} \, 4 \sin^2(\theta) f(\theta), \tag{3.160}$$

where we normalized the Haar measure so that $SU(2)$ has volume 1.

Let us now move on to $PSL(2,\mathbb{R})$. In this case there are two non-conjugate Cartan subgroups, whose algebra is generated by the Pauli matrices $i\sigma_2$ and σ_3. Let us denote these groups by H_1 and H_2. For the former algebra the situation is the same as the previous discussion, but for the Cartan algebra generated by σ_3, the characters are real: $\chi_\alpha(U) = e^a$ with $U = e^{a\sigma_3/2}$. Furthermore, we have $|W_{H_1}| = 1$ and $|W_{H_2}| = 2$. Considering a trace-class function f we get

$$\int_{PSL(2,\mathbb{R})} dg f(g) = \operatorname{vol} G \left(\int_0^{2\pi} \frac{d\theta}{2\pi}\, 4\sin^2(\theta) f(\theta) + \frac{1}{2}\int_0^\infty \frac{da}{\operatorname{vol} H_2}\, 4\sinh^2(a/2) f(a) \right). \quad (3.161)$$

Because we took here a function that is trace-class, the integrals diverge and we need to regularize them. For non-trace-class functions, such divergences will not occur as long as the functions have compact support.

Chapter 4

SYK : Beyond the IR

Given the success of the Schwarzian theory in explaining the maximally chaotic behaviour of black holes, one might hope to take the next logical step and explore its UV completion, the full SYK model. It is natural to wonder if the gravitational mode captured by the Schwarzian can be organised in a systematic expansion involving UV corrections that correspond to a stringy completion of JT gravity. The double-scaling limit of SYK discussed here provides a promising avenue for such investigation.

In this section, we will provide hints from several lines of reasoning that such an interpretation does exist. We will first review the double-scaling limit of the SYK model and review the derivation of the chord diagrams describing double-scaled SYK via a Lorentzian Liouville effective action first presented in [115]. We will provide evidence for an interpretation of the full gravitational theory as a sine-dilaton gravity. We then review a construction in minimal string theory that gives rise to a matrix version of SYK and discuss the relation with the continuum model. Finally, we will analyse the semiclassical limit of the double-scaled SYK model, making contact with the large p-SYK model.

4.1 Double-Scaled SYK

Much attention has been devoted to the solution of the SYK model in the low-energy regime where the physics is described by Schwarzian quantum mechanics. It is an interesting problem to study how UV modes can be systematically incorporated into this theory.

One way to study the physics at higher energy scales is to consider the SYK model in a double-scaling limit [17, 116–119] where tools are available to study the model with greater analytic control. We take a large number of Majorana fermions p in the SYK interaction (1.1) that scales with the total number of fermions N, holding $\frac{2p^2}{N} = \lambda$ fixed. In [117], it was shown that the partition function of the resulting theory can be deduced by summing over *chord* diagrams. In these diagrams, one introduces a Hamiltonian factor for each of k vertices on a circle and sums over all possible chord-like contractions between these vertices to compute $\mathrm{Tr}(H^k)$. The Gaussian disorder average over these contractions leads to a simple rule for computing such diagrams - one must simply assign a factor of $q = e^{-\lambda}$ for each intersection of two chords in a given diagram. This reduces the problem of computing the partition function to a combinatorial problem. A similar set of combinatorial rules correspond to computation of the correlation functions with additional rules for the crossing of chords with chords emanating from the bilocal insertion. The sum over such diagrams can be done by means of a transfer matrix and the resultant expression for the partition function can be interpreted using the representation theory of the compact quantum group $\mathcal{U}_q(su(1,1))$. Here q is a real parameter that goes between 0 and 1 and the $q \to 1$ limit can be mapped to the classical group $SL(2,R)$ after using a similarity transformation to bring it to real form. The effective diagrammatic rules follow the same group theoretic structure described in [25] - the partition function computes the sum over continuous series representations of the group with the corresponding Plancherel measure and a Hamiltonian described by the Casimir of the group. Correlation functions involve the additional insertion of $3j$ and $6j$ symbols of the group at the appropriate intersection vertices.

It is worth noting the distinction between this quantum group and the non-compact group $\mathcal{U}_q(sl(2,R))$ that describes the universal braiding properties of conformal blocks in a 2D CFT

[120]. The latter also arises more naturally in the solution of Liouville theory via bootstrap [121]. An important qualitative difference is that the Plancherel measure has non-compact support and the quantum parameter q lives on the unit circle in the complex plane. The groups are equivalent in the $q \to 1$ limit.

The resultant diagrammatic rules for correlators in the double-scaled theory can be summarised in complete analogy with those of the Schwarzian. Every graph is circumscribed by a circle, which represents the thermal circle. Inside the circle, we draw a line for every bi-local operator, which connects the corresponding two points on the boundary circle. Propagators on the circular boundary and vertices are given in terms of Euclidean time by

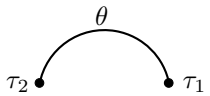

$$= \quad e^{-E(\theta)(\tau_2-\tau_1)}\,, \qquad\qquad$$

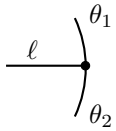

$$= \quad \gamma_\ell(\theta_1,\theta_2)\,. \tag{4.1}$$

where θ runs from 0 to π and labels continuous series representations of $\mathcal{U}_q(su(1,1))$. The Casimir takes the following value on these representations

$$E(\theta) = \frac{2\mathcal{J}}{\sqrt{1-q}}\cos\theta. \tag{4.2}$$

Notice that unlike the Schwarzian theory, the energy lives on the bounded interval $\left(-\frac{2\mathcal{J}}{\sqrt{1-q}}, \frac{2\mathcal{J}}{\sqrt{1-q}}\right)$.

The Plancherel measure factor associated with each θ variable can be expressed in terms of the q-Pochhammer symbol,

$$d\theta\,\rho(\theta) = \frac{d\theta}{2\pi}(q;q)\,\left(e^{\pm 2i\theta};q\right), \qquad\qquad (a;q) \equiv \prod_{k=0}^{\infty}\left(1-aq^k\right). \tag{4.3}$$

The time dependent factor represents the usual Schrödinger time evolution of the intermediate energy eigenstates. The vertex factor takes the following form

$$\gamma_\ell(\theta_1,\theta_2) \;=\; \sqrt{\frac{(q^{2\ell};q)}{(q^\ell e^{\pm i\theta_1 \pm i\theta_2};q)}}. \tag{4.4}$$

This vertex factor represents the matrix element of each endpoint of the bi-local operator between the corresponding two energy eigenstates and is given by the $3j$ symbol with 2 continuous series representations and one discrete series respresentation (labelled by ℓ).

The exact answer for the two point function found in [117] reads [1]

$$\langle V_1(0)V_2(t)\rangle = \prod_{i=1,2}\int d\theta_i^2 \left(q, e^{\pm 2i\theta}; q\right) \quad \theta_1,\ \ell,\ \theta_2 \tag{4.5}$$

$$= \prod_{i=1,2}\int d\theta_i \left(q, e^{\pm 2i\theta}; q\right) \quad e^{-\tau_1 E(\theta_1)-\tau_2 E(\theta_2)} \frac{\left(q^{2\ell}; q\right)}{\left(q^{\ell} e^{\pm i\theta_1 \pm i\theta_2}; q\right)}, \tag{4.6}$$

where the $\pm$ notation denotes the products of all choices of signs[2]. Here $\tau_1 + \tau_2 = \beta$ denotes the inverse temperature.

For more general correlation functions, one must assign continuous series labels to all bounded regions within the thermal circle and introduce an additional rule to include a factor for the R-matrix for every intersection of lines with discrete series labels,

θ_1, θ_t, ℓ_2, ℓ_1, θ_s, θ_4 $\quad = \quad R_{\theta_s\theta_t}\left[\begin{smallmatrix}\theta_4 & \ell_2\\ \theta_1 & \ell_1\end{smallmatrix}\right]$ (4.7)

This factor is related to the $6j$ symbol of the quantum group and an explicit expression can be found in Equation (6.3) of [117].

Let us consider more carefully the spectral density of the theory (4.3). It can also be recast in terms of a single Jacobi theta function,

$$\rho(\theta) = \sin\theta \frac{\vartheta_1\left(\frac{\theta}{\pi}|\frac{i\lambda}{2\pi}\right)}{\pi q^{\frac{1}{8}}}. \tag{4.8}$$

This form makes manifest the transformation of the measure in the opposite channel $\lambda \to \lambda^{-1}$.

[1] We use the notation $(a, b; q) = (a; q)(b; q)$.

[2] For example $f(a \pm b \pm c) = f(a+b+c)f(a+b-c)f(a-b+c)f(a-b-c)$.

Using the properties of the theta function under modular transformation, we obtain an equivalent expression

$$\rho(\theta) = -i\sqrt{\frac{2\pi}{\lambda}}e^{-\frac{2\theta^2}{\lambda}}\vartheta_1\left(\frac{2i\theta}{\lambda}\middle|\,\frac{2\pi i}{\lambda}\right). \tag{4.9}$$

As shown in [116, 117], the function shows the Schwarzian $\sinh(2\pi\sqrt{C(E-E_0)})$ behaviour near the end-points of the spectrum $\theta = 0, \pi$. The infrared part of the SYK spectrum ($\theta \sim \pi$) has been studied extensively and corresponds to the the Schwarzian mode in JT gravity. Near the center, $\theta = \pi/2$, the spectrum has a peak and can be described by a Gaussian. In the $q \to 1$ limit, the energies become unbounded and the spectrum resembles the ground state wavefunction of a classical harmonic oscillator. We will further study this limit in chapter 4. A key ingredient in this identification is that the energies of the double-scaled system (captured by the transfer matrix) correspond to the position operator in the Aric-Coon q-oscillator algebra. The dominant contribution to the spectral density in the $\lambda \to 0$ limit is

$$\rho(\theta) \to 4\sqrt{\frac{2}{\pi\lambda}}e^{-\frac{2\pi^2}{\lambda}}e^{-\frac{2}{\lambda}\left(\theta-\frac{\pi}{2}\right)^2}\sin(\theta)\sinh\left(\frac{2\pi}{\lambda}\theta\right)\sinh\left(\frac{2\pi}{\lambda}(\pi-\theta)\right). \tag{4.10}$$

One can make the dictionary with the Schwarzian variables precise in the $\lambda \to 0$ limit by zooming near the IR edge and holding

$$k = \frac{\pi-\theta}{\lambda}, \qquad C = \frac{1}{2\mathcal{J}\lambda^{3/2}}. \tag{4.11}$$

constant in this limit. Upto an overall (divergent) normalisation factor, the measure maps to

$$\rho(E) \propto \sinh\left(2\pi\sqrt{C(E-E_0)}\right). \tag{4.12}$$

Likewise, we find the Schwarzian energy spectrum $E - E_0 = \frac{k^2}{2C}$.

In this limit, we also recover the usual diagrammatic rules of the Schwarzian and obtain a precise match with the correlators of the theory. This is natural from the quantum group perspective since the group becomes classical in this regime. The θ parameter also maps to the

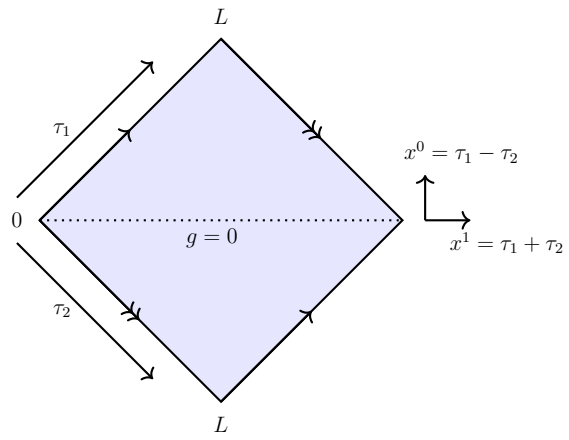

Figure 4.1: The double-scaled theory from a two-dimensional Liouville perspective with periodic identification in the null directions and vanishing boundary condition at $\tau_1 = \tau_2$. Additionally, $\tau_1 = \tau_2$ is a line of reflection symmetry for the Liouville field g.

opening angles of the 'pinched circles' in the bulk geometric picture of chapter 2 in this limit.

The solvability of the double-scaled limit hence makes it possible to exactly study properties of the SYK model that are sensitive to this particular UV completion of the Schwarzian theory.

4.2 From Chords to Liouville

In this section, we review the derivation of the diagrammatic structure of the chord diagrams from perturbation theory in the cosmological constant term of the Liouville effective action of SYK discussed in [115].

As explained in [122], one can equivalently reformulate the SYK model as an effective theory in two dimensions instead of a 1d quantum mechanical model with disorder average. This can be accomplished going by carrying out a Gaussian integral over the disorder field in the path integral corresponding to Eq (1.1) to obtain a bilocal effective action for the SYK fermions. One can further carry out the path integral over the fermions ψ by introducing a Lagrange multiplier identifying the fermion propagator with a two-dimensional bilocal field. The SYK action is then equivalently described in terms of the fundamental fields $G(\tau_1, \tau_2)$ and $\Sigma(\tau_1, \tau_2)$ where the former

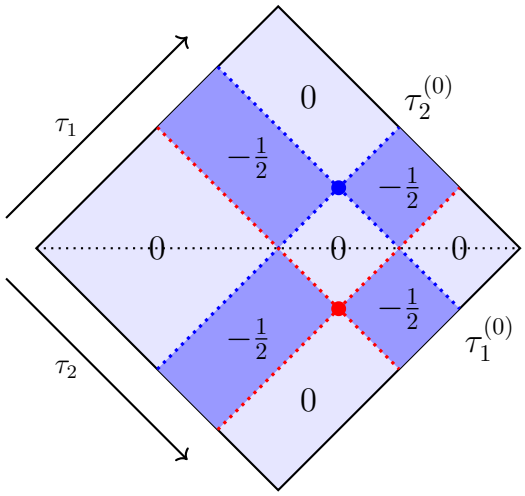

Figure 4.2: Lorentzian free field propagator $G(\tau_1, \tau_2)/8\lambda$ which satisfies the boundary condition $g(\tau_1, \tau_2) = g(\tau_2, \tau_1)$ and $g(\tau, \tau) = 0$. It vanishes in the region shaded light blue and is constant in the region shaded darker. The blue dot denotes the location of the source $\left(\tau_1^{(0)}, \tau_2^{(0)}\right)$ and the red dot shows the location of the image charge due to vanishing boundary condition at $\tau_1 = \tau_2$. One can view the two dots as sources for advanced (spacelike) propagators with equal and opposite charges so that they give the correct Green's function for $\tau_1 \geq \tau_2$ and in particular the superposition vanishes at $\tau_1 = \tau_2$. The $\tau_1 < \tau_2$ region is filled using reflection symmetry.

is identified with

$$G(\tau_1, \tau_2) \equiv \frac{1}{N} \sum_i \psi_i(\tau_1)\psi_i(\tau_2), \tag{4.13}$$

and the latter with the fermion self-energy. Fermion correlators can then be replaced by correlators of this bilocal mean field $G(\tau_1, \tau_2)$.

The resulting theory is described by the effective action[3] [56]

$$-S_E/N = \frac{1}{2}\mathrm{Tr}\log\left(\partial_\tau - \Sigma\right) - \frac{1}{2}\int d\tau_1 d\tau_2 \left[\Sigma(\tau_1, \tau_2)G(\tau_1, \tau_2) - \frac{\widehat{\mathcal{J}}^2}{2p^2}\left(2G(\tau_1, \tau_2)\right)^p\right]. \tag{4.14}$$

Analyzing the saddle point equations associated to this action, one finds that in the strong coupling limit of large $L\mathcal{J}$ the two-point function takes the form $G(\tau_1, \tau_2) \sim \mathrm{sgn}(\tau_{12})|\tau_{12}|^{-2\Delta}$ with scaling dimension $\Delta = 1/p$. In the UV regime, on the other hand $G(\tau_1, \tau_2) = \frac{\mathrm{sgn}(\tau_{12})}{2}$ takes the free field form. We will focus now on the large p limit. This means that we can approximate

[3]We use a hat to distinguish the coupling from a rescaled version that arises in the double-scaling limit that we will introduce momentarily.

the bilocal field in the following way up to $1/p^2$ corrections

$$G(\tau_1,\tau_2)=\frac{\text{sgn}(\tau_{12})}{2}e^{\Delta g(\tau_1,\tau_2)}=\frac{\text{sgn}(\tau_{12})}{2}\left(1+\frac{1}{p}g(\tau_1,\tau_2)\right), \tag{4.15}$$

and study the dynamics of $g(\tau_1,\tau_2)$. It is useful to keep in mind that since G is antisymmetric in τ_1 and τ_2, g is symmetric in it's arguments.

Noting that the Σ is $O\left(\frac{1}{p}\right)$, we can expand the action to $O\left(\frac{1}{p^2}\right)$ and do the Gaussian integral over Σ to obtain an effective Liouville action for $g(\tau_1,\tau_2)$ [17],

$$S_{\text{eff}}=\frac{1}{2\lambda}\int d^2\tau\left[\frac{1}{4}\partial_{\tau_1}g\partial_{\tau_2}g-\widehat{\mathcal{J}}^2e^g\right]. \tag{4.16}$$

This bilocal action from the point of view of the original quantum mechanical system becomes local in the two dimensional kinematic space (τ_1,τ_2). These two parameters behave like null coordinates in the flat 2d space (x^0,x^1) such that $z=\tau_1=-x^0+x^1$, $\tilde{z}=\tau_2=x^0+x^1$ and $g(\tau_1,\tau_2)\to g(z,\tilde{z})$. Then we can use this relabeling to write the action as a 2d Lorentzian theory for a scalar field g with an exponential interaction term. Note that z and $\tilde{z}$ here are not complex conjugates.

We can compare this with the usual Liouville CFT. Liouville theory with a cosmological constant μ and central charge as $c=1+6(b+1/b)^2$ is described by the *Euclidean* action

$$S_L=\frac{1}{4\pi}\int d^2z\left[\partial\phi\overline{\partial}\phi+4\pi\mu e^{2b\phi}\right]. \tag{4.17}$$

To make contact with the SYK action we can rescale $2b\phi\to g$. This turns the Liouville action into $S_L=\frac{1}{16\pi b^2}\int d^2z\left[\partial g\overline{\partial}g+4\pi\widehat{\mu}e^g\right]$, where $\widehat{\mu}=4\mu b^2$.

Despite the similar form, the action (4.16) is inherently Lorentzian. In order to assign a central charge to this theory, it is essential to analytically continue $x_0\to ix_0$. Comparing with (4.17), we again see that we need to take $b^2=i\beta^2$ purely imaginary to make contact with SYK. Notice that this problem is peculiar in that even though the action under consideration is

Lorentzian, there is no overall i in front of the action in the path integral. One needs to integrate the field g in a complex direction to obtain a convergent path integral. Also note that from the point of view of the Euclidean theory, the modular parameter of the torus on which the theory lives is purely imaginary. Finally, the corresponding CFT has central charge $13 + i\gamma$ for real γ.

In addition to the condition that $g(\tau_1, \tau_2)$ is periodic with periodicity L in both arguments, the action (4.16) is to be supplemented with the condition $g(\tau, \tau) = 0$ as the limit of small time separation coincides with the UV limit.

Following [115], let us treat this problem perturbatively in the coupling $\mathcal{J}^2$. We will denote the two dimensional coordinates collectively as τ_M with $M = 1, 2$. The kinetic term for the free field can then be inverted by the Green's function

$$\begin{aligned} G(\tau_M) &\equiv \left\langle g(\tau_M) g(\tau_M^{(0)}) \right\rangle_{\mathcal{J}=0} \\ &= -2\lambda \Big[\theta(\tau_1 - \tau_2) \Big(\theta(\tau_1 - \tau_1^{(0)}) \theta(\tau_2 - \tau_2^{(0)}) + \theta(-\tau_1 + \tau_1^{(0)}) \theta(-\tau_2 + \tau_2^{(0)}) \\ &- \theta(\tau_1 - \tau_2^{(0)}) \theta(\tau_2 - \tau_1^{(0)}) - \theta(-\tau_1 + \tau_2^{(0)}) \theta(-\tau_2 + \tau_1^{(0)}) \Big) \\ &+ \left(\tau_1 \leftrightarrow \tau_2, \tau_1^{(0)} \leftrightarrow \tau_2^{(0)} \right) \Big] \end{aligned} \tag{4.18}$$

satisfying

$$-\frac{1}{4\lambda} \partial_{\tau_1} \partial_{\tau_2} G(\tau_M) = \delta^2 \left(\tau_M - \tau_M^{(0)} \right) \tag{4.19}$$

This is the propagator consistent with the boundary condition $g(\tau, \tau) = 0$. One can view the second line as coming from an image charge located at $(\tau_2^{(0)}, \tau_1^{(0)})$ which implements the boundary condition for the Green's function. The last line simply completes the diamond by implementing the reflection symmetry.

The above expression has a simple physical interpretation - the Green's function 'clicks' whenever the intervals τ_M and $\tau_M^{(0)}$ intersect and vanishes otherwise.

Now that we have the basic setup for perturbation theory, we consider the partition function.

We consider the term at order k in the coupling $\mathcal{J}^2 = \widehat{\mathcal{J}}^2/\lambda$,

$$\frac{1}{k!}\left(\frac{\mathcal{J}^2}{2}\right)^k \int d^2\tau^{(1)} \dots d^2\tau^{(k)} \left\langle e^{g(\tau_M^{(1)})+\dots+g(\tau_M^{(k)})} \right\rangle_{\mathcal{J}=0} \tag{4.20}$$

which on applying Wick's theorem gives

$$\frac{1}{k!}\mathcal{J}^{2k} \int_{\tau_1^{(i)} \geq \tau_2^{(i)}} d^2\tau^{(1)} \dots d^2\tau^{(k)}\, e^{\frac{1}{2}\sum\limits_{i<j}\langle g(\tau_M^{(i)}) g(\tau_M^{(j)})\rangle} \tag{4.21}$$

where the sum in the exponent runs over Wick pairings. In particular, this means using the expression for the propagator (4.18) that we get -2λ whenever we have an intersection and zero otherwise. Hence, we pick up the same combinatorial factor as the usual chord diagrams of the double-scaled SYK, namely the number of intersections

$$\frac{(\mathcal{J}L)^{2k}}{(2k)!}\, e^{-\lambda\times(\#\text{ of i-j intersections})}. \tag{4.22}$$

Here, we fixed the precoefficient as follows. First notice that there is a $k!$ redundancy in assigning an index to the chords. The unrestricted integral over the τ coordinates would yield a factor of L^{2k}. Here, however the ordering of the τ coordinates corresponding to a given chord diagram is fixed resulting in the overall factor $\frac{L^{2k}}{(2k)!}$ for each chord diagram. Summing over k gives the full expression for the partition function.

Similarly insertion of bilocal observables gives the combinatorial expression for the correlators eg. for the two-point function. By expanding at order k and using Wick contractions again including the combinatorial factor from the τ integrals

$$\langle e^{\ell\lambda g(\tau_M^{(A)})}\rangle_{\mathcal{J}} = \sum_{m,n} \mathcal{J}^{\frac{m+n}{2}} \frac{\tau^m}{m!} \frac{(L-\tau)^n}{n!}\, e^{-\lambda\times(\#\text{ of i-j intersections})-\ell\lambda\times(\#\text{ of i-A intersections})} \tag{4.23}$$

where $\tau \equiv \left(\tau_1^{(A)} - \tau_2^{(A)}\right)$. Here, the capitalised A index denotes the chords corresponding to the g field inserted in the correlation function and m counts the number of vertices lying inside the

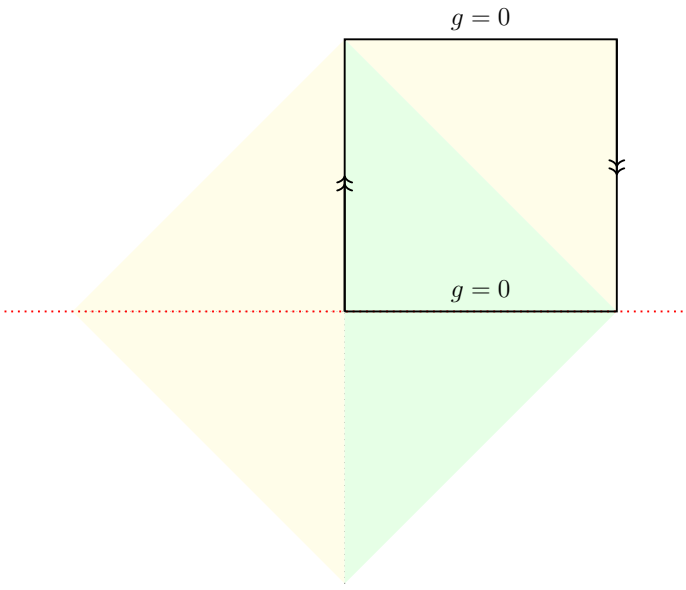

Figure 4.3: Using the reflection symmetry across the red line, we reduce the problem to solving the unoriented Liouville theory on a Möbius strip with vanishing boundary condition for the Liouville field on the edge.

segment of length τ enclosed by the bilocal operator. n counts the remaining vertices in the diagram (so $m + n$ is even) which are restricted to a given order in the $L - \tau$ interval.

It is clear that this argument readily generalises to the case where an arbitrary number of bilocal operators are inserted in any time-order. One can use the transfer matrix approach of [117] to perform the sum.

From the Liouville perspective, the above analysis suggests that we are performing perturbation theory in the cosmological constant. An important distinction in this case is that the free propagator of the theory is a step function while it is logarithmic in the Euclidean theory.

One can use the periodicity in the null directions and the symmetric boundary condition across $\tau_1 = \tau_2$ in this setup to restrict to the fundamental domain geometry that describes the system. This is the Lorentzian Liouville theory on a Möbius strip with boundary conditions such that the Liouville field vanishes at the edge of the strip as shown in Figure 4.3.

4.3 Sine Dilaton Gravity

We now consider an alternate perspective of the connection between the minimal string and JT gravity derived in [110, 47][4]. As shwos in section 3.5.4, a 'p-deformed' version of JT gravity can be derived by replacing the $(2, p)$ minimal model with a timelike Liouville CFT and coupling to gravity through an ordinary (spacelike) Liouville CFT. Using field redefinitions, this theory is equivalent to a theory of dilaton gravity with a sinh potential for the dilaton as opposed to a linear potential as in the usual JT theory. This theory corresponds to the deformation of JT gravity by the quantum group $\mathcal{U}_q(sl(2,R))$ with $q = e^{\frac{2\pi i}{p}}$. The quantum parameter lies on the unit circle in this case. In the $q \to 1$ limit, with appropriate rescaling of the fields and couplings, one can recover the linear potential.

We propose here an alternate deformation of the JT theory corresponding to the quantum group $\mathcal{U}_q(su(1,1))$. We will study the action $S = S[\varphi, \widehat{g}] + \tilde{S}[\tilde{\varphi}, \widehat{g}] + S_{gh}[b, c, \widehat{g}]$ with

$$\begin{aligned} S[\varphi] &= \frac{1}{2}\int_{\mathcal{M}} d^2x\sqrt{\widehat{g}}\left[(\widehat{\nabla}\varphi)^2 + Q\widehat{R}\varphi + 4\pi\mu e^{2b\varphi}\right] + \oint_{\partial\mathcal{M}} du\sqrt{\widehat{h}}\left[Q\widehat{K}\varphi + 2\pi\mu_B e^{b\varphi}\right] \\ \tilde{S}[\tilde{\varphi}] &= \frac{1}{2}\int_{\mathcal{M}} d^2x\sqrt{\widehat{g}}\left[(\widehat{\nabla}\tilde{\varphi})^2 + \tilde{Q}\widehat{R}\tilde{\varphi} + 4\pi\tilde{\mu} e^{2\tilde{b}\tilde{\varphi}}\right] + \oint_{\partial\mathcal{M}} du\sqrt{\widehat{h}}\left[\tilde{Q}\widehat{K}\tilde{\varphi} + 2\pi\tilde{\mu}_B e^{\tilde{b}\tilde{\varphi}}\right] \end{aligned} \tag{4.24}$$

Here, we introduced the background metric $\widehat{g}$. The background charge for the theory is $Q = b + b^{-1}$ related to the central charge via $c = 1 + 6Q^2$. Analogous expressions hold for the quantities with tilde. Moreover, we choose the parameters, $b = e^{\frac{i\pi}{4}}\overline{\beta}$ and $\tilde{b} = e^{-\frac{i\pi}{4}}\overline{\beta}$ for real $\overline{\beta}$ so that $b = i\tilde{b}$ and hence, $c + \tilde{c} + c_{gh} = 0$. The boundary interaction is included through a boundary cosmological constant term.

The field redefinitions

$$\varphi = b^{-1}\rho - b\Phi, \qquad \tilde{\varphi} = \tilde{b}^{-1}\rho - \tilde{b}\Phi, \tag{4.25}$$

[4]See [111, 123] for further discussions.

allow us to recast the action in the following form

$$S = \int_{\mathcal{M}} d^2x\sqrt{\widehat{g}}\left[2\Phi\cdot\widehat{\nabla}^2\rho + \widehat{R}(\rho-\Phi) - 4\pi\lambda e^{2\rho}\sin\left(2\overline{\beta}^2\Phi\right)\right] + 2\oint_{\partial\mathcal{M}} du\sqrt{\widehat{h}}\left[\widehat{K}(\rho-\Phi) - 2\pi\lambda_B e^{\rho}\sin\left(\overline{\beta}^2\Phi\right) - \Phi\widehat{\partial}_n\rho\right] + S_{gh} \tag{4.26}$$

where we also choose the cosmological constants to be related via $\mu = -\tilde{\mu} = -i\tilde{\lambda}$ and $\mu^B = -\tilde{\mu}^B = -i\tilde{\lambda}^B$.

In terms of the dynamical metric, $g_{\mu\nu} = e^{2\rho}\widehat{g}_{\mu\nu}$, the action is given by

$$S = -\int_{\mathcal{M}} d^2x\sqrt{g}\left[\Phi R - R\rho + 2(\nabla\rho)^2 + 4\pi\tilde{\lambda}\sin\left(2\overline{\beta}^2\Phi\right)\right] - 2\oint_{\partial\mathcal{M}} du\sqrt{h}\left[K\Phi - K\rho + 2\pi\tilde{\lambda}_B\sin\left(\overline{\beta}^2\Phi\right)\right] + S_{gh}\,. \tag{4.27}$$

Hence, the 'q-deformed' JT gravity takes the form of dilaton gravity with a sine potential. See [113, 112] for recent discussions of related deformations in JT gravity. This potential is qualitatively different from the p-deformed theory which is strongly coupled near the cutoff surface. It is not natural to use the decomposition $\Phi = \Phi_0 + \phi$ for large Φ_0 as is customary in the JT literature as it no longer splits into a topological piece. We see instead that it is the parameter $\overline{\beta}$ that controls the genus expansion.

In this case, we choose to cutoff the surface at a fixed Φ near the maximum of the potential. However, the periodic nature of the potential allows us to include additional contributions from cutoff surfaces at different hills in the potential that appear as instanton-like contributions to the path integral. This suggests the appearance of additional non-perturbative physics.

In the $\overline{\beta}\to 0$ classical limit, one recovers ordinary JT by scaling the cosmological constant to large values such that $4\pi\tilde{\lambda}\overline{\beta}^2 = \Lambda_{JT} = 1$ and $2\pi\tilde{\lambda}_B\overline{\beta}^2 = 1$. The conformal mode ρ is non-dynamical in this limit so that

$$S \overset{\beta\to 0}{\approx} -\int_{\mathcal{M}} d^2x\sqrt{g}\left[\Phi(R+2)\right] - 2\oint_{\partial\mathcal{M}} du\sqrt{h}\left[\Phi(K-1)\right]. \tag{4.28}$$

Physically, rescaling the cosmological constant to large values is the analogue of limiting to low energies so that we restrict ourselves to a single valley in the potential. Consequently, only perturbative terms survive in the strict JT limit.

Note that one could have equally well interchanged the roles of ρ and Φ in this analysis to interpret Φ as the conformal metric. Equivalently, one could parametrise $b = e^{\frac{i\pi}{4}}\beta$. This would yield the JT action but with a positive cosmological constant instead. Since the original parameter μ for the cosmological constant needs to be continued in the imaginary direction to make contact with the JT action, one may indeed think of this theory as sitting at an imaginary cosmological constant in between the postive and negative cases.

4.3.1 Geometric interpretation

It is interesting to study classical solutions in this sine dilaton gravity

$$S = -\int_{\mathcal{M}} d^2x\sqrt{g}\left[\Phi R + 4\pi\tilde{\lambda}\sin\left(2\overline{\beta}^2\Phi\right)\right] \tag{4.29}$$

Lorentzian black hole solutions are described by the metric [47],

$$ds^2 = -\frac{2\pi\lambda}{\overline{\beta}^2}\left(\cos(2\overline{\beta}^2 r) - \cos(2\overline{\beta}^2 r_h)\right)dt^2 + \left(\frac{\overline{\beta}^2}{2\pi\lambda}\right)\frac{dr^2}{\cos(2\overline{\beta}^2 r) - \cos(2\overline{\beta}^2 r_h)} \tag{4.30}$$

with $r_h = \arcsin\frac{T}{\lambda}/2\overline{\beta}^2$. Here, we have chosen gauge such that the dilaton coincides with the radial coordinate r. In order to have sensible thermodynamics, we assumed that the geometry is cutoff before $r = \frac{\pi}{4\overline{\beta}^2}$. The geometry leads to the thermodynamic relation

$$E = \frac{\pi}{\overline{\beta}^2}\sqrt{\lambda^2 - T^2} \tag{4.31}$$

Finally, the curvature

$$R = -8\pi\overline{\beta}^2\tilde{\lambda}\cos\left(2\overline{\beta}^2 r\right) \tag{4.32}$$

interpolates between a constant curvature AdS_2 region for $r \ll \overline{\beta}^{-2}$ to a flat space region near the boundary. This is different from the p-deformation where we see an exponentially growing curvature near the boundary.

4.3.2 Quantum Algebra from Poisson Sigma Model

It is well known that 2-d dilaton gravity with dilaton potential $V(X^3)$ can be recast as a Poisson Sigma model [124]

$$S = \int \left[X^a \wedge \mathcal{D}_\omega e^a + X^3 \mathrm{d}\omega + \frac{1}{2} P^{ij}(X) A_i \wedge A_j \right]. \tag{4.33}$$

with a non-linear Poisson structure on $\mathbb{R}^3$ given by

$$\{X^i, X^j\} = P^{ij}, \qquad P^{ij} = \epsilon^{ij} u_k(X). \tag{4.34}$$

The functions $u_k(X)$ are given by

$$u_a = \eta_{ab} X^b, \text{ with } a, b = 1, 2 \qquad u_3 = V(X_a X^a, X^3) \tag{4.35}$$

In particular we see that with the sine form of the potential derived above, we obtain the relation

$$[X_1, X_2] = V(X^3) = V(\phi) = 4\pi\lambda \sin\left(2\overline{\beta}^2 X^3\right) \tag{4.36}$$

which after rescaling the generators gives us the quantum algebra of $\mathcal{U}_q(su(1,1))$

$$[E, F] = \frac{K^2 - K^{-2}}{q - q^{-1}} \tag{4.37}$$

with the reality conditions $K = K^*$, $E^* = -F$ and $F^* = -E$.

Note that using the hyperbolic sine form of the dilaton potential recovers the $\mathcal{U}_q(sl(2,R))$ algebra consistent with the reality condition $K = K^*$, $E^* = -E$ and $F^* = -F$ of the above algebra and q now lies on the unit circle. These may be viewed as alternate real forms of the

$\mathcal{U}_q(sl(2,C))$ quantum algebra. The above algebra reduces to $SL(2,R)$ for the linear dilaton potential $V(\phi) = \phi$ and to $ISO(1,1)$ for $V(\phi) = 0$ corresponding to flat space JT [125].

4.4 SYK Matrix Model from Minimal Strings

The holographic dual theory to the SYK model has JT gravity as its low energy limit [12, 13, 15, 14], and it is desirable to learn more about its dynamical content or its UV completion. The main obstacle to finding this UV complete bulk dual is that the SYK model itself has thus far not found its home within string theory.

In [3] and [126], we presented a framework for a string realization of the SYK model. Our construction starts from minimal string theory [127,46,128,129] and follows the standard holographic paradigm based on open-closed string duality [6,130,131]. The main idea is to consider the world-volume theory of a large number Q of FZZT branes in $(p,1)$ string theory [44,45,132,133]. Using the large N matrix description of minimal string theory, we show that the effective theory on the FZZT branes takes the form of a matrix version of the SYK model with $J\psi^p$ interaction. The SYK fermions represent open strings between the FZZT branes and the ZZ branes that underly the matrix description of the minimal string. The continuum SYK dynamics arises upon taking the large Q limit.

The starting point for our construction is the $(p,1)$ matrix model with Q FZZT brane insertions with locations specified by the matrix X_Q which corresponds to the matrix partition function

$$Z_{pQ} = \int dA\, dB\, e^{-\mathrm{Tr}(V_p(A) - AB)} \det\big(X_Q \otimes \mathbb{1}_N - \mathbb{1}_Q \otimes B\big) \tag{4.38}$$

with A and B both $N \times N$ matrices and V_p represents a polynomial of degree p [134–136]. In the double scaling limit, this describes the partition function of Q FZZT branes in $(p,1)$ minimal string theory. Taking the large N and Q limit and adjusting the locations X_Q, this system spans the complete space of all (p,Q) minimal models and their deformations.

One can express the determinant in terms of fermionic variables ψ that are naturally interpreted as representing the open strings that stretch between the FZZT brane and the N ZZ branes that underly the matrix description of the minimal string [129–131, 127],

$$\det\big(X_Q\otimes \mathbb{1}_N - \mathbb{1}_Q\otimes B\big) \;=\; \int d\psi d\psi^\dagger \,\exp\Big(\psi^\dagger (X_Q\otimes \mathbb{1}_N - \mathbb{1}_Q\otimes B)\psi\Big) \tag{4.39}$$

with X_Q an $Q\times Q$ matrix with eigenvalues $x_1, ..., x_Q$. Hence the fermions have two indices

$$\psi_{ia}, \qquad i = 1, ..., N, \qquad a = 1, ..., Q \tag{4.40}$$

indicating that they correspond to strings that stretch between N ZZ-branes and Q FZZT branes. We will call i the color index and a the flavor index.

Starting with equation (4.38) for the partition function $Z_{p\widehat{Q}}$, and after introducing the fermionic variables via (4.39), one can first integrate out B and then integrate out A with the help of the resulting delta-function. This results in a fermionic integral

$$\begin{aligned} Z_{p\widehat{Q}} \;&=\; \int dA dB d\psi d\psi^\dagger \,\exp\big(\psi^\dagger (X_Q\otimes \mathbb{1}_N - \mathbb{1}_Q\otimes B)\psi - \mathrm{Tr}_N(V_p(A) - AB)\big) \\ &=\; \int d\psi\, d\psi^\dagger \,\exp\Big(\psi^\dagger (X_Q\otimes \mathbb{1}_N)\psi - \mathrm{Tr}_N V_p(\psi\psi^\dagger)\Big) \end{aligned} \tag{4.41}$$

with a non-linear potential given by the trace of an $N\times N$ matrix $V_p(\psi\psi^\dagger)$.

We can rewrite the potential as a trace of a $Q\times Q$ matrix by performing the *color-flavor transformation* [137]

$$\mathrm{Tr}_N\big((\psi\psi^\dagger)^k\big) = \mathrm{tr}_Q\big((\psi^\dagger\psi)^k\big) \tag{4.42}$$

with $\psi\psi^\dagger$ and $\psi^\dagger\psi$ the matrices defined by

$$(\psi\psi^\dagger)_{ij} = \sum_{a=1}^{Q} \psi_{ia}\psi^\dagger_{ja} \qquad (\psi^\dagger\psi)_{ab} = \sum_{i=1}^{N} \psi^\dagger_{ia}\psi_{ib}. \tag{4.43}$$

The partition function of the Q FZZT strings then rearranges itself in the form of a matrix version of the SYK model

$$Z_{pQ} = \int d\psi\, d\psi^\dagger \exp\Big(\sum_{i=1}^{N} \psi_i^\dagger X_Q \psi_i - N\tilde{\mathcal{J}}^2 \,\mathrm{tr}_Q\, G^p\Big) \tag{4.44}$$

with

$$G_{ab} \equiv \frac{1}{N}\sum_{i=1}^{N} \psi^\dagger_{ia}\psi_{ib} \tag{4.45}$$

This effective action can be contrasted with the non-commutative version of the SYK action, S_{NCSYK} reviewed in [3]. This is a bi-local action in the emergent time variable, or equivalently, a local action on the non-commutative torus. Introducing the two-point function G and the fermion self-energy Σ as two independent degrees of freedom living on the non-commutative torus, the action can be expressed in the following form

$$S_{\text{NCSYK}} = \int \frac{dudv}{2\pi}\Big(\sum_{i=1}^{N} \psi_i^\dagger\big(\widehat{\partial}_v - \Sigma\big)\psi_i + N\Big(\Sigma * G + \frac{\mathcal{J}^2}{2p^2} G^{*p}\Big)\Big) \tag{4.46}$$

Here, $*$ represents the non-local Moyal star product of functions on the non-commutative torus. In the $Q \to \infty$ limit, this reduces to an ordinary product of functions, provided that we work with sufficiently smooth functions G and Σ.

In [3], an explicit map was presented between the matrix SYK model and the non-commutative SYK model by employing an ensemble average over a field redefinition of the fermion. In [126], we show that such a map is not unique. In general, it is possible to enlarge the number of ZZ branes. The continuum SYK model then arises as the effective dynamics on a subspace of this enlarged space, either by carefully chosing a reparametrization of the fermions or by employing

an ensemble average.

There are several formal connections between the SYK model and minimal string theory that become apparent after taking the double scaling limit with p^2/N fixed. We can repeat the analysis of Section 4.2 but now with the complex field of Eq (4.46). In this limit, the SYK dynamics is exactly captured by an effective Liouville theory [17]

$$S[g] \;=\; \frac{\pi N}{p^2}\int \frac{dudv}{2\pi}\left(\partial_u g\,\partial_v g \;+\; 4\mathcal{J}^2 e^{2g(u,v)}\right) \tag{4.47}$$

This effective lagrangian arises from after first sending $Q\to\infty$, then integrating out the fermions and Σ field, while writing $G(u,v) = i\,\mathrm{sgn}(u,v)\left(1+\frac{2}{p}g(u,v)\right)$. Note that the lagrangian (4.47) defines a 2D field theory in Lorentzian signature but appears in the SYK functional integral without a factor of i in front. In our case, the Liouville field $g(u,v)$ is complex, but satisfies the reality condition $g(u,v)^\dagger = g(v,u)$. Hence instead of defining the model as living on the torus, we can orientifold the torus into a Möbius strip and introduce two separate Liouville fields via

$$g_+(u,v) = g(u,v), \qquad\qquad g_-(u,v) = g(v,u). \tag{4.48}$$

This doubles up the lagrangian into a sum

$$S[g] = S[g_+] + S[g_-] \tag{4.49}$$

of two Liouville lagrangians with complex central charge[5]

$$c_\pm = 13 \pm i6(\beta^2 - \beta^{-2}), \qquad \beta^2 = \frac{p^2}{2\pi N} \tag{4.50}$$

The two complex central charges add up to $c_+ + c_- = 26$. This result looks coincidental at first. Taken more seriously, however, it provides a direct hint that the bi-local effective theory of the double scaled SYK model should be viewed as a 2D worldsheet string theory. This is also

[5]This result follows from the more standard formula $c_\pm = 1+6Q_\pm^2$ with $Q_\pm = b_\pm + 1/b_\pm$ by taking $b_\pm = e^{\pm i\pi/4}\beta$.

precisely the sine-dilaton gravity theory discussed in Section 4.3.

Accordingly, the sum (4.49) of two bi-local actions (4.47) should be treated as a gravitational theory subject to Virasoro constraints. Indeed, although (4.47) looks like the lagrangian of a 2D local quantum field theory, all evidence indicates that the 2D dual to the SYK model does not have a local stress tensor. This formal similarity between double scaled SYK and non-critical string theory motivated us to look for a possible realization of SYK via D-branes in (generalized) minimal string theory and matrix models.

The properties of the dual string theory depend on which type of brane dominates and the precise dictionary one employs to may the matrix SYK model to the continuum version on the non-commutative torus. Minimal string theory resides in the regime in which the ZZ branes proliferate. The FZZT branes create a time crystal that in the large Q limit becomes a continuum emergent time direction. The dynamics of the fermionic ZZ-FZZT open strings organizes itself in the form of an SYK action.

We have argued that the worldsheet theory of the string dual of the SYK model looks similar to that of (p, q) minimal string theory, as summarized in the below table

$$\begin{array}{cc} \text{MST} & \text{SYK} \\ c_{\pm} = 13 \pm 6(b^2 + 1/b^2) & c_{\pm} = 13 \pm i6(\beta^2 - 1/\beta^2) \\ b^2 = p/q, \quad N \to \infty & \beta^2 = p^2/2\pi N, \quad q \to \infty \end{array} \tag{4.51}$$

The ratios p/q and p^2/N play the role of a worldsheet coupling constant on their respective side, while $1/N$ has its usual role as governing the strength of the string interactions.

4.5 Semiclassical Limit of Double-Scaled SYK

Having established the usefulness of the double-scaled limit of SYK as direct probe of the UV physics of SYK, let us pause to examine what this means in the classical limit. As we have seen, the Schwarzian theory arises in a triple scaling limit. If we just take the large C limit, we land

on solutions to the Lorentzian Liouville theory derived in [56]. In this section, we make this connection precise, starting directly with the results in the double-scaled theory.

4.5.1 Partition function

We saw that the partition function, when we take $\lambda \to 0$ and concentrate on low energies, agrees with the Schwarzian result. Here we consider the regime where $\lambda \to 0$, but we keep the energies finite (that is, do not take θ in the integral to be close to π).

The expression for the partition function is

$$Z = \int_0^\pi \frac{d\theta}{2\pi} (q, e^{\pm 2i\theta}; q)_\infty e^{-\frac{2\beta\mathcal{J}}{\lambda}\cos\theta}; \tag{4.52}$$

We will work up to order $1/\lambda$ when we calculate the exponent, since the λ^0 order gives finite terms, while we are interested in term that go as N in the large 'q' limit of SYK (in the notation used in [56]), which will be manifested for us as $\frac{N}{p^2}$ terms.

At this order, we use the fact that

$$(x;q)_\infty \approx \exp\left[-\frac{1}{\lambda}\mathrm{Li}_2(x)\right]. \tag{4.53}$$

Therefore we can express the large p effective action in a simplified form,

$$Z = \int_0^\pi \frac{d\theta}{2\pi} (q;q)_\infty \exp\left[-\frac{1}{\lambda}\mathrm{Li}_2(e^{2i\theta}) - \frac{1}{\lambda}\mathrm{Li}_2(e^{-2i\theta}) - \frac{2\beta\mathcal{J}\cos(\theta)}{\lambda}\right] \tag{4.54}$$

In this representation, it is easy to use the saddle point approximation. Using the definition of

the di-logarithm, the saddle point equation is[6]

$$-2i\sum_{k=1}^{\infty}\frac{e^{2i\theta k}-e^{-2i\theta k}}{k}+2\beta\mathcal{J}\sin(\theta)=4\sum_{k=1}^{\infty}\frac{\sin(2\theta k)}{k}+2\beta\mathcal{J}\sin(\theta)=2(\pi-2\theta)+2\beta\mathcal{J}\sin(\theta)=0. \tag{4.55}$$

To make contact with [56], we introduce the variable v such that $\theta=\frac{\pi}{2}+\frac{\pi v}{2}$, so that the saddle point equation becomes

$$\beta\mathcal{J}=\frac{\pi v}{\cos\frac{\pi v}{2}} \tag{4.56}$$

The di-logarithms in the exponent also simplify

$$\mathrm{Li}_2(e^{2i\theta})+\mathrm{Li}_2(e^{-2i\theta})=2\sum_{k=1}^{\infty}\frac{\cos(2\theta k)}{k^2}=\frac{\pi^2}{3}-2\pi\theta+2\theta^2=-\frac{\pi^2}{6}+\frac{\pi^2v^2}{2} \tag{4.57}$$

Assembling the terms, we obtain the partition function

$$Z\propto\exp\left[-\frac{\pi^2v^2}{2\lambda}-\frac{2\beta\mathcal{J}\cos\theta}{\lambda}\right]=\exp\left[-\frac{N}{p^2}\frac{\pi^2v^2}{4}+\frac{N}{p^2}\pi v\tan\frac{\pi v}{2}\right] \tag{4.58}$$

which is precisely the free energy computed in [56] using a more direct method.

4.5.2 Two-point function

The expression for the 2-point function is

$$\tilde{G}=\int_0^{\pi}\prod_{j=1}^{2}\left\{\frac{d\theta_j}{2\pi}(q,e^{\pm2i\theta_j};q)_\infty\right\}\exp\left[-\frac{2\tau\mathcal{J}\cos\theta_1}{\lambda}-\frac{2(\beta-\tau)\mathcal{J}\cos\theta_2}{\lambda}\right]\frac{(\tilde{q}^2;q)_\infty}{(\tilde{q}e^{i(\pm\theta_1\pm\theta_2)};q)_\infty} \tag{4.59}$$

and we denote $\tilde{q}=e^{-\tilde{\lambda}}$.

[6] In performing the sum over k, we had to assume that $0<2\theta<2\pi$, which is indeed the case.

Once again we do not keep finite in λ terms, so that to order $1/\lambda$ we have

$$\tilde{G} \sim (q;q)_\infty^2 (\tilde{q}^2;q)_\infty \int_0^\pi \frac{d\theta_1 d\theta_2}{(2\pi)^2} \exp\left[-\frac{S_0}{\lambda}\right] \tag{4.60}$$

where we defined

$$S_0 = \mathrm{Li}_2\left(e^{\pm 2i\theta_1}\right) + \mathrm{Li}_2\left(e^{\pm 2i\theta_2}\right) - \mathrm{Li}_2\left(\tilde{q}e^{i(\pm\theta_1 \pm \theta_2)}\right) + 2\mathcal{J}\tau\cos\theta_1 + 2\mathcal{J}(\beta-\tau)\cos\theta_2 \tag{4.61}$$

and by $\pm$ we mean that we should sum over all terms with all possible signs.

The saddle point equations are now given by [7]

$$\begin{aligned} &-2i\log\left(1-e^{2i\theta_1}\right) + 2i\log\left(1-e^{-2i\theta_1}\right) + i\log\left(1-e^{-\tilde{\lambda}+i(\theta_1+\theta_2)}\right) + i\log\left(1-e^{-\tilde{\lambda}+i(\theta_1-\theta_2)}\right) - \\ &- i\log\left(1-e^{-\tilde{\lambda}+i(-\theta_1+\theta_2)}\right) - i\log\left(1-e^{-\tilde{\lambda}+i(-\theta_1-\theta_2)}\right) - 2\mathcal{J}\tau\sin\theta_1 = 0 \end{aligned}$$

In the second equation, we replace $\theta_1 \leftrightarrow \theta_2$ and $\tau \leftrightarrow \beta - \tau$.

Let us work up to order $O(\tilde{\lambda}^1)$ and use the ansatz

$$\theta_1 = \theta + \alpha\tilde{\lambda} + O(\tilde{\lambda}^2), \qquad \theta_2 = \theta - \alpha\tilde{\lambda} + O(\tilde{\lambda}^2) \tag{4.62}$$

After some simplification, working to leading order we obtain the saddle equations,

$$\begin{cases} 2\theta - \pi - 2\mathcal{J}\tau\sin\theta + 2\arctan(2\alpha) = 0 \\ 2\theta - \pi - 2\mathcal{J}(\beta-\tau)\sin\theta - 2\arctan(2\alpha) = 0 \end{cases} . \tag{4.63}$$

Note that α (which was the $O(\tilde{\lambda})$ term) enters the $O(\tilde{\lambda}^0)$ equations. Also note that adding $\delta\tilde{\lambda}$ to both $\theta_{1,2}$, will not affect these equations (this is like shifting θ). Similarly, one can check that $\tilde{\lambda}^2$ terms will not affect these equations (but will enter in the $O(\tilde{\lambda})$ equations).

The sum of these two equations gives the same equation for θ as in the partition function,

[7] We use $\mathrm{Li}_1(x) = -\log(1-x)$.

and therefore with the definition of v, we get that (4.56) holds. The other equation is given by

$$\pi v + 2\arctan(2\alpha) = 2\mathcal{J}\tau\cos\left(\frac{\pi v}{2}\right). \tag{4.64}$$

We can now expand the effective action S_0 to leading order:

$$S_0 = -\frac{\pi^2}{2} + \frac{\pi^2 v^2}{2} - 2\pi v\tan\frac{\pi v}{2} + \tilde{\lambda}\left[-\log\left(\cos(\frac{\pi v}{2})^2\right) + \log\left(\cos\left(\pi v\left(\frac{1}{2}-\frac{\tau}{\beta}\right)\right)^2\right)\right] + O(\tilde{\lambda}^2). \tag{4.65}$$

After plugging in the on-shell action, we get the two-point function to this order

$$G \sim \left[\frac{\cos\frac{\pi v}{2}}{\cos\left(\pi v\left(\frac{1}{2}-\frac{\tau}{\beta}\right)\right)}\right]^{2\tilde{\lambda}/\lambda} \tag{4.66}$$

In [56] a single fermion was considered, so that $\tilde{\lambda}/\lambda = \tilde{p}/p = 1/p$ in agreement with our result.

Let us try to re-express the saddle point equations (4.61) in a manner that makes the connection with the Schwarzian more manifest. To this end, we use for our parameter range (we take $\theta_1 \geq \theta_2$)

$$\frac{d}{d\theta}\left[\mathrm{Li}_2\left(e^{-x\pm i\theta}\right)\right] = i\left(\log\left(1-e^{-x-i\theta}\right) - \log\left(1-e^{-x+i\theta}\right)\right) = -2\arctan\left[\frac{\sin\theta}{e^x-\cos\theta}\right] \tag{4.67}$$

so that the corresponding saddle point equations may be expressed as

$$\boxed{\begin{array}{rcl} (2\theta_1-\pi) + \arctan\left[\frac{\sin(\theta_1+\theta_2)}{e^x-\cos(\theta_1+\theta_2)}\right] + \arctan\left[\frac{\sin(\theta_1-\theta_2)}{e^x-\cos(\theta_1-\theta_2)}\right] &=& \mathcal{J}\tau\sin\theta_1 \\ (2\theta_2-\pi) + \arctan\left[\frac{\sin(\theta_1+\theta_2)}{e^x-\cos(\theta_1+\theta_2)}\right] - \arctan\left[\frac{\sin(\theta_1-\theta_2)}{e^x-\cos(\theta_1-\theta_2)}\right] &=& \mathcal{J}(\beta-\tau)\sin\theta_2 \end{array}}$$

Now, we may use the identifications $\theta_i = \pi - \lambda k_i$, $C = \frac{1}{2\lambda\mathcal{J}}$ and $x = \lambda\ell$ to zeroth order in λ to reproduce the saddle equations of the Schwarzian theory.

We can try to introduce angle variables to replace the arctangents in (4.68) to define angle

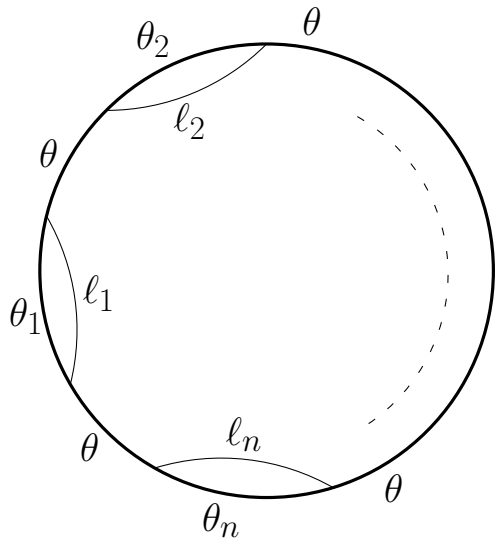

Figure 4.4: Diagram computing the time-ordered $2n$ point correlation function in the large q limit.

variables analogous to those used in Chapter 2,

$$\alpha_1 = \arctan\left[\frac{\sin(\theta_1+\theta_2)}{e^x-\cos(\theta_1+\theta_2)}\right], \qquad \alpha_2 = \arctan\left[\frac{\sin(\theta_1-\theta_2)}{e^x-\cos(\theta_1-\theta_2)}\right], \tag{4.68}$$

to obtain an equivalent system of equations in more geometric variables

$$\boxed{\begin{aligned} 2\theta_1-\pi+\alpha_1+\alpha_2 &= \mathcal{J}\tau_1\sin\theta_1 \\ 2\theta_2-\pi+\alpha_1-\alpha_2 &= \mathcal{J}\tau_2\sin\theta_2 \\ \tfrac{\sin(\theta_1+\theta_2+\alpha_1)}{\tan\alpha_1} &= \tfrac{\sin(\theta_1-\theta_2+\alpha_2)}{\tan\alpha_2} = e^x \end{aligned}}$$

Despite the simple form of these equations, it is still an open problem to see if this system also has a geometric interpretation analogous to the one in the Schwarzian case. Note that one no longer expects the bulk to be described by hyperbolic geometry in this more general setup.

4.5.3 General Recipe for Time-ordered Correlators

We consider the relevant contribution in the double scaled theory of the diagram 4.4. We henceforth drop constant factors.

$$G_n = \int \left(\prod_{i=1}^{n+1} d\theta_i \left(e^{\pm 2i\theta_i}; q \right) e^{-\frac{2\mathcal{J}}{\sqrt{\lambda(1-q)}}\tau_i \theta_i} \right) \prod_{i=1}^{n} \left(\frac{1}{\left(e^{-x_i \pm i\theta_i \pm i\theta}; q \right)} \right) \tag{4.69}$$

where we defined $x_i \equiv \lambda \ell_i$, $\theta_{n+1} \equiv \theta$ and $\sum \tau_i = \beta$.

The corresponding equations of motion are

$$2\theta_i - \pi + \arctan\left[\frac{\sin(\theta_i + \theta)}{e^{x_i} - \cos(\theta_i + \theta)} \right] + \arctan\left[\frac{\sin(\theta_i - \theta)}{e^{x_i} - \cos(\theta_i - \theta)} \right] = \mathcal{J}\tau_i \sin\theta_i \tag{4.70}$$

for $i = 1, 2 \ldots n$ and for $i = n+1$,

$$2\theta - \pi + \sum_{i=1}^{n} \left(\arctan\left[\frac{\sin(\theta_i + \theta)}{e^{x_i} - \cos(\theta_i + \theta)} \right] - \arctan\left[\frac{\sin(\theta_i - \theta)}{e^{x_i} - \cos(\theta_i - \theta)} \right] \right) = \mathcal{J}\tau_{n+1} \sin\theta \tag{4.71}$$

For the limit at hand, we can rewrite

$$S_0 \equiv -\lambda \log G_n = \sum_{i=1}^{n+1} \left(2\theta_i^2 - 2\pi\theta_i + 2\mathcal{J}\tau_i \cos\theta_i \right) - \sum_{i=1}^{n} \mathrm{Li}_2\left(e^{-x_i \pm i\theta_i \pm i\theta} \right) \tag{4.72}$$

Let us consider the ansatz

$$\theta_i = \theta_0 + x_i \alpha_i, \qquad i = 1, 2 \ldots n, \qquad \theta = \theta_0 \tag{4.73}$$

The equations of motion are

$$\left(\theta_0 - \frac{\pi}{2} \right) + \arctan\left(\alpha_i \right) = \mathcal{J}\tau_i \sin\theta_0 \tag{4.74}$$

for $i = 1, 2 \ldots n$ and for $i = n+1$,

$$(2-n)\left(\theta_0 - \frac{\pi}{2} \right) - \sum_{i=1}^{n} \arctan\left(\alpha_i \right) = \mathcal{J}\tau_{n+1} \sin\theta_0 \tag{4.75}$$

With this ansatz, there are exactly as many equations as number of variables $(n+1)$.

The sum of all these equations gives the simple relation

$$2\theta_0 - \pi = \beta\mathcal{J}\sin\theta_0 = \pi v = \beta\mathcal{J}\cos\left(\frac{\pi v}{2}\right) \tag{4.76}$$

where we introduced the notation v of Maldacena-Stanford which may be traded for θ_0.

The solution for α_i is then simply

$$\alpha_i = -\tan\left[\frac{\pi v}{2}\left(1 - \frac{2\tau_i}{\beta}\right)\right] \tag{4.77}$$

Let us record the contributions of the three different parts of (4.72) at leading and subleading order using the above ansatz.

The contribution of the measure is

$$\sum_{i=1}^{n+1}\left(2\theta_i^2 - 2\pi\theta_i\right) = 2(n+1)\theta_0(\theta_0 - \pi) + \sum_{i=1}^{n} 2x_i\alpha_i\left(2\theta_0 - \pi\right) \tag{4.78}$$

The contribution of the energy term is

$$\sum_{i=1}^{n+1}\left(2\mathcal{J}\tau_i\cos\theta_i\right) = 2\mathcal{J}\sum_{i=1}^{n+1}\tau_i\cos\theta_i - 2\mathcal{J}\sin\theta_0\sum_{i=1}^{n}\tau_i\alpha_i x_i \tag{4.79}$$

To calculate the contribution of the interaction term, we use that

$$-\mathrm{Li}_2\left(e^{-x_i\pm i\theta_i\pm i\theta}\right) = \left(2\pi\theta_0 - 2\theta_0^2\right) - 2x_i\log x_i + x_i\left(2\alpha_i\arctan(\alpha_i) - \alpha_i(-\pi + 2\theta_0) - \log\left[4\sin^2\theta_0\right]\right) \tag{4.80}$$

We can drop the terms depending only on ℓ_i and focus only on the coefficient of x_i. This gives

$$\log G_n \sim -\sum_{i=1}^{n}\ell_i\alpha_i\left(2\theta_0 - \pi + 2\arctan\alpha_i - 2\mathcal{J}\tau_i\sin\theta_0 - \alpha_i^{-1}\log\left(4\sin^2\theta_0(1+\alpha_i^2)\right)\right) \tag{4.81}$$

The first three terms here vanish from the equations of motion. Notice, that τ_{n+1} conveniently

does not make an appearance in the relevant piece of the correlation function.

Hence, consistent with (4.77), the time-ordered correlation function factorises as

$$G_n \sim \prod_{i=1}^{n} \left(\frac{\cos \frac{\pi v}{2}}{\cos\left(\pi v \left(\frac{1}{2} - \frac{\tau_i}{\beta}\right)\right)} \right)^{2\ell_i} \tag{4.82}$$

By contrast, we do not expect this factorisation for the out of time ordered correlation function due to the contribution of the R-matrix.

4.5.4 Entanglement Entropy

Next we study the entanglement entropy in partially entangled states corresponding to the double-scaled two-point functions. Our analysis will closely follow that of chapter 2. In particular, the diagrams that appear and corresponding phase transitions are completely analogous with the Schwarzian momentum replaced by the corresponding $\mathcal{U}_q(su(1,1))$ representations.

Case I: $0 < \tau < \beta/4$ $(\beta_R < \beta_L)$

We need the correlator of $2n$ operators placed periodically at a distance alternating between 2τ and $\beta - 2\tau$. For case I the channel that dominates has a contraction between operators separated a distance 2τ. We define the intermediate channel momenta θ_i and ϕ.

The configuration has a $\mathbf{Z}_n$ symmetry of permuting the replicas and a $\mathbf{Z}_2$ symmetry of time reversal. This is important for finding the saddle-point of the classical action giving this correlator. In general the correlator is given semiclassically as

$$\log G_n(\tau, \beta) = S_0 + \rho(\phi) + \sum_{i=1}^{n} \rho(\theta_i) + \sum_{i=1}^{n} \tilde{I}_i(\phi, \theta_i, \ell, \tau, \beta) \tag{4.83}$$

the explicit formula for the terms $\tilde{I}_i$ and the saddle-point equations can be obtained from the general methods explained. Here, $\rho(\theta) = 2\theta(\pi - \theta)$. Using that $\theta_i \equiv \theta$ the correlator simplifies

to

$$\log G_n(\tau,\beta) = S_0 + 2\pi\rho(\phi) + n\left[\rho(\theta) + \tilde{I}(\theta,\phi,\ell,\tau,\beta)\right] \tag{4.84}$$

Using this we can compute the Renyi entropy S_n as

$$S_n = -n^2\partial_n \frac{1}{n}\log Z_n = S_0 - n^2\frac{\partial}{\partial n}\,\frac{1}{n}\left(\rho(\phi) + n\left[\rho(\theta) + \tilde{I}(\theta,\phi,\ell,\tau,\beta)\right]\right) \tag{4.85}$$

which leads us to the simple result,

$$S_n^{\text{Renyi}} = S_0 + 2\phi(n)(\pi - \phi(n)) \tag{4.86}$$

where the saddle-point equation defining $\phi(n)$ and $\theta(n)$ is given by

$$\begin{aligned} 2\theta - \pi + \arctan\left[\frac{\sin(\theta+\phi)}{e^x - \cos(\theta+\phi)}\right] + \arctan\left[\frac{\sin(\theta-\phi)}{e^x - \cos(\theta-\phi)}\right] &= 2\mathcal{J}\tau\sin\theta \\ \frac{2\phi-\pi}{n} + \arctan\left[\frac{\sin(\theta+\phi)}{e^x - \cos(\theta+\phi)}\right] - \arctan\left[\frac{\sin(\theta-\phi)}{e^x - \cos(\theta-\phi)}\right] &= \mathcal{J}(\beta-2\tau)\sin\phi \end{aligned}$$

Indeed for $0 < \tau < \beta/4$ and any ℓ the condition $\rho(\phi(n)) < \rho(\theta(n))$ is always satisfied.

Now we can take the $n \to 1$ limit.

Case II: $\beta/4 < \tau < \beta/2$ $(\beta_L < \beta_R)$

After case I, deriving the results for case II is straightforward. The channel that dominates now has contractions between nearest neighboring operators separated by $\beta_L = \beta - 2\tau$. The Renyi entropy is given by the momentum which does not appear with a factor of n in the semiclassical action. This gives

$$S_n^{\text{Renyi}} = S_0 + 2\theta(n)(\pi - \theta(n)) \tag{4.87}$$

The saddle-point equations are different and now become

$$\begin{aligned}\frac{2\theta-\pi}{n}+\arctan\left[\frac{\sin(\theta+\phi)}{e^x-\cos(\theta+\phi)}\right]+\arctan\left[\frac{\sin(\theta-\phi)}{e^x-\cos(\theta-\phi)}\right] &= 2\mathcal{J}\tau\sin\theta\\ 2\phi-\pi+\arctan\left[\frac{\sin(\theta+\phi)}{e^x-\cos(\theta+\phi)}\right]-\arctan\left[\frac{\sin(\theta-\phi)}{e^x-\cos(\theta-\phi)}\right] &= \mathcal{J}(\beta-2\tau)\sin\phi\end{aligned}$$

which coincides with the previous case for $n=1$ but in general might be different.

4.5.5 Probe limit

The results of Section 4.5.3 are sufficient to calculate the entanglement of partially entangled thermal states in the case of double-scaled SYK.

We consider the state prepared by evolution on the Euclidean semicircle with a local operator insertion after a time τ of Euclidean evolution. Using the rules developed in this section, the relevant correlator on the n-replica manifold is

$$G_n=\left(\frac{\cos\frac{\pi v_n}{2}}{\cos\left(\pi v_n\left(\frac{1}{2}-\frac{\widehat{\tau}}{n}\right)\right)}\right)^{2\ell n} \tag{4.88}$$

where we introduced the parameters,

$$\widehat{\tau}=\min\left(\frac{2\tau}{\beta},\frac{\beta-2\tau}{\beta}\right),\qquad\qquad n\beta\mathcal{J}=\frac{\pi v_n}{\cos\left(\frac{\pi v_n}{2}\right)}. \tag{4.89}$$

This relation implies

$$\frac{\partial v_n}{\partial n}=\frac{v_n}{n}-\frac{\pi v_n}{2}\tan\left(\frac{\pi v_n}{2}\right) \tag{4.90}$$

So that the nth (modular) Renyi entropy is given by

$$\begin{aligned}S_n &= (1-n\partial_n)\log G_n\\ &= \frac{1}{2}\ell n\pi v_n\left(\tan\left(\frac{\pi v_n}{2}\right)\left(2-n\pi\tan\left(\frac{\pi v_n}{2}\right)\right)-\left(2-(n-2\widehat{\tau})\pi\tan\left(\frac{\pi v_n}{2}\right)\right)\tan\left(\pi v_n\left(\frac{1}{2}-\frac{\widehat{\tau}}{n}\right)\right)\right)\end{aligned}$$

Notice that when we take $n \to 1$, $v_n \to 1$ with $\frac{\pi v_n}{2}\tan\left(\frac{\pi v_n}{2}\right) \to 1$, we recover the Schwarzian result

$$S_n^{Sch} = 2\ell\left(n - \pi\widehat{\tau}\cot\left(\frac{\pi\widehat{\tau}}{n}\right)\right) \tag{4.91}$$

The entanglement entropy is thus

$$S_{EE} = S_0 + \frac{1}{2}\ell\pi v\left(\tan\left(\frac{\pi v}{2}\right)\left(2 - \pi\tan\left(\frac{\pi v}{2}\right)\right) - \left(2 - (1-2\widehat{\tau})\pi\tan\left(\frac{\pi v}{2}\right)\right)\tan\left(\pi v\left(\frac{1}{2} - \widehat{\tau}\right)\right)\right)$$

Plugging in the zero-point contribution (4.58), we obtain

$$S_0^{(n)} = \frac{\pi^2 v_n}{4\lambda}\left(v_n - 2v_n\sec^2\left(\frac{\pi v_n}{2}\right) + n\tan^2\left(\frac{\pi v_n}{2}\right)\left(2 + \pi v_n\tan\left(\frac{\pi v_n}{2}\right)\right)\right) \tag{4.92}$$

4.5.6 Summary of Limits of Double Scaled SYK

We summarise the various order of limits of the double-scaled SYK partition function/correlators in Fig 4.5. The effective actions for the two-point function that appear at intermediate stages are given as follows. We use the notation, $x = \lambda\ell$, $C = \frac{1}{2\lambda\mathcal{J}}$, $\theta_i = \lambda k_i$ and $\beta\mathcal{J} = \frac{\pi v}{\cos\left(\frac{\pi v}{2}\right)} \implies v = 1 - \frac{2}{\beta\mathcal{J}} + \frac{4}{(\beta\mathcal{J})^2} + \ldots$.

The effective action for the two-point function in the full double-scaled theory is then

$$\begin{aligned} S_{DS}[\theta_1,\theta_2,\ell,\lambda,\mathcal{J}] &= -\log\left(q, e^{\pm 2i\theta_1}; q\right) - \log\left(q, e^{\pm 2i\theta_2}; q\right) + \frac{2}{\sqrt{1-q}}\tau\cos\theta_1 \\ &\quad + \frac{2}{\sqrt{1-q}}(\beta-\tau)\cos\theta_2 + \log\left(q^\ell e^{\pm i\theta_1 \pm i\theta_2}; q\right) \end{aligned} \tag{4.93}$$

The intermediate large p effective action follows from the saddle point of the above action,

$$S_\lambda[\theta_1,\theta_2,x,\mathcal{J}] = \mathrm{Li}_2\left(e^{\pm 2i\theta_1}\right) + \mathrm{Li}_2\left(e^{\pm 2i\theta_1}\right) - \mathrm{Li}_2\left(e^{-x\pm i\theta_1\pm i\theta_2}\right) + 2\mathcal{J}\tau\cos\theta_1 + 2\mathcal{J}(\beta-\tau)\cos\theta_2$$

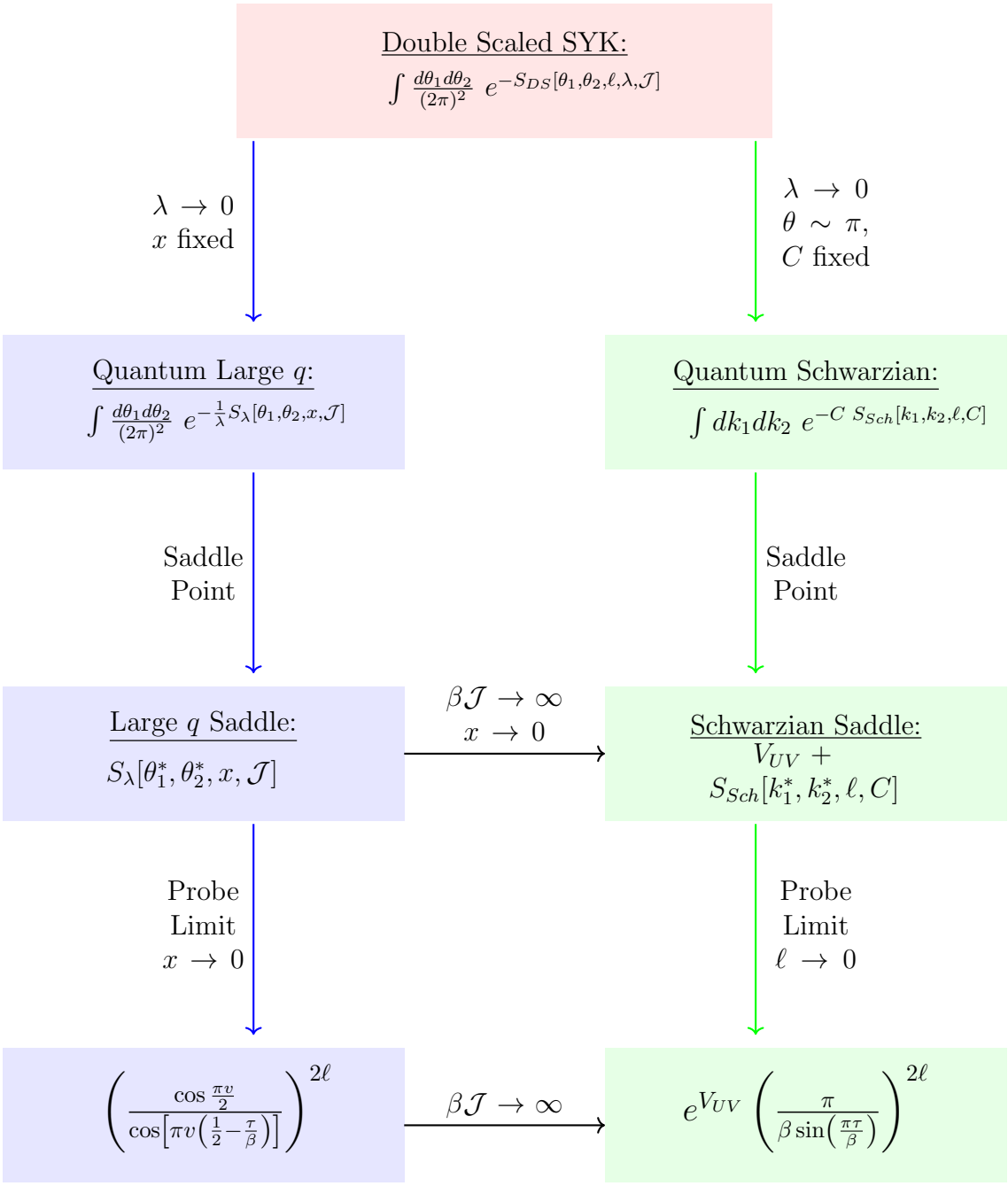

Figure 4.5: Web of limits of the two-point function in the double-scaled theory.

By contrast, the Schwarzian action arises after restricting to the IR region,

$$\begin{aligned} S_{Sch}[k_1, k_2, \ell, C] &= -\frac{1}{C}\log\left(k_1 \sinh(2\pi k_1)\right) - \frac{1}{C}\log\left(k_2 \sinh(2\pi k_2)\right) + \frac{\tau}{2}\left(\frac{k_1}{C}\right)^2 \\ &\quad + \frac{(\beta-\tau)}{2}\left(\frac{k_2}{C}\right)^2 - \frac{1}{C}\log\left(\Gamma(\ell \pm k_1 \pm k_2)\right) \end{aligned} \tag{4.94}$$

The divergent factor V_{UV} denotes an additional contribution coming from the UV modes in the triple scaling limit that goes to the Schwarzian.

Chapter 5

Conclusions and Outlook

In this thesis, we have explored 2d holography from various different viewpoints. The new tools developed here have far-reaching consequences in helping us understand the interplay between gravity, spacetime and quantum information. These developments have also sparked interest in several lines of enquiry that motivate future research.

In chapter 2, motivated by the geometric approach of [51] to pure states in the SYK model, we have studied the holographic dual of a general class of partially entangled thermal states (PETS) specified by the insertion of the single scaling operators into the euclidean time evolution that creates the thermo-field double state. We studied the bulk dual of a PETS in the low energy approximation of the SYK model described by the Schwarzian theory. We argued that the partially entangled thermal states describe a composite black hole with two horizons, separated by an expanded interior region with a massive bulk particle. We computed the entanglement entropy of these states and compared with the usual holographic RT prescription. We argued, both from an entanglement wedge and a tensor network perspective, that a one-sided reconstruction can be extended into the interior geometry of the black hole.

It would be interesting to generalize this setup to higher dimensions, maybe using SYK-like models such as [138–141] or 2D generalizations of the Schwarzian action [142]. The bulk membrane dual to the PETS might have a more interesting structure in these cases. Another

interesting application would be to study, even within AdS_2, how to apply the GJW teleportation protocol [143] in this context. Since entanglement is a resource for these kinds of operations, it should be harder to make the PETS wormhole traversable.

One important point which we leave for future work is to study partially entangled states in the regime where the entanglement is a finite fraction of N. Semi-classically, these states look like factorized black hole geometry as indicated in panel c) of figure 2.5. The physics of this transition depends on the microscopic SYK dynamics. This looks like a hard problem, but may be tractable using dynamical mean field theory or via numerical methods.

Another interesting modification of the thermo-field double state is obtained by considering the insertion of a topological interface. A topological interface in a 2D CFT is defined by considering a boundary state in the tensor product of two identical CFTs and then using the folding trick [144] [145] to reorient it such that the reflection from left-movers into right-movers is replaced by a transmission from CFT_1 to CFT_2 (see e.g. [146]). Since the resulting interface is topological (commutes with the Virasoro algebra), inserting it into the euclidean path integral of the TFD state does not lead to any (localizable) gravitational backreaction. In particular, the effective temperature on both sides will always be the same. Hence the quantum numbers that specify the topological interface should be considered as non-trivial potential quantum numbers of the state associated with the ER bridge of a two-sided black hole geometry [147–149].

The results of the chapter are closely related to the developments leading to an explanation of a unitary Page curve during the black hole evaporation process in [84, 83, 85]. These papers considered a holographic setup where the bulk theory is coupled to a non-gravitating external bath which collects the Hawking quanta emitted by the black hole in AdS. As a consequence, one can restate the black hole information problem in this context as a derivation of the Page curve for the entropy corresponding to the density matrix of the radiation that is consistent with unitarity. The central idea behind this derivation is the phase transition that gives rise to a new quantum extremal surface behind the horizon of the black hole dubbed an 'island'. In our treatment of the Schwarzian correlation function, this entropy may be viewed as arising from the

mixed density matrix arising from a sum over multiple operators in our multi-partite setup. The phase transition between the two types of replica diagrams corresponds to the transition between the entropy of the black hole and the radiation and gives rise to the plateau in the entropy at the Page time [84]. It would also be interesting to give a derivation of the evaporation process of a Hawking pair using probe operators in this setup.

In chapter 3, we derived a systematic four-fold classification of boundary conditions in JT gravity. We gave a geometric interpretation of classical solutions in each case and discussed various factorisation and ensemble-averaging properties. In particular, we showed that the boundaries with $K > 1$ factorise at the level of the path integral. We also provided a prescription to insert boundaries with different boundary conditions in the matrix integral language as special operators in the matrix model.

Thus far, we have only considered two-dimensional dilaton gravities, but most of our analysis could also be applied to higher-dimensional gravity theories, albeit now with $g_{\mu\nu}$ and $K_{\mu\nu}$ as phase space variables. The DD and DN are relatively straightforward as they map onto the canonical and microcanonical ensembles in the higher dimensional field theory [74,150]; however, it would be interesting to figure out the higher-dimensional analogs of the ND and NN boundary conditions considered in this chapter of the thesis.[1]

A particularly tractable theory of gravity that shares many features with the theory of gravity considered here is three-dimensional gravity in its Chern-Simons formulation. In this case, the gauge algebra is $sl(2,R) \times sl(2,R)$ and gives rise to two gauge fields A and $\overline{A}$. We can consider various boundary conditions on these gauge fields that in the second order formulation correspond to fixing certain components of the metric and extrinsic curvature. The fixed ND boundary condition would be one where the Chern-Simons theory does not have any boundary terms and is purely topological. It would therefore be interesting to study the exact computation of the partition functions in that case.

Recently there has been a great effort in trying to define two-dimensional gravity for finite

[1]Fixing the trace of the extrinsic curvature in higher dimensional gravity appears to be a better behaved boundary condition (together with fixing the conformal class of the metric), as reviewed in [151].

patches of space-time [90, 152, 108].[2] In doing so, one deforms the putative quantum mechanics dual with a particular operator that depends solely on the Hamiltonian and coupling constant. This is a well-known story in the standard Dirichlet case, but it would be interesting to determine whether other boundary conditions can also be insightful for defining gravity at finite cutoff. For instance, the spectrum of the deformed quantum mechanics theory is known to exhibit a complexification of the energy levels at high energy,[3] signaling the presence of a UV cutoff. However, upon Laplace transforming in ϕ (functionally), we arrive at the ND boundary conditions, whose partition function is simple and topological. It would be interesting to use the simplicity of the ND partition functions, say for the disk, to study the DD finite cutoff theory in more detail. In particular, using the techniques above, we can, in principle, determine what happens when the cutoff surface is brought inside all the way to the center of the disk, where we expect it to reproduce the Bekenstein-Hawking entropy. Putting the DN boundary conditions (the microcanonical ensemble) can also be considered at finite cutoff, which we hope could shed more light on the complexification of the previously discussed energies. See also [156] for a discussion of these ideas in three dimensions.

When studying the ND boundary conditions, we have seen that all perturbative corrections in e^{ϕ_0} vanish provided that $k > 1$. It is then natural to wonder if this statement is also true non-perturbatively for a UV completion of JT gravity, such as its matrix integral completion.[4] In particular, we expect that the kernel presented in section 3.2.3, when integrated against non-perturbative terms in the partition function, would kill these terms in addition to the perturbative terms. If the non-perturbative completion is specified by a matrix model, this translates to the expectation value of the operator (3.82) vanishing.

It would be interesting to use the results of [33] to study a non-perturbative completion of JT gravity via the corresponding double-scaled matrix model to check if this is true. A complete

[2] See also, [153] for the original proposal with a three-dimensional bulk, or [154, 155] for higher-dimensional analogs.

[3] See [91] for a entirely different approach that did not yield such a complexification.

[4] Alternatively, requiring that all non-perturbative corrections vanish for $k > 1$ can be viewed as a condition on the possible UV completions of JT gravity.

understanding of this requires detailed knowledge of such non-perturbative corrections, including their exact form at exponentially small energies. Nevertheless, one cannot rule out the possibility that a careful application of the integration contour for the kernel, together with some universal analytic properties of the non-perturbative contributions, can indeed lead to this conclusion.

It would also be interesting to carry out a similar analysis for the supersymmetric cousins of JT gravity studied in [81] and obtain the analog of our kernel, specifically for the ($\alpha \in \{0, 1, 2\}$, $\beta = 2$) Altland-Zirnbauer ensembles. The advantage of these JT supergravity models is that their non-perturbative behavior is under much better control than in standard JT. It is interesting to note that these theories exhibit a truncation in the perturbative series, even with standard boundary conditions in some cases. Hence, they are better suited to study factorization properties, α-branes, and non-perturbative phenomena.

In chapter 4, we explored various strategies to study the SYK model beyond the Schwarzian limit. We derived a matrix version of the SYK model where the role of the continuum time coordinate was played by a large stack of FZZT branes. We also showed that it was possible to derive the chord-diagram expansion of double-scaled SYK using perturbation theory in the cosmological constant operator in Lorentzian signature. These observations hint at a possible embedding within the framework of non-critical string theory. We also studied the semiclassical limit of double-scaled SYK commonly referred to as the 'large-q SYK' in the literature.

Perhaps the most radical feature of this proposal is that time is emergent. Continuous time only arises after taking the strict large Q limit. Some earlier hint that time in SYK should be viewed as possibly discrete are found in the chord diagram expansion of the double scaled SYK theory [117,116], where time evolution is most effectively captured by means of a transfer matrix and the energy spectrum runs over a finite range, suggesting an interpretation as a quasi-energy of a system with a discrete time evolution.

It is also an interesting problem to explore the Liouville theory on the Mobius strip - in particular one could try to use the unoriented Liouville Mobius strip amplitude [157] and transform to fixed length basis to reproduce the partition function as well as higher-point functions. This

would provide very strong evidence for the link between the two theories. Another possibility avenue to explore is the connection between the double-scaled SYK theory and 3d de-Sitter gravity starting from $SL(2, C)$ Chern-Simons theory. One anticipates the emergence of the compact quantum group instead of the non-compact quantum group as in the AdS case.

Our story is far from finished. Given the central place of the SYK model as a prototype of low dimensional holography with the same dynamical properties as a quantum black hole, it is clearly important to find its connection with string theory. Our analysis aims to take a concrete step in that direction.

Bibliography

[1] A. Goel, H.T. Lam, G.J. Turiaci and H. Verlinde, *Expanding the Black Hole Interior: Partially Entangled Thermal States in SYK*, *JHEP* **02** (2019) 156 [1807.03916].

[2] A. Goel, L.V. Iliesiu, J. Kruthoff and Z. Yang, *Classifying boundary conditions in JT gravity: from energy-branes to α-branes*, 2010.12592.

[3] A. Goel and H. Verlinde, *Towards a String Dual of SYK*, 2103.03187.

[4] G. 't Hooft, *Dimensional reduction in quantum gravity*, *Conf. Proc. C* **930308** (1993) 284 [gr-qc/9310026].

[5] L. Susskind, *The World as a hologram*, *J. Math. Phys.* **36** (1995) 6377 [hep-th/9409089].

[6] J.M. Maldacena, *The Large N Limit of Superconformal Field Theories and Supergravity*, *Int. J. Theor. Phys.* **38** (1999) 1113 [hep-th/9711200].

[7] E. Witten, *Anti-de Sitter space and holography*, *Adv. Theor. Math. Phys.* **2** (1998) 253 [hep-th/9802150].

[8] S.S. Gubser, I.R. Klebanov and A.M. Polyakov, *Gauge theory correlators from noncritical string theory*, *Phys. Lett. B* **428** (1998) 105 [hep-th/9802109].

[9] O. Aharony, S.S. Gubser, J.M. Maldacena, H. Ooguri and Y. Oz, *Large N field theories, string theory and gravity*, *Phys. Rept.* **323** (2000) 183 [hep-th/9905111].

[10] A. Kitaev, *Talks given at the Fundamental Physics Prize Symposium and KITP seminars*, .

[11] J. Maldacena, D. Stanford and Z. Yang, *Diving into traversable wormholes*, *Fortsch. Phys.* **65** (2017) 1700034 [1704.05333].

[12] A. Almheiri and J. Polchinski, *Models of AdS_2 backreaction and holography*, *JHEP* **11** (2015) 014 [1402.6334].

[13] J. Maldacena, D. Stanford and Z. Yang, *Conformal symmetry and its breaking in two dimensional Nearly Anti-de-Sitter space*, *PTEP* **2016** (2016) 12C104 [1606.01857].

[14] K. Jensen, *Chaos in AdS_2 Holography*, *Phys. Rev. Lett.* **117** (2016) 111601 [1605.06098].

[15] J. Engelsöy, T.G. Mertens and H. Verlinde, *An investigation of AdS_2 backreaction and holography*, *JHEP* **07** (2016) 139 [1606.03438].

[16] S. Sachdev and J. Ye, *Gapless spin fluid ground state in a random, quantum Heisenberg magnet*, *Phys. Rev. Lett.* **70** (1993) 3339 [cond-mat/9212030].

[17] J.S. Cotler, G. Gur-Ari, M. Hanada, J. Polchinski, P. Saad, S.H. Shenker et al., *Black Holes and Random Matrices*, *JHEP* **05** (2017) 118 [1611.04650].

[18] R. Jackiw, *Lower Dimensional Gravity*, *Nucl. Phys.* **B252** (1985) 343.

[19] C. Teitelboim, *Gravitation and Hamiltonian Structure in Two Space-Time Dimensions*, *Phys. Lett.* **126B** (1983) 41.

[20] D. Stanford and E. Witten, *Fermionic Localization of the Schwarzian Theory*, *JHEP* **10** (2017) 008 [1703.04612].

[21] A. Kitaev and S.J. Suh, *Statistical mechanics of a two-dimensional black hole*, *JHEP* **05** (2019) 198 [1808.07032].

[22] Z. Yang, *The Quantum Gravity Dynamics of Near Extremal Black Holes*, *JHEP* **05** (2019) 205 [1809.08647].

[23] D. Bagrets, A. Altland and A. Kamenev, *Sachdev–Ye–Kitaev model as Liouville quantum mechanics*, *Nucl. Phys. B* **911** (2016) 191 [1607.00694].

[24] T.G. Mertens, G.J. Turiaci and H.L. Verlinde, *Solving the Schwarzian via the Conformal Bootstrap*, *JHEP* **08** (2017) 136 [1705.08408].

[25] T.G. Mertens, *The Schwarzian Theory - Origins*, 1801.09605.

[26] A. Almheiri, D. Marolf, J. Polchinski and J. Sully, *Black Holes: Complementarity or Firewalls?*, *JHEP* **02** (2013) 062 [1207.3123].

[27] A. Almheiri, D. Marolf, J. Polchinski, D. Stanford and J. Sully, *An Apologia for Firewalls*, *JHEP* **09** (2013) 018 [1304.6483].

[28] K. Papadodimas and S. Raju, *Black Hole Interior in the Holographic Correspondence and the Information Paradox*, *Phys. Rev. Lett.* **112** (2014) 051301 [1310.6334].

[29] E. Verlinde and H. Verlinde, *Black Hole Entanglement and Quantum Error Correction*, *JHEP* **10** (2013) 107 [1211.6913].

[30] S. Ryu and T. Takayanagi, *Holographic derivation of entanglement entropy from AdS/CFT*, *Phys. Rev. Lett.* **96** (2006) 181602 [hep-th/0603001].

[31] J.M. Maldacena, J. Michelson and A. Strominger, *Anti-de Sitter fragmentation*, *JHEP* **02** (1999) 011 [hep-th/9812073].

[32] J.M. Maldacena, *Eternal black holes in anti-de Sitter*, *JHEP* **04** (2003) 021 [hep-th/0106112].

[33] P. Saad, S.H. Shenker and D. Stanford, *JT gravity as a matrix integral*, 1903.11115.

[34] H.T. Lam, T.G. Mertens, G.J. Turiaci and H. Verlinde, *Shockwave S-matrix from Schwarzian Quantum Mechanics*, *JHEP* **11** (2018) 182 [1804.09834].

[35] L.V. Iliesiu, S.S. Pufu, H. Verlinde and Y. Wang, *An exact quantization of Jackiw-Teitelboim gravity*, *JHEP* **11** (2019) 091 [1905.02726].

[36] A. Blommaert, T.G. Mertens and H. Verschelde, *The Schwarzian Theory - A Wilson Line Perspective*, 1806.07765.

[37] M. Mirzakhani, *Simple geodesics and Weil-Petersson volumes of moduli spaces of bordered Riemann surfaces*, *Invent. Math.* **167** (2006) 179.

[38] A.M. Polyakov, *Quantum Geometry of Bosonic Strings*, *Phys. Lett. B* **103** (1981) 207.

[39] N. Seiberg, *Notes on quantum Liouville theory and quantum gravity*, *Prog. Theor. Phys. Suppl.* **102** (1990) 319.

[40] H. Dorn and H. Otto, *On correlation functions for noncritical strings with c <= 1 d >= 1*, *Phys. Lett. B* **291** (1992) 39 [hep-th/9206053].

[41] A.B. Zamolodchikov and A.B. Zamolodchikov, *Structure constants and conformal bootstrap in Liouville field theory*, *Nucl. Phys. B* **477** (1996) 577 [hep-th/9506136].

[42] Y. Nakayama, *Liouville field theory: A Decade after the revolution*, *Int. J. Mod. Phys. A* **19** (2004) 2771 [hep-th/0402009].

[43] V.G. Knizhnik, A.M. Polyakov and A.B. Zamolodchikov, *Fractal Structure of 2D Quantum Gravity*, *Mod. Phys. Lett. A* **3** (1988) 819.

[44] V. Fateev, A.B. Zamolodchikov and A.B. Zamolodchikov, *Boundary Liouville field theory. 1. Boundary state and boundary two point function*, hep-th/0001012.

[45] J. Teschner, *Remarks on Liouville theory with boundary*, *PoS* **tmr2000** (2000) 041 [hep-th/0009138].

[46] N. Seiberg and D. Shih, *Minimal string theory*, *Comptes Rendus Physique* **6** (2005) 165 [hep-th/0409306].

[47] T.G. Mertens and G.J. Turiaci, *Liouville quantum gravity – holography, JT and matrices*, 2006.07072.

[48] G.W. Moore, N. Seiberg and M. Staudacher, *From loops to states in 2-D quantum gravity*, *Nucl. Phys.* **B362** (1991) 665.

[49] A.B. Zamolodchikov, *Three-point function in the minimal Liouville gravity*, *Theor. Math. Phys.* **142** (2005) 183 [hep-th/0505063].

[50] A. Belavin and A. Zamolodchikov, *On Correlation Numbers in 2D Minimal Gravity and Matrix Models*, *J. Phys. A* **42** (2009) 304004 [0811.0450].

[51] I. Kourkoulou and J. Maldacena, *Pure states in the SYK model and nearly-AdS_2 gravity*, 1707.02325.

[52] A. Almheiri, A. Mousatov and M. Shyani, *Escaping the Interiors of Pure Boundary-State Black Holes*, 1803.04434.

[53] A. Almheiri, X. Dong and D. Harlow, *Bulk Locality and Quantum Error Correction in AdS/CFT*, *JHEP* **04** (2015) 163 [1411.7041].

[54] A. Kitaev, *Talk given at IAS workshop.* , .

[55] Y. Gu, A. Lucas and X.-L. Qi, *Spread of entanglement in a Sachdev-Ye-Kitaev chain*, *JHEP* **09** (2017) 120 [1708.00871].

[56] J. Maldacena and D. Stanford, *Remarks on the Sachdev-Ye-Kitaev model*, *Phys. Rev.* **D94** (2016) 106002 [1604.07818].

[57] X. Dong, *The Gravity Dual of Renyi Entropy*, *Nature Commun.* **7** (2016) 12472 [1601.06788].

[58] A. Lewkowycz and J. Maldacena, *Generalized gravitational entropy*, *JHEP* **08** (2013) 090 [1304.4926].

[59] P. Nayak, A. Shukla, R.M. Soni, S.P. Trivedi and V. Vishal, *On the Dynamics of Near-Extremal Black Holes*, *JHEP* **09** (2018) 048 [1802.09547].

[60] B. Czech, J.L. Karczmarek, F. Nogueira and M. Van Raamsdonk, *The Gravity Dual of a Density Matrix*, *Class. Quant. Grav.* **29** (2012) 155009 [1204.1330].

[61] H. Verlinde, *Poking Holes in AdS/CFT: Bulk Fields from Boundary States*, 1505.05069.

[62] T. Banks, M.R. Douglas, G.T. Horowitz and E.J. Martinec, *AdS dynamics from conformal field theory*, hep-th/9808016.

[63] A. Hamilton, D.N. Kabat, G. Lifschytz and D.A. Lowe, *Holographic representation of local bulk operators*, *Phys. Rev. D* **74** (2006) 066009 [hep-th/0606141].

[64] D. Kabat, G. Lifschytz and D.A. Lowe, *Constructing local bulk observables in interacting AdS/CFT*, *Phys. Rev. D* **83** (2011) 106009 [1102.2910].

[65] M. Headrick, V.E. Hubeny, A. Lawrence and M. Rangamani, *Causality & holographic entanglement entropy*, *JHEP* **12** (2014) 162 [1408.6300].

[66] F. Pastawski, B. Yoshida, D. Harlow and J. Preskill, *Holographic quantum error-correcting codes: Toy models for the bulk/boundary correspondence*, *JHEP* **06** (2015) 149 [1503.06237].

[67] I. Heemskerk, D. Marolf, J. Polchinski and J. Sully, *Bulk and Transhorizon Measurements in AdS/CFT*, *JHEP* **10** (2012) 165 [1201.3664].

[68] T. Faulkner and A. Lewkowycz, *Bulk locality from modular flow*, *JHEP* **07** (2017) 151 [1704.05464].

[69] D.L. Jafferis, A. Lewkowycz, J. Maldacena and S.J. Suh, *Relative entropy equals bulk relative entropy*, *JHEP* **06** (2016) 004 [1512.06431].

[70] A. Almheiri, T. Anous and A. Lewkowycz, *Inside out: meet the operators inside the horizon. On bulk reconstruction behind causal horizons*, *JHEP* **01** (2018) 028 [1707.06622].

[71] A. Almheiri, *Talk given at IAS workshop, December 6, 2017.*, .

[72] T. Takayanagi, *Holographic Dual of BCFT*, *Phys. Rev. Lett.* **107** (2011) 101602 [1105.5165].

[73] G.W. Gibbons and S.W. Hawking, *Action integrals and partition functions in quantum gravity*, *Phys. Rev. D* **15** (1977) 2752.

[74] J.D. Brown and J.W. York, *Microcanonical functional integral for the gravitational field*, *Phys. Rev. D* **47** (1993) 1420.

[75] A. Almheiri and B. Kang, *Conformal Symmetry Breaking and Thermodynamics of Near-Extremal Black Holes*, *JHEP* **10** (2016) 052 [1606.04108].

[76] U. Moitra, S.K. Sake, S.P. Trivedi and V. Vishal, *Jackiw-Teitelboim Gravity and Rotating Black Holes*, 1905.10378.

[77] S. Sachdev, *Universal low temperature theory of charged black holes with AdS_2 horizons*, *J. Math. Phys.* **60** (2019) 052303 [1902.04078].

[78] A. Ghosh, H. Maxfield and G.J. Turiaci, *A universal Schwarzian sector in two-dimensional conformal field theories*, *JHEP* **05** (2020) 104 [1912.07654].

[79] L.V. Iliesiu and G.J. Turiaci, *The statistical mechanics of near-extremal black holes*, 2003.02860.

[80] P. Saad, S.H. Shenker and D. Stanford, *A semiclassical ramp in SYK and in gravity*, 1806.06840.

[81] D. Stanford and E. Witten, *JT Gravity and the Ensembles of Random Matrix Theory*, 1907.03363.

[82] A. Blommaert, T.G. Mertens and H. Verschelde, *Eigenbranes in Jackiw-Teitelboim gravity*, *JHEP* **02** (2019) 168 [1911.11603].

[83] A. Almheiri, T. Hartman, J. Maldacena, E. Shaghoulian and A. Tajdini, *Replica Wormholes and the Entropy of Hawking Radiation*, *JHEP* **05** (2020) 013 [1911.12333].

[84] G. Penington, S.H. Shenker, D. Stanford and Z. Yang, *Replica wormholes and the black hole interior*, 1911.11977.

[85] A. Almheiri, T. Hartman, J. Maldacena, E. Shaghoulian and A. Tajdini, *The entropy of Hawking radiation*, 2006.06872.

[86] D. Marolf and H. Maxfield, *Transcending the ensemble: baby universes, spacetime wormholes, and the order and disorder of black hole information*, *JHEP* **08** (2020) 044 [2002.08950].

[87] S.R. Coleman, *Black Holes as Red Herrings: Topological Fluctuations and the Loss of Quantum Coherence*, *Nucl. Phys. B* **307** (1988) 867.

[88] S.B. Giddings and A. Strominger, *Loss of Incoherence and Determination of Coupling Constants in Quantum Gravity*, *Nucl. Phys. B* **307** (1988) 854.

[89] S.B. Giddings and A. Strominger, *Baby Universes, Third Quantization and the Cosmological Constant*, *Nucl. Phys. B* **321** (1989) 481.

[90] L.V. Iliesiu, J. Kruthoff, G.J. Turiaci and H. Verlinde, *JT gravity at finite cutoff*, 2004.07242.

[91] D. Stanford and Z. Yang, *Finite-cutoff JT gravity and self-avoiding loops*, 2004.08005.

[92] J. Maldacena, G.J. Turiaci and Z. Yang, *Two dimensional Nearly de Sitter gravity*, 1904.01911.

[93] J. Cotler, K. Jensen and A. Maloney, *Low-dimensional de Sitter quantum gravity*, *JHEP* **06** (2020) 048 [1905.03780].

[94] Y. Chen, V. Gorbenko and J. Maldacena, *Bra-ket wormholes in gravitationally prepared states*, 2007.16091.

[95] T. Anous, J. Kruthoff and R. Mahajan, *Density matrices in quantum gravity*, *SciPost Phys.* **9** (2020) 045 [2006.17000].

[96] J.W. York, *Role of conformal three-geometry in the dynamics of gravitation*, *Phys. Rev. Lett.* **28** (1972) 1082.

[97] M. Mirzakhani, *Weil-Petersson volumes and intersection theory on the moduli space of curves*, *J. Am. Math. Soc.* **20** (2007) 1.

[98] H.A. González, D. Grumiller and J. Salzer, *Towards a bulk description of higher spin SYK*, *JHEP* **05** (2018) 083 [1802.01562].

[99] V. Godet and C. Marteau, *New boundary conditions for AdS_2*, 2005.08999.

[100] K. Isler and C.A. Trugenberger, *Gauge theory of two-dimensional quantum gravity*, *Physical Review Letters* **63** (1989) 834.

[101] A.H. Chamseddine and D. Wyler, *Gauge theory of topological gravity in 1+ 1 dimensions*, *Physics Letters B* **228** (1989) 75.

[102] J. Balog, L. Feher and L. Palla, *Coadjoint orbits of the Virasoro algebra and the global Liouville equation*, *Int. J. Mod. Phys. A* **13** (1998) 315 [hep-th/9703045].

[103] A. Lyapunov, *The general problem of stability of motion (in Russian)*, Ph.D. thesis, University of Kharkov, 1892.

[104] A.M. Polyakov, *Gauge Fields and Strings*, vol. 3 (1987).

[105] J.M. Maldacena, *Non-Gaussian features of primordial fluctuations in single field inflationary models*, *JHEP* **05** (2003) 013 [astro-ph/0210603].

[106] O. Aharony, M. Berkooz and E. Silverstein, *Multiple trace operators and nonlocal string theories*, *JHEP* **08** (2001) 006 [hep-th/0105309].

[107] E. Witten, *Multitrace operators, boundary conditions, and AdS / CFT correspondence*, hep-th/0112258.

[108] D.J. Gross, J. Kruthoff, A. Rolph and E. Shaghoulian, *Hamiltonian deformations in quantum mechanics, $T\overline{T}$, and the SYK model*, *Phys. Rev. D* **102** (2020) 046019 [1912.06132].

[109] M. Guica and R. Monten, *$T\overline{T}$ and the mirage of a bulk cutoff*, 1906.11251.

[110] D. Stanford and N. Seiberg, *Unpublished*, .

[111] D. Kapec and R. Mahajan, *Comments on the Quantum Field Theory of the Coulomb Gas Formalism*, 2010.10428.

[112] H. Maxfield and G.J. Turiaci, *The path integral of 3D gravity near extremality; or, JT gravity with defects as a matrix integral*, 2006.11317.

[113] E. Witten, *Matrix Models and Deformations of JT Gravity*, 2006.13414.

[114] A. Knapp, *Representation Theory of Semisimple Groups: An Overview Based on Examples*, Princeton Mathematical Series, Princeton University Press (2001).

[115] D. Stanford, *Talk given at KITP, 2018*, .

[116] M. Berkooz, P. Narayan and J. Simon, *Chord diagrams, exact correlators in spin glasses and black hole bulk reconstruction*, *JHEP* **08** (2018) 192 [1806.04380].

[117] M. Berkooz, M. Isachenkov, V. Narovlansky and G. Torrents, *Towards a full solution of the large N double-scaled SYK model*, *JHEP* **03** (2019) 079 [1811.02584].

[118] M. Berkooz, V. Narovlansky and H. Raj, *Complex Sachdev-Ye-Kitaev model in the double scaling limit*, 2006.13983.

[119] M. Berkooz, N. Brukner, V. Narovlansky and A. Raz, *The double scaled limit of Super–Symmetric SYK models*, 2003.04405.

[120] S. Jackson, L. McGough and H. Verlinde, *Conformal Bootstrap, Universality and Gravitational Scattering*, *Nucl. Phys. B* **901** (2015) 382 [1412.5205].

[121] B. Ponsot and J. Teschner, *Liouville bootstrap via harmonic analysis on a noncompact quantum group*, hep-th/9911110.

[122] A. Kitaev, *Talks given at the Fundamental Physics Prize Symposium and KITP seminars*, .

[123] G.J. Turiaci, M. Usatyuk and W.W. Weng, *Dilaton-gravity, deformations of the minimal string, and matrix models*, 2011.06038.

[124] A.C. Hirshfeld and T. Schwarzweller, *Poisson sigma models*, in *International Workshop on Physical Variables in Gauge Theories*, 9, 1999 [hep-th/0001026].

[125] T. Mertens, *Talk given at Workshop on Qubits and Black Holes, IAS Princeton, 2020*, .

[126] P. Gao, A. Goel and H. Verlinde, *to appear*, .

[127] N. Seiberg and D. Shih, *Branes, rings and matrix models in minimal (super)string theory*, *JHEP* **02** (2004) 021 [hep-th/0312170].

[128] J.M. Maldacena, G.W. Moore, N. Seiberg and D. Shih, *Exact vs. semiclassical target space of the minimal string*, *JHEP* **10** (2004) 020 [hep-th/0408039].

[129] D. Kutasov, K. Okuyama, J.-w. Park, N. Seiberg and D. Shih, *Annulus amplitudes and ZZ branes in minimal string theory*, *JHEP* **08** (2004) 026 [hep-th/0406030].

[130] J. McGreevy and H.L. Verlinde, *Strings from tachyons: The c=1 matrix reloaded*, *JHEP* **12** (2003) 054 [hep-th/0304224].

[131] I.R. Klebanov, J.M. Maldacena and N. Seiberg, *D-brane decay in two-dimensional string theory*, *JHEP* **07** (2003) 045 [hep-th/0305159].

[132] D. Gaiotto and L. Rastelli, *A Paradigm of Open / Closed Duality: Liouville D-Branes and the Kontsevich Model*, *JHEP* **07** (2005) 053 [hep-th/0312196].

[133] A. Hashimoto, M.-x. Huang, A. Klemm and D. Shih, *Open/closed string duality for topological gravity with matter*, *JHEP* **05** (2005) 007 [hep-th/0501141].

[134] J.M. Daul, V.A. Kazakov and I.K. Kostov, *Rational theories of 2-D gravity from the two matrix model*, *Nucl. Phys.* **B409** (1993) 311 [hep-th/9303093].

[135] V.A. Kazakov and I.K. Kostov, *Instantons in noncritical strings from the two matrix model*, in *From fields to strings: Circumnavigating theoretical physics. Ian Kogan memorial collection (3 volume set)*, pp. 1864–1894, 2004, DOI [hep-th/0403152].

[136] B. Eynard, *Large N expansion of the 2 matrix model*, *JHEP* **01** (2003) 051 [hep-th/0210047].

[137] A. Altland and J. Sonner, *Late time physics of holographic quantum chaos*, 2008.02271.

[138] Y. Gu, X.-L. Qi and D. Stanford, *Local criticality, diffusion and chaos in generalized Sachdev-Ye-Kitaev models*, *JHEP* **05** (2017) 125 [1609.07832].

[139] G. Turiaci and H. Verlinde, *Towards a 2d QFT Analog of the SYK Model*, *JHEP* **10** (2017) 167 [1701.00528].

[140] J. Murugan, D. Stanford and E. Witten, *More on Supersymmetric and 2d Analogs of the SYK Model*, *JHEP* **08** (2017) 146 [1706.05362].

[141] M. Berkooz, P. Narayan, M. Rozali and J. Simón, *Comments on the Random Thirring Model*, *JHEP* **09** (2017) 057 [1702.05105].

[142] G. Turiaci and H. Verlinde, *On CFT and Quantum Chaos*, *JHEP* **12** (2016) 110 [1603.03020].

[143] P. Gao, D.L. Jafferis and A.C. Wall, *Traversable Wormholes via a Double Trace Deformation*, *JHEP* **12** (2017) 151 [1608.05687].

[144] M. Oshikawa and I. Affleck, *Boundary conformal field theory approach to the critical two-dimensional Ising model with a defect line*, *Nucl. Phys. B* **495** (1997) 533 [cond-mat/9612187].

[145] C. Bachas, J. de Boer, R. Dijkgraaf and H. Ooguri, *Permeable conformal walls and holography*, *JHEP* **06** (2002) 027 [hep-th/0111210].

[146] E.M. Brehm, I. Brunner, D. Jaud and C. Schmidt-Colinet, *Entanglement and topological interfaces*, *Fortsch. Phys.* **64** (2016) 516 [1512.05945].

[147] H. Verlinde, *ER = EPR revisited: On the Entropy of an Einstein-Rosen Bridge*, 2003.13117.

[148] H. Verlinde, *Wormholes in Quantum Mechanics*, 2105.02129.

[149] H. Verlinde, *Deconstructing the Wormhole: Factorization, Entanglement and Decoherence*, 2105.02142.

[150] G. Compere and D. Marolf, *Setting the boundary free in AdS/CFT*, *Class. Quant. Grav.* **25** (2008) 195014 [0805.1902].

[151] E. Witten, *A Note On Boundary Conditions In Euclidean Gravity*, 1805.11559.

[152] D.J. Gross, J. Kruthoff, A. Rolph and E. Shaghoulian, $T\overline{T}$ *in* AdS_2 *and Quantum Mechanics*, *Phys. Rev. D* **101** (2020) 026011 [1907.04873].

[153] L. McGough, M. Mezei and H. Verlinde, *Moving the CFT into the bulk with* $T\overline{T}$, *JHEP* **04** (2018) 010 [1611.03470].

[154] T. Hartman, J. Kruthoff, E. Shaghoulian and A. Tajdini, *Holography at finite cutoff with a* T^2 *deformation*, *JHEP* **03** (2019) 004 [1807.11401].

[155] M. Taylor, *TT deformations in general dimensions*, 1805.10287.

[156] E. Coleman and V. Shyam, *Conformal Boundary Conditions from Cutoff* AdS_3, 2010.08504.

[157] Y. Hikida, *Liouville field theory on a unoriented surface*, *JHEP* **05** (2003) 002 [hep-th/0210305].